FACULTEIT WETENSCHAPPEN
DEPARTEMENT CHEMIE
AFDELING MOLECULAIR DESIGN EN SYNTHESE
LABORATORIUM COORDINATIECHEMIE

KATHOLIEKE
UNIVERSITEIT
LEUVEN

Liquid-crystalline complexes of transition metals and rare earths with substituted 1,10-phenanthroline ligands

Proefschrift ingediend voor het behalen van de graad van
Doctor in de Wetenschappen

Thomas Cardinaels

Mei 2006

Promotor:
Prof. Dr. Koen Binnemans

Copyright Faculteit Wetenschappen, Departement Chemie
ISBN 90-8649-009-3
Wettelijk depot D/2006/10.705/6
UDC 544.25

Leden van de examencommissie:

Prof. Dr. Koen Binnemans (promotor)
Prof. Dr. Christiane Görller-Walrand
Prof. Dr. Wim Dehaen
Prof. Dr. Steven De Feyter
Prof. Dr. Christ Glorieux
Prof. Dr. Duncan W. Bruce (University of York, UK)

Dankwoord (Acknowledgements)

In de loop van mijn doctoraatsonderzoek realiseerde ik mij dat vele inzichten en ideeën meestal tot stand komen door (soms verregaande) discussies met anderen. Bij deze gelegenheid wil ik dan ook een aantal mensen bedanken die mij geholpen hebben met de verwezenlijking van mijn doctoraatsthesis.

Eerst en vooral wil ik ons diensthoofd Prof. Dr. Christiane Görller-Walrand en mijn promotor Prof. Dr. Koen Binnemans bedanken. Zij hebben mij de mogelijkheid gegeven om onderzoek te verrichten in hun onderzoeksgroep. Koen, bedankt om mij "mijn ding" te laten doen gedurende vier jaar en voor de enorme input aan ideeën en wetenschappelijke feedback.

Secondly, I would like to thank Prof. Duncan W. Bruce for an amazing year in Exeter. Duncan, I really suffered to obtain my first phenanthroline-containing liquid crystal, but it was worth it, and I promise you if I get the opportunity, I'll finish the synthesis of the other homologues. I also want to thank Dr. Loc Nguyen, the only Vietnamese guy I know, but he's one of a kind. Thank you for all your advice concerning organic synthesis.

Tijdens de laatste twee jaar van mijn doctoraatsonderzoek heb ik mogen samenwerken met Jan Ramaekers. Bedankt voor al het werk, de B52's en de sportieve inspanningen die we samen verzet hebben.

Daarnaast wil ik vier doctors bedanken die mij het leven in de "200F" wat gemakkelijker (of soms moeilijker) hebben gemaakt door de vele discussies en voor hun bijdrage aan mijn doctoraatsthesis. Bedankt Dr. Kris Driesen, voor uw wijze raad en het opnemen en bespreken van de luminescentiespectra. Bedankt Dr. Tanja Parac-Vogt, voor de structuurbepalingen in oplossing via NMR-spectrometrie.

Bedankt Dr. Rik Van Deun, voor de vele besprekingen op allerhande gebied en bedankt Dr. Peter Nockemann, voor de vele tips, discussies en de kristalstructuurbepalingen.

Graag wil ik Prof. Dr. Wim Dehaen bedanken voor zijn wijze raad betreffende organische synthese en Karel Duerinckx en Prof. Dr. Suzanne Toppet voor de hulp bij NMR-metingen. Ook de twee laborantes van ons labo, Petra Bloemen en Leen Van Nerum wil ik bedanken voor de CHN-analyses, de massaspectra en de zuiveringen via HPLC.

Prof. Dr. Luc Van Meervelt, Kristof Van Hecke en Dr. Peter Nockemann wil ik bedanken voor de kristalstructuurbepalingen.

For all the hard work concerning X-ray diffraction and molecular modeling, I would like to thank Dr. Daniel Guillon, Dr. Benoît Heinrich, Dr. Cyril Bourgogne and Dr. Bertrand Donnio. Bertrand, your way of thinking about liquid crystals has changed my way of thinking, and has made me a better scientist. I have great respect for people like you, who realize there is more in life than science.

Verder wil ik mijn collega's, ex-collega's en de mensen van de "200F" bedanken voor de aangename werkomgeving: Jan, Pacco (bedankt voor al het "chillen"), Fias (onze "rumba-fever" zal ik nooit vergeten), Philip (mijn trouwe bureaugenoot), Ben, Kelly, Kyra, Karel, Nele, Els, Karen, Katleen, Linda… Ook Rita en Pol mag ik zeker niet vergeten voor de hulp op allerhande gebied.

Voor de financiële steun wil ik het Fonds voor Wetenschappelijk Onderzoek Vlaanderen (FWO-Vlaanderen) bedanken.

Ik wil ook zeker mijn familie en vrienden bedanken en in het bijzonder mijn ouders en mijn zus, die altijd voor mij klaarstaan. Om te eindigen wil ik mijn lieve vriendin Eve bedanken. Bedankt voor alle steun en het vertrouwen in deze kerel!

Contents

Introduction **1**

Chapter 1: Liquid crystals **5**
1.1 Introduction 5
1.2 Classification of mesophases 8
1.2.1 Calamitic molecules 8
1.2.2 Discotic molecules 12
1.2.3 Bent-core molecules 14
1.2.4 Polycatenar molecules 17
1.2.5 Metallomesogens 19
1.3 Mesophase characterization 20
1.3.1 Polarizing optical microscopy 20
1.3.2 Differential Scanning Calorimetry 22
1.3.3 X-ray diffraction 25

Chapter 2: Phenanthrolines **29**
2.1 Introduction 29
2.2 Liquid-crystalline phenanthrolines 30

Chapter 3: A tetracatenar liquid crystal based on 1,10-phenanthroline **37**
3.1 Introduction 37
3.2 Synthesis 37
3.3 Results and discussion 40
3.3.1 X-ray single crystal structure 40
3.3.2 Thermal behavior 41

3.4 Conclusions 46
3.5 Experimental section 46
3.5.1 Techniques 46
3.5.2 Synthesis 48

Chapter 4: Design of high coordination number metallomesogens by decoupling of the complex-forming and mesogenic groups 57
4.1 Introduction 57
4.2 Synthesis 62
4.3 Results and discussion 68
4.3.1 Solution studies 68
4.3.2 Thermal behavior 73
4.3.3 Luminescence properties 94
4.4 Conclusions 100
4.5 Experimental section 101
4.5.1 Techniques 101
4.5.2 Synthesis 103

Chapter 5: Imidazo[4,5-f]-1,10-phenanthrolines: versatile ligands for the design of metallomesogens with complex molecular architectures 127
5.1 Introduction 127
5.2 Synthesis and characterization 127
5.2.1 Synthesis and characterization of the ligands 127
5.2.2 Synthesis and characterization of the metal complexes 135
5.3 Results and discussion 142
5.3.1 Thermal behavior of the ligands 142
5.3.2 Thermal behavior of the palladium(II) and platinum(II) complexes 148

5.3.3 Thermal behavior of the rhenium(I) complexes 149
5.3.4 Thermal behavior of the ruthenium(II) complexes 149
5.3.5 Thermal behavior of the nickel(II) complexes 149
5.3.6 Thermal behavior of the uranyl complex 151
5.4 Conclusions 159
5.5 Experimental section 160
5.5.1 Techniques 160
5.5.2 Synthesis 162
5.5.2.1 Synthesis of precursors and ligands 162
5.2.2.2 Synthesis of metal precursors 186
5.2.2.3. Synthesis of metal complexes 188

General conclusions and summary **207**

Samenvatting **215**

List of publications **221**

Appendix A: X-ray diffraction of mesophases **223**
A.1 Nematic phase 223
A.2 Smectic phases 223
A.3 Columnar phases 227
A.3.1 Hexagonal columnar phase 230
A.3.2 Rectangular columnar phase 232
A.4 Cubic phases 235

Appendix B: Treatment of glass cover slips **237**
B.1 Treatment of glass cover slips to obtain planar orientation 238
B.2 Treatment of glass cover slips to obtain homeotropic orientation 239

Abbreviations

Col_h	hexagonal columnar mesophase
Col_r	rectangular columnar mesophase
Cr	crystalline or semicrystalline phase
d	layer spacing
dec	decomposition
DMF	*N,N*-dimethylformamide
DMSO	dimethyl sulfoxide
DSC	differential scanning calorimetry
ESI-MS	electron spray ionization mass spectrometry
I	isotropic phase
Ln	lanthanide ion
N	nematic phase
ñ	director of the liquid crystal
phen	1,10-phenanthroline
POM	polarizing optical microscopy
ppm	parts per million
SmA	smectic A phase
SmC	smectic C phase
THF	tetrahydrofuran
tta	2-thenoyltrifluoroacetonate
XRD	X-ray diffraction

Introduction

Liquid crystals are extraordinary materials that represent a state of matter, intermediate between disordered liquids and ordered solids. They can be considered as anisotropic liquids as they combine the anisotropic properties of crystals and the fluidity of liquids. An important development has been the synthesis of metal-containing liquid crystals, the so-called *metallomesogens*, which combine the properties of both liquid crystals and metals (magnetic and optical properties, redox activity). There is strong interest in the development of new ligands, as the choice of ligand will determine which metals can be complexed, while specific properties can be obtained on complexation to a metal center. In this point of view, 1,10-phenanthroline is a very interesting ligand. It is one of the most versatile ligands in coordination chemistry as it can form complexes with a wide variety of metals and also because it allows the synthesis of luminescent metal complexes. There are only a few examples of liquid crystals based on the 1,10-phenanthroline core. This is due to the relative unavailability of suitable substituted phenanthrolines as starting materials. However, from a general point of view, 1,10-phenanthroline is very suitable as a basic unit for the design of liquid-crystalline materials. The extended conjugated π-system and the permanent dipole moment are favorable for the emergence of mesophases via π-π stacking and dipole-dipole interactions of the rigid cores.

The objective of this PhD thesis is to investigate how 1,10-phenanthroline can be functionalized so that the resulting compounds are liquid crystals themselves or that they can serve as ligands for the design of metal-

containing liquid crystals. Two substitution patterns are investigated: 3,8-disubstitution and 5,6-disubstitution. These two substitution patterns can lead to classes of mesogenic molecules with a totally different molecular shape. The focus of this work is on the synthesis of 1,10-phenanthroline ligands and corresponding metal complexes, and on the thermal behavior of these compounds. The metals considered in this study are both d-block and f-block elements, so that a wide variety of different metal complexes can be obtained.

Besides some general terms used in liquid-crystalline research, in **Chapter 1**, an overview of the different types of liquid-crystalline phases is given and the techniques used to identify these phases are described.
In **Chapter 2**, a literature overview about phenanthrolines is presented.
A tetracatenar liquid crystal prepared by Sonogashira chemistry is described in **Chapter 3**. The compound is structurally and thermally characterized.
The synthesis of mesomorphic high coordination number metallomesogens by coupling mesogenic 4-cyanobiphenyl groups via a long alkyl spacer to a substituted imidazo[4,5-f]-1,10-phenanthroline, which acts as the coordinating group is presented in **Chapter 4**. Complexes of rhenium(I), yttrium(III), lanthanum(III), neodymium(III), samarium(III), europium(III), erbium(III), and ytterbium(III) were prepared. A study of the thermal behavior of both the ligands and metal complexes as well as the optical properties of the luminescent lanthanide β-diketonate complexes is performed. Also the solution structure of the diamagnetic complexes is investigated by NMR spectroscopy.
Finally in **Chapter 5**, the synthesis of mesomorphic alkoxylated 2-aryl-substituted imidazo[4,5-f]-1,10-phenanthrolines and corresponding metal complexes is described. Metal complexes were made with different d-block transition metals, including nickel(II), palladium(II), platinum(II),

ruthenium(II), and rhenium(I), as well as with trivalent lanthanide ions and with uranyl. The influence of the metal ion (metal-to-ligand ratio), the substitution pattern and the chain length on the thermal properties is discussed.

1.1. Introduction

Materials can be classified by considering their physical aggregation state as solids, liquids and gasses. However, there exist two other states of matter, namely the plasma state and the liquid-crystalline state.
In the crystalline solid state, the molecules are ordered in a crystal lattice. The molecules have 3-dimensional positional and orientational order. In the liquid phase, the molecules have neither positional nor orientational order, and the molecules are randomly oriented and free to flow. The liquid-crystalline phase is situated between the crystalline phase and the liquid phase and is therefore defined as *mesophase* (*mesos* = between). Materials that have liquid-crystalline properties are named *mesogens*. The order of the crystalline phase is partly lost and the molecules have some degree of mobility.
One way to obtain a mesophase is by heating the crystalline phase (*thermotropic* liquid crystals, Figure 1.1). When such a compound is heated, it will melt into the liquid-crystalline phase at the *melting point*. On further heating, the liquid crystal transforms into an isotropic liquid at the *clearing point*. When the mesophase is found on both heating and cooling a material, the phase is termed *enantiotropic*. When the mesophase only appears on cooling a material and is therefore metastable, the phase is termed *monotropic*.

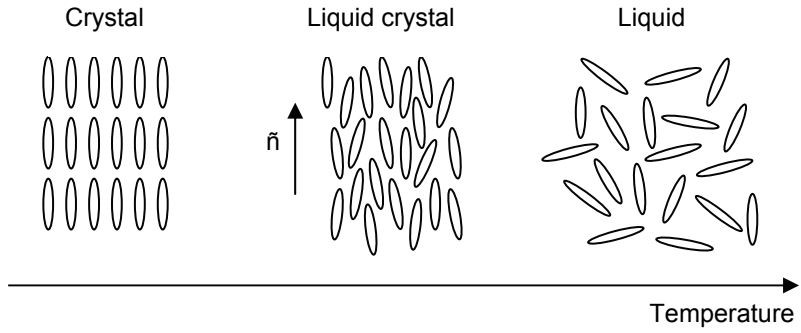


Figure 1.1: Schematic thermal behavior of a thermotropic liquid crystal.

Another way to induce liquid-crystalline behavior (or *mesomorphism*) is the addition of a solvent, such as water, to the solid phase (*lyotropic* liquid crystals). The types of mesophases formed, depend on the concentration of the compound in the solution and on the temperature.

Liquid crystals combine order and mobility, which make them very useful materials which have properties of both solids and liquids.[1-5] Lyotropic mesophases are of prime importance for living organisms, because cell membranes are examples of lyotropic systems formed by self-assembly of phospholipids in an aqueous medium into lamellar phases (Figure 1.2).[6] DNA, which contains all the genetic information, exhibits lyotropic mesomorphic behavior at sufficiently high concentrations.

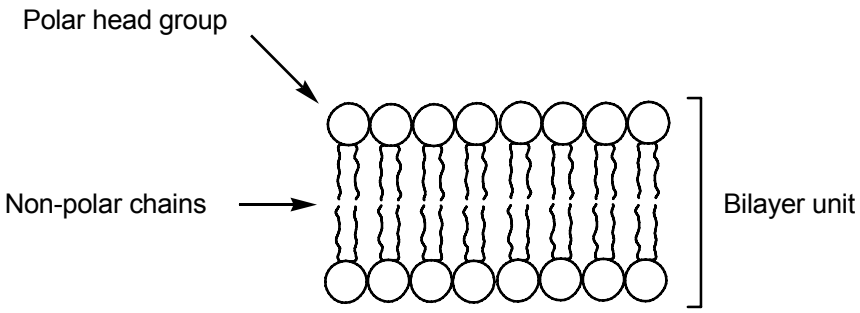


Figure 1.2: Lamellar arrangement of phospholipids.

Thermotropic liquid crystals are used in many applications such as displays (LCDs) and temperature sensors. Since this work considers only low molar mass thermotropic liquid crystals, the further discussion is devoted to this type of materials only.

Many factors determine the type of mesophases formed by thermotropic liquid crystals, but the molecular shape is by far the most important one. Liquid-crystalline phases are therefore classified according to the shape of the mesogenic molecule. This shape can be rodlike (*calamitic* mesogens), disclike (*discotic* mesogens) or V-shaped (*bent-core* or *banana shaped* mesogens). *Polycatenar* liquid crystals have a structure intermediate between that of rodlike and disclike molecules and are also considered as a separate class of thermotropic liquid crystals. Another factor which determines the type of mesophase is space filling.[7] The whole space must be reachable by the mesogenic molecules. This space filling requirement adds extra limitations to the structures that can be displayed by thermotropic liquid crystals. The issue of space filling is further described in appendix A.

1.2 Classification of mesophases

1.2.1 Calamitic molecules

Nematic phase

The *nematic phase* (N) is the least ordered phase and has a lower viscosity than any other type of mesophase. The long molecular axis of the molecules is on average parallel to a preferential direction, indicated by the vector ñ, which is known as the *director* (Figure 1.3).

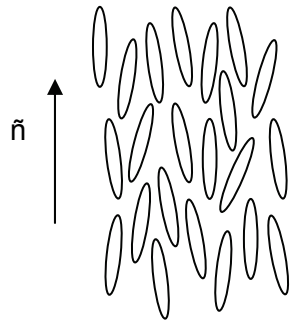


Figure 1.3: Schematic representation of the molecular order in the nematic phase.

Chiral nematic phase

In the *chiral nematic phase* (N*), the director precesses through the material, describing a helix (Figure 1.4). The pitch of a chiral nematic phase is the distance along the helix over which the director rotates by 360°.

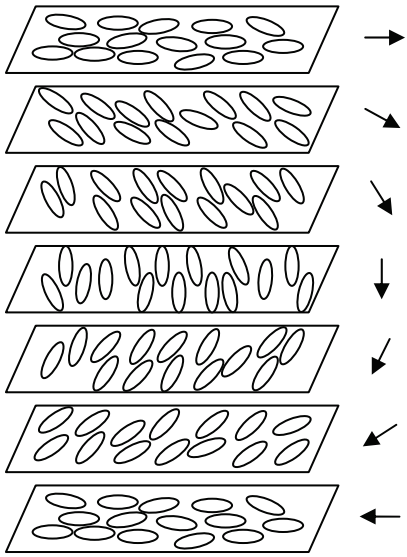


Figure 1.4: Schematic representation of the molecular order in the chiral nematic phase.

Smectic phases

The *smectic phases* (Sm) are more ordered than the nematic phase. They possess some positional ordering of the molecules into layers, in addition to the orientational order.

The *smectic A phase* (SmA) is the most disordered smectic phase (Figure 1.5). Like the nematic phase, the molecules point with their long molecular axis on average in the same direction, but in addition, they are stacked into layers, with the orientational direction perpendicular to the layer plane. When the molecules are tilted within the layers, a *smectic C phase* (SmC) is obtained (Figure 1.5).

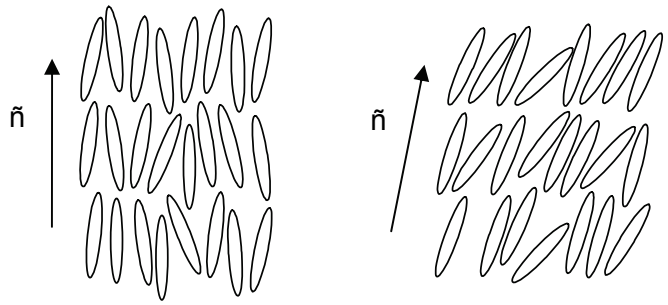


Figure 1.5: Schematic representation of the SmA (left) and the SmC (right) phase.

If hexagonal symmetry is introduced in the smectic A phase, the *smectic B phase* (SmB) is obtained (Figure 1.6). It is a more ordered, and hence less fluid phase than the SmA and the SmC phase.

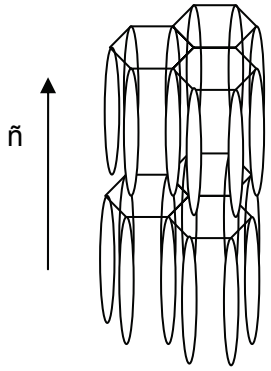


Figure 1.6: Schematic representation of the SmB phase.

The *smectic F phase* (SmF) and the *smectic I phase* (SmI) are tilted hexagonal structures. For the SmF phase the tilt is towards an edge of the hexagonal net, while for the SmI phase the tilt is towards a corner of the net.

In addition, the SmC, SmF, and SmI phases may exist as chiral modifications (SmC*, SmF*, and SmI*).
There are also *crystal smectic phases*, which are characterized by the appearance of inter-layer correlations and, in some cases, by the loss of molecular rotational freedom (labeled B, E, G, H, J, and K).

Cubic phases

Cubic phases are mesophases of cubic symmetry. Because of their high symmetry, their physical properties are no longer anisotropic. No defect texture is observed by polarizing optical microscopy (vide infra) and the image between crossed polarizers remains black. The cubic mesophases are very viscous and often their formation kinetics are very slow. Although cubic mesophases are very common for lyotropic liquid crystals, where a cubic phase is possible between any pair of phases, there are only relatively few examples of cubic mesophases in thermotropic liquid crystals.[8] Whereas a cubic mesophase can relatively easy be detected when it is present between two anisotropic mesophases, it is difficult to observe the formation of the cubic phase when it is formed by cooling an isotropic liquid. In this case, a deformation of air bubbles in the melt is observed, as well as a sharp increase in the viscosity of the liquid.

1.2.2 Discotic molecules

Discotic molecules can also form a nematic phase: the *discotic nematic phase* (N_D). Analogous to the calamitic nematic phase, the discotic nematic phase possesses only orientational order of the short molecular axes (Figure 1.7).

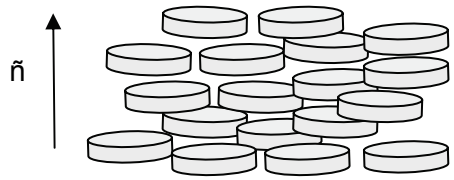


Figure 1.7: Schematic representation of the discotic nematic phase (N_D).

In addition to the N_D phase, there are a whole series of columnar phases. These phases consist of columns of discotic molecules and differ by the positional ordering of the columns. In the *columnar nematic phase* (N_{col}), short columns are ordered in a nematic way (Figure 1.8).

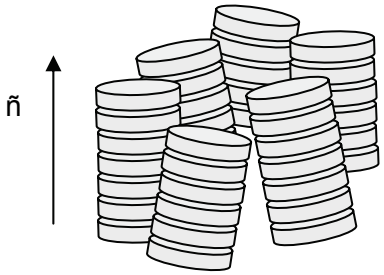


Figure 1.8: Schematic representation of the columnar nematic phase (N_{col}).

If the columns are arranged into a hexagonal pattern, a *hexagonal columnar phase* (Col_h) is obtained. Other types of columnar phases are the

rectangular columnar phase (Col_r) and the *oblique columnar phase* (Col_o). A schematic representation of the Col_h phase is shown in Figure 1.9. A schematic representation of the 2D lattices of the Col_r and the Col_o phases is shown in Figure 1.10.

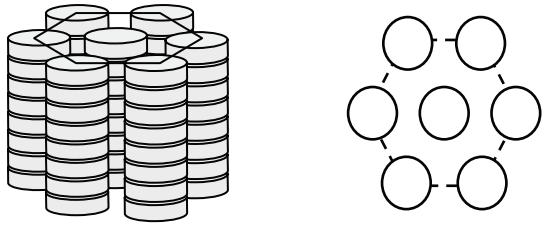


Figure 1.9: Schematic representation of the hexagonal columnar phase (plane group p6mm).

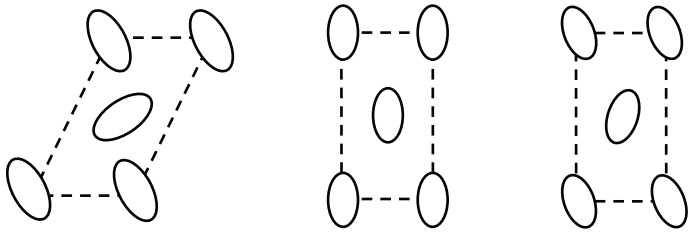


Figure 1.10: Schematic representation of the 2D lattices of the oblique columnar phase (left, plane group p1) and the rectangular columnar phase (middle, plane group c2mm; right, plane group p2gg).

In some types of columnar phase, the order of the molecules within the columns is a-periodical (disordered columnar phase), while in other cases there is an ordered, regular stacking inside the columns (ordered columnar phase).

1.2.3 Bent-core molecules

Liquid-crystalline molecules with a bent molecular shape, so-called *banana-shaped* liquid crystals, have recently attracted much scientific attention because of their unique mesomorphism (Figure 1.11).[9-11]

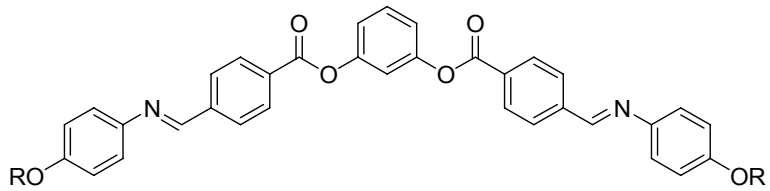


Figure 1.11: General structure of the most intensively investigated type of bent-core (banana-shaped) liquid crystals.

The special shape and the polarity of these molecules lead to a stacking of the molecules in layers, with the polar bend of the molecules pointing in the same direction. Such a directed packing results in a polarization parallel to the layers. Energetically, this is not favorable and therefore the layered structures are modified in order to escape from a macroscopic polarization. There are several ways, leading to the formation of new liquid-crystalline phases (Figure 1.12). The most simple one, is the formation of a rectangular columnar phase (Col_r in Figure 1.12), also known as the B_1 phase, which is usually formed when the core-core interactions are dominant. When the aliphatic chains are sufficiently long, a lamellar arrangement is more favorable, resulting in the formation of polar smectic phases with an antiparallel stacking of the layers (SmP_A in Figure 1.12). Because the polarization of adjacent layers is cancelled out, this phase is antiferroelectric. By application of an electric field, the antiparallel stacking of the layers can be transformed into a parallel stacking, resulting in a ferroelectric polar smectic phase (SmP_F). Usually, in most of these polar

smectic phases (SmP) the molecules are tilted (SmCP or B_2 phase), but also non-tilted (SmAP) and double tilted (SmC_G) phases exist.

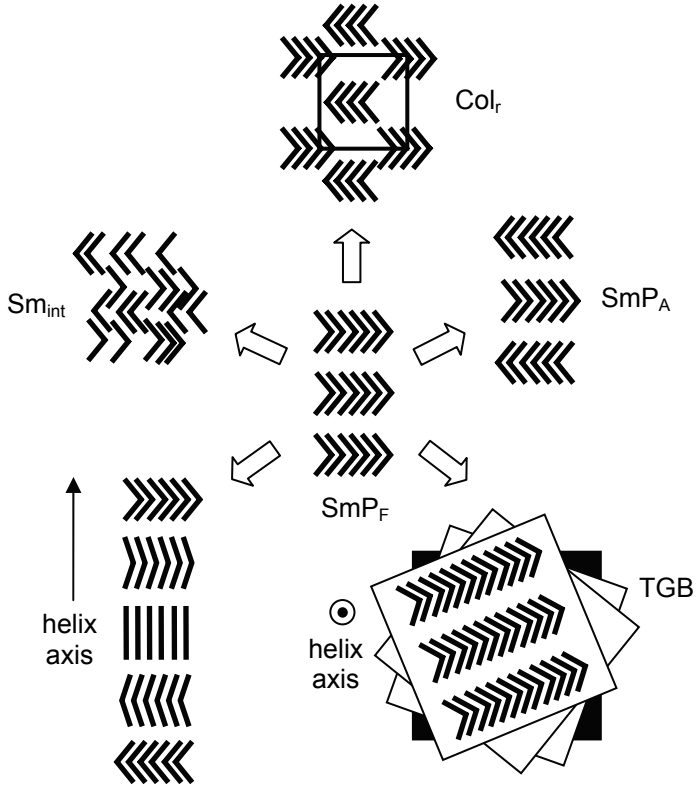


Figure 1.12: Possible ways to escape from a macroscopic polarization in mesophases built up from bent-core molecules. Abbreviations: Sm_{int} = intercalated smectic phase; SmP_A = smectic phase with antiferroelectric correlation between adjacent layers; SmP_F = smectic phase with ferroelectric correlation between adjacent layers (macroscopically polar ordered); TGB = twisted grain boundary structure.

For the SmCP phase, four possible states can be distinguished depending on the relative tilt sense and the polar order of the molecules in adjacent layers (Figure 1.13). For these SmCP phases, a handedness (and thus chirality) is observed, depending on the tilt sense of the molecules. Also non-polar intercalated phases exist, denoted as Sm_{int} or B_6 phases (Figure 1.12).
Another way to escape from macroscopic polarization is the formation of a helical supermolecular structure. Examples are the plastic crystal B_4 phase, which has a twisted grain boundary structure (TGB in Figure 1.12) and the B_7 phase, which has a very complex structure.

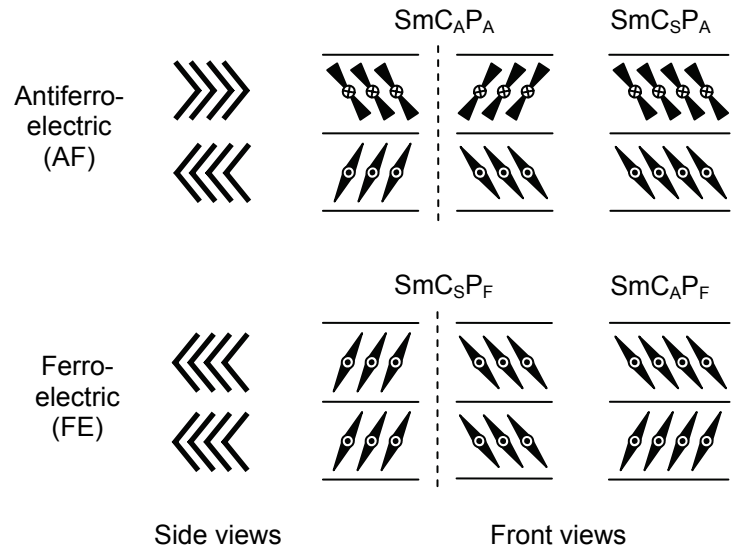


Figure 1.13: The four possible states of SmCP phases that are distinguished by the relative tilt sense and the polar order in adjacent layers. The notations C_S and C_A refer to synclinic and anticlinic tilt while P_F and P_A refer to ferroelectric (FE) and antiferroelectric (AF) polar order in adjacent layers.

1.2.4 Polycatenar molecules

Polycatenar (literally *many-tailed*) liquid crystals consist of an extended, linear, normally aromatic core that is decorated with several long alkoxy chains at both ends (Figure 1.14).[12]

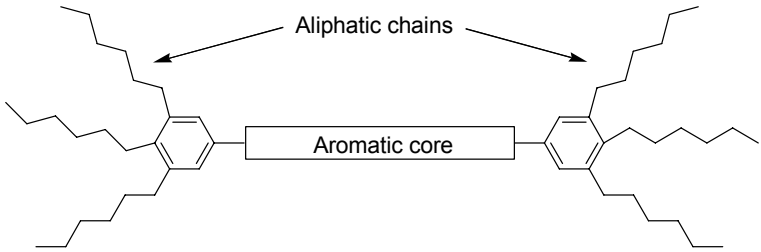


Figure 1.14: General structure of polycatenar liquid crystals. In this figure a hexacatenar liquid crystal is shown.

The nomenclature of polycatenar systems is related to the number of terminal chains, so that those containing four chains are named *tetracatenar*, those with six chains *hexacatenar* and so on. The chains can be placed in different positions leading to several isomeric possibilities. In general, the core of a polycatenar mesogen consists of at least four rings, usually aromatic. Additionally, there must be a balance between the number of chains attached to the core and the length of the core to obtain mesomorphic properties. In general, the core must have as many rings as terminal chains.
Polycatenar mesogens have aroused interest due to their rich mesomorphism, and tetracatenar mesogens with the terminal chains in the 3- and 4-positions are the most interesting polycatenar mesogens. They can show nematic, lamellar, cubic and columnar mesophases in the same series at differing chain lengths, making them quite unique liquid-crystalline

materials.[13] At short chain lengths, nematic and/or SmC phases are observed, while at longer chain lengths, columnar phases are observed.

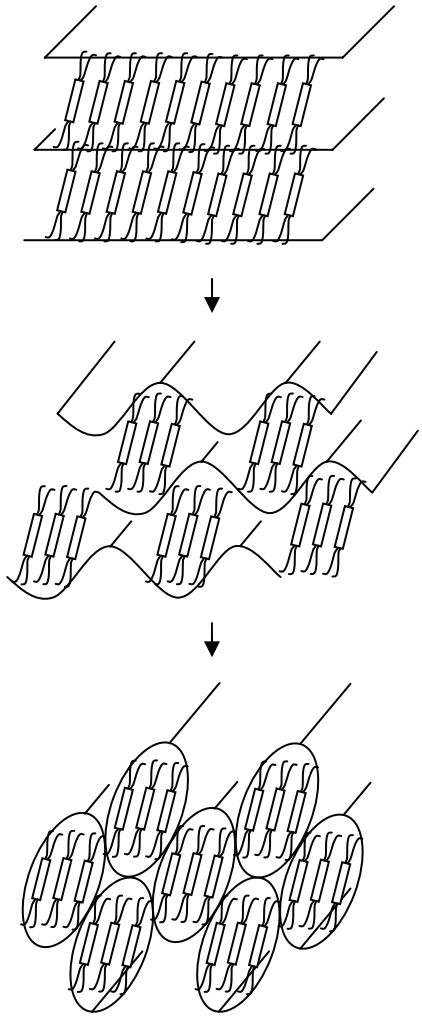


Figure 1.15: Model for the formation of the columnar mesophases.[14]

When the chain length is short, the materials have a rodlike shape and so nematic or smectic phases are expected. With these systems, it is always the tilted SmC phase which is observed: at the interface between the rigid core and the chains, the cross-sectional area of the chains is greater than that of the core and so to fill space efficiently, the cores must tilt. However, at longer chain lengths and/or at higher temperatures, the chains occupy a greater volume and, in order to compensate this additional volume, the cores tilt even further. Eventually, the smectic layers can no longer hold together and they break up, leading to the formation of a columnar phase (Figure 1.15). The transition from the SmC phase to the columnar phase normally takes place gradually (one or two compounds showing both phases) and is classically achieved via a cubic phase.

1.2.5 Metallomesogens

Metallomesogens are metal-containing liquid crystals and they are multifunctional molecular materials.[15-18] These interesting compounds have properties that are typical for both liquid crystals and d-group transition metals or rare earths. In the mesophase, the molecules of metallomesogens are ordered like in classic organic liquid crystals, and their optical, magnetic, electric, and mechanical properties are anisotropic. But at the same time, metallomesogens can have the redox activity or can exhibit the magnetic and optical properties of d-block or f-block metals. The metallomesogens will be further discussed in the introduction of chapter 4.

1.3 Mesophase characterization

Three techniques are commonly used to characterize a mesophase, namely hot-stage polarizing optical microscopy (POM), differential scanning calorimetry (DSC) and X-ray diffraction (XRD).

1.3.1 Polarizing optical microscopy

The use of polarizing optical microscopy for the identification of mesophases is based on the birefringence of a mesophase, which means that the mesophase has more than one refractive index. Figure 1.16 shows the experimental setup that is used to perform microscopy studies. The microscope is equipped with two polarizers; one is placed between the light source and the hot-stage and the other is localized between the hot-stage and the observer. The polarizers can be rotated, but are typically placed in a crossed configuration in which their polarization directions are perpendicular. In this way, only birefringent materials, like liquid crystals, can show an image to the observer as they are able to change the polarization direction of the incident light.

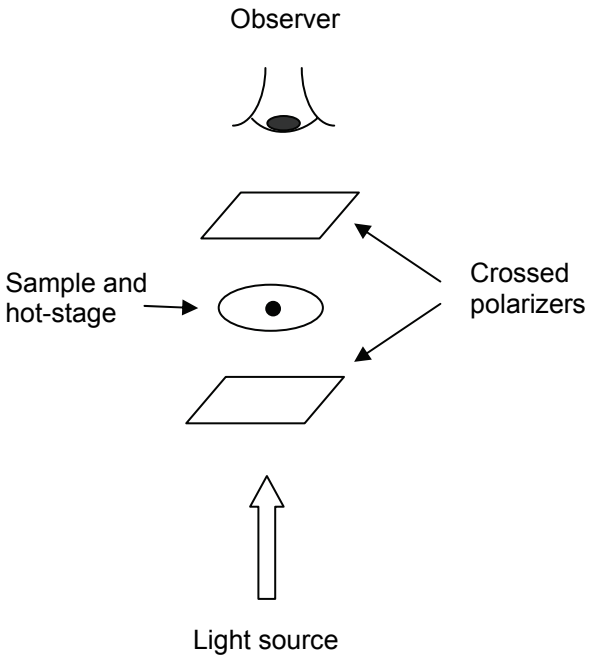


Figure 1.16: Experimental setup for polarizing optical microscopy.

Isotropic materials only possess one refractive index and cannot change the polarization direction of the incident light beam. Therefore, they appear black between crossed polarizers.

In a typical microscopy experiment, the mesomorphic compound is placed between two glass cover slips and positioned on the hot stage. When light passes through the mesophase, two refracted rays result and these interfere with one another to give characteristic interference patterns. These patterns are called *textures* (or *defect textures*), and they are diagnostic for a particular mesophase. The best textures can be obtained on cooling from the isotropic liquid.

1.3.2 Differential Scanning Calorimetry

Transitions between the solid phase and a mesophase, between mesophases or between a mesophase and the isotropic phase are accompanied by a change in enthalpy (and thus in entropy $\Delta S = \Delta H/T$). The magnitude of the enthalpy change is related to the amount of order that is lost during the transition. In a DSC experiment, the enthalpy change accompanying a phase transition is measured. There exist two types of DSC techniques: *power compensation* DSC and *heat flux* DSC. Only heat flux DSC will be discussed, because this technique was used for all the DSC experiments in this work.

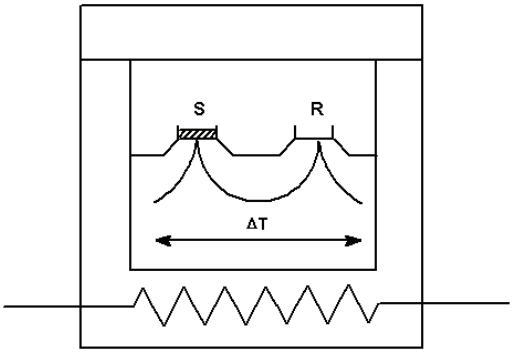


Figure 1.17: Heat flux DSC cell; S = sample, R = reference.

Heat flux DSC uses one furnace to heat both sample and reference (Figure 1.17). When the sample undergoes a phase transition, it will show a temperature lag compared to the reference. When the sample mass is known and the temperature lag can be measured very accurately, the energy of the transition (the enthalpy change) can be calculated. DSC provides information which cannot always be obtained from microscopy. Sometimes

a phase transition is accompanied with only a very small textural change, which might be overlooked by the observer. On the other hand, not all textural changes result from a phase change. Therefore, the DSC technique is strictly complementary to optical microscopy and the two should always be used together.

Liquid-crystalline materials can exhibit a rich variety of phases and phase transitions. Phase transitions can be first-order or second-order. A first-order phase transition is characterized by a discontinuous jump in the first derivative of the Gibbs free energy G. The enthalpy H, entropy S and volume V can all be defined by appropriate first derivatives of the Gibbs free energy and all change discontinuously at a first-order transition. A second-order phase transition is characterized by a continuous first derivative of the Gibbs free energy, but a discontinuous second derivative. In this case, the heat capacity C_p will exhibit a discontinuous jump. The experimental acquisition of high-quality $C_p(T)$ and/or $H(T)$ data is the first step in a calorimetric study of liquid crystals and their phase transitions. The second step is a theoretical analysis of these data in order to gain insight into the basic physical model that determines the thermal and other properties.
If the intermolecular interactions responsible for ordering in the system are sufficiently long-range, the system can be described by a Landau mean-field model. Mean-field models are approximations in which only the long-range aspects of enthalpy fluctuations are taken into account and the short-range fluctuations in the order are ignored. The order present in a system can be described by a so-called order parameter θ, which is zero in the disordered phase and non-zero in the ordered phase.

The Landau model assumes the Gibbs free energy G, to be analytic and a function of a long-range order parameter θ, given by:

$$G(\theta, T) = G_0(T) + \alpha(T)\theta + A(T)\theta^2 + B(T)\theta^3 + C(T)\theta^4 + \ldots \qquad (1.1)$$

where $G_0(T)$ is the Gibbs free energy of the disordered phase. It should be noted that θ is associated with a particular state of the system, the equilibrium value $<\theta>$ being defined by the minimum of the Gibbs free energy. The symmetry of the phases under consideration determines the number of non-zero terms in this expansion.

In reality, C_p is related to the behavior of short-range order rather than long-range order. Unfortunately, models taking short-range order parameter fluctuations into account are much more difficult to handle and analytical solutions are only available for some special cases. However, sophisticated renormalization group analyses have been carried out for several types of n vector order parameter models of which the three-dimensional cases are of particular relevance for liquid crystals. A more detailed treatment of theoretical analysis is beyond the scope of this thesis, but is given in references 1-5.

1.3.3 X-ray diffraction

X-ray diffraction is the best method for the characterization of mesophases. X-rays interact with the clouds of electrons, present in the mesophase and are scattered accordingly. The various scattered wavelets combine, undergoing constructive or destructive interference, following Bragg's law, which relates the angle of incidence θ of the X-ray beam with the wavelength λ (usually $\lambda = 1.5405$ Å) and the distance d between two atomic layers:

$$n\lambda = 2d\sin\theta \qquad (1.2)$$

The experimental setup is shown in Figure 1.18. A powder sample is placed in a glass capillary which can be heated. When X-rays are sent through the powder sample, diffraction occurs, resulting in a pattern of diffracted X-rays, which is collected by a detector.

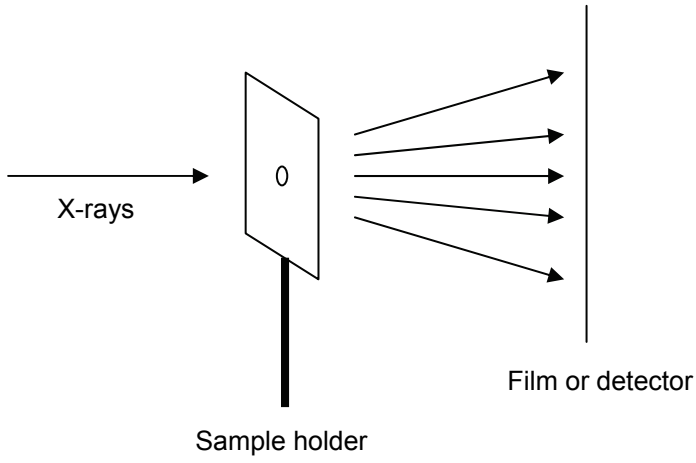


Figure 1.18: Experimental setup for XRD powder measurements.

The intensity I of the diffracted X-rays is measured as a function of the diffraction angle (2θ), leading to a diffraction pattern containing several diffraction peaks. The position of the diffraction peaks is related to a separation between layers of scattering atoms. The sharpness of the peaks is related to the extent to which these separations extend periodically over large distances. The intensity of diffraction peaks is related to the number of scattering atoms. Using this information (position, intensity and sharpness of diffraction peaks), the structure of the mesophase can be revealed.

1.4 References

1. Collings, P. J.; Hird, M., Eds.; *Introduction to Liquid Crystals*; Taylor and Francis: London, 1997.
2. Collings, P. J.; *Liquid Crystals: Nature's Delicate Phase of Matter*; IOP Publishing Ltd: Bristol, 1990.
3. Demus, D.; Goodby, J.; Gray, G. W.; Spiess, H.-W.; Vill, V., Eds.; *Handbook of Liquid Crystals*; Wiley-VCH: Weinheim, 1998.
4. Hamley, I. W.; *Introduction to Soft Matter*; John Wiley & Sons, Ltd: Chichester, 2000.
5. Kumar, S.; *Liquid Crystals: Experimental Study of Physical Properties and Phase Transitions*; University Press: Cambridge, 2001.
6. Goodby, J. W. *Liq Cryst.* **1998**, *24*, 25.
7. (a) Bruce, D. W.; Donnio, B.; Hudson, S. A.; Levelut, A.-M.; Megtert, S.; Petermann, D.; Veber, M. *J. Phys. II France* **1995**, *5*, 289. (b) Donnio, B.; Heinrich, B.; Allouchi, H.; Kain, J.; Diele, S.; Guillon, D.; Bruce, D. W. *J. Am. Chem. Soc.* **2004**, *126*, 15258. (c) Tschierske, C. *J. Mater. Chem.* **1998**, *8*, 1485.
8. Diele, S.; Göring, P. In: *Handbook of Liquid Crystals*; Demus, D.; Goodby, J.; Gray, G. W.; Spies, H.-W.; Vill, V., Eds.; Wiley-VCH: Weinheim, 1998; Volume 2B, Chapter XIII, pp 887-900.
9. Dantlgraber, G.; Eremin, A.; Diele, S.; Hauser, A.; Kresse, H.; Pelzl, G.; Tschierske, C. *Angew. Chem., Int. Ed.* **2002**, *41*, 2408.
10. Tschierske, C. *J. Mater. Chem.* **2001**, *11*, 2647.
11. Tschierske, C. *Curr. Opin. Colloid Interface S.* **2002**, *7*, 69.
12. Nguyen, H.-T.; Destrade, C.; Malthête, J. *Adv. Mater*. **1997**, *9*, 375.
13. Fazio, D.; Mongin, C.; Donnio, B.; Galerne, Y.; Guillon, D.; Bruce, D. W. *J. Mater. Chem.* **2001**, *11*, 2852.

14. Donnio, B.; Bruce, D. W. *J. Chem. Soc., Dalton Trans.* **1997**, 2745.
15. Bruce, D. W. In: *Inorganic Materials*, 2nd ed.; Bruce, D. W., O'Hare, D., Eds.; Wiley: Chichester, 1996; Chapter 8, pp 429-522.
16. Donnio, B.; Bruce, D. W. *Struct. Bonding* **1999**, *95*, pp 193-247.
17. Donnio, B.; Guillon, D.; Deschenaux, R.; Bruce, D. W. In: *Comprehensive Coordination Chemistry II*; McCleverty, J. A.; Meyer, T. J., Eds.; Elsevier: Oxford, 2003; Vol. 7, Chapter 7.9, pp 357-627.
18. Serrano, J. L., Ed.; *Metallomesogens: Synthesis, Properties and Applications*; VCH: Weinheim, 1996.

2.1 Introduction

The choice of ligand will determine which metals can be complexed, while complexation can result in specific properties. Oligopyridines, such as 2,2'-bipyridine (bipy) and 1,10-phenanthroline (phen), are very interesting in this point of view, because they form complexes with a wide variety of metals in different oxidation states, which when designed correctly, may exhibit potentially interesting luminescent properties (Figure 2.1).[1]



Figure 2.1: Structure of 2,2'-bipyridine (left) and 1,10-phenanthroline (right).

Bipyridine exists in the *transoid* state when uncomplexed and has no net electric dipole moment (Figure 2.2). On the other hand, the *cisoid* state occurs when coordinating a metal so that *N,N'*-coordination is possible (Figure 2.2). In the latter case, there is a lateral dipole moment of 3.5 D on the ligand.[2]

In contrast to 2,2'-bipyridine, 1,10-phenanthroline has a conformation fixed by the exocyclic double bond. 1,10-Phenanthroline has a permanent lateral dipole moment of 4.1 D and is ready set up for *N,N'*-coordination.[2]

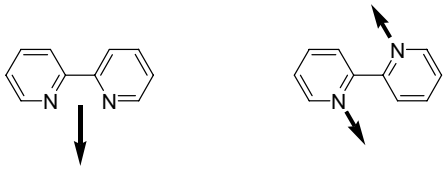


Figure 2.2: Local dipole moments in the cisoid (left) and transoid (right) conformation of 2,2'-bipyridine.

There exist several other isomeric phenanthrolines, depending on the position of the two nitrogens, for example 1,7-phenanthroline and 4,7-phenanthroline (Figure 2.3).



Figure 2.3: 1,7-phenanthroline (left) and 4,7-phenanthroline (right).

2.2 Liquid-crystalline phenanthrolines

The first 1,10-phenanthroline containing liquid crystals were reported by Bousquet and Bruce.[3] These were linear 3,8-disubstituted 1,10-phenanthrolines (Figure 2.4) in which an alkylated phenyl group was coupled to the phenanthroline unit via a single bond or a triple carbon-carbon bond.

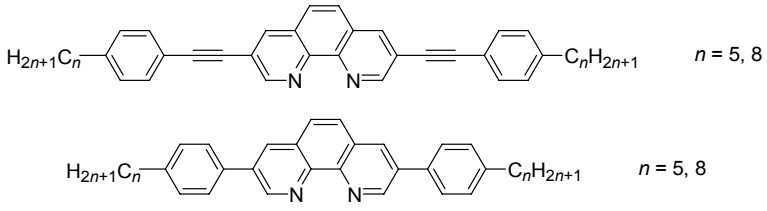


Figure 2.4: 3,8-Disubstituted 1,10-phenanthrolines reported by Bousquet and Bruce.[3]

The 3,8-disubstituted 1,10-phenanthrolines showed nematic and smectic phases, but the melting points (above 100 °C) and clearing points (approached 300 °C or decomposition occurred before clearing) were very high. Therefore methyl groups were introduced in the 2- and 9-positions (Figure 2.5), leading to a small drop in the clearing/decomposition temperatures. These compounds exhibited a nematic phase.

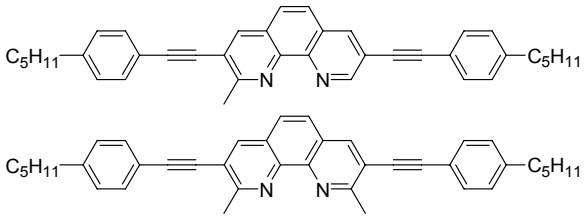


Figure 2.5: 3,8-Disubstituted 1,10-phenanthrolines with additional methyl groups in the 2- and 9-positions.

Also 3-monosubstituted 1,10-phenanthrolines were reported by Bousquet and Bruce, but did not show mesomorphism (Figure 2.6).[3]

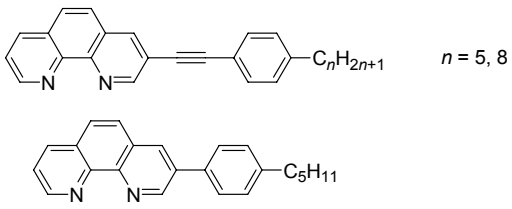


Figure 2.6: 3-Monosubstituted 1,10-phenanthrolines reported by Bousquet and Bruce.[3]

Related tetracatenar ligands and their corresponding rhenium(I) complexes were reported by Bruce and co-workers[4] and their structure is shown in Figure 2.7. The ligands showed nematic and smectic C phases at shorter chain lengths and a hexagonal columnar phase for longer-chain homologues. The rhenium(I) complexes were not mesomorphic at shorter chain lengths and the longer-chain homologues only showed hexagonal columnar phases, but with higher clearing points and a wider mesomorphic range than the corresponding ligands.

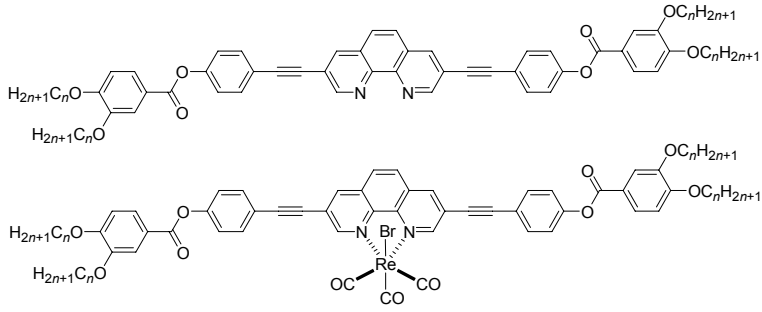


Figure 2.7: Tetracatenar 1,10-phenanthrolines and corresponding rhenium(I) complexes reported by Bruce and co-workers.[4]

Very recently, Ziessel and co-workers reported mesomorphic copper(I) complexes derived from non-symmetrical 1,10-phenanthrolines.[5] The structure of the ligands is shown in Figure 2.8. Figure 2.9 shows the structure of the corresponding copper(I) complexes. The ligands were liquid-crystalline only at longer chain lengths (n = 12, 16) and showed an unstable (n = 12) and a stable cubic phase (n = 16). The corresponding copper(I) complexes have a non-planar geometry and were mesomorphic only at longer chain lengths (n = 12, 16). They showed an oblique columnar phase (Col_o). The driving force for the organization in liquid-crystalline phases for both ligands and complexes is hydrogen bonding.

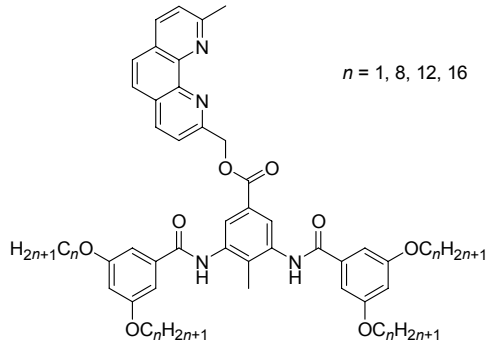


Figure 2.8: Structure of the non-symmetrical 1,10-phenanthrolines reported by Ziessel and co-workers.[5]

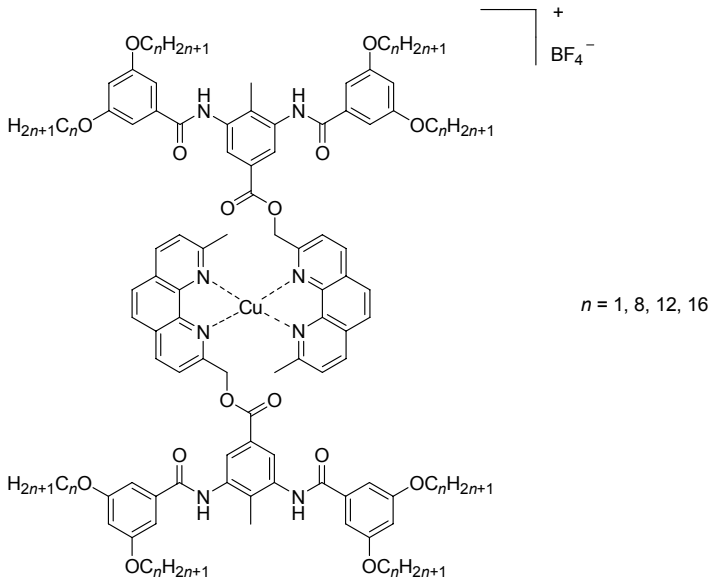


Figure 2.9: Structure of the copper(I) complexes of non-symmetrical 1,10-phenanthrolines reported by Ziessel and co-workers.[5]

2.3 References

1. (a) Sammes, P. G.; Yahioglu, G. *Chem. Soc. Rev.* **1994**, *23,* 327. (b) Hiort, C.; Lincoln, P.; Norden, B. *J. Am. Chem. Soc.* **1993**, *115,* 3448. (c) Hartshorn, R. M.; Barton, J. K. *J. Am. Chem. Soc.* **1992**, *114,* 5919. (d) Binnemans, K.; Lenaerts, P.; Driesen, K.; Görller-Walrand, C. *J. Mater. Chem.* **2004**, *14,* 191. (e) Bellusci, A.; Barberio, G.; Crispini, A.; Ghedini, M.; La Deda, M.; Pucci, D. *Inorg. Chem.* **2005**, *44,* 1818. (f) Bünzli, J. C. G.; Moret, E.; Foiret, V.; Schenk, K. J.; Wang, M. Z.; Jin, L. P. *J. Alloy. Compd.* **1994**, *207,* 107.
2. Fielding, P. E.; Le Fevre, R. J. W. *J. Chem. Soc.* **1951**, 1811.
3. Bousquet, S. J. P.; Bruce, D. W. *J. Mater. Chem.* **2001**, *11*, 1769.
4. (a) Date, R. W.; Iglesias, E. F.; Rowe, K. E.; Elliot, J. M.; Bruce, D. W. *Dalton Trans.* **2003**, 1914. (b) Smirnova, A. I.; Fazio, D.; Iglesias, E. F.; Hall, C. G.; Guillon, D.; Donnio, B.; Bruce, D. W. *Mol. Cryst. Liq. Cryst.* **2003**, *396*, 227.
5. Ziessel, R.; Pickaert, G.; Camerel, F.; Donnio, B.; Guillon, D.; Cesario, M.; Prangé, T. *J. Am. Chem. Soc*. **2004**, *126*, 12403.

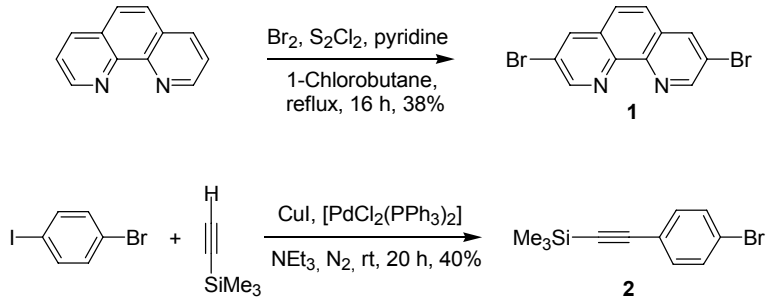
A tetracatenar liquid crystal based on 1,10-phenanthroline — Chapter 3

3.1 Introduction

The first 3,8-disubstituted 1,10-phenanthroline containing liquid crystals were reported by Bousquet and Bruce (see Chapter 2), and showed smectic and nematic phases.[1] Related tetracatenar ligands and their corresponding rhenium(I) complexes were reported to show a hexagonal columnar mesophase (see Chapter 2).[2] In this case, in order to develop a long aromatic core to counterbalance the bulky metallic fragment, ester linkages and triple bonds were used to connect the aromatic units. From a synthetic point of view, the connection of building blocks via ester bonds is straightforward, but the resulting liquid crystals have a limited chemical stability in basic and acidic conditions and have a reduced thermal stability. Therefore, to overcome these problems, we designed a rigid and chemically stable tetracatenar system with acetylenic linking groups. In this chapter, the synthesis, solid state structure and mesophase structure of a rigid tetracatenar compound based on the 1,10-phenanthroline core is presented.

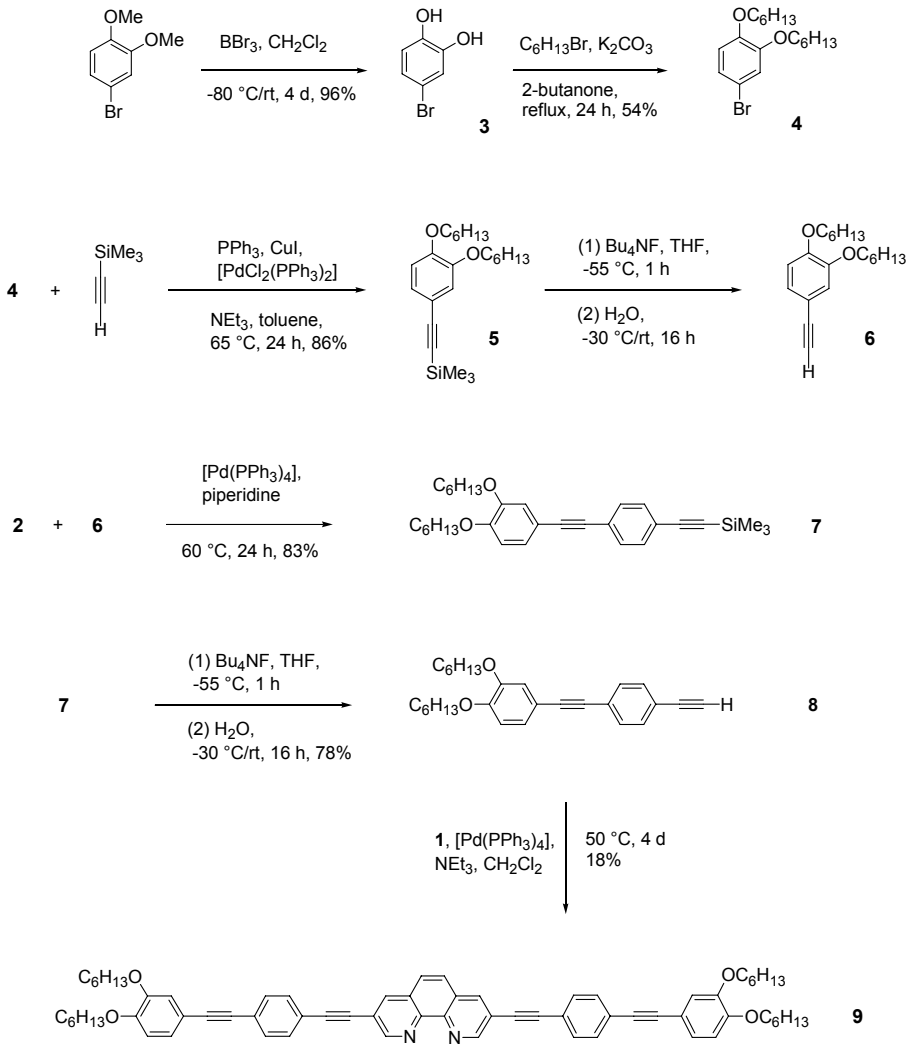
3.2 Synthesis

For the synthesis of phenanthroline **9**, a convergent methodology based on two successive Sonogashira couplings between appropriate aryl halides and phenyl acetylenes was developed.[3]



Scheme 3.1: Synthesis of precursors.

The central 3,8-dibromo-1,10-phenanthroline unit (**1**) is not available commercially and was synthesized according to a literature procedure described by Saitoh and co-workers[4] (scheme 3.1). For the two-chain component **8**, the synthesis started by conversion of 4-bromoveratrole into the corresponding catechol by reaction with BBr_3; *O*-alkylation then gave **4**. The first Sonogashira coupling between **4** and trimethylsilylacetylene gave **5**, which was transformed almost quantitatively into **6** with Bu_4NF. The precursor **2** was prepared via a palladium-catalyzed cross-coupling reaction between 1-bromo-4-iodobenzene and trimethylsilylacetylene using the differential reactivity of the iodo and bromo functions (scheme 3.1). Compound **6** and precursor **2** were then coupled via a second Sonogashira coupling to give **7**, which yielded acetylene **8** with Bu_4NF.



Scheme 3.2: Synthesis of the 1,10-phenanthroline-based ligand.

Finally, acetylene **8** and 3,8-dibromophenanthroline (**1**) were coupled via a third Sonogashira reaction to give **9** (Scheme 3.2). The purification of 9 was very tedious and could only be achieved by repeated preparative HPLC. The structure of the final compound **9** was confirmed by ^{1}H and ^{13}C NMR spectroscopy, elemental analysis, mass spectrometry and single-crystal X-ray analysis.

3.3 Results and discussion

3.3.1 X-ray single crystal structure

The X-ray single crystal structure of **9** (Figures 3.1 and 3.2) shows the non-planarity of the whole molecule in the solid state. The phenyl rings adjacent to the 1,10-phenanthroline ring are out of plane with the latter (dihedral angles are 25.1(1)° and 56.1(1)°, respectively and in turn, the outer phenyl rings are out of plane with respect to the phenyl rings (37.6(1)° and 45.3(2)°, respectively). The molecules are arranged in antiparallel pairs by an offset, intermolecular π-π-stacking (smallest distance between the centroids of two of the phenanthroline rings is 3.660(2) Å); only two rings of the phenanthroline moiety are involved in the stacking. Additionally, intermolecular, edge-to-face CH/π interactions (ca. 3.8 Å) are observed between phenyl rings next to the phenanthroline core. Interdimeric H-bonds (ca. 2.65 Å), resulting in a staircase arrangement of the pairs, help in the stabilization of the crystalline phase.

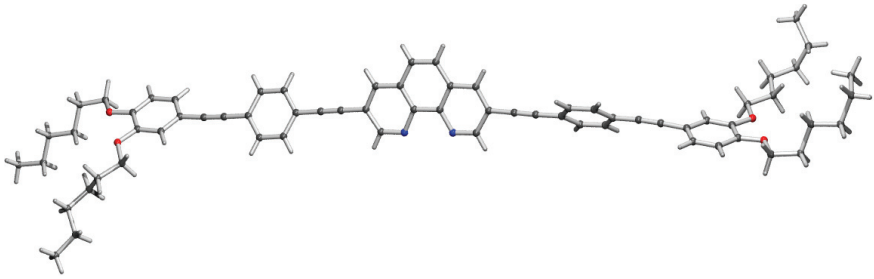


*Figure 3.1: Molecular structure of **9**, determined by single-crystal X-ray diffraction.*

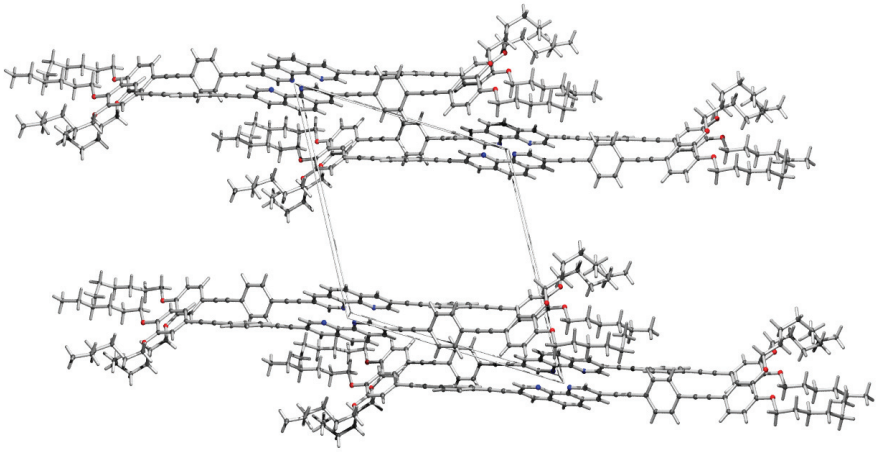


*Figure 3.2: Packing of molecules of **9** in the crystal structure.*

3.3.2 Thermal behavior

The thermal behavior of compound **9** was examined by polarizing optical microscopy, differential scanning calorimetry (DSC) and by small-angle X-ray diffraction on a powder sample and the following mesomorphism was elucidated:

Cr 158 (57.1) SmC 231 (1.1) I

Figure 3.3 shows the Schlieren and fingerprint textures of **9** between crossed polarizers, typical for a smectic C phase. This texture was obtained by placing the sample on a glass cover slip but without a glass cover slip on top of the sample. In Figure 3.4, the broken fan texture of the same compound can be seen, which was obtained by placing the sample between two glass cover slips.

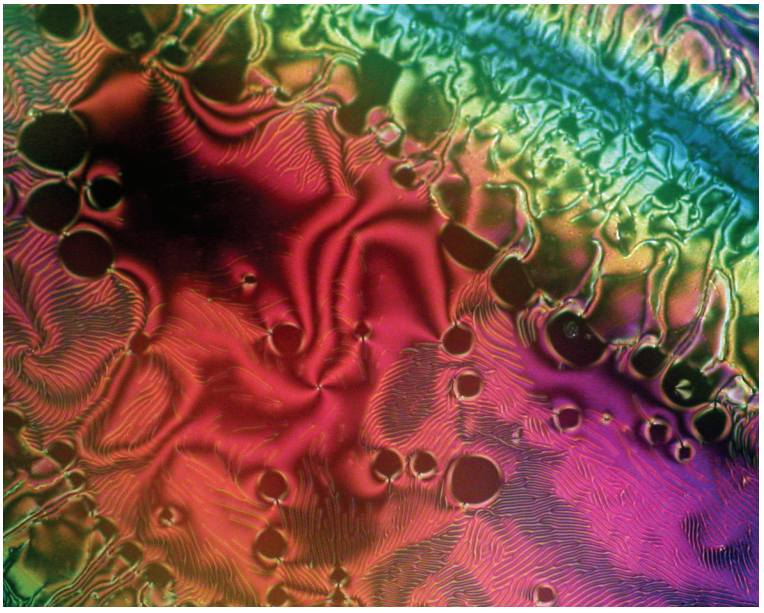


*Figure 3.3: Natural optical texture of the smectic C phase of **9** at 225 °C (200× magnification).*

The DSC profile of **9** contains an endothermic peak at 158 °C (ΔH = 57.1 kJ mol^{-1}) that corresponds to the melting point, and a small, endothermic peak at 231 °C (ΔH = 1.1 kJ mol^{-1}) that corresponds to the clearing point.

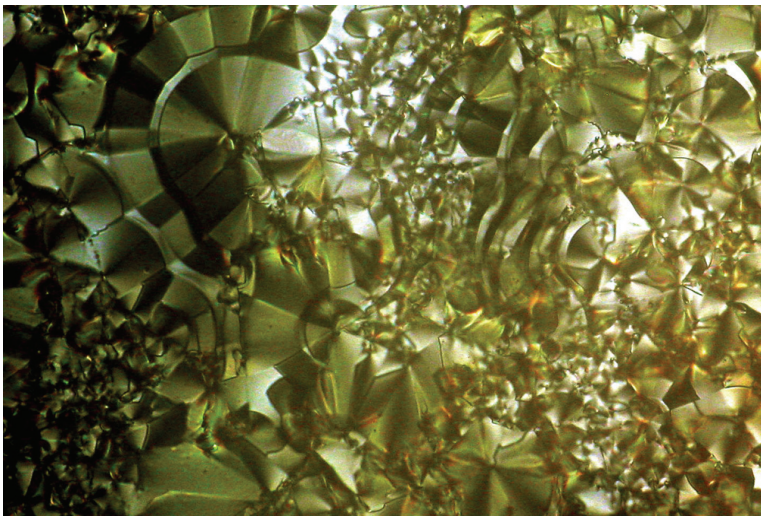


*Figure 3.4: Broken fan shape texture of **9** at 200 °C (200× magnification).*

Small-angle XRD confirmed the lamellar nature of the mesophase. At 200 °C, two sharp reflections in the spacing ratio 1:2 were observed in the small-angle part corresponding to the periodicities d = 32.0 Å and $d_{1/2}$ = 16.0 Å, and were indexed as the 001 and 002 reflections, respectively (Figure 3.5). In the wide-angle part, the diffuse halo characteristic of the molten chains in the liquid-like order, was observed at ca. 4.5 Å. Along with this broad scattering, another weak halo was seen at about 8.2 Å, which likely corresponds to the arrangement of the dimers, reminiscent of the crystalline phase.

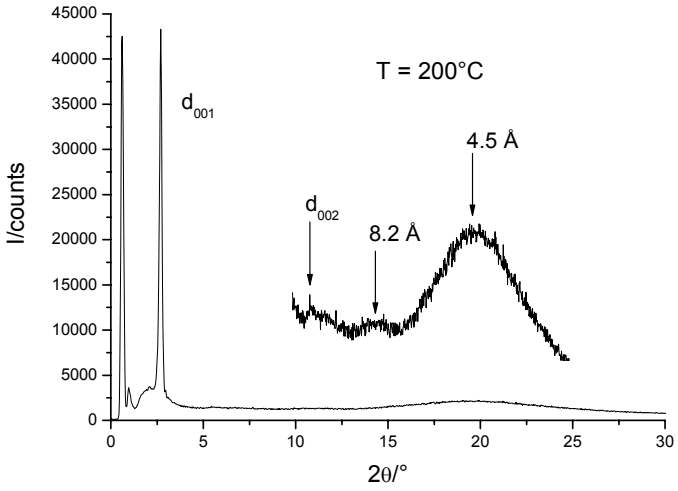


*Figure 3.5: X-Ray diffractogram of **9** in the smectic mesophase at 200 °C.*

According to a procedure described elsewhere,[5] it is possible to use the crystallographic data and the variation of the chain volume to express the molecular volume at 200 °C (in the mesophase) as a sum of contributing, partial volumes i.e. aromatic core (V_{ar}) and chains (V_{ch}), according to $V_{mol} = V_{ar} + V_{ch}$, where V_{ar} = 795 Å^3 and V_{ch} = 830 Å^3, so that V_{mol} = 1625 Å^3. The molecular area found in such a way ($A_{mol} = V_{mol}/d$ = 50.8 Å^2) and the area occupied by one aliphatic chain (a_{ch} = ½A$_{mol}$ = 25.4 Å^2) are perfectly consistent with the observation of a smectic C phase.[6] The large area occupied by the molten chains then allows compensation of the molecular tilt, φ, which can be estimated to be about 50° with respect to the layer normal ($\cos^{-1}\{32/50\} = \cos^{-1}\{d/l\}$). However, the molecular tilt contains contributions from the tilt of the rigid core and of the chains, which need not be the same.[7] In such cases, the tilt shown by the rigid core is often much

greater,[6,8] and we can obtain an estimate of it if we assume that volume fractions can be used to evaluate the thickness of each part in the layer, such that $f_{ar} = V_{ar}/V_{mol}$. This suggests an aromatic sub-layer 15.6 Å thick ($d_{ar} = f_{ar}d$), i.e. corresponding to a pronounced core tilt estimated at ca. 62°. This would leave aliphatic layers thicknesses of 16.4 Å (2 × 8.2 Å), effectively identical to the length of the chains in their most elongated conformation; such agreement is considered acceptable given the approach adopted. Such large tilts are expected in polycatenar systems due to the need to accommodate both the rigid core and the chains into a lamellar structure, as discussed elsewhere.[6,9] The tilt increases with increasing terminal chain length until the phase can no longer be considered as simply lamellar, and the mesomorphism changes to columnar, either directly,[10] *via* a lamellar columnar phase[9] or via a cubic phase.[11] Figure 3.6 shows a model for the molecules of compound **9** in the mesophase.

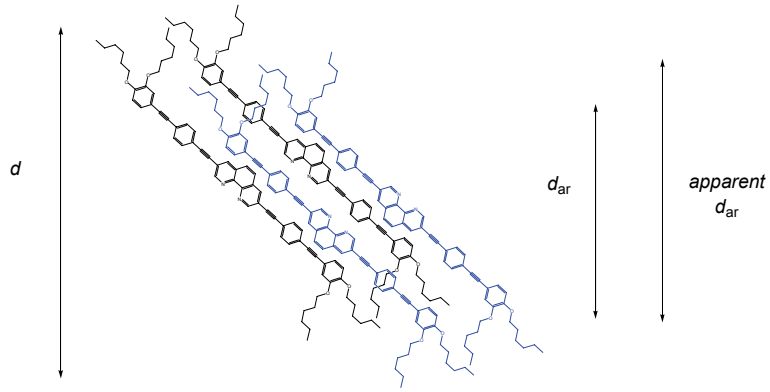


*Figure 3.6: Model of the molecules of **9** in the mesophase.*

3.4 Conclusions

A tetracatenar molecule was designed based on the 1,10-phenanthroline core and with acetylenic linking groups. The use of these acetylenic linking groups resulted in a molecule with a higher thermal stability than the corresponding molecules with an ester linking group. Moreover the molecule is much more rigid. The tetracatenar molecule exhibits a smectic C phase. Because of the tedious purification procedures, compound **9** could only be obtained in small quantities so far; enough for its full characterization, but not for the preparation of metal complexes.

3.5 Experimental section

Single-crystal X-ray diffraction was performed by Dr. Peter Nockemann, Kristof Van Hecke and Prof. Dr. Luc Van Meervelt. Characterization of the mesophase by X-ray diffraction and following discussion was performed by Dr. Bertrand Donnio and Dr. Daniel Guillon.

3.5.1 Techniques

The nuclear magnetic resonance (NMR) spectra were recorded on a Bruker Avance 300 spectrometer (operating at 300 MHz) or a Bruker AMX-400 (operating at 400 MHz). Elemental analyses were obtained on a CE Instruments EA-1110 elemental analyzer. Optical textures of the mesophases were observed with an Olympus BX60 polarizing microscope equipped with a LINKAM THMS600 hot stage and a LINKAM TMS93 programmable temperature-controller. DSC traces were recorded with a Mettler-Toledo DSC821e module. Preparative HPLC was performed on a Waters instrument, equipped with a 600 Controller, a 600E Multisolvent Delivery System and a 996 Photodiode Array Detector, using a Xterra MS

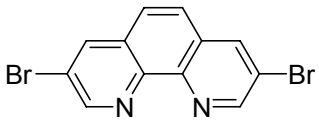
C18 30 mm x 100 mm column. Electrospray ionization (ESI) spectra were recorded on a Thermo Finnigan LCQ Advantage mass spectrometer. The XRD patterns were obtained with two different experimental setups. In all cases, a linear monochromatic Cu-Kα_1 beam (λ = 1.5405 Å) was obtained using a sealed-tube generator (900 W) equipped with a bent quartz monochromator. In the first setup, the transmission Guinier geometry was used, whereas a Debye-Scherrer-like geometry was used in the second experimental setup. In all cases, the crude powder was filled in Lindemann capillaries of 1 mm diameter. An initial set of diffraction patterns was recorded on an image plate; periodicities up to 80 Å can be measured, and the sample temperature controlled to within ± 0.3 °C. The second set of diffraction patterns was recorded with a curved Inel CPS 120 counter gas-filled detector linked to a data acquisition computer; periodicities up to 60 Å can be measured, and the sample temperature controlled to within ± 0.05 °C. In each case, exposure times were varied from 1 to 24 h.

Crystal data for compound **9**: crystals grown from dichloromethane, intensity data were collected on a SMART 6000 diffractometer equipped with CCD detector using Cu-Kα radiation (λ = 1.54178 Å). The images were interpreted and integrated with the program SAINT from Bruker,[12] $C_{68}H_{72}N_2O_4$, M = 981.28, triclinic, P-1, a = 10.3183(4), b = 17.5597(6), c = 17.9247(6) Å, α = 118.281(2), β = 100.373(2), γ = 94.895(2), V = 2758.18(18) Å^3, T = 100 K, Z = 2, D_c = 1.182 g cm^{-3}, μ(Cu-Kα) = 0.560 mm^{-1}, F(000) = 1052.0, crystal size 0.35 × 0.15 × 0.1 mm, 10058 independent reflections (R_{int} = 0.1203). Final R = 0.0796 for 4633 reflections with $I > 2\sigma(I)$ and $\omega R2$ = 0.2328 for all data. The structure was solved by direct methods and refined by full-matrix least-squares on F^2 using the SHELXTL program package.[13] Non-hydrogen atoms were refined anisotropically and the hydrogen atoms in the riding mode with isotropic temperature factors fixed at 1.2 times U(eq) of the parent atoms (1.5 times

for methyl groups). No solvent molecules were detected in the asymmetric unit. CCDC-269316 contains the supplementary crystallographic data for this compound and can be obtained from the Cambridge Crystallographic Data Centre, 12 Union Road, Cambridge CB2 1EZ, UK; fax: +44-1223-336033; or deposit@ccdc.cam.uk).

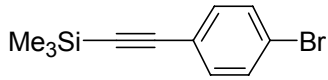
3.5.2 Synthesis

(a) 3,8-Dibromo-1,10-phenanthroline (1)



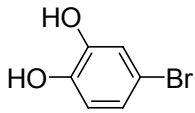
A stirred solution of 1-chlorobutane (200 ml) containing 1,10-phenanthroline (0.028 mol, 5.0 g), S_2Cl_2 (0.091 mol, 12.3 g), pyridine (0.090 mol, 7.1 g) and Br_2 (0.088 mol, 14.0 g) was heated under reflux for 16 h. After cooling to room temperature, the solid formed was separated and an aqueous solution of sodium hydroxide (excess) and chloroform (100 ml) was added. The organic layer was separated and washed with water. Then the organic layer was dried over $MgSO_4$ and the solvent was removed under reduced pressure. The crude product was purified on a silica column with chloroform/methanol (96:4) as the eluent to obtain a colorless solid. The product was crystallized from tetrachloroethylene (25 ml) and dried in a vacuum oven at 50 °C. Yield: 38% (3.6 g). δ_H (300 MHz, $CDCl_3$): 7.63 (s, 2H, H-aryl), 8.27 (s, 2H, H-aryl), 9.05 (s, 2H, H-aryl). Calcd. for $C_{12}H_6Br_2N_2 \cdot 0.25H_2O$: C 42.08, H 1.91, N 8.18. Found: C 42.01, H 1.47, N 8.00. M.p.: 281-283 °C (lit. m.p.: 270-273 °C[14]).

(b) 4-Trimethylsilylbromobenzene (2)



1-Bromo-4-iodobenzene (0.021 mol, 5.94 g), $[PdCl_2(PPh_3)_2]$ (0.00021 mol, 0.147 g) and copper(I) iodide (0.00021 mol, 0.040 g) were dissolved in a degassed solution of triethylamine (100 ml). After 20 minutes, trimethylsilylacetylene (0.025 mol, 2.46 g) was added and the mixture was stirred for 20 hours at room temperature. The solvent was evaporated to give a brown solid. The product was purified on a silica column with hexane as the eluent to obtain a white solid. Yield: 40% (2.15 g). δ_H (300 MHz, $CDCl_3$): 0.27 (s, 9H, CH_3), 7.35 (d, 2H, J_o = 8.5 Hz), 7.44 (d, 2H, J_o = 8.5 Hz). Calcd. for $C_{11}H_{13}BrSi$: C 52.18, H 5.17. Found: C 51.81, H 4.98. M.p.: 61-62 °C.

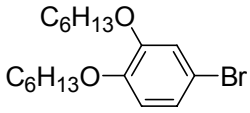
(c) 3,4-Dihydroxybromobenzene (3)



BBr_3 (0.084 mol, 84 ml of a 1 M solution in dichloromethane) was dissolved in dry dichloromethane (50 ml) at –80 °C. A solution of 4-bromoveratrole (0.026 mol, 5.64 g) in dry dichloromethane (50 ml) was added dropwise. The resulting mixture was allowed to warm slowly to room temperature and stirred under a nitrogen atmosphere for 4 d. Water (60 ml) was added and the reaction mixture was extracted using diethyl ether. The organic extract was washed several times with water, dried over $MgSO_4$ and the solvent was removed under reduced pressure. An oil was obtained and dried under

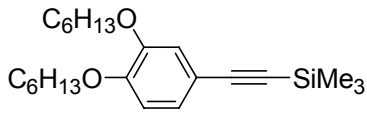
vacuum to give a gray compound. The crude product was used in the next synthesis step without further purification. Yield: 96% (4.74 g). δ_H (300 MHz, $CDCl_3$): δ = 5.53 (s, 1H, HO-aryl), 5.72 (s, 1H, HO-aryl), 6.66 (d, 1H, H-aryl, J_o = 8.5 Hz), 6.81 (dd, 1H, H-aryl, J_o = 8.5 Hz, J_m = 2.3 Hz), 6.92 (d, 1H, H-aryl, J_m = 2.3 Hz).

(d) 3,4-Dihexyloxybromobenzene (4)



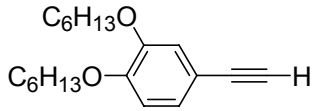
A mixture of 3,4-dihydroxybromobenzene **3** (0.016 mol, 3.02 g), 1-bromohexane (0.064 mol, 10.56 g) and potassium carbonate (0.090 mol, 12.44 g) in butanone (200 ml) was heated under reflux for 24 hours protected by a guard tube. The mixture was allowed to cool to room temperature and poured into water (350 ml). The organic layer was separated off and the aqueous layer extracted with chloroform. The combined organic layers were dried over anhydrous $MgSO_4$ and the solvent was removed under reduced pressure. The crude product was purified on a silica column with hexane/ethyl acetate (90:10) as the eluent to obtain a colorless oil. Yield: 54% (3.07 g). δ_H (300 MHz, $CDCl_3$): 0.83 (m, 6H, CH_3), 1.26–1.39 (m, 12H, CH_2), 1.72 (m, 4H, –C**H**$_2$–CH_2–O–), 3.88 (m, 4H, –C**H**$_2$–O–), 6.68 (d, 1H, H-aryl, J_o = 9.1 Hz), 6.90 (m, 2H, H-aryl). Calcd. for $C_{18}H_{29}BrO_2$: C 60.50, H 8.18. Found: C 60.84, H 8.67.

(e) 3,4-Di(hexyloxy)trimethylsilylphenylacetylene (5)



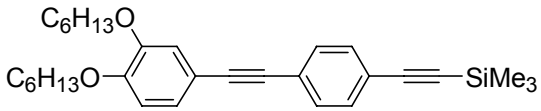
3,4-Dihexyloxybromobenzene **4** (0.018 mol, 6.43 g), CuI (0.18 mmol, 0.034 g), $[PdCl_2(PPh_3)_2]$ (0.18 mmol, 0.126 g) and triphenylphosphine (0.36 mmol, 0.094 g) were dissolved in triethylamine (65 ml) and toluene (40 ml) under a nitrogen atmosphere and stirred for 1 h. Trimethylsilylacetylene (0.036 mol, 3.54 g) was added and the mixture was heated to 65 °C and stirred for 24 hours. The solution was filtered off and the solvent evaporated to give a brown oil. The oil was dissolved in dichloromethane and washed with water and brine. The organic layer was dried over $MgSO_4$ and the solvent was removed under reduced pressure. The crude product was purified on a silica column with dichloromethane as the eluent to obtain a yellow oil. Yield: 86% (5.77 g). δ_H (300 MHz, $CDCl_3$): 0.26 (s, 9H, CH_3), 0.92 (t, 6H, CH_3), 1.35–1.48 (m, 12H, CH_2), 1.83 (m, 4H, –C**H**$_2$–CH_2–O–), 3.99 (m, 4H, –C**H**$_2$–O–), 6.80 (d, 1H, H-aryl, J_o = 8.3 Hz), 6.99 (d, 1H, H-aryl, J_m = 1.7 Hz), 7.03 (dd, 1H, H-aryl, J_o = 8.3 Hz, J_m = 1.7 Hz). Calcd. for $C_{23}H_{38}O_2Si{\cdot}0.25H_2O$: C 72.86, H 10.24. Found: C 72.75, H 10.23.

(f) 3,4-Dihexyloxyphenylacetylene (6)



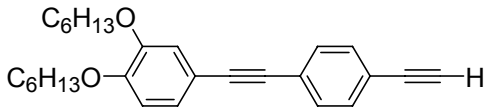
3,4-Di(hexyloxy)trimethylsilylphenylacetylene **5** (0.015 mol, 5.77 g) was dissolved in dry THF (100 ml) and the solution was cooled to –55 °C. Bu_4NF (0.026 mol, 26 ml of a 1 M solution in THF) was added and the reaction mixture was stirred for 1 hour. Then the solution was allowed to warm to –30 °C at which point water (100 ml) was added. The reaction mixture was allowed to warm up to room temperature and stirred for 16 hours under a nitrogen atmosphere. The solvent was evaporated and the resulting oil dissolved in dichloromethane and washed with water and brine. The organic layer was dried over $MgSO_4$ and the solvent was removed under reduced pressure. The crude product was purified on a silica column with dichloromethane as the eluent to obtain a yellow oil. Yield: 98% (4.44 g). δ_H (300 MHz, $CDCl_3$): 0.77 (t, 6H, CH_3), 1.20–1.33 (m, 12H, CH_2), 1.68 (m, 4H, –C**H**$_2$–CH_2–O–), 2.86 (s, 1H, –C≡C–H), 3.85 (m, 4H, –C**H**$_2$–O–), 6.67 (d, 1H, H-aryl, J_o = 8.3 Hz), 6.86 (d, 1H, H-aryl, J_m = 1.9 Hz), 6.91 (dd, 1H, H-aryl, J_o = 8.3 Hz, J_m = 1.9 Hz). Calcd. for $C_{20}H_{30}O_2 \cdot 0.5H_2O$: C 77.13, H 10.03. Found: C 77.29, H 10.35.

(g) Alkyne 7



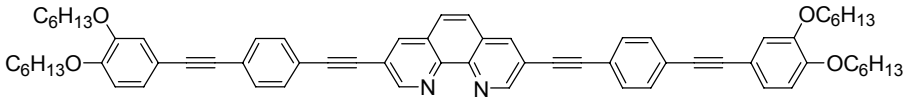
To a degassed solution of piperidine (40 ml) were added 4-trimethylsilylbromobenzene **2** (6.6 mmol, 1.67 g) and $[Pd(PPh_3)_4]$ (0.33 mmol, 0.38 g). The solution was flushed with nitrogen and stirred for 20 minutes. Then 3,4-dihexyloxyphenylacetylene **6** (13.2 mmol, 4.0 g) was added. The mixture was flushed with nitrogen and heated to 60 °C for 24 hours. The mixture was poured into a saturated aqueous solution of ammonium chloride and extracted with diethyl ether. The organic layer was washed with water and brine. The organic layer was then dried over $MgSO_4$ and the solvent was removed under reduced pressure. The crude product was purified on an alumina column with hexane/ethyl acetate (98:2) as the eluent to obtain a yellow solid. Yield: 83% (2.61 g). δ_H (300 MHz, $CDCl_3$): 0.27 (s, 9H, CH_3), 0.93 (m, 6H, CH_3), 1.36–1.49 (m, 12H, CH_2), 1.85 (m, 4H, –C**H**$_2$–CH_2–O–), 4.02 (m, 4H, –C**H**$_2$–O–), 6.86 (d, 1H, H-aryl, J_o = 8.3 Hz), 7.05 (d, 1H, H-aryl, J_m = 2.1 Hz), 7.09 (dd, 1H, H-aryl, J_o = 8.3 Hz, J_m = 2.1 Hz), 7.45 (s, 4H, H-aryl). Calcd. for $C_{31}H_{42}O_2Si$: C 78.43, H 8.92. Found: C 77.94, H 9.37. M.p.: 53-56 °C.

(h) Alkyne 8



Compound **7** (5.5 mmol, 2.61 g) was dissolved in dry THF (50 ml) and the solution was cooled to –55 °C. Bu_4NF (13.75 mmol, 13.75 ml of a 1 M solution in THF) was added and the reaction mixture was stirred for 1 hour. Then the solution was allowed to warm up to –30 °C at which point water was added (50 ml). The reaction mixture was allowed to warm up to room temperature and stirred for 16 hours under a nitrogen atmosphere. The solvent was evaporated and the resulting solid dissolved in dichloromethane and washed with water and brine. The organic layer was dried over $MgSO_4$ and the solvent was removed under reduced pressure. The crude product was purified on an alumina column with hexane/ethyl acetate (97:3) as the eluent to obtain a colorless solid. Yield: 78% (1.73 g). δ_H (300 MHz, $CDCl_3$): 0.84 (m, 6H, CH_3), 1.27–1.40 (m, 12H, CH_2), 1.76 (m, 4H, –C**H**$_2$–CH_2–O–), 3.09 (s, 1H, –C≡C–H), 3.94 (m, 4H, –C**H**$_2$–O–), 6.77 (d, 1H, H-aryl, J_o = 8.3 Hz), 6.96 (d, 1H, H-aryl, J_m = 1.7 Hz), 7.00 (dd, 1H, H-aryl, J_o = 8.3 Hz, J_m = 1.7 Hz), 7.38 (s, 4H, H-aryl). Calcd. for $C_{28}H_{34}O_2$: C 83.54, H 8.51. Found: C 83.16, H 8.92. M.p.: 71-72 °C.

(i) Tetracatenar Phenanthroline 9



To a degassed solution of dichloromethane (10 ml) and triethylamine (4 ml) were added 3,8-dibromo-1,10-phenanthroline **1** (0.41 mmol, 0.14 g) and [$Pd(PPh_3)_4$] (0.025 mmol, 0.028 g). The solution was flushed with nitrogen and stirred for 20 minutes. Then acetylene **8** (1.24 mmol, 0.5 g) was added. The mixture was flushed with nitrogen and heated to 50 °C for 4 days. The solvent was evaporated and the resulting product dissolved in chloroform. The organic layer was washed with water and brine. The organic layer was then dried over $MgSO_4$ and the solvent was removed under reduced pressure. The crude product was purified by preparative HPLC using a reversed phase column with THF/H_2O (75:25) as the eluent to obtain a yellow solid. Yield: 18% (0.074 g). δ_H (400 MHz, $CDCl_3$): 0.91 (m, 12H, CH_3), 1.25–1.48 (m, 24H, CH_2), 1.83 (m, 8H, –C**H**$_2$–CH_2–O–), 4.01 (m, 8H, –C**H**$_2$–O–), 6.84 (d, 2H, H-aryl, J_o = 8.2 Hz), 7.05 (s, 2H, H-aryl), 7.09 (d, 1H, H-aryl, J_o = 8.2 Hz), 7.53 (m, 8H, H-aryl), 7.79 (b, s, 2H, H-aryl), 8.35 (b, s, 2H, H-aryl), 9.27 (b, s, 2H, H-aryl). δ_C (100 MHz, $CDCl_3$): 13.97 (CH_3), 22.58 (CH_2), 25.66 (CH_2), 25.68 (CH_2), 29.17 (CH_2), 29.21 (CH_2), 31.56 (CH_2), 69.20 (CH_2), 69.35 (CH_2), 87.46 (C), 88.03 (C), 92.28 (C), 93.92 (C), 113.36 (CH), 114.97 (C), 116.81 (CH), 121.70 (C), 124.38 (C), 125.15 (CH), 126.93 (CH), 131.48 (CH), 131.73 (CH), 137.98 (CH), 148.86 (C), 150.09 (C). Calcd. for $C_{68}H_{72}N_2O_4 \cdot H_2O$: C 81.73, H 7.46, N 2.80. Found: C 82.18, H 7.10, N 2.45. ESI-MS (Acetonitrile, m/z): 981.6, $[M + H]^+$.

3.6 References

1. Bousquet, S. J. P.; Bruce, D. W. *J. Mater. Chem.* **2001**, *11*, 1769.
2. Date, R. W.; Iglesias, E. F.; Rowe, K. E.; Elliot, J. M.; Bruce, D. W. *Dalton Trans.* **2003**, 1914.
3. (a) Sonogashira, K.; Tohda, Y.; Hagihara, N. *Tetrahedron Lett.* **1975**, *50*, 4467. (b) Sonogashira, K. *J. Organomet. Chem.* **2002**, *653*, 46.
4. Saitoh, Y.; Koizumi, T.-A.; Osakada, K.; Yamamoto, T. *Can. J. Chem*. **1997**, *75*, 1336.
5. Donnio, B.; Heinrich, B.; Allouchi, H.; Kain, J.; Diele, S.; Guillon, D.; Bruce, D. W. *J. Am. Chem. Soc*. **2004**, *126*, 15258.
6. Guillon, D.; Heinrich, B.; Ribeiro, A. C.; Cruz, C.; Nguyen, H.-T. *Mol. Cryst. Liq. Cryst.* **1998**, *317*, 51.
7. Bartolino, R.; Doucet, J.; Durand, G. *Ann. Phys*. **1978**, *3*, 389.
8. Allouchi, H.; Cotrait, M.; Guillon, D.; Heinrich, B.; Nguyen, H.-T. *Chem. Mater*. **1995**, *7*, 2252.
9. Fazio, D.; Mongin, C.; Donnio, B.; Galerne, Y.; Guillon, D.; Bruce, D. W. *J. Mater. Chem.* **2001**, *11*, 2852.
10. Date, R. W.; Iglesias, E. F.; Rowe, K. E.; Elliot, J. M.; Bruce, D. W. *Dalton Trans.* **2003**, 1914.
11. Rowe, K. E.; Bruce, D. W. *J. Mater. Chem.* **1998**, *8*, 331.
12. SAINT, Bruker Analytical X-ray Systems Inc., Madison, WI, manual ver. 5/6.0, 1997.
13. SHELXTL-PC, Bruker Analytical X-ray Systems Inc., Madison, WI, manual ver. 5.1, 1997.
14. Tzalis, D.; Tor, Y.; Failla, S.; Siegel, J. S. *Tetrahedron Lett.* **1995**, *36*, 3489.

Design of high coordination number metallomesogens by decoupling of the complex-forming and mesogenic groups

Chapter 4

4.1 Introduction

The first metallomesogens were designed in such a way that they mimicked the shape of rodlike (calamitic) organic liquid crystals. To exhibit a mesophase, the shape anisotropy of the complex must be sufficient. The choice of the metal ion was restricted previously to those ions that are able to form complexes with a linear or a square planar coordination. Therefore, many of the earlier described metallomesogens contain rhodium(I), iridium(I), nickel(II), copper(II), palladium(II), platinum(II), or silver(I) as the central metal ion. It is a challenge to design metallomesogens with coordination geometries other than linear or square planar ones. Only few metallomesogens have a tetrahedral metal center, because a tetrahedral coordination geometry is difficult to combine with the requirement of structural anisotropy and good lateral interactions for mesophase formation.[1] Due to the stronger geometrical constraints, it is even more difficult to obtain metallomesogens with a coordination number of six or even higher.[2] The first metallomesogens with an octahedral coordination sphere were the 1,4,7-triazacyclononane tricarbonyl and trichloro metal complexes ([$ML(CO)_3$], with M = W, Cr, and Mo, and [$FeCl_3L$]) described by Lattermann and co-workers (Figure 4.1).[3] Bruce and co-workers prepared the first octahedral metallomesogens with a calamitic shape (Figure 4.2).[4] Ghedini and co-workers described octahedral platinum(IV) complexes (Figure 4.3).[5] Binnemans, Bruce, Galyametdinov and co-workers

described rare-earth-containing liquid crystals, which have a coordination number of eight or nine Figure 4.4).[6]

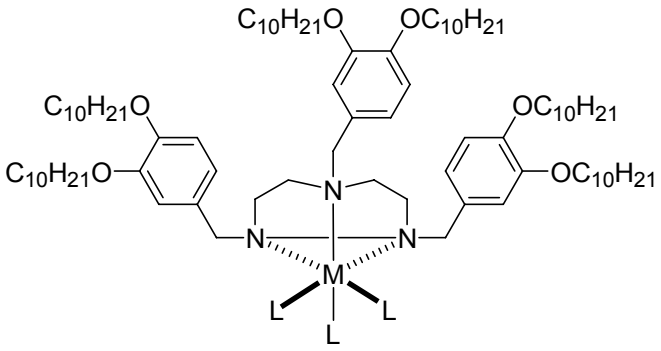


Figure 4.1: 1,4,7-Triazacyclononane tricarbonyl and trichloro metal complexes described by Lattermann and co-workers (M = W, Cr, Mo and L = CO; M = Fe and L = Cl).[3]

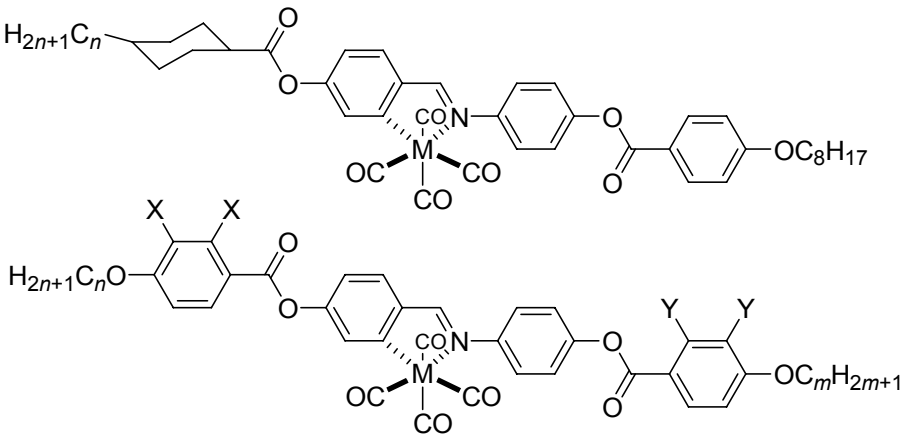


Figure 4.2: The first octahedral metallomesogens with a calamitic shape prepared by Bruce and co-workers (M = Re(I), Mn(I); X, Y = H or F).[4]

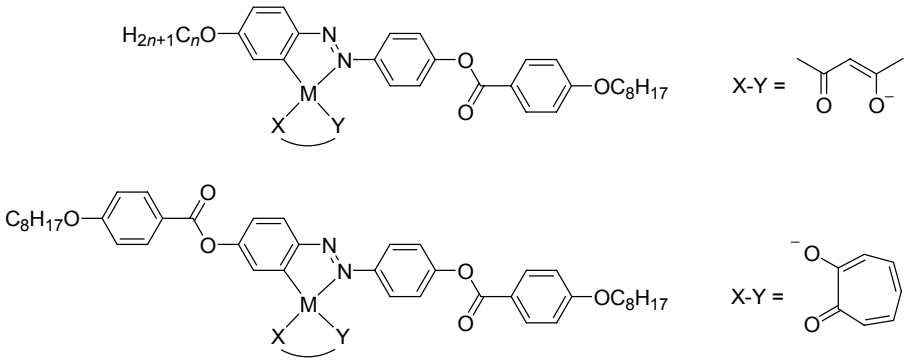


Figure 4.3: Octahedral platinum(IV) complexes described by Ghedini and co-workers (M = PtI_2, PtIMe).[5]

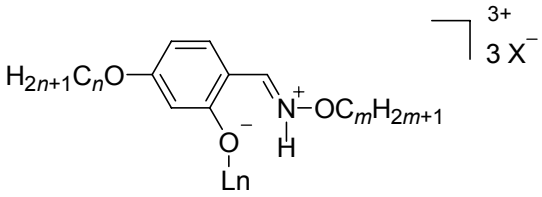


Figure 4.4: Rare-earth-containing liquid crystals described by Binnemans, Bruce, Galyametdinov and co-workers (X = NO_3^-, Cl^-, DOS, alkylsulfate).[6]

Other types of rare-earth-containing liquid crystals have then been studied by the research groups of Piguet and Bünzli,[7] and Serrano.[8] Swager made mesomorphic β-diketonate complexes with an octahedral (Figure 4.5),[9] and with a square antiprismatic (Figure 4.6) coordination.[10] Also ferrocene-containing liquid crystals are examples of high coordination number metallomesogens.[11] A popular approach to overcome the disturbance of the rodlike shape of the ligands after complex formation with a bulky transition metal fragment, is to increase the number of phenyl groups in order to increase the anisotropy of the ligands.[12] Inevitably, this will lead to higher transition temperatures and to a lower thermal stability of the metal complexes.

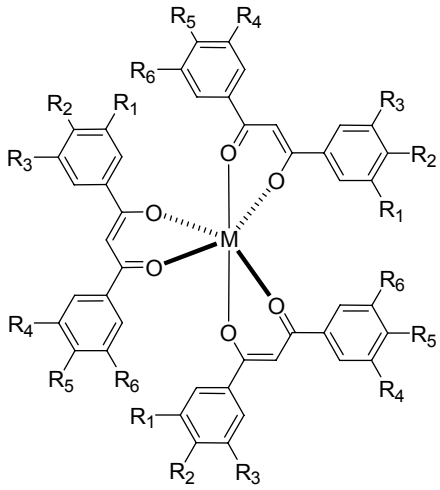


Figure 4.5: β-Diketonate complexes with an octahedral coordination described by Swager (M = Fe(III), Co(III), Mn(III), Cr(III); R_1, R_2, R_3, R_4, R_5, R_6 = alkoxy chain or H).[9]

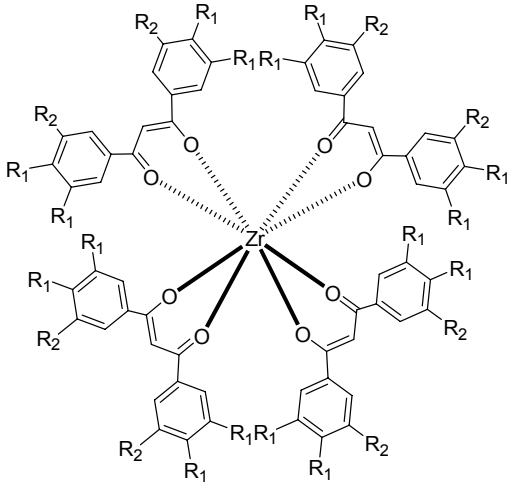


Figure 4.6: β-Diketonate complexes with a square antiprismatic coordination described by Swager ($R_1 = R_2 = OC_nH_{2n+1}$; $R_1 = OC_8H_{17}$, R_2 = H; $R_1 = R_2 = R–/S–O(CH_2)_2C^*HMe(CH_2)_3CHMe_2$).[10]

One can also increase the number of alkyl chains attached to the coordination unit, but in this case the metal complexes exhibit columnar mesophases as a rule.[9,10] It is evident that alternative approaches to obtain high coordination number metallomesogens with nematic or smectic mesophases are a scientific challenge, especially when these compounds ought to have low or moderate transition temperatures. As far as this matter is concerned, particularly the work of Deschenaux and co-workers is inspiring, because they found methods to obtain liquid-crystalline C_{60} fullerenes,[13] the bulky fullerene being incompatible with the requirements for structural anisotropy. Typically, classical mesogenic groups such as cholesteryl or cyanobiphenyl groups are linked to the fullerene moiety by long flexible chains. Saez and co-workers were able to prepare liquid-crystalline clusters on the basis of octasilsesquioxane by using a similar strategy.[14]

In this chapter, we describe the design of high coordination number metallomesogens, which exhibit nematic or lamellar columnar phases. The basic idea is to decouple the mesogenic groups from the metal-coordinating group by a flexible spacer. In this way, the system resembles to a covalent host-guest system where the metal complex (the guest) is dissolved in the liquid-crystal host, but phase separation is prevented by covalently linking the metal complex to the mesogenic moiety. This approach is illustrated for rhenium(I) and rare-earth complexes of 2-arylimidazo[4,5-f]-1,10-phenanthroline derivatives. The ligand is bearing one, two, or three cyanobiphenyl groups separated from the coordinating core by long alkyl chains. The rhenium(I) compounds are six-coordinate metallomesogens, and the rare-earth complexes are eight-coordinate systems. The influence of the number of mesogenic groups and of the nature of the metal ion on the mesomorphic properties of the complexes are investigated. The rare-earth complexes are not only luminescent themselves, but they are also

completely soluble in the liquid crystal 4'-pentyl-4-cyanobiphenyl (5CB). This allows obtaining strongly luminescent liquid-crystal mixtures.

4.2 Synthesis

The inspiration to develop the materials presented in this chapter came from previous work on liquid-crystalline rare-earth complexes with β-diketonate ligands. Mesomorphism was observed in adducts of long-chain salicylaldimine Schiff bases with tris(dibenzoylmethanato)lanthanide(III) complexes.[6e,15] Similarly, highly ordered smectic mesophases were found in complexes of rare earths with mesogenic β-diketonates.[16] Mesomorphic analogues of the tris(2-thenoyltrifluoroacetonato)(1,10-phenanthroline) lanthanide(III) complexes, $[Ln(tta)_3(phen)]$ were synthesized, because of the good luminescence performance of these complexes. For instance, the europium(III) complex $[Eu(tta)_3(phen)]$ is one of the best known red-emitting molecular luminescent materials (Htta = 2-thenoyltrifluoroacetone or 4,4,4-trifluoro-1-(thiophen-2-yl)butane-1,3-dione).[17] The complexes $[Nd(tta)_3(phen)]$, $[Er(tta)_3(phen)]$, and $[Yb(tta)_3(phen)]$ emit in the near-infrared region of the electromagnetic spectrum. Taking into account the structure of the 2-thenoyltrifluoroacetonate ligand, it is difficult to induce mesomorphism in the $[Ln(tta)_3(phen)]$ complexes by modification of the β-diketonate ligand. Therefore, modification has to be made by functionalization of the 1,10-phenanthroline moiety. The most reactive positions in 1,10-phenanthroline are the 5- and 6-positions. The first trials we made was by using 5-amino-1,10-phenanthroline. This molecule was previously used to attach $[Eu(tta)_3(phen)]$ to a sol-gel silica matrix,[18] or to a Merrifield resin.[19] However, the low solubility in common organic solvents and the low photochemical stability of 5-amino-1,10-phenanthroline, renders its chemistry rather difficult and impractical. In contrast, 1,10-

phenanthroline-5,6-dione is a more convenient starting product. 1,10-Phenanthroline is oxidized to 1,10-phenanthroline-5,6-dione according to a method described by Hiort et al.,[20] followed by the transformation of the dione to the 2-arylimidazo[4,5-f]1,10-phenanthrolines by reaction with a substituted benzaldehyde and ammonium acetate in hot glacial acetic acid. The synthetic route is similar to the method of Steck and Day for the preparation of 2-substituted phenanthrimidazoles.[21] By choosing different substituents on the benzaldehyde, the structure and thus the mesophase behavior of the corresponding ligands and metal complexes can in principle be tuned. Although a single compound can be transformed into a mesogenic analogue by attaching for example long alkyl chains, we have selected another methodology, namely by attaching mesogenic groups via a long alkyl chain to the 1,10-phenanthroline derivative. The mesogenic group in this case is a cyanobiphenyl group, linked to the alkyl chain by an ether linkage group. In this respect, 4'-hydroxy-4-biphenylcarbonitrile is a very useful mesogenic building block to design large liquid-crystalline compounds. We have chosen a flexible alkyl chain with eleven carbon atoms. Although different approaches are possible, we coupled 4'-hydroxy-4-biphenylcarbonitrile and 11-bromo-undecanol via the OH group by a Mitsunobu reaction,[22] so that the unit consisting of the flexible chain and the mesogenic group can be coupled to a hydroxybenzaldehyde by a classic Williamson ether reaction. For the Mitsunobu reaction, diisopropyl azodicarboxylate (DIAD) was preferred to diethyl azodicarboxylate (DEAD) as the reagent, because DIAD is more convenient and safer to use. The mesomorphic properties of 4'-(10-bromoundecyloxy)-4-cyanobiphenyl (**11**) have been described by other authors in the past.[23] Three different hydroxybenzaldehydes were used in this study: 4-hydroxybenzaldehyde, 3,4-dihydroxybenzaldehyde and 3,4,5-trihydroxybenzaldehyde. Depending on the hydroxybenzaldehyde used, one, two, or three mesogenic groups

could be coupled via a flexible chain to the substituted 1,10-phenanthroline. An overview of the benzaldehyde precursors and ligands is given in Figure 4.7 and Figure 4.8, respectively. The synthesis of ligand $\mathbf{L_I}$ is described in Scheme 4.1. The other ligands $\mathbf{L_{II}}$ and $\mathbf{L_{III}}$ were prepared by following a similar method starting from 3,4-dihydroxybenzaldehyde and from 3,4,5-trihydroxybenzaldehyde, respectively.

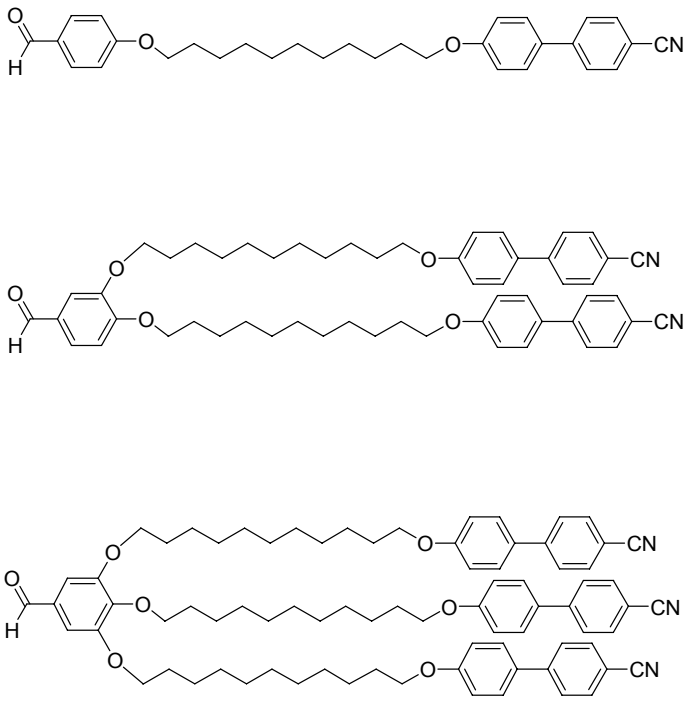


Figure 4.7: Overview of benzaldehyde precursors.

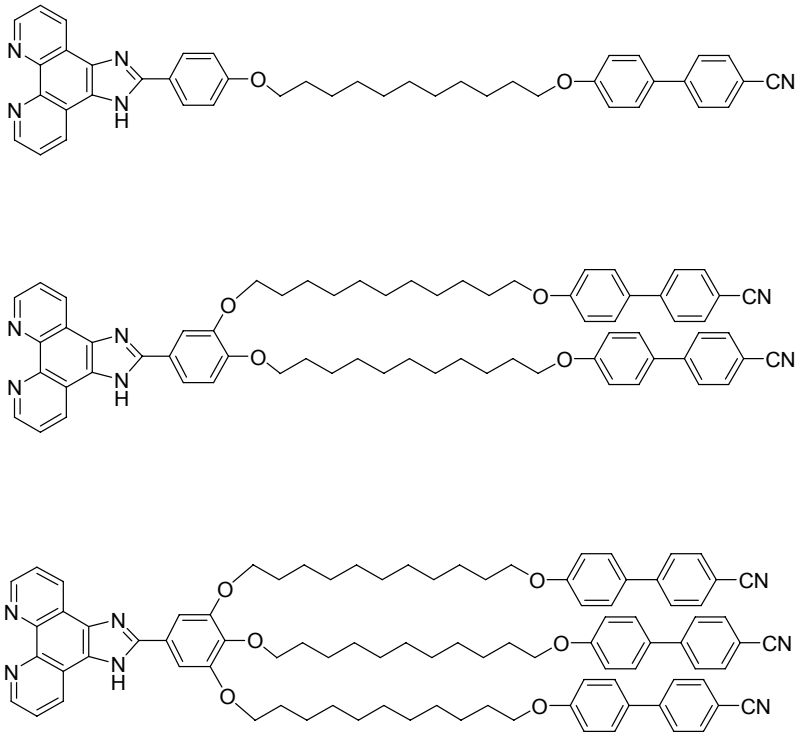
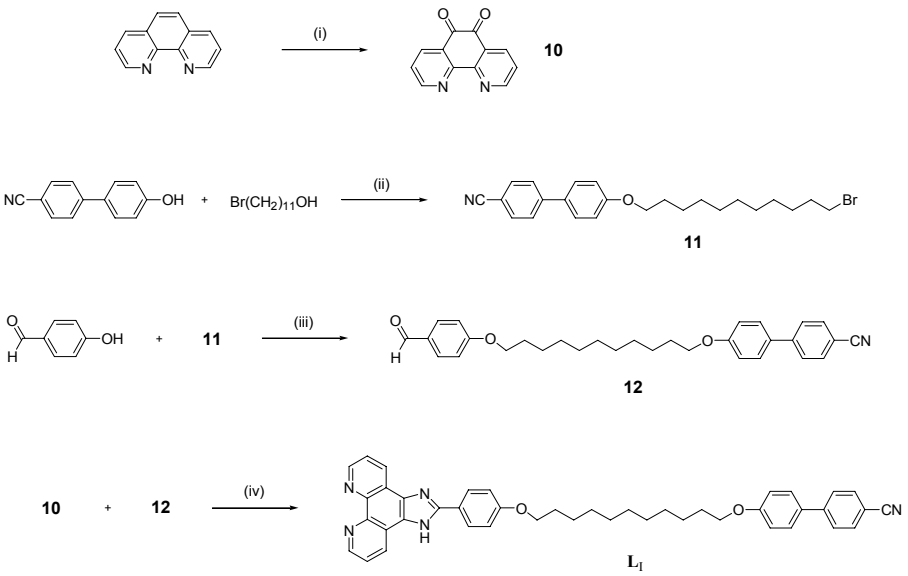


Figure 4.8: Overview of the imidazo[4,5-f]1,10-phenanthroline ligands.

A crystal structure of the methanol adduct of 2-phenylimidazo[4,5-f]-1,10-phenanthroline showed that all the 19 carbon atoms and the 4 nitrogen atoms are coplanar,[24] so it is very likely that the core of our phenanthroline derivatives is flat as well. From the analysis of the bound lengths, it was concluded that the molecule is very extensively conjugated. The 2-arylimidazo[4,5-f]-1,10-phenanthrolines have a tendency to form strong H-bonded adducts with methanol or other lower alcohols. For this reason, it is preferable to exclude these solvents from the synthetic procedure if one wants to obtain solvent-free 2-arylimidazo[4,5-f]-1,10-phenanthrolines.



Scheme 4.1: Synthesis of ligand $\mathbf{L_I}$*. Experimental conditions: (i)* H_2SO_4/HNO_3*, NaBr; (ii)* PPh_3*, DIAD, THF; (iii)* K_2CO_3*/KI, 2-butanone; (iv)* NH_4OAc*, HOAc.*

Complexes of rhenium(I) and of trivalent rare-earth ions were prepared from the different 2-arylimidazo[4,5-f]-1,10-phenanthroline ligands. Rhenium(I) was chosen rather than group 10 metals since they tend to give more thermally and chemically stable complexes with ligands derived from 2,2'-bipyridine and 1,10-phenanthroline and since mesophases could be observed for these complexes as found by Bruce and co-workers.[25,12b,12c] Another interesting feature is that the rhenium(I) complexes containing the bulky [$ReBr(CO)_3$] fragment have an large dipole moment due to the polar Re-Br bond. This dipole, in combination with the number of 4-cyanobiphenyl groups attached, is expected to influence the arrangement of

the molecules in the mesophase and the solid phase. The trivalent rare-earth ions were selected in such a way that the steady decrease of the ionic radius over the lanthanide series (*lanthanide contraction*) was reflected; indeed, the decrease of the ionic radius often influences the thermal properties of the compounds.[26] Moreover, the choice of rare-earth ions was also determined by the physical properties of the ions: lanthanum(III) and yttrium(III) compounds are diamagnetic, so that they can be conveniently studied by NMR techniques. The neodymium(III), samarium(III), europium(III), erbium(III), and ytterbium(III) ions were chosen because of their photoluminescent properties.

Rhenium(I), yttrium(III), lanthanum(III), neodymium(III), samarium(III), europium(III), erbium(III), and ytterbium(III) complexes of ligands $\mathbf{L_I}$, $\mathbf{L_{II}}$, and $\mathbf{L_{III}}$ were therefore prepared. The rhenium(I) complexes were obtained by reaction between the ligand and rhenium(I) pentacarbonyl bromide in toluene (molar ratio 1:1). The rare-earth complexes were prepared by reaction of the ligand and a tris(2-thenoyltrifluoroacetonate)lanthanide dihydrate complex, $[Ln(tta)_3(H_2O)_2]$ (Ln = Y, La, Nd, Sm, Eu, Er, Yb), in chloroform (molar ratio 1:1). The complexes were characterized by CHN elemental analysis, by IR spectroscopy, and by electrospray mass spectrometry (ESI-MS). The structures of complexes $[ReBr(CO)_3\mathbf{L_{II}}]$ and $[Ln(tta)_3\mathbf{L_{II}}]$ (Ln = Y, La, Nd, Sm, Eu, Er, Yb) are shown in Figures 4.9 and 4.10, respectively. It should be mentioned that all the ligands and metal complexes were obtained as monohydrates. The bonded water molecule could not be removed, even not after a long drying period in a vacuum oven (below the melting point of the compounds).

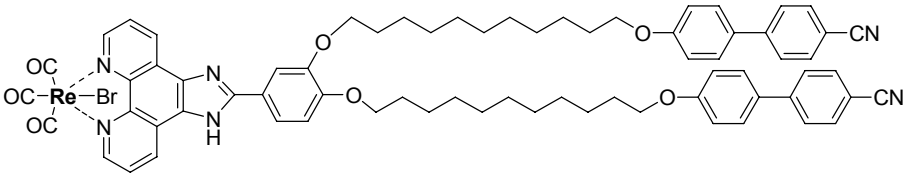


Figure 4.9: Rhenium(I) complex of ligand $\boldsymbol{L_{II}}$.

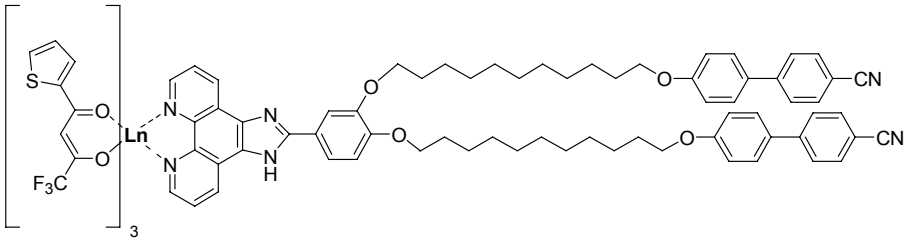


Figure 4.10: Rare-earth complexes of ligand $\boldsymbol{L_{II}}$
(Ln = Y, La, Nd, Sm, Eu, Er, Yb).

4.3 Results and discussion

4.3.1 Solution studies

The coordination mode of the metal ion in solution was examined by measuring one- and two-dimensional proton NMR spectra of the diamagnetic [$ReBr(CO)_3\mathbf{L_{II}}$] and [$Ln(tta)_3\mathbf{L_{II}}$] (Ln = Y, La) complexes which were then compared to the proton NMR spectra of the ligands $\mathbf{L_{II}}$ and that of 2-thenoyltrifluoroacetone (Htta). The proton NMR resonances of the free ligand $\mathbf{L_{II}}$ are sharp and show the expected splitting pattern (Figure 4.11).

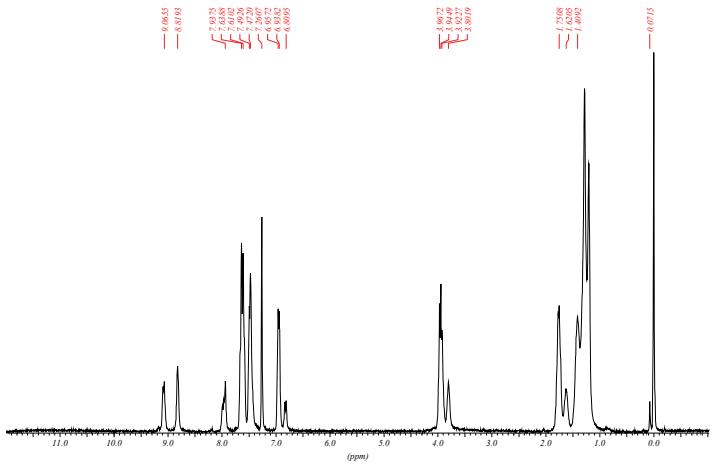


Figure 4.11: Proton NMR spectrum of ligand $\boldsymbol{L_{II}}$ *in* $CDCl_3$ *at room temperature.*

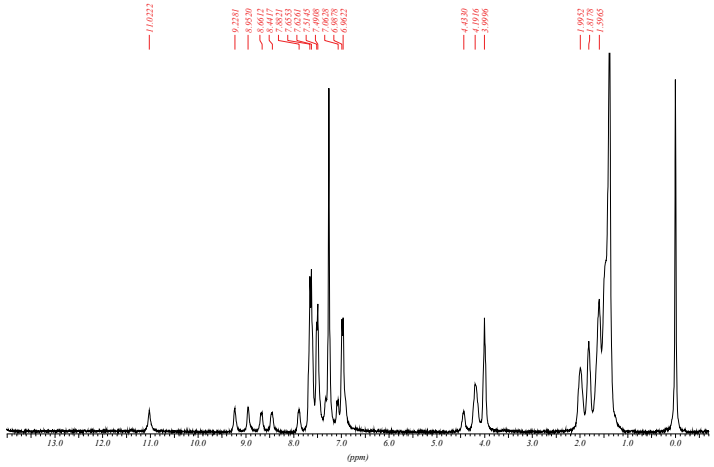


Figure 4.12: Proton NMR spectrum of $[ReBr(CO)_3\boldsymbol{L_{II}}]$ *in* $CDCl_3$ *at room temperature.*

Upon coordination to the rhenium(I)-containing moiety [$ReBr(CO)_3$], the proton signals of the 1,10-phenanthroline unit shifted between 0.14 and 0.39 ppm downfield, as compared to the corresponding protons of the free ligand (Figure 4.12). The magnitude of the observed downfield shifts is consistent with the 1,10-phenanthroline ligand coordination to rhenium(I).[27,28] While the proton signals of the aryl group attached to the imidazole ring also experienced a slight downfield shift, the aromatic protons of cyanobiphenyl groups were unaffected by the coordination to rhenium(I), indicating that there was no interaction between the cyano group and the metal center.

In the proton NMR spectrum of the [$La(tta)_3\mathbf{L_{II}}$] complex the resonances of 1,10-phenanthroline were broadened and shifted between 0.11 and 0.35 ppm downfield compared to those of the free ligand (Figure 4.13). These downfield shifts are comparable to the values found for other diamagnetic lanthanum(III) complexes of 1,10-phenanthroline.[29,30] No signals of free 1,10-phenanthroline were observed in the spectrum. Similarly, no evidence for free 2-thenoyltrifluoroacetone was observed. Uncoordinated 2-thenoyltrifluoroacetone exists in $CDCl_3$ solutions 100% in the enol form, displaying a prominent enol proton resonance at 14.84 ppm. Upon complexation of the ligand to lanthanum(III) in [$La(tta)_3\mathbf{L_{II}}$], this resonance disappears which indicates full coordination of the 2-thenoyltrifluoroacetonate ligand to the lanthanum(III) ion. At room temperature, the proton NMR resonances of the 1,10-phenanthroline unit in the [$Y(tta)_3\mathbf{L_{II}}$] complex was significantly broadened, while the methine signal at 6.33 pm was rather sharp (Figure 4.14). Variable temperature proton NMR spectra of [$Y(tta)_3\mathbf{L_{II}}$] were measured in order to investigate the possible dynamic process which led to the broadening of the NMR resonances. Upon lowering the temperature to –25 °C, the 1,10-phenanthroline peaks sharpened while the methine peak of the 2-thenoyltrifluoroacetonate ligand broadened into a hump consisting of at

least three overlapping signals (Figure 4.15). The dynamic processes which take place in solution of the [Y(tta)$_3$**L$_{II}$**] complex are difficult to elucidate. These may involve exchange of the ligands or partial dissociation of the 1,10-phenanthroline derivative and of one or more 2-thenoyltrifluoroacetonate ligands from the yttrium(III) ion. In addition, conformational freezing of the three β-diketonate ligands or other coordination modes could be also possible. Variable temperature NMR spectra of the [La(tta)$_3$**L$_{II}$**] complex also showed splitting of the 2-thenoyltrifluoroacetonate methine resonances upon lowering the temperature to –25 °C, indicative of similar dynamic processes as that suggested for the [Y(tta)$_3$**L$_{II}$**] complex (Figure 4.16). Similar dynamic behavior was previously observed in solutions of other rare-earth complexes with β-diketonate ligands.[15]

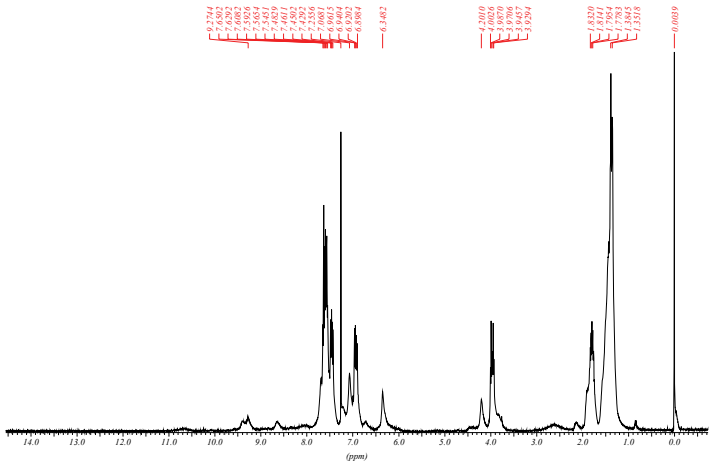


*Figure 4.13: Proton NMR spectrum of [La(tta)$_3$**L$_{II}$**] in $CDCl_3$ at room temperature.*

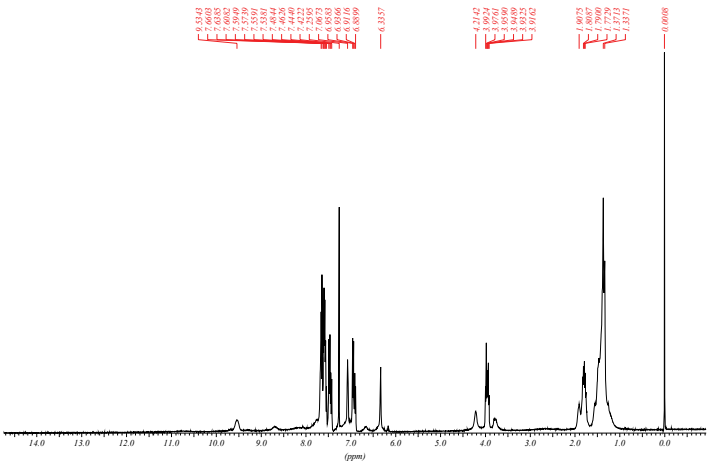


*Figure 4.14: Proton NMR spectrum of [Y(tta)$_3$**L$_{II}$**] in $CDCl_3$ at room temperature.*

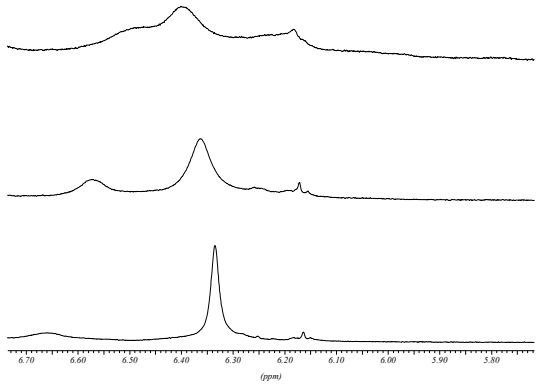


*Figure 4.15: Methine resonance of the tta ligand in [Y(tta)$_3$**L$_{II}$**] at 248 K (top), 268 K (middle) and 288 K (bottom).*

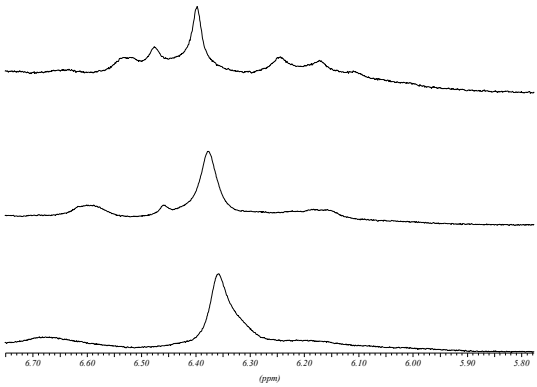


*Figure 4.16: Methine resonance of the tta ligand in [La(tta)$_3$**L$_{II}$**] at 248 K (top), 268 K (middle) and 288 K (bottom).*

4.3.2 Thermal behavior

The thermal behavior of the different benzaldehyde precursors, phenanthroline derivatives, and metal complexes was investigated by differential scanning calorimetry (DSC), polarizing optical microscopy (POM), and by small-angle X-ray diffraction on powder samples. Determination of accurate transition temperatures was not easy because no well-resolved thermograms of the imidazo[4,5-f]-1,10-phenanthroline ligands and of the corresponding metal complexes were obtained by DSC. The absence of a distinct melting peak can be attributed to the low crystallinity of the compounds, a consequence of their non-linear, oligomeric-like structures, some of them being even obtained as waxy solids after synthesis. The three precursor aldehydes (**12**, **13**, **14**) exhibit a nematic phase, which is monotropic for **12**, and enantiotropic for **13** and **14**, though over a narrow temperature range.

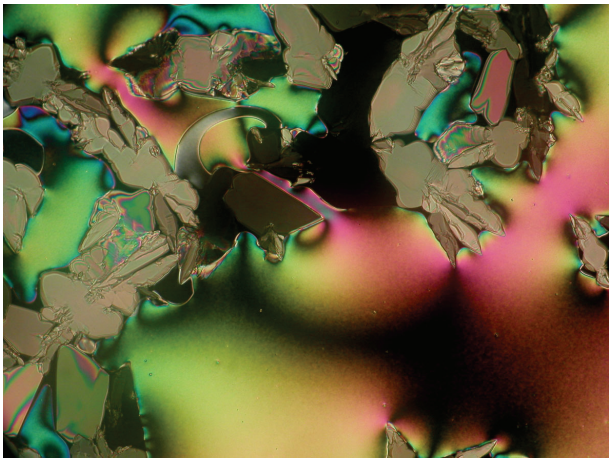


*Figure 4.17: Optical texture of the nematic phase of **12** upon cooling at 85 °C. The compound has partially crystallized out.*

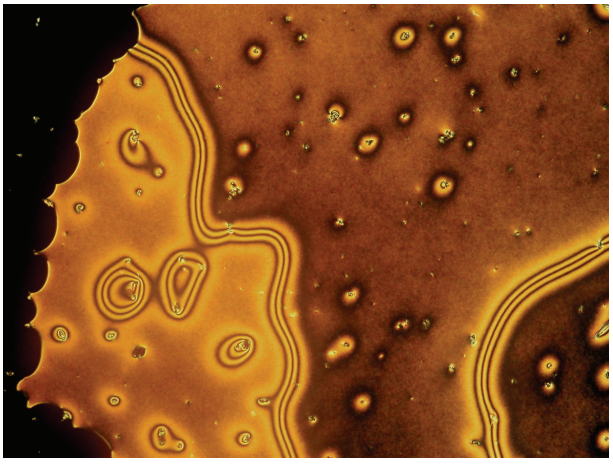


*Figure 4.18: Optical texture of the nematic phase of **13** upon cooling at 80 °C.*

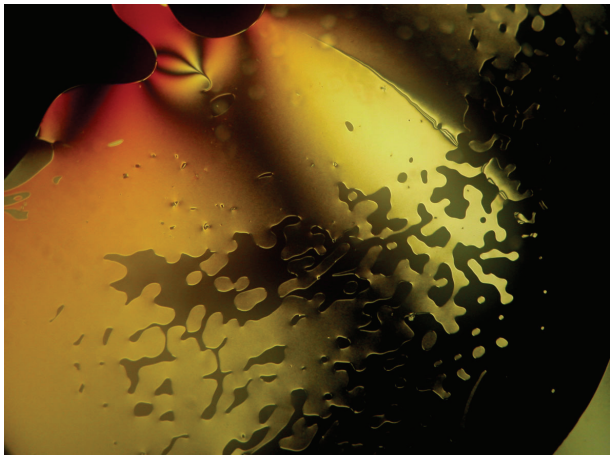


*Figure 4.19: Optical texture of the nematic phase of **14** upon cooling at 110 °C.*

The nematic phase of **12**, **13**, and **14** was identified on the basis of its optical texture observed by polarizing optical microscopy, showing Schlieren textures with two and four brushes (see Figure 4.17, 4.18, and 4.19, respectively).

Table 4.1: Transition temperatures and mesophases of the precursor aldehydes.

Compd.	Transition temperatures (°C)[a]	ΔH_m (kJ mol^{-1})[a]	ΔH_c (kJ mol^{-1})[a]
12	Cr · 95 (N · 89) · I	55.5	-
13	Cr · 54 · N · 89 · I	25.6	4.6
14	Cr · 104 · N · 111 · I	86.2	3.8

[a] Abbreviations: Cr = crystalline or semicrystalline phase; N = nematic phase; I = isotropic liquid. ΔH_m = enthalpy change at the melting point; ΔH_c = enthalpy change at the clearing point.

An overview of the transition temperatures of the precursor aldehydes is given in Table 4.1.

Quite interestingly, both the ligands $\mathbf{L_I}$ and $\mathbf{L_{II}}$ and all their metal-adduct derivatives, except the [$ReBr(CO)_3\mathbf{L_I}$] complex, exhibit a N phase with similar transition temperatures with the melting points ranging between 75 and 92 °C and the clearing temperatures between 124 and 138 °C, and with an average mesomorphic temperature range of about 40 to 50 °C. A slight decrease of the transition temperatures, but with a constant mesomorphic temperature domain, was achieved with the ligand $\mathbf{L_{III}}$ and the rhenium(I) derivative [$ReBr(CO)_3\mathbf{L_{III}}$]. However, the europium(III) complex of this ligand showed a mesophase over a small temperature range of only 9 °C. In most cases, it was only possible to observe a defect texture after inducing birefringence by pressing with a needle on the glass cover slips of the microscope preparations. Some of the samples tend to orient nearly perpendicular to the glass slide surface to give a homeotropic texture, and by pressing the glass cover slips this orientation is disrupted. An overview of the transition temperatures is given in Table 4.2.

All the compounds exhibit enantiotropic mesophases, except the rhenium(I) complex [$ReBr(CO)_3\mathbf{L_I}$], which forms a monotropic nematic mesophase. Deduced from observations by polarizing optical microscopy, the rare-earth complexes systematically exhibit a nematic phase. The characteristic texture was recognized by the formation of Schlieren textures with two- and four-brushes point defects, along with large homeotropic areas. No sign of an additional more ordered phase was detected. X-ray diffraction experiments on powder samples were sufficient to confirm the correct assignment of the nematic phase. Indeed, the observation of a broad scattering signal in the small-angle region instead of the presence of sharp intense peaks in the temperature range of the mesophase, confirmed the absence of 1D or 2D long-range correlated positional ordering. This broad signal corresponds to

lateral short-range molecular correlations of the order of the molecular length, typical of the orientational nematic ordering. In the wide-angle part, the signal at ca. 4.5 Å, attributed to the lateral short-range order of the molten chains and cyanobiphenyl moieties, was also observed.

Table 4.2: Transition temperatures and mesophases of the substituted imidazo[4,5-f]-1,10-phenanthroline ligands and the corresponding metal complexes.

Compound	Transition temperatures (°C)[a]	Temperature range, ΔT (°C)
L_I	Cr · 80 · N · 124 · I	44
[$ReBr(CO)_3$**L_I**]	Cr · 260 (N · 158) · I	-
[$Nd(tta)_3$**L_I**]	Cr · 86 · N · 138 · I	52
[$Eu(tta)_3$**L_I**]	Cr · 89 · N · 138 · I	49
L_{II}	Cr · 75 · N · 128 · I	53
[$ReBr(CO)_3$**L_{II}**]	Cr · 81 (SmA_{Col} · 65) · N · 128 · I	47
[$Y(tta)_3$**L_{II}**]	Cr · 89 · N · 127 · I	38
[$La(tta)_3$**L_{II}**]	Cr · 84 · N · 124 · I	40
[$Nd(tta)_3$**L_{II}**]	Cr · 85 · N · 124 · I	39
[$Sm(tta)_3$**L_{II}**]	Cr · 86 · N · 124 · I	38
[$Eu(tta)_3$**L_{II}**]	Cr · 86 · N · 125 · I	39
[$Er(tta)_3$**L_{II}**]	Cr · 90 · N · 127 · I	37
[$Yb(tta)_3$**L_{II}**]	Cr · 92 · N · 127 · I	35
L_{III}	Cr · 48 · SmA_{Col} · 94 · I	46
[$ReBr(CO)_3$**L_{III}**]	Cr · 49 · Col_rL · 105 · I	56
[$Eu(tta)_3$**L_{III}**]	Cr · 83 · N · 92 · I	9

[a] Abbreviations: Cr = crystalline or semicrystalline phase; N = nematic phase; SmA_{Col} = unconventional smectic A phase with an in-plane short-range ordered columnar stacking; Col_rL = unconventional smectic phase with a long-range ordered 2D columnar packing (see text); I = isotropic liquid. ΔH values are not given as no well-resolved thermograms could be obtained by DSC.

The lanthanide ion has only a small influence on the transition temperatures. However, a slight increase of the melting temperatures is observed going along the lanthanide series from lanthanum(III) to ytterbium(III). The effect of the ionic radius on the transition temperatures is additionally illustrated by the similar melting points of the yttrium(III) complex [Y(tta)$_3$**L$_{II}$**] and the erbium (III) complex [Er(tta)$_3$**L$_{II}$**] (the ionic radius of yttrium(III) and erbium(III) is very similar). A small increase in the clearing points is observed going along the lanthanide series. The limited effect of the lanthanide ion on the transition temperatures is in striking contrast to the lanthanide(III) alkanoates,[31] and Schiff's base complexes with nitrate counterions for which either the mesophase stability was considerably decreased or the liquid-crystalline properties totally suppressed, going along the lanthanide series from lanthanum(III) to lutetium(III).[32] The thermal behavior is quite similar to alkoxy-substituted bis(phthalocyaninato)-lanthanide(III) complexes,[6g] and the small influence of the lanthanide ion on the mesomorphic behavior can be attributed to the rather large contribution of organic ligands (phenanthroline derivative and coligands).

As for the three imidazo[4,5-f]-1,10-phenanthroline ligands, both **L$_I$** and **L$_{II}$** exhibit a nematic phase, whereas in the case of **L$_{III}$**, the crystal phase transforms on heating into a smectic-like phase with a short-range ordering of columns (vide infra). The nematic phase of **L$_I$** and **L$_{II}$** was identified on the basis of its optical texture observed by polarizing optical microscopy, showing Schlieren textures with two and four brushes, whereas for **L$_{III}$**, no characteristic texture was obtained, except from the presence of large homeotropic areas. In the case of the nematogenic ligands **L$_I$** and **L$_{II}$**, X-ray diffraction patterns resembled those described above for the rare-earth complexes, and the same explanations are given.

As for the mesophase of **L$_{III}$**, in the X-ray diffraction pattern recorded at 80 °C, two sharp, small-angle reflections of high intensity, in the ratio 1:2,

attributed to the lamellar periodicity ($d = d_{001}$ = 50.0 Å), and to its first harmonics (d_{002} = 25.0 Å) were observed (Figure 4.20). This periodicity of 50 Å corresponds to a multilayered smectic phase formed by the piling of phenanthroline- and cyanobiphenyl-containing sublayers alternating with the aliphatic spacer sublayer. Additionally, broad reflections at ca. 14 Å (*D* in Figure 4.20) and at 4.6 Å were observed. The reflection at 4.6 Å corresponds to the usual lateral periodicity within the molten chains sublayer, whereas the reflection at 14 Å corresponds to some lateral periodicity within the sublayer occupied by the phenanthroline groups, very likely to a ribbon's width of stacked phenanthrolines. This latter assumption is supported by the fact that phenanthroline-like cores show, like other discotic cores, a strong tendency to stack into columns to give columnar phases with typical stacking periodicities ranging between 3.3 and 3.6 Å.[33]

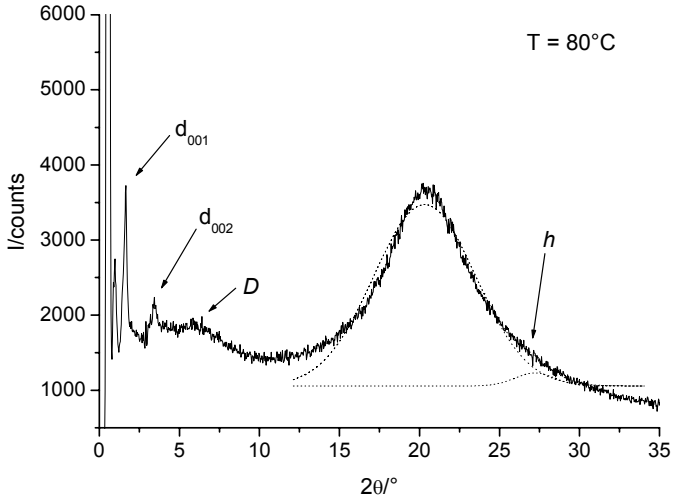


Figure 4.20: X-ray pattern of the SmA_{Col}-type phase of $\boldsymbol{L_{III}}$ *at 80 °C. The following diffraction peaks are observed: d_{001} = 50.0 Å, d_{002} = 25.0 Å, D = 14.0 Å, and the two broad reflections at 4.6 Å and 3.5 Å (h), respectively.*

Indeed, the peak located at 4.6 Å is much wider than in classical disordered smectic phases as the wing of the signal extends to ca. $2\theta = 30°$. The peak shape analysis eventually reveals a superposition of two broad signals, that of 4.6 Å and another weak one at 3.3-3.5 Å (*h* in Figure 4.20).

To have a more precise description of the molecular arrangement, a quantitative discussion based on the measured periodicities and calculated partial molecular volumes is proposed. Given the alternate packing of the phenanthroline rings, it is therefore necessary to consider two molecules in a head-to-tail arrangement to calculate the area occupied by the three terminal mesogenic units at the interface between the smectic layers. Such an area $A = 2V_M/d$ is directly deduced from the molecular volume ($V_M \approx 2400$ Å^3 estimated at 80 °C) and the layer thickness ($d = 50$ Å) and is found to be ca. 96 Å^2. This calculation thus gives a molecular area per mesogenic unit of 32 Å^2, which is larger than the well-known cross section of the cyanobiphenyl groups of about 20–24 Å^2. In this case, the sublayers containing the cyanobiphenyl groups are either partially interdigitated, as in the case of the SmA_d phase,[34] or the aliphatic spacers and the cyanobiphenyl groups are tilted with an angle ψ of about 50°, but without any correlation in the tilt direction, as in the SmA phase of the de Vries type. Let us recall that in the de Vries SmA phase, the molecules are assumed to be tilted as in the SmC phase resulting from either tilted layers being stacked in a random fashion,[35] or the molecules being tilted without long-range order in the direction of tilt within the layer.[35,36]

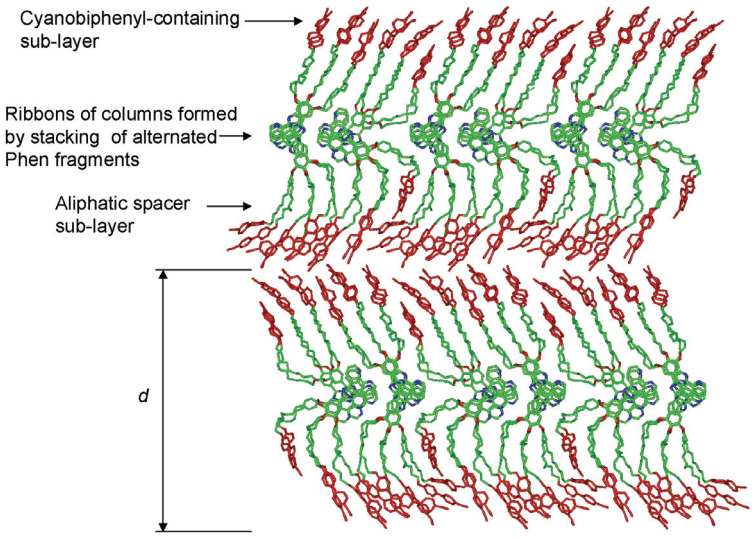


Figure 4.21: Representation of the alternated packing of $\boldsymbol{L_{III}}$ *in the* SmA_{Col} *phase built from two snapshots of a single layer obtained by MD calculations. The columns forming ribbons can be seen from the alternated stacking of the phenanthroline heterocycles. The cyanobiphenyl mesogens are randomly tilted (see text).*

In the case of the phenanthroline-rich slabs, the heterocycles occupy a transverse area of 48 $Å^2$ and are packed in such a way that short columns are formed. The ratio of this transverse area with the ribbon periodicity in the X-ray diffraction pattern (14 Å) gives a stacking periodicity of 3.4 Å (within the ribbons). The particular nature of this arrangement in layers was found consistent with molecular dynamics calculations, for which a density of 1 was found. A snapshot of this modelized structure is shown in Figure 4.21. This smectic phase cannot be simply referred to as a classical SmA phase due to the presence of the short columns within layers. Such unusual

structure is similar to the SmA phase formed by the charge transfer assembly of tetrathiofulvalene and tetracyanoquinodimethane reported by Davidson et al.[37] and that formed by *ortho*-palladated bipyridine[38] and di-copper bis-(terpyridine)[1c] complexes reported by Ziessel and co-workers in which the aromatic cores of the molecules stacked into small columns randomly oriented within smectic layers. Therefore, the mesophase would be more appropriately defined as a *lamellar phase with short-range columnar order within the layers*, i.e., a *lamello-columnar phase*[39] and labeled SmA_{Col} phase.

The rhenium(I) complexes also exhibit an interesting thermal behavior, which is extremely dependent on the ligand type. The first derivative, based on $\mathbf{L_I}$, [$ReBr(CO)_3\mathbf{L_I}$], exhibits a high-temperature monotropic nematic phase as recognized by POM. The rhenium(I) complex of $\mathbf{L_{II}}$, [$ReBr(CO)_3\mathbf{L_{II}}$], exhibits an enantiotropic nematic phase and a monotropic smectic-like phase. Not unambiguously ascertained by POM alone (Figure 4.22), both mesophases were eventually fully identified by the combination of both POM and XRD techniques. The X-ray diffraction patterns of the nematic phase recorded at 80, 100, and 120 °C are similar to the patterns obtained with the other nematogens, but in addition local orderings consisting of *cybotactic smectic clusters* were observed. This local layering was in fact heralding the formation of a lower-temperature smectic-like phase. Indeed, the pattern recorded at 60 °C on cooling, revealed two sharp, weakly intense, small-angle reflections, in the ratio 1:2, which are characteristic of a layered structure, with a periodicity *d* of 45.3 Å. In addition, weak and diffuse signals in the wide-angle part were detected at about 4.6 and 3.3 Å corresponding to the lateral short-range order of the molten chains and cyanobiphenyl groups and to the alternated stacking of the phenanthroline rings, respectively, as for $\mathbf{L_{III}}$. The supramolecular

organization of the complex within the smectic phase thus resembles that of the ligand $\mathbf{L_{III}}$ described above (SmA_{Col} phase), with an alternation of mesogenic-rich layers and phenanthroline-metal layers.

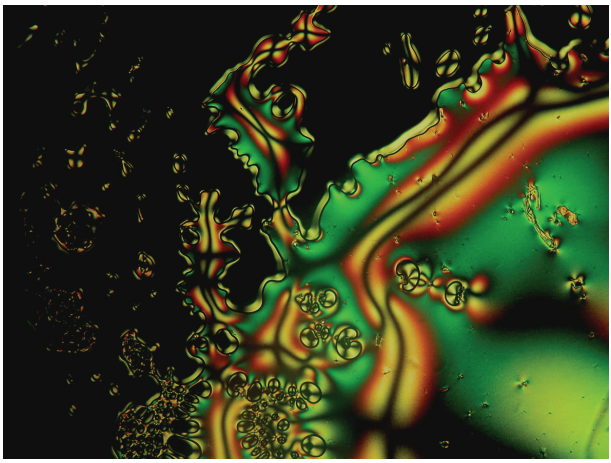


*Figure 4.22: Optical texture of the nematic phase of [ReBr(CO)$_3$**L$_{II}$**] upon cooling at 100 °C.*

The same analysis as above, by estimating the molecular volume close to 1900 Å^3, gives a molecular area, $A = 2V_M/d \approx 84$ Å^2. This results in a molecular area per mesogenic unit of 42 Å^2, which is large (about twice) compared to the transverse cross-section of one cyanobiphenyl group (20-24 Å^2). This therefore suggests that the packing of the mesogens within the sublayer can be most likely described as a non-tilted monolayer (i.e., a layer containing one thickness of cyanobiphenyls) with complete interdigitation of the cyanobiphenyl groups from the molecules of adjacent layers (zip-like), and it is now consistent with an area per mesogenic groups of 21 Å^2. In the case of the phenanthroline/rhenium-rich slabs, the heterocycles transverse area is also 42 Å^2, which is smaller than in the $\mathbf{L_{III}}$ ligand case,

despite the bulky metallic fragment. This could indicate an out-of-plane tilting of the piled heterocycles. A representation of this molecular arrangement in the SmA_{Col} phase is shown below, for which the likeliness is supported by MD calculations (Figure 4.23).

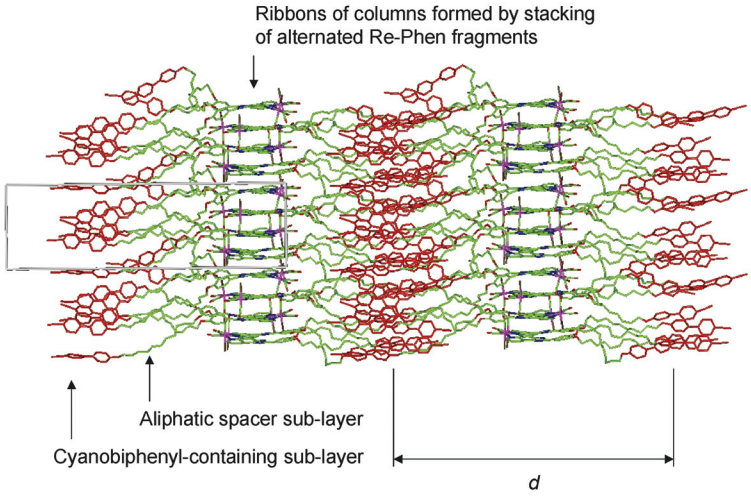


*Figure 4.23: Snapshot of the packing of [ReBr(CO)$_3$**L$_{II}$**] in the alternated SmA_{Col} phase obtained from MD calculations. Short columns forming ribbons can be seen from the alternated stacking of the phenanthroline heterocycles.*

Finally, the [ReBr(CO)$_3$**L$_{III}$**] complex exhibits a mesophase, but the strongly birefringent and sand-like texture seen by POM (Figure 4.24) was not characteristic of any particular mesophase. The use of hydrophilic and hydrophobic treated glass slides did not help for a concluding assignment either.

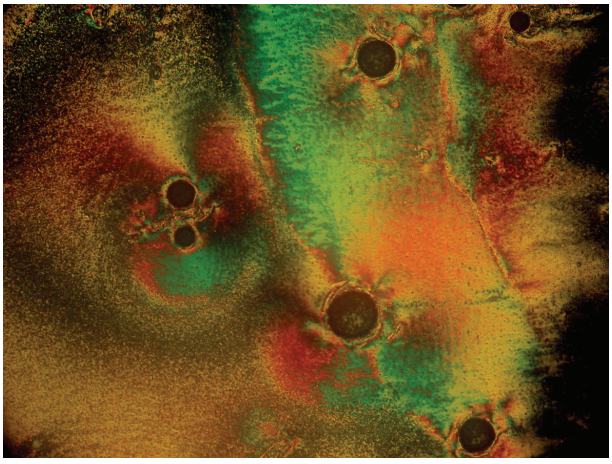


*Figure 4.24: Optical texture of the Col_rL phase of [ReBr(CO)$_3$**L**$_{III}$] upon cooling at 90 °C.*

The X-ray diffraction pattern recorded at 80 °C (Figure 4.25), shown as a representative example of the different temperatures at which the experiment was done, contains a set of five sharp reflections and four scattering halos (Table 4.3). The sharp reflections (1–5) in the low-angle region were indexed in the following 2D rectangular lattice with the parameters a = 82.0 Å, b = 36.7 Å, S = 3010 Å^2 (Figure 4.26). The broad signal 7 in the wide-angle part detected at about 4.5 Å corresponds to the lateral short-range order of the molten chains and cyanobiphenyl groups (D_0). The reflection 8 (h_0 = 3.3 Å) corresponds to the stacking of the phenanthroline heterocycles into columns. From the FWHM (full width at half maximum) of this reflection, a correlation length of about 100 Å is deduced, corresponding to columns of about 30 phenanthroline units.

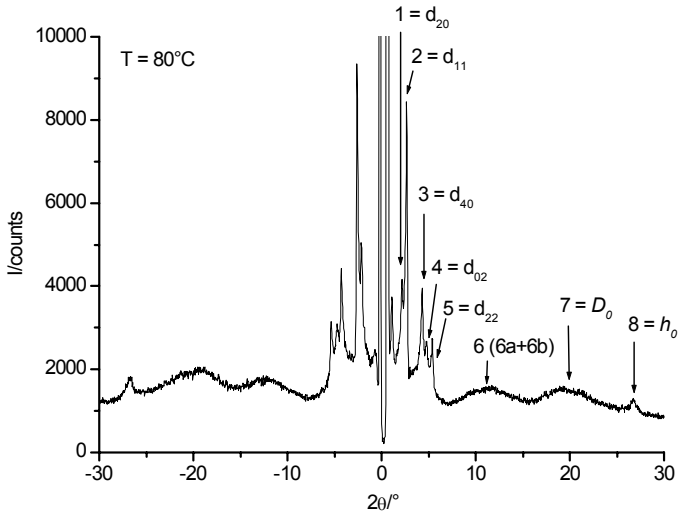


*Figure 4.25: Representative X-ray diffraction pattern of the Col$_r$L phase of [ReBr(CO)$_3$**L$_{III}$**] at 80 °C.*

Moreover, the spacing of reflection 8 corresponds to the distance between phenanthroline heterocycles, being very close to the value found for analogous phenanthroline-containing compounds in the crystalline state or for other macrocycles in columnar phases in general.[33] This indicates that the scattering vector is nearly parallel to both the columnar axis and the normal to the heterocycle's plane and that, consequently, these species are not tilted within the columns. The piling of the sublayers containing the columns formed by the phenanthroline complexes and of the cyanobiphenyl-containing sublayers alternating with aliphatic sublayers (spacer) has an overall periodicity of $a/2$ (i.e., d_{20}).

*Table 4.3: Low- and wide-angle bragg reflections collected from the X-ray diffraction pattern of [ReBr(CO)$_3$**L$_{III}$**] at 80 °C.*

Reflection[a)]	$d_{meas.}$/Å[b)]	I[c)]	L[c)]	*hk*[c)]	$d_{calc.}$/Å[b)]	Assignment
1	41.0	M	S	20	41.0	Rectangular lattice
2	33.5	VS	S	11	33.5	Rectangular lattice
3	20.55	M	S	40	20.5	Rectangular lattice
4	18.6	W	S	02	18.35	Rectangular lattice
5	16.6	W	S	22	16.75	Rectangular lattice
6a	8.8		br			~2D_0
6b	6.7		br			~2h_0
7	4.5		22			D_0
8	3.3		100			h_0

[a] Reflection number.

[b] d_{meas} and d_{calc} are the measured and calculated diffraction spacing.

[c] I is the intensity of the reflections: VS, very strong; M, medium; W, weak; L, sharp reflection (S), broad reflection (br) or correlation length value obtained from the Scherrer Guinier-modified formula; *hk* are the indexations of the reflections. D_0, average mesogen distance; h_0, average stacking distance.

This attribution is justified by the absence of the (10) and (30) reflections and by the surprisingly high intensity of the (40) reflection with respect to the (20) reflection, consistent with a peak of electronic density associated to the cyanobiphenyl sublayers. Finally, another broad signal (6) is observed between 7 and 15° (2θ) whose shape allows the decomposition into two diffuse reflections centered around ca. 8.8–9.0 Å (6a) and ca. 6.7–7.0 Å (6b), respectively (vide infra).

In contrast to classical discotic molecules, the amphipathic moiety is connected to only one side of the phenanthroline ring. This results in the micro-segregation of the rhenium-phenanthroline complexes and of the amphipathic moieties in adjacent sublayers. Again, the packing corresponds to a lamellar columnar phase consisting in the superposition of two types of sublayers separated by the aliphatic continuum stemmed by the spacer: one slab contains the columns formed by the complexes, and the other one accommodates the cyanobiphenyl mesogens. This packing is thus similar to that described above for $\mathbf{L_{III}}$ and [$ReBr(CO)_3\mathbf{L_{II}}$], except that the short-range correlated ribbons of stacked phenanthroline heterocycles are replaced by the long-range correlated two-dimensional rectangular organization of the columns formed by the stacked rhenium-phenanthroline complexes. Therefore, and for consistency with the previous results, we may label this *lamellar columnar phase* as Col_rL since both the columnar and lamellar orderings are long-range correlated.

In the crystalline phase of related compounds such as the chlorotricarbonyl(1,10-phenanthroline)rhenium(I), 6.5 Å is the minimum rhenium-rhenium distance.[40] This value is also twice the distance corresponding to the stacking of the heterocycles (6b, $2h_0$ = 6.6 Å). Therefore, neighboring heterocycles within the columns have to stack with a shift on their orientation around the columnar axis. As in phthalocyanine systems packed in columnar phases,[33] a signal corresponding to this

additional dimer's periodicity is expected in the diffractogram; and indeed, this distance corresponds to the location of the reflection 6b (vide supra). For the description of the packing within the sublayers, the molecular area and the number of molecules per slice of section $a \times b$ and of thickness 2×3.33 Å (from the alternated stacked phenanthrolines) need to be calculated. The volume of this slice (ca. 20 000 $Å^3$) corresponds to an occupation of eight molecules of 2500 $Å^3$ in consistency with the molecular volume determination. Since the lattice contains two sublayers of cyanobiphenyl mesogens and each molecule three of these mesogens, about twelve mesogens are contained in a sublayer slice 6.7 Å thick. This corresponds to a molecular area of $36.7 \times 2 \times 3.33/12 = 20.4$ $Å^2$, which is consistent with the transverse cross section of one cyanobiphenyl group (20 to 24 $Å^2$). This value of the molecular area per mesogen is identical to that found for the rhenium(I) complex $[ReBr(CO)_3\mathbf{L_{II}}]$ discussed previously, and therefore the packing of the mesogens within the sublayer can also be classed as a non-tilted monolayer case. Again, this up and down arrangement of the mesogens within such a totally interdigitated monolayer results in a doubling of the in-plane periodicity, and the corresponding signal is expected in the X-ray pattern; indeed, this distance (8.8 Å) corresponds to the position of reflection 6a ($2D_0$).

From this complete analysis, the rectangular lattice contains four columns of stacked rhenium-phenanthroline complexes and that the average intercolumnar distance is therefore equal to $b/2$, i.e., 18.3 Å. This value is larger than the 14 Å found for the average ribbon periodicity in the ligand's pattern: in this case, the discrepancy corresponds to the organization of the rhenium-bromotricarbonyl moiety between the columns. The doubling of the lattice along both the a axis and b axis is revealed by the presence of the reflection (11), while the reflections (10) and (01) are absent. This lattice doubling should result from different repartitions of the electronic density

around the columns. Moreover, it would probably be related to the organization on the electron-rich rhenium moiety, since the reflection (11) is highly intense. As the most simple columnar organization consistent with the lattice doubling, the following schematic view of a packing with a *p2mg* symmetry is proposed (Figure 4.26). The ellipsoid center coincides with the columnar axis, and the ellipsoid ends stand for a peak of electronic density.

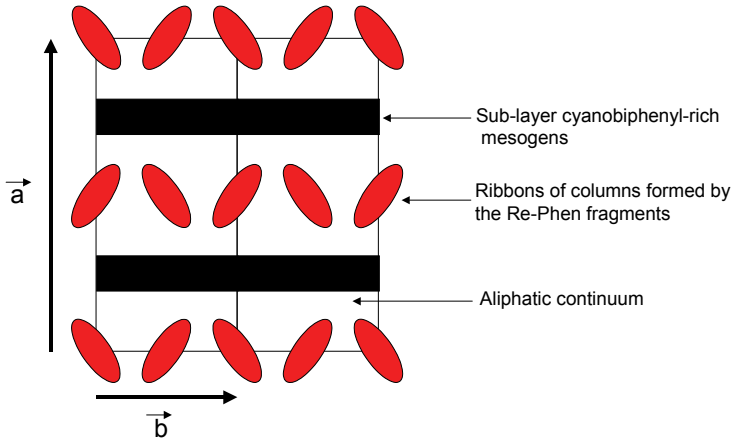


*Figure 4.26: Model representing the Col$_r$L phase of [ReBr(CO)$_3$**L**$_{III}$]: in red, elliptic cross sections of the columns formed by the stacking of the rhenium-phenanthroline fragments, arranged in a rectangular lattice ($\vec{a}$, $\vec{b}$) with the p2mg plane group; in black, sublayers formed by the cyanobiphenyl mesogenic units. The rest of the lattice is occupied by the aliphatic chains.*

The strong effect of the rhenium(I) ion on the mesomorphic behavior can be attributed to the additional dipole moment due to the polar Re-Br bond. This results in specific interactions with neighboring molecules and has a large influence on the arrangement of the molecules in the mesophase and the solid phase.

The ligands and corresponding metal complexes may be regarded as non-symmetric flexible dimer, trimer and tetramer liquid crystals, many of which are described in the literature.[41] In general, there is a difference in mesomorphic behavior between symmetric and non-symmetric dimers. Symmetric dimers show monolayer smectic phases and nematic phases, depending on the spacer length; non-symmetric dimers show interdigitated smectic phases, nematic phases and intercalated smectic phases, depending on the spacer length. The smectic phase formation may be considered in terms of a microphase separation in which the mesogenic units form one domain, while the alkyl chains constitute another. There are two possible driving forces behind this separation: energetically if the mean of the "mesogenic unit - mesogenic unit" and "chain - chain" interactions is more favorable than the mixed "mesogenic unit - chain" interaction then phase separation will occur, or entropically the interaction between a core and a chain acts to order the chain and hence, is unfavorable. Traditionally, dimer or oligomer liquid crystals consist of molecules, comprising usually rodlike mesogenic units linked end-to-end via a flexible alkyl chain containing between 3 and 12 methylene groups. In this point of view, the ligands and complexes described in this chapter are somewhat different. The 2-phenyl-imidazo[4,5-f]-1,10-phenanthroline fragment is a coordinating unit and the mesogenic units are not connected end-to-end, but are all connected to the coordinating unit via a flexible alkyl spacer. However, the ligands and complexes described in this chapter also show nematic and lamellar phases (although with additional columnar order within the layers), depending on the number of mesogenic units and on the type of metal fragment. For a large number of mesogenic units (as in the case of $\mathbf{L_{III}}$, which contains three mesogenic units), a microphase separation is induced leading to the formation of a lamellar columnar phase. Complexation to rhenium(I) (except for the rhenium(I) complex $[ReBr(CO)_3\mathbf{L_I}]$, which contains only

one mesogenic unit) results in favorable interactions between the rhenium-phenanthroline units and thus in the formation of lamellar columnar phases. The additional (short- or long-range) columnar order within the layers can be attributed to the good stacking abilities of the 2-phenyl-imidazo[4,5-f]-1,10-phenanthroline units. The lanthanide complexes show nematic phases, which can be explained by the introduction of the bulky [$Ln(tta)_3$] fragment. The interactions between the bulky [$Ln(tta)_3$]-phenanthroline fragments are not favorable to induce a microphase separation so that only nematic phases are obtained.

As mentioned before, the concept of decoupling of the mesogenic groups from the coordinating group was inspired on the work of Deschenaux and co-workers concerning liquid-crystalline fullerenes.[13] Saez and co-workers used the same strategy to prepare liquid-crystalline octasilsesquioxane derivatives.[14] Compared to the fullerene and octasilsesquioxane core, the 2-phenyl-imidazo[4,5-f]-1,10-phenanthroline fragment is rather small and has no spherical shape. Also, the incorporation of a metal ion, as in the case of the metal complexes described in this chapter, is different. Let us consider only the low generation dendrimers based on the fullerene and octasilses-quioxane core, as these can be most easily be compared to the ligands and complexes described in this chapter. The liquid-crystalline fullerenes and octasilsesquioxanes with terminally attached mesogenic groups all exhibit SmA phases. For the mesomorphic octasilsesquioxanes, association of the mesogenic units with one another changed the globular shape of the octasilsesquioxane core into a cylindrical one, resulting in the formation of a smectic A phase. For the mesomorphic fullerenes, the organization is determined by steric factors: the suitable adequacy between the cross-sectional areas of the fullerene moiety and that of the mesogenic groups (to fill the space in an optimized way), produces a smectic A phase. However, it

is also possible to obtain nematic phases in dendrimers functionalized with laterally attached mesogenic units,[42] in a similar way as occurs in side-chain liquid crystal polymers.[43]

Considering the ligands and metal complexes described in this chapter, we can assume that when the number of mesogenic groups is large (as in the case of $\mathbf{L_{III}}$, which contains three mesogenic units) and/or when there are additional specific interactions by the introduction of the [$ReBr(CO)_3$] fragment (except for the rhenium(I) complex [$ReBr(CO)_3\mathbf{L_I}$], which contains only one mesogenic unit), interactions between the mesogenic units with another and between the coordinating units with another result in the formation of a lamellar arrangement. In addition we have shown that for the lamellar columnar phases formed by ligand $\mathbf{L_{III}}$ and the rhenium(I) complexes [$ReBr(CO)_3\mathbf{L_{II}}$] and [$ReBr(CO)_3\mathbf{L_{III}}$], there is a good adequacy between the cross-sectional areas of the coordinating unit and that of the mesogenic groups. In the case of a small number of mesogenic units (as in the case of $\mathbf{L_I}$ and $\mathbf{L_{II}}$, which contain only one or two mesogenic units, respectively) and for the lanthanide complexes, nematic phases are observed. These results are in contrast to the observations for liquid-crystalline dendrimers with terminally attached mesogenic units, which in general form lamellar phases (end-on attachment of the mesogenic groups favors smectic phase formation, while side-on attachment favors nematic phase formation).[42g] However, in comparison to the liquid-crystalline dendrimers, the number of mesogenic units is small; the interaction between the mesogenic units with another and between the coordinating units with another being insufficient or unfavorable for the emergence of more ordered mesophases. Also, it is possible that the number of mesogenic units is too small in order to compensate the large cross-sectional area of the coordinating units so that the formation of more ordered mesophases is suppressed.

4.3.3 Luminescence properties

The trivalent lanthanide ions are well-known for their intense luminescence. This luminescence is not only of interest for optical applications, but the fine structure in the luminescence spectrum of the europium(III) can also be used to probe the symmetry of the first coordination sphere of rare-earth complexes. The luminescence spectrum of europium(III) is sensitive to small structural changes in the first coordination sphere. The luminescence properties of the mesomorphic neodymium(III), samarium(III), europium(III), erbium(III), and ytterbium(III) compounds were studied in the solid state at room temperature. The spectroscopic and photophysical properties of these complexes are very comparable with those of the $[Ln(tta)_3(phen)]$ complexes, where Ln = Nd, Sm, Eu, Er, Yb, tta = 2-thenoyltrifluoroacetonate, and phen = 1,10-phenanthroline. Although both the samarium(III) and europium(III) compounds emit in the visible spectral region, the red europium(III) luminescence is much brighter than the reddish samarium(III) luminescence. These findings are in agreement with the fact that $[Eu(tta)_3(phen)]$ is one of the best-performing red-emitting molecular luminescent materials. Because most of the luminescence output is concentrated in the $^5D_0 \rightarrow {}^7F_2$ transition of Eu^{3+}, the red color is very bright and has a high monochromaticity. The luminescence quantum yield of the complexes dissolved in DMF was calculated and compared with that of the $[Eu(tta)_3(phen)]$ complex. The values are 28 (± 2) %, 19 (± 2) %, and 23 (± 1) % for the europium(III) complexes of the ligands $\mathbf{L_I}$, $\mathbf{L_{II}}$, $\mathbf{L_{III}}$, respectively. The luminescence quantum yield reported for $[Eu(tta)_3(phen)]$ in DMF is 36%.[44] The addition of the imidazole ring makes the energy transfer less favorable, but the systems remain efficient luminescent materials with a good luminescence quantum yield.

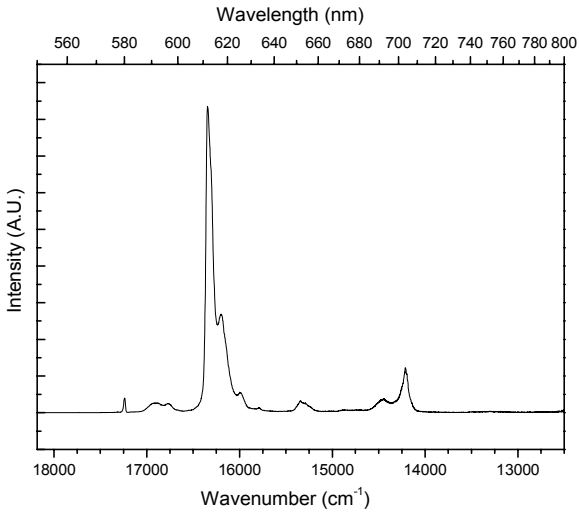


*Figure 4.27: Luminescence spectrum of [Eu(tta)$_3$**L$_I$**] in the solid state at room temperature. The excitation wavelength is 350 nm. The transitions in the spectrum start from the $^5D_0$ state and end at the ^7F_J levels (J = 0-4).*

The luminescence spectrum of the compound [Eu(tta)$_3$**L$_I$**] is shown in Figure 4.27. The fact that only one emission peak is observed for the $^5D_0 \rightarrow {}^7F_0$ transition (580 nm) in the three europium(III) complexes we studied, is a good indication that the local surroundings of all the europium(III) ions are very similar. Only two crystal-field transitions are observed for the $^5D_0 \rightarrow {}^7F_2$ transition (612 nm), but the broadening of the crystal-field transition at the high-energy side (shorter wavelengths) indicates that there are two overlapping crystal-field transitions. The degeneracy of the $^7F_1$ level (observable in the $^5D_0 \rightarrow {}^7F_1$ transition at 592 nm) is totally removed, so that the Eu^{3+} is a site of low symmetry (orthorhombic or lower). The intensity ratio $I(^5D_0 \rightarrow {}^7F_2)/I(^5D_0 \rightarrow {}^7F_1)$ is 15.4, 10.8, and 14.8 for the complexes [Eu(tta)$_3$**L$_I$**], [Eu(tta)$_3$**L$_{II}$**], and [Eu(tta)$_3$**L$_{III}$**] respectively. Changes induced by the extra side chains appear to have an influence, but

the values are also comparable to the values calculated for $[Eu(tta)_3(phen)]$ and $[Eu(tta)_3(H_2O)_2]$. These complexes have a ratio of 11 and 18, respectively. The luminescence lifetime of the $^5D_0 \rightarrow {}^7F_2$ transition was determined by measurement of the luminescence decay curves. Values of 278 (± 8) μs, 327 (± 10) μs, and 282 (± 9) μs were found for the monoexponential decay curves of the europium complexes $[Eu(tta)_3\mathbf{L_I}]$, $[Eu(tta)_3\mathbf{L_{II}}]$, and $[Eu(tta)_3\mathbf{L_{III}}]$ respectively. These decay times are very similar. It can be concluded that the mesogenic groups have a small influence on the spectroscopic properties but overall there is no indication that there are systematic changes. Small, local variations in the first coordination sphere are responsible for the different luminescence behavior.

The neodymium(III), erbium(III), ytterbium(III), but also the samarium(III) are emitting in the near-infrared. These ions show luminescence in the telecommunication low-loss regions of silica. Luminescence can be observed for the complexes of these trivalent lanthanide ions with ligands $\mathbf{L_I}$, $\mathbf{L_{II}}$, and $\mathbf{L_{III}}$. The luminescence of the erbium(III) complexes is the most difficult to measure, but the energy transfer in the mesogenic systems is efficient, and luminescence can be observed at 1530 nm. The luminescence spectra of $[Nd(tta)_3\mathbf{L_I}]$, $[Sm(tta)_3\mathbf{L_{II}}]$, $[Er(tta)_3\mathbf{L_{II}}]$, and $[Yb(tta)_3\mathbf{L_{II}}]$ are shown in Figure 4.28, 4.29, 4.30, and 4.31, respecively.

The lanthanide(III) complexes of the ligands $\mathbf{L_I}$, $\mathbf{L_{II}}$, and $\mathbf{L_{III}}$ are well soluble in the nematic liquid host 4'-pentyl-4-cyanobiphenyl (5CB). Although we did not determine quantitative solubility values, the solubility of the complexes described in this paper is much higher than the solubility of the parent $[Ln(tta)_3(phen)]$ complexes.[45] This good solubility in comparison with that of other lanthanide(III) complexes can be explained by the structural similarities between the host matrix and the guest molecules. After all, each lanthanide complex contains 4-cyanobiphenyl groups attached to the periphery of the 1,10-phenanthroline group and exhibits a

nematic phase. Luminescent liquid-crystal mixtures can be obtained by doping the lanthanide complexes into the liquid-crystal host matrix. Heating the sample above the clearing point of the liquid-crystal host 5CB led in this case to a decrease in luminescence intensity. This decrease is larger than what can be expected from the decrease of the luminescence intensity by a stronger radiationless deactivation of the excited states of the lanthanide(III) ion. The decrease in luminescence intensity is due to the less pronounced scattering of the excitation light in the isotropic liquid than in the mesophase. When there is more scattering of the excitation light, more light can be absorbed by the ligand chromophores of the lanthanide complexes. So far, only limited literature data on the spectroscopic and photophysical properties of adducts of tris β-diketonato lanthanide(III) complexes with 2-arylimidazo[4,5-f]1,10-phenanthrolines are available in comparison with the adducts of 1,10-phenanthroline.[46] The main differences of the 2-arylimidazo[4,5-f]1,10-phenanthroline adducts with respect to the 1,10-phenanthroline adducts is the more extended conjugation in the former molecules, which results in different positions of the ligand triplet levels and an altered energy transfer to the lanthanide ions.

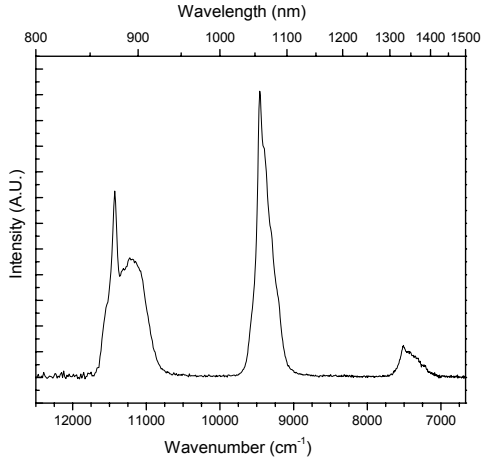


*Figure 4.28: Luminescence spectrum of [Nd(tta)$_3$**L$_I$**] at room temperature. The transitions in the spectrum start from the $^4F_{3/2}$ state and end at the ^4I_J levels (J = 9/2-13/2).*

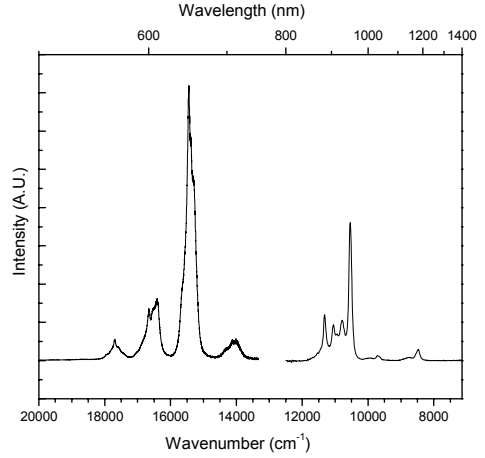


*Figure 4.29: Luminescence spectrum of [Sm(tta)$_3$**L$_{II}$**] at room temperature. The transitions in the visible region start from the $^4G_{5/2}$ state and end at the ^6H_J levels (J = 5/2-11/2). The transitions in the near-infrared region start from the $^4G_{5/2}$ state and end at the $^6H_{15/2}$ level and the ^6F_J levels (J = 5/2-9/2).*

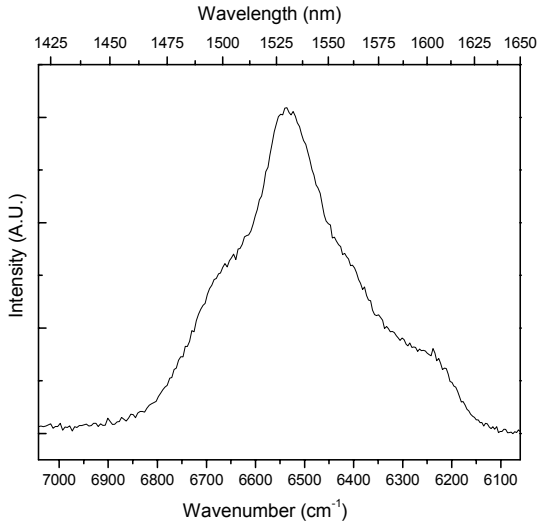


*Figure 4.30: Luminescence spectrum of [Er(tta)$_3$**L$_{II}$**] at room temperature. The emission corresponds to the $^4I_{13/2} \rightarrow {}^4I_{15/2}$ transition.*

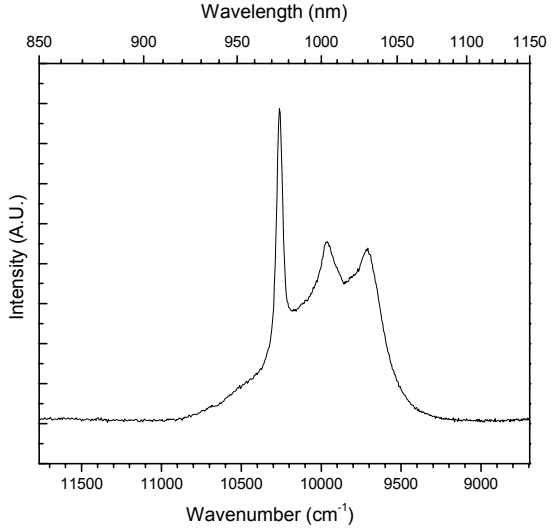


*Figure 4.31: Luminescence spectrum of [Yb(tta)$_3$**L$_{II}$**] at room temperature. The emission corresponds to the $^2F_{5/2} \rightarrow {}^2F_{7/2}$ transition.*

4.4 Conclusions

In this chapter, several liquid-crystalline metal complexes with a high coordination number (eight or nine) have been obtained by attaching mesogenic groups via a flexible alkyl spacer to the coordinating unit. The approach is illustrated for rhenium(I) complexes and for rare-earth complexes. Although we have chosen the 4-cyanobiphenyl group as the mesogenic promoter and a 1,10-phenanthroline derivative as the coordinating group, the concept of decoupling of the mesophase-inducing groups and the coordination groups can be extended to other mesogenic groups and ligands. Examples of possible mesogenic groups can be 4-alkoxybiphenyl or cholesteryl derivatives. This concept is different from other studies on metallomesogens, where the key idea to obtain high coordination number metallomesogens is to increase the number of long alkyl chains attached to the central metal core. The advantage of our approach is that in our case metallomesogens showing a nematic phase can be obtained, whereas metallomesogens with a large number of long alkyl chains often form columnar mesophases. Unconventional phases were also obtained for the rhenium(I) complexes bearing two or three cyanobiphenyl groups. An interesting feature of the rare-earth complexes studied in this work, is their good solubility in nematic liquid-crystal solvents, so that by a doping procedure luminescent liquid crystals can be obtained. In these anisotropic solvents, the crystal-field fine structure of the dissolved lanthanide complexes is well resolved.

4.5 Experimental section

The solution studies were performed by Dr. Tanja Parac-Vogt. Characterization of the mesophases by X-ray diffraction and following discussion was performed by Dr. Bertrand Donnio, Dr. Benoît Heinrich and Dr. Daniel Guillon. The molecular dynamics calculations were performed by Dr. Cyril Bourgogne. The luminescence spectra were recorded and discussed by Dr. Kris Driesen.

4.5.1 Techniques

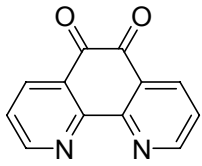
The nuclear magnetic resonance (NMR) spectra were recorded on a Bruker Avance 300 spectrometer (operating at 300 MHz) or a Bruker AMX-400 (operating at 400 MHz). FTIR spectra were recorded on a Bruker IFS-66 spectrometer, using the KBr pellet method. Elemental analyses were obtained on a CE Instruments EA-1110 elemental analyzer. Optical textures of the mesophases were observed with an Olympus BX60 polarizing microscope equipped with a LINKAM THMS600 hot stage and a LINKAM TMS93 programmable temperature-controller. DSC traces were recorded with a Mettler-Toledo DSC821e module. The XRD patterns were obtained with two different experimental setups, and in all cases, the powdered sample was filled in Lindemann capillaries of 1 mm diameter. A linear monochromatic CuKα_1 beam (λ = 1.5405 Å) obtained with a sealed-tube generator (900 W) and a bent quartz monochromator were used (both generator and monochromator were manufactured by Inel). One set of diffraction patterns was registered with a curved counter Inel CPS 120, for which the sample temperature is controlled within ±0.05 °C; periodicities up to 60 Å can be measured. The other set of diffraction patterns was registered on Image Plate. Periodicities up to 90 Å can be measured, and the sample temperature is controlled within ±0.3 °C. The molecular dynamics

calculations were performed on an SGI Origin 2800 20 CPU computer and on an SGI Octane workstation using the DISCOVER 3 molecular mechanics package from Accelrys (www.accelrys.com) with the esff force field. For all models, prior to the dynamics, the systems were minimized to a gradient of 0.1 kcal mol^{-1}. The simulation then consisted of a 50 ps cycle from 373 to 353 K, and a 200 ps isotherm at 353 K in the NVT-PBC ensemble and with a 1 fs time step.

Photoluminescence spectra have been recorded on an Edinburgh Instruments FS900 spectrofluorimeter. This instrument is equipped with a 450 W xenon arc lamp, a microsecond flashlamp and a red-sensitive photomultiplier (250-850 nm). All the photoluminescence spectra were recorded at room temperature and have been corrected for the sensitivity of the detector at the different wavelengths. The quantum yield of the europium sample was determined using an integrating sphere (150 mm diameter, $BaSO_4$ coating) of Edinburgh Instruments. The quantum yield can be defined as the integrated intensity of luminescence signal divided by the integrated intensity of the absorption signal. Only the intense luminescence band around 612 nm of the europium(III) emission was measured by the integrating sphere, but this intensity value was corrected by taking into account the relative intensity of the other transitions (as determined from the steady state luminescence spectrum. The absorption intensity was obtained by subtracting the integrated intensity of the light source (with the europium sample in the integrating sphere) from the integrated intensity of the light source (with a blank sample in the integrating sphere). The blank sample used contained the solvent DMF.

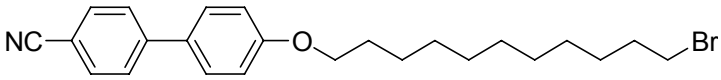
4.5.2 Synthesis

(a) 1,10-Phenanthroline-5,6-dione (10)



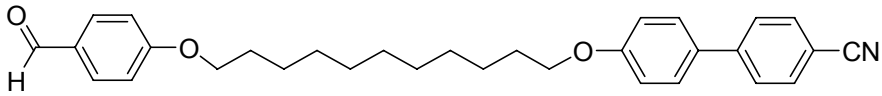
1,10-Phenanthroline monohydrate (0.0504 mol, 10.00 g) was added in small portions under stirring to 60 ml of concentrated sulfuric acid in a round-bottom flask (500 ml) equipped with a reflux condenser. After the solid compound was dissolved, sodium bromide (0.0504 mol, 5.19 g) was added, followed by 30 ml of 70% nitric acid. The mixture was heated to 105 °C for 6 hours. The temperature was then lowered to 95 °C and the reflux condenser was removed to allow the bromine vapors to escape for a period of 16 hours. After being cooled, the mixture was poured onto 800 g of ice and was carefully neutralized to pH 7 with about 300 ml of a 10 M solution of sodium hydroxide. The turbid solution was filtered and the solid residue was extracted with 5 × 200 ml of boiling water. The insoluble material was removed from the cooled extraction liquid by filtration and the combined aqueous solutions were extracted with dichloromethane, dried over anhydrous $MgSO_4$, and the solvent was removed under reduced pressure. The crude product was recrystallized from toluene to obtain orange crystals. Yield: 30% (3.18 g). δ_H (300 MHz, $CDCl_3$): 7.58–7.62 (dd, 2H, H-aryl, J_o = 8.1 Hz, J_o = 4.8 Hz), 8.53 (dd, 2H, H-aryl, J_o = 8.1 Hz, J_m = 1.8 Hz), 9.12 (dd, 2H, H-aryl, J_o = 4.8 Hz, J_m = 1.8 Hz). Calcd. for $C_{12}H_6N_2O_2 \cdot 0.33H_2O$: C 66.67, H 3.11, N 12.96. Found: C 67.25, H 2.77, N 12.99. M.p.: 257 °C (lit. m.p.: 258 °C[47]).

(b) 4'-(10-Bromodecyloxy)-4-cyanobiphenyl (11)



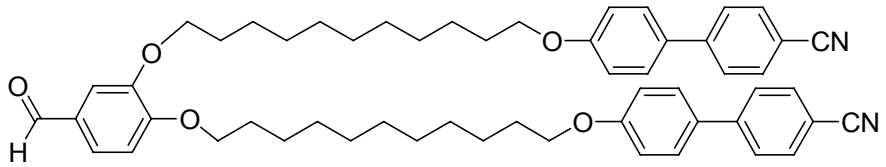
Bromide **11** was prepared by adding diisopropyl azodicarboxylate (DIAD) (0.0256 mol, 5.18 g) dropwise to an ice-cooled stirred solution of 4'-hydroxy-4-biphenylcarbonitrile (0.0256 mol, 5.00 g), 11-bromo-1-undecanol (0.0256 mol, 6.43 g) and triphenylphosphine (0.0256 mol, 6.72 g) in dry THF, in a nitrogen atmosphere. The solution was allowed to warm up to room temperature and stirred for 24 hours. The solvent was removed under reduced pressure and the crude product was purified on a silica column with $CHCl_3$ as the eluent. The product was recrystallized from hexane to obtain white crystals. Yield: 67% (7.35 g). δ_H (300 MHz, $CDCl_3$): 1.32–1.51 (m, 14H, CH_2), 1.82–1.92 (m, 4H, –C**H**$_2$–CH_2–Br and –C**H**$_2$–CH_2–O–), 3.42 (t, 2H, –C**H**$_2$–Br), 4.02 (t, 2H, –C**H**$_2$–O–), 7.02 (d, 2H, H-aryl, J_o = 8.8 Hz), 7.52 (d, 2H, H-aryl, J_o = 8.8 Hz), 7.63–7.72 (m, 4H, H-aryl). δ_C (75 MHz, $CDCl_3$): 26.43, 28.56, 29.15, 29.63, 29.75, 29.81, 29.85, 29.92, 33.24, 34.45, 68.57, 110.44, 115.50, 119.52, 127.47, 128.72, 131.64, 132.97, 145.69, 160.22. IR (KBr-pellet, cm^{-1}): 2918, 2850 (s, aliphatic C–H stretch), 2222 (m, ν(C≡N)). Calcd. for $C_{24}H_{30}BrNO$: C 67.29, H 7.06, N 3.27. Found: C 67.32, H 7.00, N 3.35. EI (m/z): 427.2, M^+. M.p.: 77 °C (a monotropic nematic phase is formed upon cooling at 66 °C).

(c) Aldehyde 12



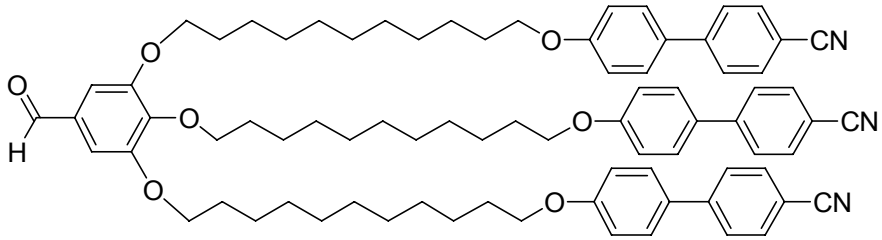
Aldehyde **12** was prepared by adding bromide **11** (0.0070 mol, 3.00 g) to a solution of 4-hydroxybenzaldehyde (0.0070 mol, 0.85 g) and potassium carbonate (0.0070 mol, 0.97 g) in 2-butanone (50 ml). A catalytic amount of potassium iodide was added and the mixture was refluxed for 24 hours protected by a guard tube. After the reaction mixture was cooled to room temperature, it was poured into 200 ml of water. The organic layer was separated and the aqueous layer was extracted with dichloromethane. The combined organic layers were dried over anhydrous $MgSO_4$ and the solvent was removed under reduced pressure. The crude product was recrystallized from ethyl acetate. Yield: 70% (2.30 g). δ_H (300 MHz, $CDCl_3$): 1.34–1.49 (m, 14H, CH_2), 1.80–1.87 (m, 4H, –C**H**$_2$–CH_2–O–), 4.00–4.07 (m, 4H, –C**H**$_2$–O–), 6.99–7.02 (m, 4H, H-aryl), 7.52 (d, 2H, H-aryl, J_o = 8.8 Hz), 7.63–7.72 (m, 4H, H-aryl), 7.83 (d, 2H, H-aryl, J_o = 8.1 Hz), 9.89 (s, 1H, CH=O). δ_C (75 MHz, $CDCl_3$): 26.37, 26.44, 29.46, 29.63, 29.73, 29.78, 29.93, 68.56, 68.82, 110.44, 115.15, 115.47, 119.53, 127.47, 128.72, 130.15, 131.66, 132.40, 132.97, 145.67, 160.20, 164.65, 191.23. IR (KBr-pellet, cm^{-1}): 2922, 2852 (s, aliphatic C–H stretch), 2222 (m, ν(C≡N)), 1689 (s, ν(C=O)). Calcd. for $C_{31}H_{35}NO_3 \cdot 0.33H_2O$: C 78.28, H 7.56, N 2.94. Found: C 78.38, H 7.08, N 2.97. ESI-MS (Acetonitrile, m/z): 470.3, $[M + H]^+$.

(d) Aldehyde 13



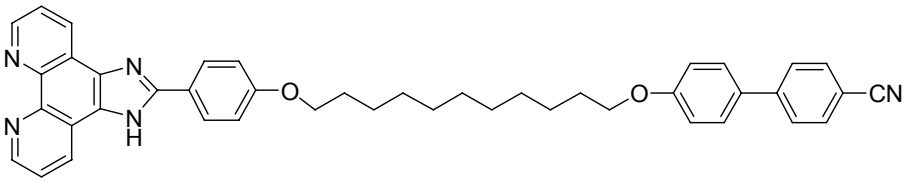
Aldehyde **13** was prepared by adding bromide **11** (0.0145 mol, 6.20 g) to a solution of 3,4-dihydroxybenzaldehyde (0.0072 mol, 1.00 g) and potassium carbonate (0.0145 mol, 2.00 g) in 2-butanone (100 ml). A catalytic amount of potassium iodide was added and the mixture was refluxed for 24 hours protected by a guard tube. After the reaction mixture was cooled to room temperature, it was poured into 200 ml of water. The organic layer was separated and the aqueous layer was extracted with dichloromethane. The combined organic layers were dried over anhydrous $MgSO_4$ and the solvent was removed under reduced pressure. The crude product was recrystallized from ethyl acetate. Yield: 60% (3.62 g). δ_H (300 MHz, $CDCl_3$): 1.34–1.49 (m, 28H, CH_2), 1.77–1.90 (m, 8H, –C**H**$_2$–CH_2–O–), 3.99–4.11 (m, 8H, –C**H**$_2$–O–), 6.95–7.01 (m, 5H, H-aryl), 7.41–7.44 (m, 2H, H-aryl), 7.52 (d, 4H, H-aryl, J_o = 8.0 Hz), 7.62–7.70 (m, 8H, H-aryl), 9.84 (s, 1H, CH=O). δ_C (75 MHz, $CDCl_3$): 26.37, 26.46, 29.38, 29.46, 29.64, 29.75, 29.81, 29.93, 29.98, 68.56, 69.50, 110.46, 111.29, 112.18, 115.48, 119.50, 127.06, 127.45, 128.70, 130.29, 131.64, 132.95, 145.66, 149.83, 155.05, 160.20, 191.39. IR (KBr-pellet, cm^{-1}): 2919, 2849 (s, aliphatic C–H stretch), 2224 (m, ν(C≡N)), 1685 (s, ν(C=O)). Calcd. for $C_{55}H_{64}N_2O_5$: C 79.29, H 7.74, N 3.36. Found: C 78.98, H 8.08, N 3.45. ESI-MS (Acetonitrile, m/z): 833.3, $[M + H]^+$.

(e) Aldehyde 14



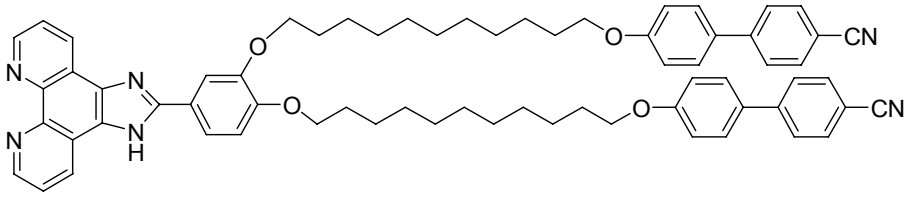
Aldehyde **14** was prepared by adding bromide **11** (0.0070 mol, 3.00 g) to a solution of 3,4,5-trihydroxybenzaldehyde monohydrate (0.0023 mol, 0.40 g) and potassium carbonate (0.0070 mol, 0.97 g) in 2-butanone (50 ml). A catalytic amount of potassium iodide was added and the mixture was refluxed for 24 hours protected by a guard tube. After the reaction mixture was cooled to room temperature, it was poured into 200 ml of water. The organic layer was separated and the aqueous layer was extracted with dichloromethane. The combined organic layers were dried over anhydrous $MgSO_4$ and the solvent was removed under reduced pressure. The crude product was recrystallized from toluene. Yield: 47% (1.30 g). δ_H (300 MHz, $CDCl_3$): 1.34–1.49 (m, 42H, CH_2), 1.77–1.87 (m, 12H, –C**H**$_2$–CH_2–O–), 3.98–4.10 (m, 12H, –C**H**$_2$–O–), 7.01 (dd, 6H, H-aryl, J_o = 8.8 Hz, J_m = 2.5 Hz), 7.10 (s, 2H, H-aryl), 7.52 (dd, 6H, H-aryl, J_o = 8.7 Hz, J_m = 1.9 Hz), 7.63–7.71 (m, 12H, H-aryl), 9.84 (s, 1H, CH=O). δ_C (75 MHz, $CDCl_3$): 26.44, 29.64, 29.76, 29.81, 29.95, 29.98, 30.04, 30.75, 68.56, 69.62, 74.01, 108.26, 110.46, 115.48, 119.49, 127.44, 128.70, 131.66, 131.87, 132.95, 144.22, 145.64, 153.91, 160.20, 191.65. IR (KBr-pellet, cm^{-1}): 2922, 2850 (s, aliphatic C–H stretch), 2222 (m, ν(C≡N)), 1693 (s, ν(C=O)). Calcd. for $C_{79}H_{93}N_3O_7$: C 79.30, H 7.83, N 3.51. Found: C 79.10, H 7.66, N 3.34. ESI-MS (MeOH, m/z): 1218.7, $[M + Na]^+$.

(f) Ligand L_I



Ligand $\mathbf{L_I}$ was prepared by adding aldehyde **12** (0.0021 mol, 1.00 g) to a warm solution of 1,10-phenanthroline-5,6-dione (0.0021 mol, 0.45 g) and ammonium acetate (0.0085 mol, 0.66 g) in 30 ml of glacial acetic acid. The mixture was heated to 90 °C for 3 hours. After the reaction mixture was cooled to room temperature, it was poured into 100 ml of water and neutralized to pH 7 with an aqueous ammonia solution. The precipitate was filtered, washed with distilled water and dried. The crude product was purified on a silica column with $CHCl_3$/MeOH (90:10) as the eluent. Since the compound holds solvents firmly, it was dried in a vacuum oven at 60 °C. Yield: 36% (0.50 g). δ_H (400 MHz, DMSO-d6, 333K): 1.31–1.50 (m, 14H, CH_2), 1.69–1.80 (m, 4H, –C**H**$_2$–CH_2–O–), 4.01 (t, 2H, –C**H**$_2$–O–), 4.09 (t, 2H, –C**H**$_2$–O–), 7.02 (d, 2H, H-aryl, J_o = 8.8 Hz), 7.15 (d, 2H, H-aryl, J_o = 8.8 Hz), 7.62 (d, 2H, H-aryl, J_o = 8.8 Hz), 7.76–7.81 (m, 6H, H-aryl), 8.20 (d, 2H, H-aryl, J_o = 8.9 Hz), 8.90 (d, 2H, H-aryl, J_o = 7.3 Hz), 9.03 (d, 2H, H-aryl, J_o = 4.2 Hz), 13.40 (b, s, 1H, N–H). δ_C (100 MHz, DMSO-d6, 333K): 25.44, 28.66, 28.78, 28.84, 28.95, 67.87, 67.95, 109.25, 115.06, 115.28, 118.81, 122.75, 123.07, 126.81, 127.90, 128.20, 129.40, 130.45, 132.62, 143.66, 144.39, 147.54, 150.90, 159.49, 160.08. IR (KBr-pellet, cm^{-1}): 3404 (m, ν(N–H)), 2920, 2850 (s, aliphatic C–H stretch), 2224 (m, ν(C≡N)). Calcd. for $C_{43}H_{41}N_5O_2 \cdot H_2O$: C 76.19, H 6.39, N 10.33. Found: C 76.51, H 6.22, N 9.87. ESI-MS (Acetonitrile, m/z): 660.5, $[M + H]^+$.

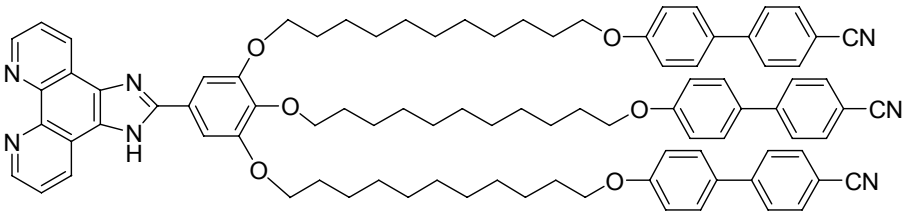
(g) Ligand L_{II}



Ligand **L_{II}** was prepared by adding aldehyde **13** (0.0024 mol, 2.00 g) to a warm solution of 1,10-phenanthroline-5,6-dione (0.0024 mol, 0.50 g) and ammonium acetate (0.0096 mol, 0.74 g) in 30 ml of glacial acetic acid. The mixture was heated to 90 °C for 3 hours. After the reaction mixture was cooled to room temperature, it was poured into 100 ml of water and neutralized to pH 7 with an aqueous ammonia solution. The precipitate was filtered, washed with distilled water and dried. The crude product was purified on a silica column with $CHCl_3$/MeOH (90:10) as the eluent. Since the compound holds solvents firmly, it was dried in a vacuum oven at 60 °C. Yield: 35% (0.86 g). δ_H (400 MHz, DMSO-d6, 333K): 1.27–1.47 (m, 28H, CH_2), 1.64–1.76 (m, 8H, –C**H**$_2$–CH_2–O–), 3.92–3.96 (m, 4H, –C**H**$_2$–O–), 4.03–4.10 (m, 4H, –C**H**$_2$–O–), 6.96 (dd, 4H, H-aryl, J_o = 8.8 Hz, J_m = 2.4 Hz), 7.13 (d, 1H, H-aryl, J_o = 8.2 Hz), 7.56 (d, 4H, H-aryl, J_o = 8.8 Hz), 7.72 (d, 4H, H-aryl, J_o = 8.5 Hz), 7.75–7.79 (m, 6H, H-aryl), 7.87 (m, 2H, H-aryl), 8.91 (d, 2H, H-aryl, J_o = 8.1 Hz), 9.01 (d, 2H, H-aryl, J_o = 4.1 Hz), 13.55 (b, s, 1H, N–H). δ_C (100 MHz, DMSO-d6, 333K): 25.06, 25.15, 25.17, 28.29, 28.32, 28.35, 28.43, 28.45, 28.51, 28.56, 28.63, 67.42, 68.50, 68.97, 108.84, 112.65, 114.02, 114.78, 118.37, 119.49, 122.65, 122.80, 126.33, 127.72, 129.23, 129.99, 132.17, 142.99, 143.92, 147.02, 148.74, 150.20, 150.56, 159.05. IR (KBr-pellet, cm^{-1}): 3435 (s, ν(N–H)), 2924, 2853 (s, aliphatic C–H stretch), 2224 (m, ν(C≡N)). Calcd. for

$C_{67}H_{70}N_6O_4 \cdot H_2O$: C 77.28, H 6.97, N 8.07. Found: C 77.76, H 6.99, N 8.11. ESI-MS (Acetonitrile, m/z): 1023.5, $[M + H]^+$.

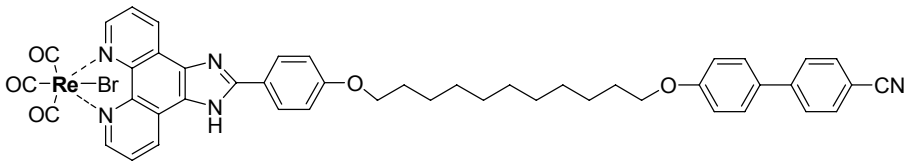
(h) Ligand L_{III}



Ligand $\mathbf{L_{III}}$ was prepared by adding aldehyde **14** (0.58 mmol, 0.700 g) to a warm solution of 1,10-phenanthroline-5,6-dione (0.58 mmol, 0.123 g) and ammonium acetate (5.8 mmol, 0.450 g) in 30 ml of glacial acetic acid. The mixture was heated to 90 °C for 3 hours. After the reaction mixture was cooled to room temperature, it was poured into 100 ml of water and neutralized to pH 7 with an aqueous ammonia solution. The precipitate was filtered, washed with distilled water and dried. The crude product was purified on a silica column with $CHCl_3$/MeOH (90:10) as the eluent. Since the compound holds solvents firmly, it was dried in a vacuum oven at 60 °C. Yield: 25% (0.200 g). δ_H (300 MHz, DMSO-d6, 343K): 1.27–1.52 (m, 42H, CH_2), 1.69–1.83 (m, 12H, –C**H**$_2$–CH_2–O–), 3.97–3.99 (m, 8H, –C**H**$_2$–O–), 4.15 (t, 4H, –C**H**$_2$–O–), 7.00 (d, 6H, H-aryl, J_o = 8.1 Hz), 7.59–7.62 (m, 8H, H-aryl), 7.76 (m, 14H, H-aryl), 8.90 (d, 2H, H-aryl, J_o = 7.7 Hz), 9.02 (b, s, 2H, H-aryl). δ_C (100 MHz, DMSO-d6, 333K): 25.43, 25.59, 28.68, 28.71, 28.81, 28.89, 28.91, 28.98, 29.02, 29.85, 67.82, 69.16, 72.74, 105.81, 109.23, 115.19, 118.77, 122.98, 125.19, 126.74, 128.13, 128.84, 129.47, 130.41, 132.58, 139.58, 143.76, 144.33, 147.65, 150.75, 153.09, 159.45. IR (KBr-pellet, cm^{-1}): 3446 (m, ν(N–H)), 2924, 2852 (s,

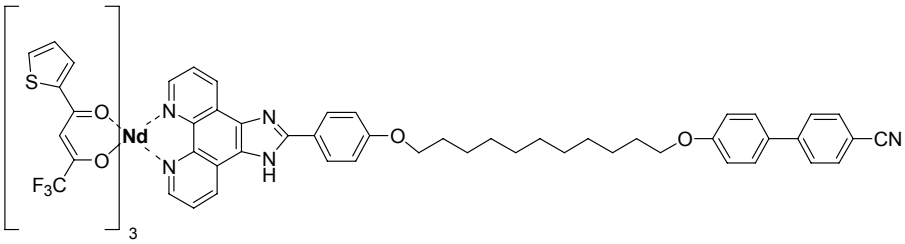
aliphatic C–H stretch), 2224 (m, ν(C≡N)). Calcd. for $C_{91}H_{99}N_7O_6 \cdot H_2O$: C 77.80, H 7.25, N 6.98. Found: C 77.38, H 7.21, N 6.74. ESI-MS (Acetonitrile, m/z): 1386.7, $[M + H]^+$.

(i) Rhenium(I) complex $[ReBr(CO)_3L_I]$



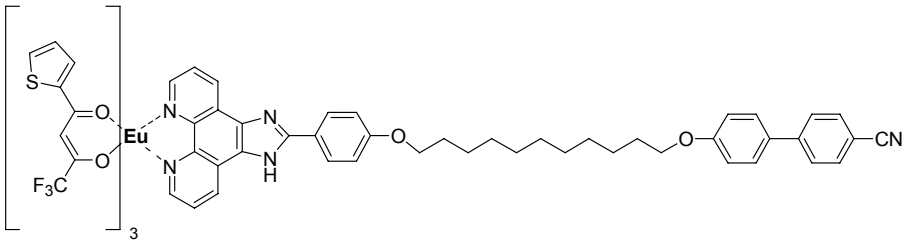
Rhenium(I) complex $[ReBr(CO)_3\mathbf{L_I}]$ was prepared by adding rhenium(I) pentacarbonyl bromide, $[ReBr(CO)_5]$ (0.17 mmol, 0.068 g) to a solution of ligand $\mathbf{L_I}$ (0.17 mmol, 0.110 g) in toluene. The mixture was refluxed for 3 hours. Then the solvent was removed under reduced pressure and the crude product was purified on a silica column with $CHCl_3$/MeOH (95:5) as the eluent. The complex was dissolved in a minimum amount of $CHCl_3$ and precipitated in hexane. The yellow precipitate was filtered off and dried in a vacuum oven at 60 °C. Yield: 45% (0.077 g). IR (KBr-pellet, cm^{-1}): 3404 (m, ν(N–H)), 2926, 2852 (s, aliphatic C–H stretch), 2226 (m, ν(C≡N)). Calcd. for $C_{46}H_{41}BrN_5O_5Re \cdot H_2O$: C 53.75, H 4.22, N 6.81. Found: C 53.87, H 4.20, N 6.63. ESI-MS (Acetonitrile, m/z): 1008.1, $[M - H]^-$.

(j) Neodymium complex [Nd(tta)$_3$L$_I$]



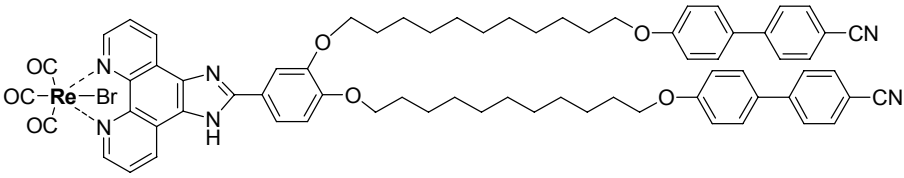
Neodymium(III) complex [Nd(tta)$_3$**L$_I$**] was prepared by adding a solution of Nd(tta)$_3$.2H$_2$O (0.076 mmol, 0.064 g) in $CHCl_3$ to a solution of ligand **L$_I$** (0.076 mmol, 0.050 g) in $CHCl_3$. The mixture was refluxed for 1 hour. Then the solvent was removed under reduced pressure. The product was dissolved in a minimum amount of $CHCl_3$ and precipitated in hexane. The yellow precipitate was filtered off and dried in a vacuum oven at 60 °C. Yield: 80% (0.089 g). IR (KBr-pellet, cm^{-1}): 3406 (m, ν(N–H)), 2928, 2854 (s, aliphatic C–H stretch), 2226 (m, ν(C≡N)). Calcd. for $C_{67}H_{53}F_9N_5NdO_8S_3 \cdot H_2O$: C 54.17, H 3.73, N 4.71. Found: C 54.15, H 3.76, N 4.84. ESI-MS (Acetonitrile, m/z): 1466.9, $[M - H]^-$.

(k) Europium complex [Eu(tta)$_3$L$_I$]



Europium(III) complex [Eu(tta)$_3$**L$_I$**] was prepared starting from ligand **L$_I$** (0.076 mmol, 0.050 g) and Eu(tta)$_3$·2H$_2$O (0.076 mmol, 0.065g) using the procedure described for the Nd-complex **Nd-L**[4] to yield the product as a yellow powder. Yield: 80% (0.090 g). IR (KBr-pellet, cm^{-1}): 3446 (m, ν(N–H)), 2928, 2854 (s, aliphatic C–H stretch), 2226 (m, ν(C≡N)). Calcd. for $C_{67}H_{53}EuF_9N_5O_8S_3 \cdot H_2O$: C 53.89, H 3.71, N 4.69. Found: C 53.55, H 3.68, N 4.78. ESI-MS (Acetonitrile, m/z): 1473.9, $[M - H]^-$.

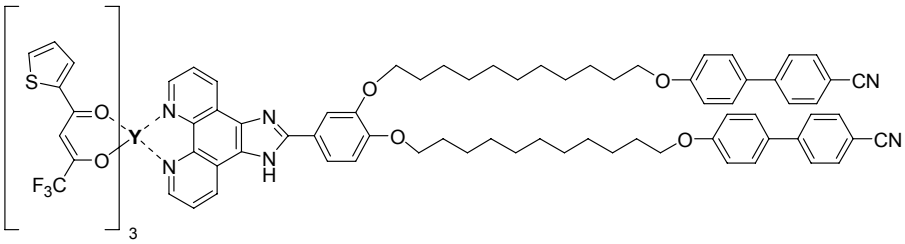
(l) Rhenium(I) complex [ReBr(CO)$_3$L$_{II}$]



Rhenium(I) complex [ReBr(CO)$_3$**L$_{II}$**] was prepared by adding rhenium(I) pentacarbonyl bromide, [ReBr(CO)$_5$] (0.098 mmol, 0.040 g) to a solution of ligand **L$_{II}$** (0.098 mmol, 0.100 g) in toluene. The mixture was refluxed for 3 hours. Then the solvent was removed under reduced pressure and the crude product was purified on a silica column with CHCl$_3$/MeOH (95:5) as the eluent. The complex was dissolved in a minimum amount of CHCl$_3$ and

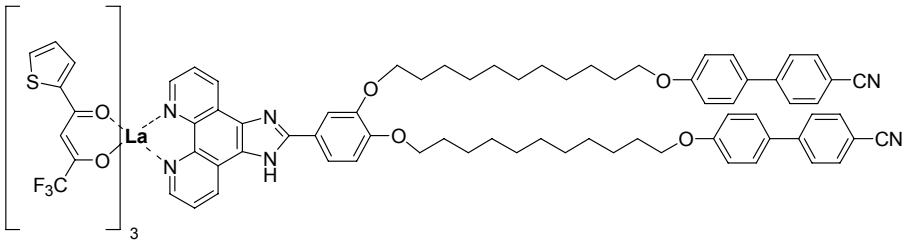
precipitated in hexane. The yellow precipitate was filtered off and dried in a vacuum oven at 60 °C. Yield: 75% (0.100 g). IR (KBr-pellet, cm^{-1}): 3430 (m, ν(N–H)), 2926, 2853 (s, aliphatic C–H stretch), 2225 (m, ν(C≡N)). Calcd. for $C_{70}H_{70}BrN_6O_7Re \cdot H_2O$: C 60.42, H 5.22, N 6.04. Found: C 60.52, H 5.18, N 6.00. ESI-MS (Acetonitrile, m/z): 1371.4, $[M - H]^-$.

(m) Yttrium complex of ligand $[Y(tta)_3L_{II}]$



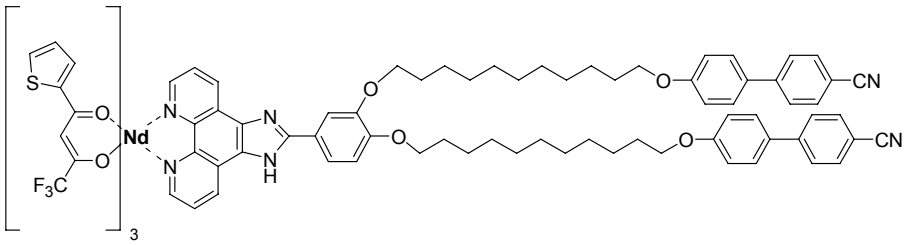
Yttrium(III) complex $[Y(tta)_3\mathbf{L_{II}}]$ was prepared by adding a solution of $Y(tta)_3 \cdot 2H_2O$ (0.098 mmol, 0.077g) in $CHCl_3$ to a solution of ligand $\mathbf{L_{II}}$ (0.098 mmol, 0.100 g) in $CHCl_3$. The mixture was refluxed for 1 hour. Then the solvent was removed under reduced pressure. The product was dissolved in a minimum amount of $CHCl_3$ and precipitated in hexane. The yellow precipitate was filtered off and dried in a vacuum oven at 60 °C. Yield: 88% (0.154 g). IR (KBr-pellet, cm^{-1}): 3406 (m, ν(N–H)), 2927, 2854 (s, aliphatic C–H stretch), 2225 (m, ν(C≡N)). Calcd. for $C_{91}H_{82}F_9N_6O_{10}S_3Y \cdot H_2O$: C 60.93, H 4.72, N 4.69. Found: C 61.22, H 4.70, N 4.62. ESI-MS (Acetonitrile, m/z): 1774.1, $[M - H]^-$.

(n) Lanthanum complex [La(tta)$_3$L$_{II}$]



Lanthanum(III) complex [La(tta)$_3$**L$_{II}$**] was prepared starting from ligand **L$_{II}$** (0.098 mmol, 0.100 g) and La(tta)$_3$·2H$_2$O (0.098 mmol, 0.082g) using the procedure described for the Y-complex to yield the product as a yellow powder. Yield: 79% (0.141 g). IR (KBr-pellet, cm^{-1}): 3411 (m, ν(N–H)), 2927, 2854 (s, aliphatic C–H stretch), 2225 (m, ν(C≡N)). Calcd. for $C_{91}H_{82}F_9LaN_6O_{10}S_3 \cdot H_2O$: C 59.28, H 4.59, N 4.56. Found: C 58.85, H 4.49, N 4.26. ESI-MS (Acetonitrile, m/z): 1824.2, [M - H]$^-$.

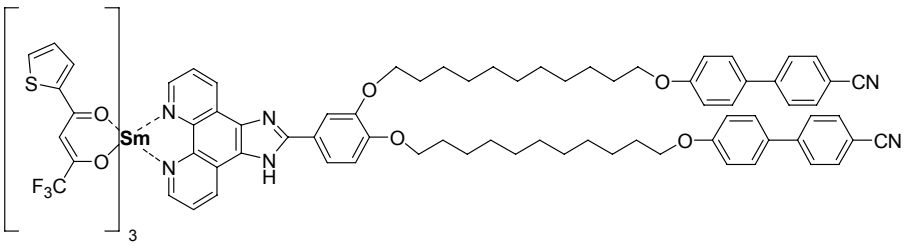
(o) Neodymium complex [Nd(tta)$_3$L$_{II}$]



Neodymium(III) complex [Nd(tta)$_3$**L$_{II}$**] was prepared starting from ligand **L$_{II}$** (0.098 mmol, 0.100 g) and Nd(tta)$_3$·2H$_2$O (0.098 mmol, 0.082 g) using the procedure described for the Y-complex to yield the product as a yellow powder. Yield: 84% (0.150 g). IR (KBr-pellet, cm^{-1}): 3431 (m, ν(N–H)),

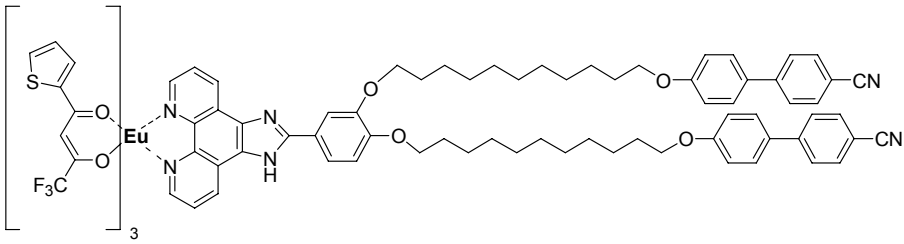
2927, 2854 (s, aliphatic C–H stretch), 2228 (m, ν(C≡N)). Calcd. for $C_{91}H_{82}F_9N_6NdO_{10}S_3 \cdot H_2O$: C 59.11, H 4.58, N 4.54. Found: C 59.16, H 4.61, N 4.43. ESI-MS (Acetonitrile, m/z): 1829.9, $[M - H]^-$.

(p) Samarium complex $[Sm(tta)_3L_{II}]$



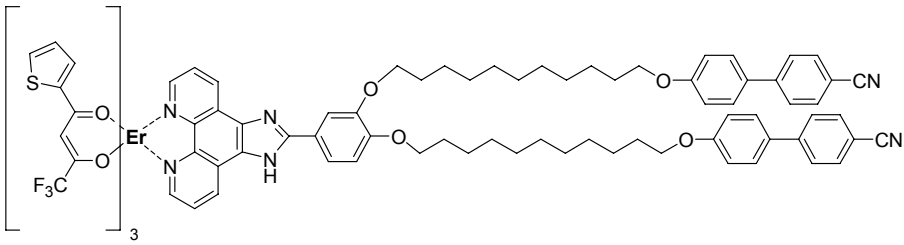
Samarium(III) complex $[Sm(tta)_3\mathbf{L_{II}}]$ was prepared starting from ligand $\mathbf{L_{II}}$ (0.098 mmol, 0.100 g) and $Sm(tta)_3 \cdot 2H_2O$ (0.098 mmol, 0.083 g) using the procedure described for the Y-complex to yield the product as a yellow powder. Yield: 81% (0.146 g). IR (KBr-pellet, cm^{-1}): 3421 (m, ν(N–H)), 2927, 2854 (s, aliphatic C–H stretch), 2225 (m, ν(C≡N)). Calcd. for $C_{91}H_{82}F_9N_6O_{10}S_3Sm \cdot H_2O$: C 58.91, H 4.56, N 4.53. Found: C 59.13, H 4.47, N 4.40. ESI-MS (Acetonitrile, m/z): 1835.7, $[M - H]^-$.

(q) Europium complex [Eu(tta)$_3$L$_{II}$]



Europium(III) complex [Eu(tta)$_3$**L$_{II}$**] was prepared starting from ligand **L$_{II}$** (0.098 mmol, 0.100 g) and Eu(tta)$_3$·2H$_2$O (0.098 mmol, 0.084g) using the procedure described for the Y-complex to yield the product as a yellow powder. Yield: 85% (0.150 g). IR (KBr-pellet, cm^{-1}): 3431 (m, ν(N–H)), 2926, 2853 (s, aliphatic C–H stretch), 2225 (m, ν(C≡N)). Calcd. for $C_{91}H_{82}EuF_9N_6O_{10}S_3 \cdot H_2O$: C 58.86, H 4.56, N 4.53. Found: C 59.30, H 4.08, N 4.38. ESI-MS (Acetonitrile, m/z): 1836.9, $[M - H]^-$.

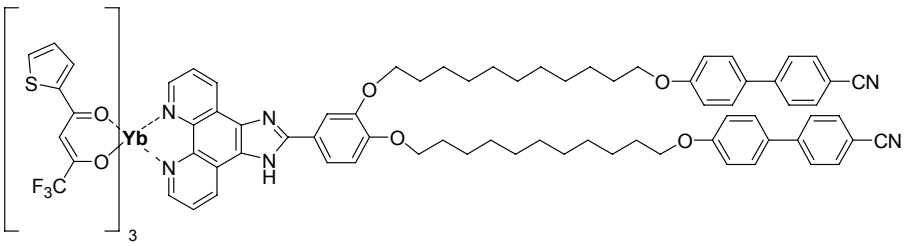
(r) Erbium complex [Er(tta)$_3$L$_{II}$]



Erbium(III) complex[Er(tta)$_3$**L$_{II}$**] was prepared starting from ligand **L$_{II}$** (0.098 mmol, 0.100 g) and Er(tta)$_3$·2H$_2$O (0.098 mmol, 0.085g) using the procedure described for the Y-complex to yield the product as a yellow powder. Yield: 81% (0.147 g). IR (KBr-pellet, cm^{-1}): 3406 (m, ν(N–H)),

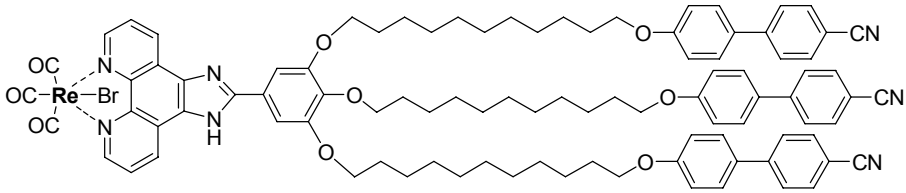
2927, 2854 (s, aliphatic C–H stretch), 2225 (m, ν(C≡N)). Calcd. for $C_{91}H_{82}ErF_9N_6O_{10}S_3 \cdot H_2O$: C 58.38, H 4.52, N 4.49. Found: C 58.73, H 4.47, N 4.43. ESI-MS (Acetonitrile, m/z): 1851.1, $[M - H]^-$.

(s) Ytterbium complex [Yb(tta)$_3$L$_{II}$]



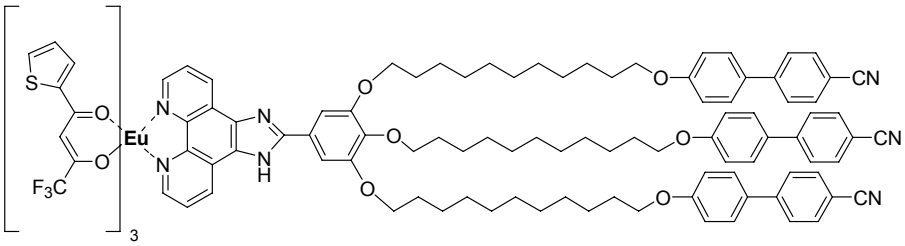
Ytterbium(III) complex [Yb(tta)$_3$**L$_{II}$**] was prepared starting from ligand **L$_{II}$** (0.098 mmol, 0.100 g) and Yb(tta)$_3$·2H$_2$O (0.098 mmol, 0.086g) using the procedure described for the Y-complex to yield the product as a yellow powder. Yield: 84% (0.153 g). IR (KBr-pellet, cm^{-1}): 3421 (m, ν(N–H)), 2927, 2854 (s, aliphatic C–H stretch), 2225 (m, ν(C≡N)). Calcd. for $C_{91}H_{82}F_9N_6O_{10}S_3Yb \cdot H_2O$: C 58.20, H 4.51, N 4.48. Found: C 58.28, H 4.42, N 4.29. ESI-MS (Acetonitrile, m/z): 1857.8, $[M - H]^-$.

(t) Rhenium(I) complex [ReBr(CO)$_3$L$_{III}$]



Rhenium(I) complex [ReBr(CO)$_3$**L$_{III}$**] was prepared by adding rhenium(I) pentacarbonyl bromide, [ReBr(CO)$_5$] (0.043 mmol, 0.018 g) to a solution of ligand **L$_{III}$** (0.043 mmol, 0.060 g) in toluene. The mixture was refluxed for 3 hours. Then the solvent was removed under reduced pressure and the crude product was purified on a silica column with $CHCl_3$/MeOH (95:5) as the eluent. The complex was dissolved in a minimum amount of $CHCl_3$ and precipitated in hexane. The yellow precipitate was filtered off and dried in a vacuum oven at 60 °C. Yield: 47% (0.035 g). IR (KBr-pellet, cm^{-1}): 3446 (m, ν(N–H)), 2922, 2850 (s, aliphatic C–H stretch), 2224 (m, ν(C≡N)). Calcd. for $C_{94}H_{99}BrN_7O_9Re \cdot H_2O$: C 64.33, H 5.80, N 5.59. Found: C 64.12, H 5.69, N 5.42. ESI-MS (Acetonitrile, m/z): 1734.4, $[M - H]^-$.

(u) Europium complex [Eu(tta)$_3$L$_{III}$]



Europium(III) complex [Eu(tta)$_3$**L$_{III}$**] was prepared by adding a solution of Eu(tta)$_3$·2H$_2$O (0.054 mmol, 0.046 g) in $CHCl_3$ to a solution of ligand **L$_{III}$** (0.054 mmol, 0.075 g) in $CHCl_3$. The mixture was refluxed for 1 hour. Then the solvent was removed under reduced pressure. The product was dissolved in a minimum amount of $CHCl_3$ and precipitated in hexane. The yellow precipitate was filtered off and dried in a vacuum oven at 60 °C. Yield: 88% (0.105 g). IR (KBr-pellet, cm^{-1}): 3448 (m, ν(N–H)), 2926, 2852 (s, aliphatic C–H stretch), 2226 (m, ν(C≡N)). Calcd. for $C_{115}H_{111}EuF_9N_7O_{12}S_3·H_2O$: C 62.21, H 5.13, N 4.42. Found: C 62.41, H 5.18, N 4.58. ESI-MS (Acetonitrile, m/z): 1099.7, $[M - 2H]^{2-}$.

4.6 References

1. (a) Neve, F.; Ghedini, M.; De Munno, G.; Levelut, A. M. *Chem. Mater*. **1995**, *7*, 688. (b) Douce, L.; El-ghayoury, A.; Skoulios, A.; Ziessel, R. *Chem. Commun*. **1999**, 2033. (c) Ziessel, R.; Douce, L.; El-ghayoury, A.; Harriman, A.; Skoulios, A. *Angew. Chem.*, *Int. Ed*. **2000**, *39*, 1489. (d) Giménez, R.; Manrique, A. B.; Uriel, S.; Barbera, J.; Serrano, J. L. *Chem. Commun.* **2004**, 2064.
2. Bruce, D. W. *Adv. Mater.* **1994**, *6*, 699.
3. (a) Lattermann, G.; Schmidt, S.; Kleppinger, R.; Wendorf, J. H. *Adv. Mater*. **1992**, *4*, 30. (b) Schmidt, S.; Lattermann, G.; Kleppinger, R.; Wendorff, J. H. *Liq. Cryst*. **1994**, *16*, 693. (c) Walf, G. H.; Benda, R.; Litterst, F. J.; Stebani, U.; Schmidt, S.; Lattermann, G. *Chem. Eur. J*. **1998**, *4*, 93.
4. (a) Bruce, D. W.; Liu, X. H. *J. Chem. Soc., Chem. Commun.* **1994**, 729. (b) Morrone, S.; Harrison, G.; Bruce, D. W. *Adv. Mater*. **1995**, *7*, 665. (c) Morrone, S.; Guillon, D.; Bruce, D. W. *Inorg. Chem*. **1996**, *35*, 7041.
5. (a) Ghedini, M.; Pucci, D.; Crispini, A.; Barberio, G. *Organometallics* **1999**, *18*, 2116. (b) Ghedini, M; Pucci, D.; Barberio, G. *Liq. Cryst.* **2000**, *27*, 1277.
6. (a) Galyametdinov, Yu. G.; Ivanova, G. I.; Ovchinnikov, I. V. *Bull. Acad. Sci. USSR, Div. Chem. Sci. (Engl. Transl.)* **1991**, *40*, 1109; *Izv. Akad. Nauk SSSR, Ser. Khim.* **1991**, 1232. (b) Galyametdinov, Yu.; Athanassopoulou, M. A.; Griesar, K.; Kharitonova, O.; Soto Bustamante, E. A.; Tinchurina, L.; Ovchinnikov, I.; Haase, W. *Chem. Mater.* **1996**, *8*, 922. (c) Binnemans, K.; Bruce, D. W.; Collinson, S. R.; Van Deun, R.; Galyametdinov, Yu. G.; Martin, F. *Philos. Trans. R. Soc. London, Ser. A* **1999**, *357*, 3063.

(d) Binnemans, K.; Galyametdinov, Yu. G.; Van Deun, R.; Bruce, D. W.; Collinson, S. R.; Polishchuk, A. P.; Bikchantaev, I.; Haase, W.; Prosvirin, A.V.; Tinchurina, L.; Litvinov, I.; Gubajdullin, A.; Rakhmatullin, A.; Uytterhoeven, K.; Van Meervelt, L. *J. Am. Chem. Soc.* **2000**, *122*, 4335. (e) Binnemans, K.; Lodewyckx, K. *Angew. Chem.* **2001**, *113*, 248; *Angew. Chem.*, *Int. Ed.* **2001**, *40*, 242. (f) Binnemans, K.; Lodewyckx, K.; Donnio, B.; Guillon, D. *Chem. Eur. J*. **2002**, *8*, 1101. (g) Binnemans, K.; Sleven, J.; De Feyter, S.; De Schryver, F. C.; Donnio, B.; Guillon, D. *Chem. Mater.* **2003**, *15*, 3930.

7. (a) Nozary, H.; Piguet, C.; Rivera, J.-P.; Tissot, P.; Morgantini, P.-Y.; Weber, J.; Bernardinelli, G.; Bünzli, J.-C. G.; Deschenaux, R.; Donnio, B.; Guillon, D. *Chem. Mater.* **2002**, *14*, 1075. (b) Terazzi, E.; Benech, J. M.; Rivera, J. P.; Bernardinelli, G.; Donnio, B.; Guillon, D.; Piguet, C. *Dalton Trans.* **2003**, 769. (c) Suarez, S.; Mamula, O.; Imbert, D.; Piguet, C.; Bünzli, J. C. G. *Chem. Commun.* **2003**, 1226. (d) Guillet, E.; Imbert, D.; Scopelliti, R.; Bünzli, J. C. G. *Chem. Mater.* **2004**, *16*, 4063. (e) Terazzi, E.; Torelli, S.; Bernardinelli, G.; Rivera, J.-P.; Benech, J.-M.; Bourgogne, C.; Donnio, B.; Guillon, D.; Imbert, D.; Bünzli, J.-C. G.; Pinto, A.; Jeannerat, D.; Piguet, C. *J. Am. Chem. Soc.* **2005**, *127*, 888. (f) Terazzi, E.; Suarez, S.; Torelli, S.; Nuzary, H.; Imbert, D.; Mamula, O.; Rivera, J.-P.; Guillet, E.; Benech, J.-M.; Bernardinelli, G.; Scopelliti, R.; Donnio, B.; Guillon, D.; Bünzli, J.-C. G.; Piguet, C. *Adv. Funct. Mater.* **2006**, *16*, 157.

8. Marcos, M.; Omenat, A.; Barbera, J.; Duran, F.; Serrano, J. L. *J. Mater. Chem.* **2004**, *14*, 3321.

9. (a) Zheng, H.; Swager T. M. *J. Am. Chem. Soc*. **1994**, *116*, 761. (b) Swager, T. M.; Zheng, H. *Mol. Cryst. Liq. Cryst*. **1995**, *260*, 301.

(c) Trzaska, S. T.; Hsu, H. F.; Swager, T. M. *J. Am. Chem. Soc*. **1999**, *121*, 4518; Corrigendum, *ibid*. 4544.

10. Trzaska, S. T.; Zheng, H.; Swager, T. M. *Chem. Mater*. **1999**, *11*, 130.
11. Deschenaux, R.; Goodby, J. W. *Ferrocene-Containing Thermotropic Liquid Crystals*. In: *Ferrocene: Homogeneous Catalysis, Organic Synthesis, Materials Science*; Togni, A., Hayashi, T., Eds.; VCH: Weinheim, Germany, 1995; Chapter 9, pp 471-495.
12. (a) Rowe, K. E.; Bruce, D. W. *J. Mater. Chem*. **1998**, *8*, 331. (b) Rowe, K. E.; Bruce D. W. *J. Chem. Soc., Dalton Trans*. **1996**, 3913. (c) Rowe, K. E.; Bruce, D. W. *Mol. Cryst. Liq. Cryst*. **1999**, *326*, 15. (d) Jacq, P.; Malthête, J. *Liq. Cryst*. **1996**, *21*, 291. (e) Campillos, E.; Deschenaux, R.; Levelut, A. M.; Ziessel, R. *J. Chem. Soc., Dalton Trans*. **1996**, 2533. (f) Seo, J. S.; Yoo, Y. S.; Choi, M. G. *J. Mater. Chem*. **2001**, *11*, 1332.
13. (a) Chuard, T.; Deschenaux, R. *Helv. Chim. Acta* **1996**, *79*, 736. (b) Chuard, T.; Deschenaux, R.; Hirsch, A.; Schönberger, H. *Chem. Commun.* **1999**, 2103. (c) Dardel, B.; Deschenaux, R.; Even, M.; Serrano, E. *Macromolecules* **1999,** *32*, 5193. (d) Dardel, B.; Guillon, D.; Heinrich, B.; Deschenaux, R. *J. Mater. Chem.* **2001**, *11*, 2814.
14. (a) Mehl, G. H.; Saez, I. M. *Appl. Organomet. Chem*. **1999**, *13*, 261. (b) Saez, I. M.; Goodby, J. W. *J. Mater. Chem.* **2001**, *11*, 2845. (c) Saez, I. M.; Goodby, J. W. *Liq. Cryst.* **1999**, *26*, 1101. (d) Saez, I. M.; Goodby, J. W. *J. Mater. Chem.* **2005**, *15*, 26.
15. Binnemans, K.; Lodewyckx, K.; Parac-Vogt, T. N.; Van Deun, R.; Goderis, B.; Tinant, B.; Van Hecke, K.; Van Meervelt, L. *Eur. J. Inorg. Chem*. **2003**, 3028.

16. Galyametdinov, Yu. G.; Malykhina, L. V.; Haase, W.; Driesen, K.; Binnemans, K. *Liq. Cryst.* **2002**, *29*, 1581.

17. (a) Zhong, G. L.; Kim, K.; Jin, J. I. *Synth. Met*. **2002**, *129*, 193. (b) Adachi, C.; Baldo, M. A.; Forrest, S. R. *J. Appl. Phys.* **2000**, *87*, 8049. (c) Sano, T.; Fujita, M.; Fujii, T.; Hamada, Y.; Shibata, K.; Kuroki, K. *Jpn. J. Appl. Phys.*, **1995**, *34*, 1883. (d) Li, H. H.; Inoue, S.; Machida, K.; Adachi, G. *Chem. Mater*. **1999**, *11*, 3171. (e) Kido, J.; Okamoto, Y. *Chem. Rev*. **2002**, *102*, 2357. (f) Binnemans, K. Rare-Earth β-Diketonates. In: *Handbook on the Physics and Chemistry of Rare Earths*; Gschneidner, K. A., Bünzli, J. C. G., Jr., Pecharsky, V. K., Eds.; Elsevier: Amsterdam, 2005; Vol. 35, Chapter 225, pp 107-272.

18. (a) Binnemans, K.; Lenaerts, P.; Driesen, K.; Görller-Walrand, C. *J. Mater. Chem.* **2004**, *14*, 191. (b) Lenaerts, P.; Ryckebosch, E.; Driesen, K.; Van Deun, R.; Nockemann, P.; Görller-Walrand, C.; Binnemans, K. *J. Lumin.* **2005**, *114*, 77.

19. Lenaerts, P.; Driesen, K.; Van Deun, R.; Binnemans, K. *Chem. Mater.* **2005**, *17*, 2148.

20. Hiort, C.; Lincoln, P.; Norden, B. *J. Am. Chem. Soc.* **1993**, *115*, 3448.

21. Steck, E. A.; Day, A. R. *J. Am. Chem. Soc.* **1943**, *65*, 452.

22. Mitsunobu, O. *Synthesis* **1981**, 1.

23. (a) Imrie, C. T.; Karasz, F. E.; Attard, G. S. *J. Macromol. Sci.*, *Part A* **1994**, *31*, 1221. (b) Everaars, M. D.; Marcelis, A. T. M.; Sudholter, E. J. R. *Langmuir* **1996**, *12*, 3964. (c) Percec, V.; Asandei, A. D.; Hill, D. H.; Crawford, D. *Macromolecules* **1999**, *32*, 2597. (d) Cook, A.; Badriya, S.; Greenfield, S.; McKeown, N. B. *J. Mater. Chem.* **2002**, *12***,** 2675. (e) Kouwer, P. H. J.; Mehl, G. H. *J. Am. Chem. Soc.* **2003**, *125*, 11172.

24. (a) Lin, H. W.; Zhu, W. X. *Chin. J. Chem.* **2003**, *21*, 1054. (b) Wu, J. Z.; Wang, L.; Yang, G.; Ji, L. N.; Katsaros, N.; Koutsodimou, A. *Cryst. Res. Technol.* **1996**, *31*, 857.
25. (a) Bruce, D. W.; Liu, H. X., *Liq. Cryst.* **1995**, *18*, 156. (b) Date, R. W.; Fernandez Iglesias, E.; Rowe, K. E.; Elliott, J. M.; Bruce, D. W. *Dalton Trans.* **2003**, 1914.
26. Binnemans, K.; Görller-Walrand, C. *Chem. Rev.* **2002**, *102*, 2303.
27. Wrighton, M. S.; Morse, D. L. *J. Am. Chem. Soc*. **1974**, *96*, 998.
28. Itokazu, M. K.; Polo, A. S.; De Faria, D. L. A.; Bignozzi, C. A.; Iha, N. Y. I. *Inorg. Chim. Acta,* **2001**, *313*, 149.
29. Khan, A. A.; Saxena, A. K.; Iftikhar, K. *Polyhedron* **1997**, *16*, 4143.
30. Iftikhar, K. *Polyhedron* **1996**, *15*, 1113.
31. Binnemans, K.; Jongen, L.; Görller-Walrand, C.; D'Olieslager, W.; Hinz, D.; Meyer, G. *Eur. J. Inorg. Chem*. **2000**, 1429.
32. Binnemans, K.; Van Deun, R.; Bruce, D. W.; Galyametdinov, Y. G. *Chem. Phys. Lett.* **1999**, *300*, 509.
33. Weber, P.; Guillon, D.; Skoulios, A. *Liq. Cryst.* **1991**, *9*, 369.
34. (a) Seurin, P.; Guillon, D.; Skoulios, A. *Mol. Cryst. Liq. Cryst.* **1981**, *71*, 37. (b) Guillon, D.; Skoulios, A. *Mol. Cryst. Liq. Cryst.* **1983**, *91*, 341. (c) Hardouin, F.; Levelut, A. M.; Achard, M. F.; Sigaud, G. *J. Chim. Phys.* **1983**, *80*, 53. (d) Hardouin, F. *Physica A* **1986**, *140*, 359).
35. De Vries, A. *Mol. Cryst. Liq. Cryst.* **1977**, *41*, 27.
36. De Vries, A. *Mol. J. Chem. Phys.* **1979**, *71*, 25.
37. Davidson, P.; Levelut, A. M.; Strzelecka, H.; Gionis, V. *J. Phys. (Orsay, Fr.)* **1983**, *44*, 823.
38. El-ghayoury, A.; Douce, L.; Skoulios, A.; Ziessel, R. *Angew. Chem., Int. Ed*. **1998**, *37*, 1255.
39. Tschierske, C. *Annu. Rep. Prog. Chem., Ser. C* **2001**, *97*, 191.

40. Haddad, S. F.; Marshall, J. A.; Crosby, G. A.; Twamley, B. *Acta Crystallogr., Sect. E* [Online] **2002**, *58*, 559 – CCDC 198307.

41. Imrie, C. T.; Luckhurst, G. R. In: *Handbook of Liquid Crystals*; Demus, D.; Goodby, J.; Gray, G. W.; Spies, H.-W.; Vill, V., Eds.; Wiley-VCH: Weinheim, 1998; Volume 2B, Chapter X, pp 801-833.

42. (a) Saez, I. M.; Goodby, J. W.; Richardson, R. M. *Chem. Eur. J.* **2001**, *7*, 2758. (b) Tsiourvas, D.; Stathopoulu, K.; Sideratou, Z.; Paleos, C. M. *Macromolecules* **2002**, *35*, 1746. (c) Barberá, J.; Giménez, R.; Marcos, M.; Serrano, J. L. *Liq. Cryst.* **2002**, *29*, 309. (d) Mehl, G. H.; Elsässer, R.; Goodby, J. W.; Veith, M. *Mol. Cryst. Liq. Cryst.* **2001**, *364*, 219. (e) Saez, I. M.; Goodby, J. W. *J. Mater. Chem.* **2001**, *11*, 2845. (f) Campidelli, S.; Eng, C.; Saez, I. M.; Goodby, J. W.; Deschenaux, R. *Chem. Commun.* **2003**, 1520. (g) Saez, I. M.; Goodby, J. W. *Chem. Eur. J.* **2003**, *9*, 4869.

43. (a) Hessel, F.; Finkelmann, H. *Polym. Bull.* **1985**, *14*, 375. (b) Keller, P.; Harduin, F.; Mauzac, M.; Achard, M. F. *Mol. Cryst. Liq. Cryst*. **1988**, *155*, 171.

44. Filipescu, N.; Mushrush, G. W.; Hurt, C. R.; McAvory, N. *Nature* **1966**, *211*, 960.

45. (a) Binnemans, K.; Moors, D. *J. Mater. Chem.* **2002**, *12*, 3374. (b) Van Deun, R.; Moors, D.; De Fré, B.; Binnemans, K. *J. Mater. Chem.* **2003**, *13*, 1520.

46. (a) Gao, D. Q.; Bian, Z. Q.; Wang, K. Z.; Jin, L. P.; Huang, C. H. *J. Alloys Compds.* **2003**, *358*, 188. (b) Bian, Z. Q.; Wang, K. Z.; Jin, L. P. *Polyhedron* **2002**, *21*, 313.

47. Dickeson, J. E.; Summers, L. A. *Aust. J. Chem.* **1970**, *23*, 1023.

Imidazo[4,5-f]-1,10-phenanthrolines: versatile ligands for the design of metallomesogens with complex molecular architectures

Chapter 5

5.1 Introduction

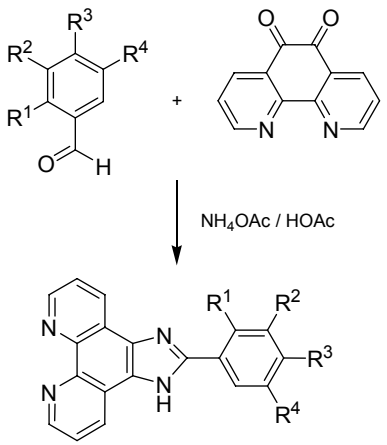
In this chapter, we discuss the influence of the metal ion and complex geometry, the mesogen geometry, the substitution pattern, and the alkoxy chain length on the mesomorphic properties of imidazo[4,5-f]-1,10-phenanthroline based derivatives. The structure and thermal behavior of these compounds is different from that of the related imidazo[4,5-f]-1,10-phenanthrolines bearing 4-cyanobiphenyl groups connected via a long alkyl spacer, described in chapter 4. The compounds presented in this chapter have a 1:1, a 1:2 or a 1:3 metal-to-ligand ratio, depending on the metal ion. 1:1 square planar palladium(II) and platinum(II) complexes, octahedral ruthenium(II) and rhenium(I) complexes, 1:2 octahedral nickel(II) complexes, and a uranyl complex in the 1:3 ratio are described.

5.2 Synthesis and characterization

5.2.1 Synthesis and characterization of the ligands

The 2-arylimidazo[4,5-f]-1,10-phenanthrolines were prepared by a condensation reaction between 1,10-phenanthroline-5,6-dione and an appropriate polyalkoxy benzaldehyde in the presence of ammonium acetate and glacial acetic acid. The synthetic route is similar to the method of Steck and Day for the preparation of 2-substituted phenanthrimidazoles.[1] 1,10-Phenanthroline is oxidized to 1,10-phenanthroline-5,6-dione according to a method described by Hiort et al. (see chapter 4).[2] Structure variations

includes the choice of different chain substitution patterns for the benzaldehyde as well as the variation of the alkoxy chain length. 4-Hydroxybenzaldehyde, 3,4-dihydroxybenzaldehyde, 3,5-dihydroxy-benzaldehyde, 2,3,4-trihydroxybenzaldehyde, 2,4,5-trihydroxybenzaldehyde and 3,4,5-trihydroxybenzaldehyde were used as starting products. They were all prepared as their tetradecyloxy polyether homologues (L^{V}, L^{VIII}, L^{IX}, L^{X}, L^{XI}) or as hexadecyloxy ether ones (L^{I}). The 3,4-dialkoxybenzaldehyde series was prepared with various chain lengths (OC_2H_5, OC_6H_{13}, $OC_{10}H_{21}$, $OC_{14}H_{29}$, $OC_{16}H_{33}$, $OC_{18}H_{37}$, L^{II}, L^{III}, L^{IV}, L^{V}, L^{VI}, and L^{VII}, respectively). We also investigated the influence of alkylation of the N-atom of the five-member imidazole ring. The synthesis of the ligands is outlined in Scheme 5.1. An overview of the different ligands is given in Figure 5.1. All the imidazo[4,5-f]-1,10-phenanthrolines were characterized by CHN analysis, IR spectroscopy, ^{1}H and ^{13}C NMR spectroscopy and by mass spectrometry.



Scheme 5.1: Synthesis of the imidazo[4,5-f]-1,10-phenanthroline ligands.

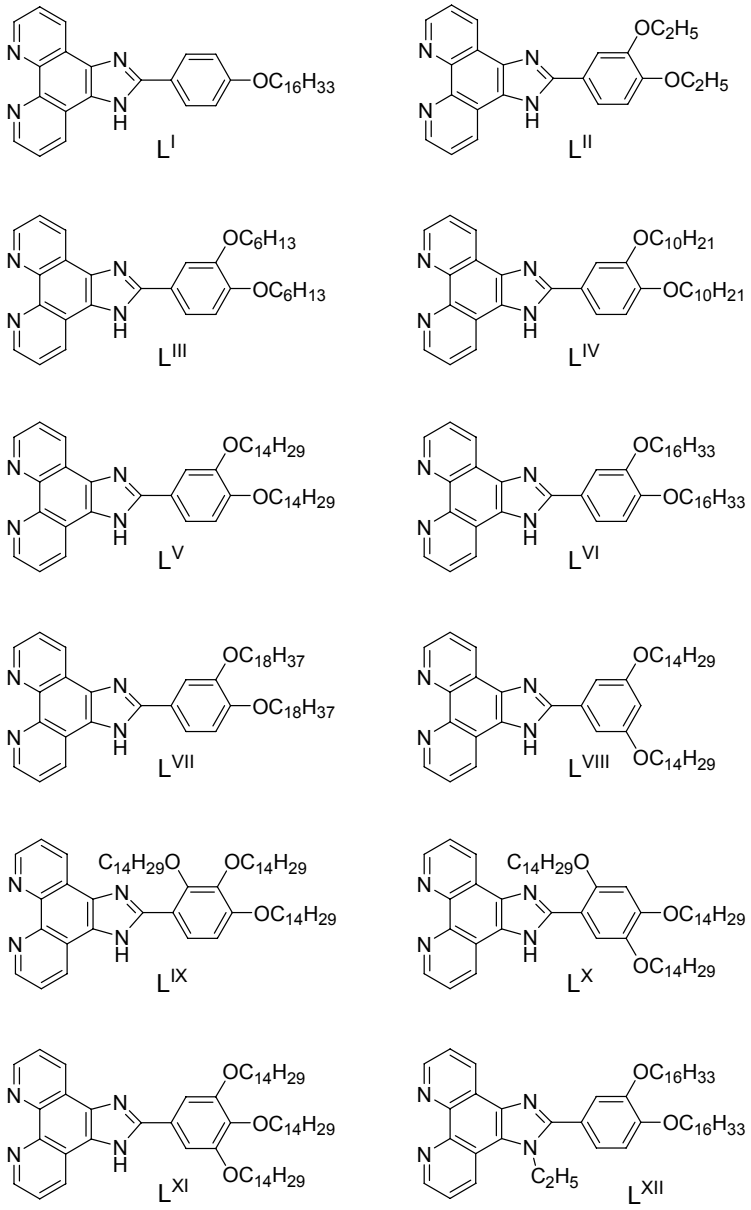


Figure 5.1: Overview of the imidazo[4,5-f]-1,10-phenanthroline ligands.

In chapter 4, we presented the synthesis of liquid-crystalline imidazo[4,5-f]-1,10-phenanthrolines containing mesogenic 4-cyanobiphenyl groups, the synthesis of which has been successfully applied for the imidazo[4,5-f]-1,10-phenanthrolines containing only aliphatic chains. However, the solubility of these two classes of ligands is very different. The imidazo[4,5-f]-1,10-phenanthrolines containing mesogenic 4-cyanobiphenyl groups are only soluble in dichloromethane, chloroform, tetrahydrofuran and hot toluene. Therefore, only metal complexes of which the corresponding metal salt precursor is soluble in a solvent which is able to dissolve the ligand, were prepared for the 4-cyanobiphenyl-substituted ligands: complexes of lanthanides (with 2-thenoyltrifluoroacetonate as a coligand) and rhenium(I). The corresponding metal precursors $[ReBr(CO)_5]$ and $[Ln(tta)_3{\cdot}2H_2O]$ (Htta = 2-thenoyltrifluoroacetone or 4,4,4-trifluoro-1-(thiophen-2-yl)butane-1,3-dione) are soluble in toluene and chloroform, respectively, which are solvents that also dissolve the ligands. Unfortunately, many metal salts like $NiCl_2{\cdot}6H_2O$, *cis*-$[RuCl_2(bipy)_2]$ and $UO_2(CF_3SO_3)_2$ are soluble only in water, methanol or ethanol, rendering the preparation of the corresponding coordination complexes rather difficult. The imidazo[4,5-f]-1,10-phenanthrolines containing only aliphatic chains are soluble in diethyl ether, hexane and warm ethanol, besides to dichloromethane, chloroform, tetrahydrofuran and toluene. Complexes of nickel(II), ruthenium(II) and uranium(VI) could now be prepared without experiencing solubility problems. We tried to obtain lanthanide complexes with the 2-thenoyltrifluoroacetonate fragments of ligand L^{XI}, but all trials were unsuccessful due to too high solubility of the lanthanide complexes; the lanthanide complexes could not be selectively precipitated, so that the complex obtained by precipitation by addition of ethanol were always contaminated with the free ligand. The $Eu(tta)_3$ complex of L^{III} could be obtained in good purity, but this europium(III) complex was not

mesomorphic. For the ligands with the short alkyl chains, the lanthanide complexes have a lower solubility than the ligands, so that these complexes can be selectively precipitated.

It should be mentioned that all the ligands bind 0.5 equivalent of water (or ethanol). The bonded water molecule could not be removed, even not after a long drying period in a vacuum oven (below the melting point of the compounds). Looking at the molecular structure of L^I (Figure 5.2 and Figure 5.3), which was determined by single crystal X-ray diffraction, it is very likely that all the ligands form dimers, in which a water or ethanol molecule connects two ligands via strong hydrogen bonding. Strong intermolecular N-H···O hydrogen bonds appear between the imidazo nitrogen and an ethanol solvent molecule (average H···O distance: 2.01 Å). These ethanol molecules are also bridged by hydrogen bonds to a nitrogen of the phenanthroline part of a second L^I ligand to arrange in dimers with the alkyl chains pointing into opposite directions (average H···N distance: 2.23 Å). The asymmetric unit contains one crystallographically independent molecule.

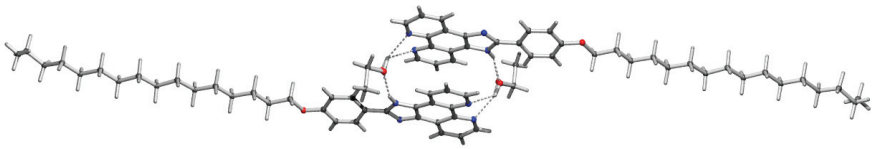


Figure 5.2: Molecular structure of ligand L^I. The bridging by ethanol molecules to dimers of the ligand is shown.

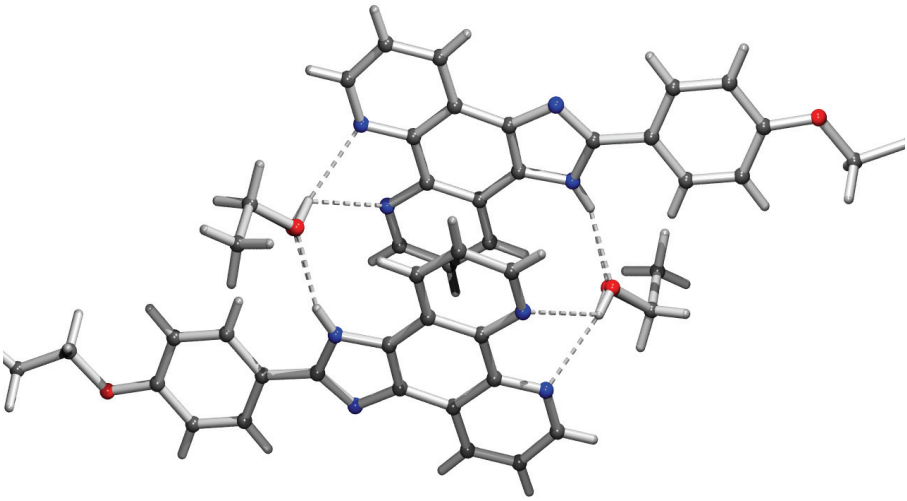


Figure 5.3: Cutout from the molecular structure of ligand L^{I}. The bridging by ethanol molecules to dimers of the ligand is shown.

The ^{1}H and ^{13}C NMR spectra of L^{XII} (the ligand with one of the N-atoms of the imidazole ring alkylated with an ethyl group) were compared with the spectra of all the other ligands (no alkylation of the N atoms of the imidazole ring). For L^{XII}, all the heteroaromatic carbons (six tertiary and seven quaternary carbon atoms of imidazo[4,5-f]-1,10-phenanthroline) could be assigned via two-dimensional ^{1}H-^{13}C correlation spectroscopy (HMQC and HMBC). For the other ligands, an intermolecular exchange reaction of the N-H occurs between the two N-atoms of the imidazole ring (prototropic tautomerism). The rate of this exchange reaction depends on many factors, such as concentration, solvent and temperature. In the case of a fast exchange reaction, three resonances assigned to tertiary carbon atoms and four resonances assigned to quaternary carbon atoms should be

observed in the ^{13}C NMR spectrum and the chemical shifts should be an average of the values of the ligand L^{XII}.

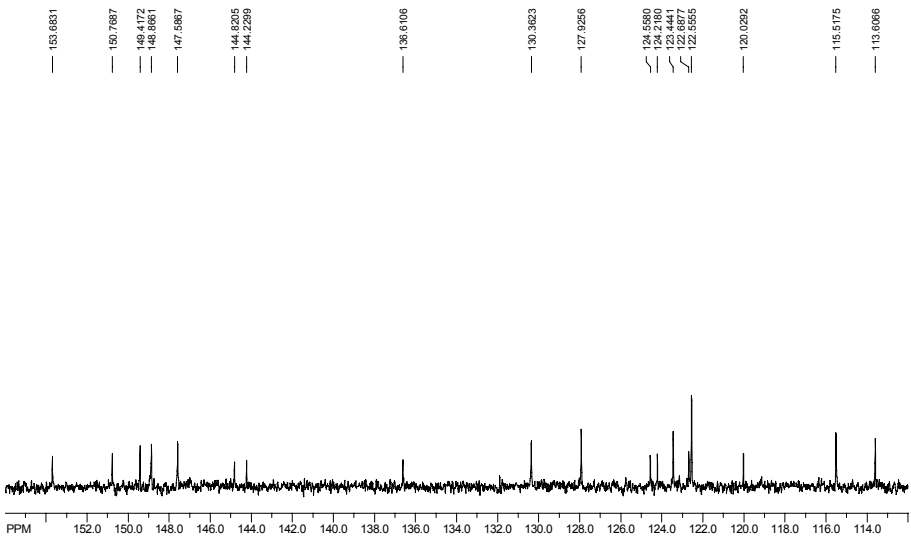


Figure 5.4: ^{13}C NMR spectrum of L^{XII}. Only the region of aromatic carbon atoms is shown. The six tertiary carbon atoms give sharp signals at 123.4 (2x), 127.9, 130.4, 147.6, and 148.9 ppm. The seven quaternary carbon atoms give sharp signals at 120.0, 124.2, 124.6, 136.6, 144.2, 144.8, and 153.7 ppm.

For a very slow exchange reaction, the chemical shift values are expected to be similar to those of the ligand L^{XII}. For an intermediate exchange rate (the most frequently observed situation), broadened resonances for the tertiary and quaternary carbon atoms are observed at an average value, but usually the two resonances of quaternary carbon atoms of the imidazole ring are broadened beyond detection. The resonance of the quaternary carbon atom between the two N atoms (i.e. in the 2-position of the imidazole ring) is not

affected by the exchange process and gives rise to a sharp signal at 152-154 ppm. For all the ligands, the carbons of the substituted aryl group, attached to imidazo[4,5-f]-1,10-phenanthroline, give sharp signals. The ^{13}C NMR spectrum of L^{XII} and L^{XI} are shown in Figure 5.4 and Figure 5.5 respectively.

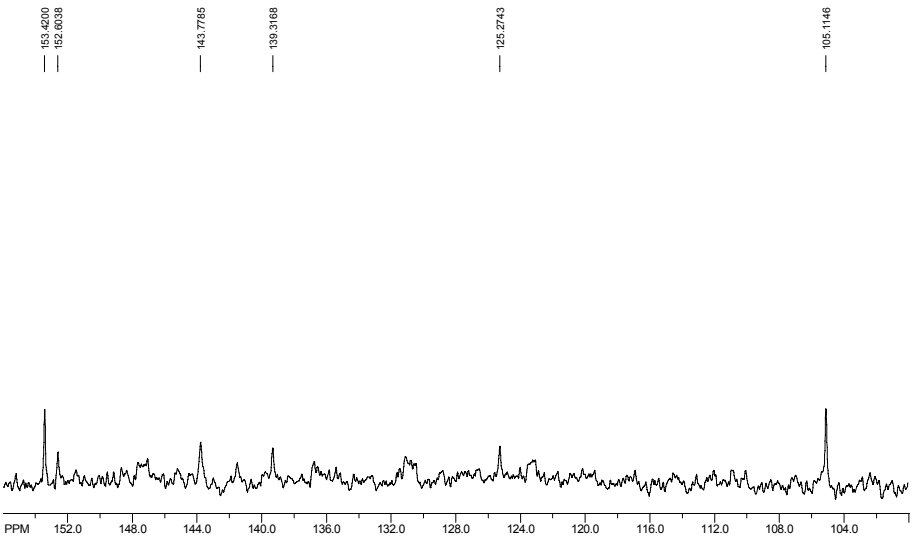


Figure 5.5: ^{13}C NMR spectrum of L^{XI}. Only the region of aromatic carbon atoms is shown. The six tertiary carbon atoms give broad signals at 123, 131, and 147.5 ppm. The quaternary carbon atom in the 2-position of the imidazole ring gives a sharp signal at 152.6 ppm. Two quaternary carbon atoms give one signal at 143.8 ppm. The other quaternary carbon atoms are broadened beyond detection.

5.2.2 Synthesis and characterization of the metal complexes

The palladium(II) and platinum(II) complex were synthesized by a ligand exchange reaction between ligand L^{XI} and $[MCl_2(NCPh)_2]$ (M = Pt, Pd) respectively (1:1.3 molar ratio) in chloroform. The rhenium(I) complexes were synthesized by reaction between the corresponding ligand and $[ReBr(CO)_5]$ (1:1 molar ratio) in toluene. The ruthenium(II) complexes were prepared by reaction between the corresponding ligand and *cis*-$[RuCl_2(bipy)_2]$ (1:1 molar ratio) in an ethanol/water (50:50) mixture. The nickel(II) complexes were synthesized by reaction between the corresponding ligand and $NiCl_2{\cdot}6H_2O$ (2:1 molar ratio) in ethanol. The uranyl complex was synthesized by reaction between ligand L^{XI} and uranyl triflate (3:1 molar ratio) in ethanol. All the metal complexes were characterized by CHN analysis and by mass spectrometry. The uranyl complex was additionally characterized by IR spectroscopy, ^{1}H and ^{13}C NMR spectroscopy. Except for the uranyl complex, all the metal complexes contain water for the same reason as that given for the ligands. Due to its unconventional propeller-like structure, the uranyl complex could be obtained free of bonded water molecules. An overview of the different types of metal complexes is given in Figure 5.6 (with ligand L^{XI} as the complexing ligand). Figure 5.7 shows the structure of the uranyl complex.

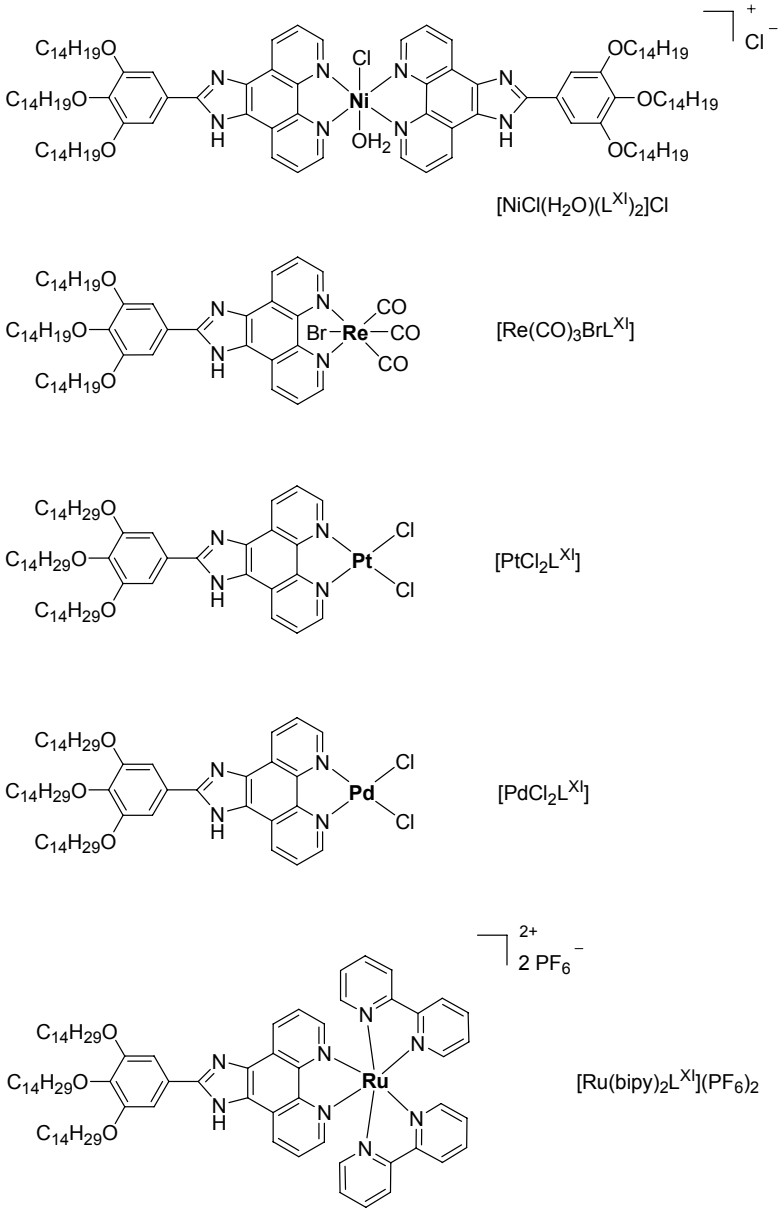


Figure 5.6: Overview of the different types of metal complexes with ligand L^{XI} as the complexing ligand.

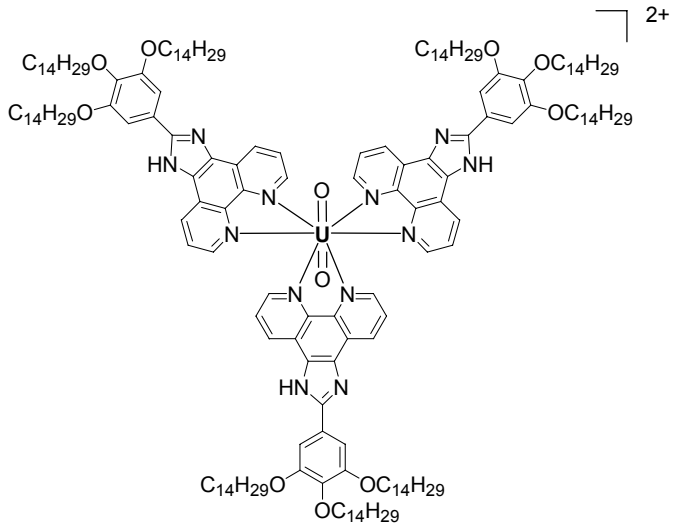


Figure 5.7: Structure of the uranyl complex. The two non-coordinating triflate counter ions have been omitted.

Many trials were made to obtain single crystals of metal complexes of imidazo[4,5-f]-1,10-phenanthroline ligands with none or with short alkyl chains. Crystallization of the metal complexes turned out to be a difficult task. Single crystals of the rhenium(I) complex $[ReBr(CO)_3L^{XIII}]$ and of the europium(III) complex $[Eu(tta)_3L^{XIII}]$ were obtained and examined by X-ray diffraction (L^{XIII} is phenylimidazo[4,5-f]-1,10-phenanthroline). For the molecular structure of the rhenium(I) complex $[ReBr(CO)_3L^{XIII}]$, three carbonyl ligands, one bromide ion and one L^{XIII} ligand are coordinated to the rhenium(I) ion (Figure 5.8). The coordination number of the rhenium(I) ion is six, and the coordination polyhedron can be described as a slightly distorted octahedron. Strong intermolecular N-H···O hydrogen bonds appear between the imidazo nitrogen and the oxygen of a solvent DMF molecule

(average H···O distance: 1.93 Å). The asymmetric unit contains one crystallographically independent molecule.

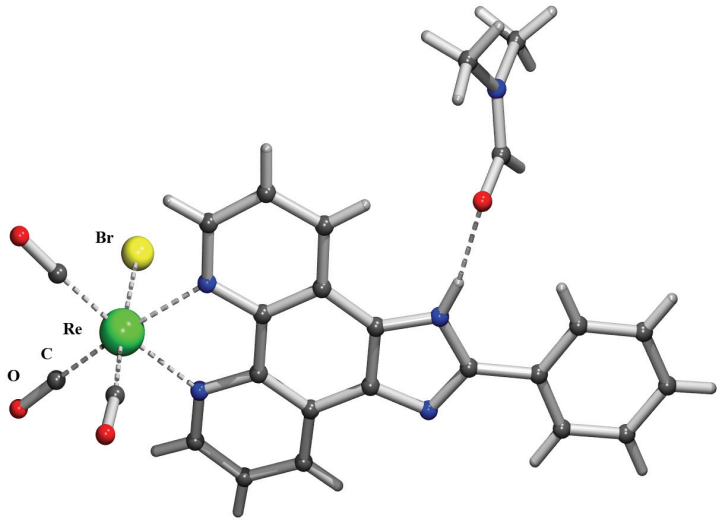


Figure 5.8: Molecular structure of the rhenium(I) complex [ReBr(CO)$_3$L^{XIII}]·DMF.

The molecular structure of [Eu(tta)$_3$L^{XIII}] shows very clearly that three bidentate coordinating 2-thenoyltrifluoroacetonate ligands and one L^{XIII} ligand are coordinated to the europium ion without any solvent coordination to the lanthanide ion (Figure 5.9). The coordination number of the europium(III) ion is eight, and the coordination polyhedron can be described as a slightly distorted square antiprism. Strong intermolecular N-H···O hydrogen bonds appear between the imidazo nitrogen and a methanol solvent molecule (average H···O distance: 1.94 Å). These methanol molecules are also bridged by hydrogen bonds to a second [Eu(tta)$_3$L^{XIII}] complex to arrange in dimers with the L^{XIII} ligands pointing in opposite

directions (Figure 5.10). Considering also the hydrogen bonds between methanol molecules, a two-dimensional network is formed (Figure 5.11). The asymmetric unit contains one crystallographically independent molecule.

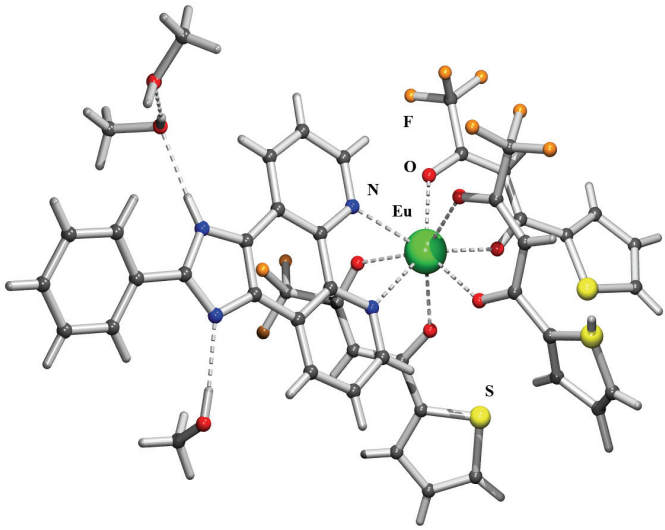


Figure 5.9: Molecular structure of the europium complex $[Eu(tta)_3L^{XIII}]\cdot MeOH$. The hydrogen bridging with solvent molecules is shown.

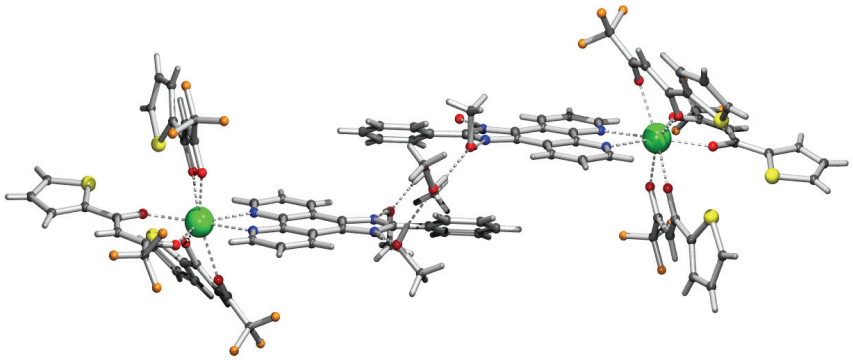


Figure 5.10: Molecular structure of the europium complex $[Eu(tta)_3L^{XIII}]\cdot MeOH$. The hydrogen bridging with solvent molecules and the arrangement to dimers is shown.

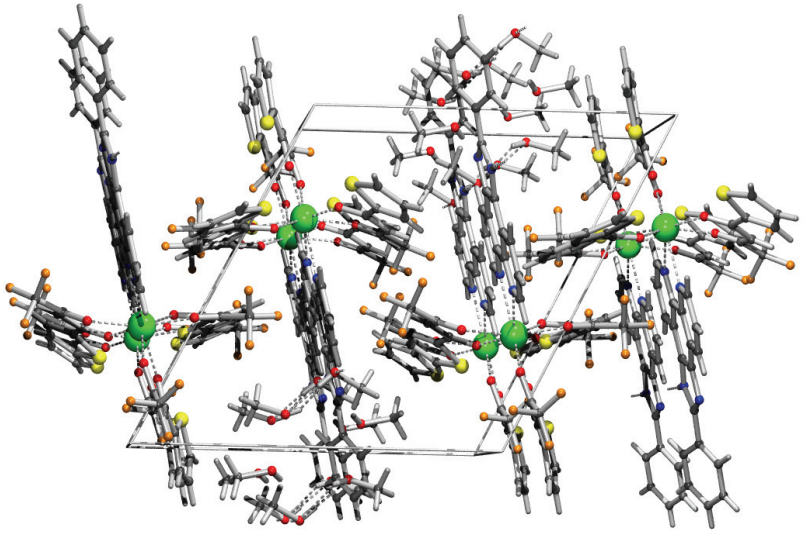


Figure 5.11: Packing in the crystal structure of the europium complex $[Eu(tta)_3L^{XIII}]\cdot MeOH$.

For the complexes of which we were unable to get single crystals of a sufficient quality for X-ray diffraction, we had to rely on literature data of crystal structures of similar ligands. So far, only very few examples of crystal structures of imidazo[4,5-f]-1,10-phenanthrolines have been published.[3,4] Therefore we considered in the first place metal complexes of 1,10-phenanthroline. The palladium(II) and platinum(II) complexes cause no problems, because all the reported crystal structures have a square planar coordination sphere.[5] Therefore, one can safely assume that the palladium(II) and platinum(II) complexes of the imidazo[4,5-f]-1,10-phenanthrolines have a square-planar coordination sphere as well. The coordination sphere of the nickel(II) complexes is more difficult to determine. All the crystal structures reported for bis(1,10-phenanthroline) nickel(II) complexes show an octahedral coordination for the nickel(II) center, and the two 1,10-phenanthroline ligands are in general in a cis-position.[6] Interestingly, all the complexes with chloro anions, have one chloride ion coordinated to nickel(II) and the second chloride ion is in the second coordination sphere.[7] The sixth ligand in the coordination sphere is a water molecule. The same structure is found for a complex with bromo ions as well.[8] A tetradentate 1,10-phenanthroline forces the two other ligands into a trans conformation.[9] By analogy, we assume that in our nickel(II) complexes one chloro ligand and one aqua ligand coordinates to the nickel(II) center, together with two imidazo[4,5-f]-1,10-phenanthrolines. A second chloride is in the second coordination sphere, making the complex an ionic metallomesogen. One can also assume that the coordination sphere is a distorted octahedron, and that the distortion is so that the two imidazo[4,5-f]-1,10-phenanthroline ligands interact via π-π stacking with one other or with neighboring imidazo[4,5-f]-1,10-phenanthroline molecules. In order to obtain more information about the coordination sphere of the nickel(II) complexes, we investigated the nickel(II) complexes

by conductivity and by analysis with silver(I) as in Werner's original work (where $AgNO_3$ is used to discriminate between inner sphere and outer sphere chloride ions).[10] The electric conductivity of a solution of the nickel(II) complexes in THF was the same as that of the pure solvent. However, no conclusions can be drawn because it is possible that the counterions are electrostatically bonded (ion pair formation). When a solution of $AgNO_3$ in a THF/water mixture is added to a solution of the nickel(II) complexes in THF, a precipitate of AgCl is formed. This indicates that there are chloride ions present in the second coordination sphere. However, one has to be cautious to draw conclusions because nickel(II) complexes are kinetically much more labile than the classical cobalt(III) Werner-type of complexes. For the uranyl complex, it is reasonable to assume that its first coordination sphere is comparable with that observed for the $[UO_2(phen)_3](OTf)_2$ complex, with an equal population of right-handed and left-handed helices.[11,12] The coordination polyhedron can be described as a bi-end-capped trigonal antiprism.

5.3 Results and discussion

5.3.1 Thermal behavior of the ligands

The thermal behavior of the ligands was studied by polarizing optical microscopy (POM), differential scanning calorimetry (DSC) and X-ray diffraction. Mesophase formation depends very much on the substitution pattern of the ligand and on the alkoxy chain length. The results of these investigations are reported in Table 5.1.

Most ligands are deprived of mesomorphic properties: L^{I} (which contains only one long aliphatic chain), L^{VIII} (two chains in the 3- and 5-positions), L^{IX}, L^{X}, L^{XI} (three chains in the 2,3,4-, 2,4,5-, and 3,4,5-positions), and the 3,4-disubstituted ligand with ethoxy chains (L^{II}) are not liquid-crystalline.

The paraffinic part of L^{I} is clearly not sufficient to compensate the large 1,10-phenanthroline moiety to induce microphase segregation and thus mesomorphism. The absence of mesomorphism for the 3,5-disubstituted and 2,4,5-trisubstituted ligands (L^{VIII} and L^{X}, respectively) is also not surprising as compounds with such substitution chain-pattern usually do not reach criteria of space-filling (chain deficiency).[13] The lack of mesophases for the 2,3,4- and the 3,4,5- trisubstituted ligands L^{IX} and L^{XI} was on the contrary unexpected, but can be attributed to the long lateral chain in the 2-position, which reduces the lateral π-stacking of the molecules (L^{IX}) or to the reduction of the molecular anisotropy of the molecule (L^{XI}).

Ligand L^{XII}, for which one nitrogen of the imidazole ring is alkylated, is not mesomorphic either. This small ethyl chain is not situated in the plane of the flat aromatic core of the molecule and thus reduces the lateral π-stacking of the molecules. Also hydrogen bonding between neighboring molecules and thus the ability for the formation of dimers (vide supra) is suppressed. Mesophases were observed only for the 3,4-disubstituted ligands L^{III}, L^{IV}, L^{V}, L^{VI} and L^{VII}. The compounds L^{III}, L^{IV}, L^{V} were obtained as glassy solids. They transformed upon heating into a mesophase and became isotropic on further heating. This thermal behavior was reversible and on cooling, the compounds did not crystallize, but formed a glass. However, this amorphous physical appearance was thermodynamically not stable as after a few months the compounds started to crystallize. The small crystallites melted directly into the isotropic phase over a large temperature range, but on cooling a mesophase was formed again. The ligands L^{VI} and L^{VII} were obtained as semi- or partially crystalline solid materials, which showed a monotropic thermal behavior. Examination of the mesophase behavior of the ligands by POM was not easy as the molecules were prone to orient perpendicularly to the glass slide surface giving rise to a homeotropic texture. Pressing on the cover slip induced luminous flashes. Treatment of

the glass cover slips with sulfochromic acid, to favor a planar orientation, did not yield characteristic textures enabling the correct mesophase assignment.

Table 5.1: Transition temperatures and phase behavior of the imidazo[4,5-f]-1,10-phenanthroline ligands.

Ligand	Transition temperatures (°C)[a]
L^{I}	Cr 162 I
L^{II}	Cr 345 I
L^{III}	g 91 N 128 I
L^{IV}	g 60 N 95 I
L^{V}	g 64 M 82 I
L^{VI}	Cr 113 (M 79) I
L^{VI}·2EtOH	Cr 135 Col_h 140 SmX 190 I
L^{VII}	Cr 116 (M 77) I
L^{VIII}	Cr 158 I
L^{IX}	Cr 77 I
L^{X}	Cr 81 I
L^{XI}	Cr 83 I
L^{XII}	Cr 122 I

[a] Abbreviations: Cr = crystalline or semi- or partially crystalline phase; g = glass; N = nematic phase; Col_h = hexagonal columnar phase; SmX = disordered smectic phase (SmA or SmC); M = unidentified mesophase; I = isotropic liquid; ( ) metastable monotropic phase.

Because most of the mesophases are monotropic, the X-ray diffraction patterns were carried out on cooling from the isotropic liquid, 10 °C below the clearing point. By X-ray diffraction, supported by POM observations, the mesophase formed by ligands L^{III} and L^{IV} was identified as nematic. In the small-angle region, a rather broad scattering signal was observed instead of sharp intense peaks, which confirmed the absence of 1D or 2D long-range correlated positional ordering. This broad signal corresponds to lateral short-range molecular correlations of the order of the molecular length, typical of the orientational nematic ordering. In the wide-angle part, a weak and diffuse signal at ca. 4.6 Å was observed, attributed to the liquid-like order of the molten chains. For the mesophase behavior of ligands L^{V} and L^{VII}, in the X-ray pattern were observed at large angles the broad scattering at ca. 4.6 Å, indicative of the liquid-like order of the system, along with one sharp, small-angle reflection of high intensity indicating that the complexes are self-organized into ordered mesostructures. Unfortunately no additional peaks in the small-angle region could be observed, necessary for further identification of the mesophases.

The most striking feature is the influence of solvent molecules on the thermal behavior of the ligands. As mentioned before, all the ligands contain 0.5 equivalents of water, which leads to the formation of dimers. To examine the influence of solvent molecules, L^{VI} was recrystallized from ethanol. After drying the compound under reduced pressure, a 1:2 ethanol adduct L^{VI}·2EtOH could be obtained. The presence of ethanol molecules changed the thermal behavior of L^{VI} dramatically. The ethanol free ligand (which contains 0.5 equivalents of water) shows a monotropic unidentified mesophase, whereas, the 1:2 ethanol adduct shows two phases, a low temperature hexagonal columnar mesophase, and a smectic phase just below the isotropic liquid, as identified by X-ray diffraction. At 135 °C, in the small-angle region of the X-ray pattern, seven sharp reflections were

observed with reciprocal spacings in the ratio 1, $\sqrt{3}$, 2, $\sqrt{7}$, 3, $\sqrt{12}$, $\sqrt{13}$. They were indexed as (*hk*) = (10), (11), (20), (21), (30), (22), and (31) of a hexagonal lattice. In addition, a broad scattering halo was observed at ca. 4.6 Å, corresponding to the liquidlike order of the molten aliphatic chains. Along with this broad scattering, another weak halo was seen at ca. 8.0 Å, which likely corresponds to the stacking periodicity along the columnar axis. At 140 °C, two sharp small-angle reflections were observed. Analysis of their profiles indicated that they belong to different families, and were thus associated to two different phases that co-exist. At 160 °C, two sharp reflections were observed in the ratio 1:2, indicative of a lamellar structure and were indexed as the 001 and 002 reflections, respectively. In addition, two broad scattering halos were seen at ca. 4.6 Å (h_{ch}) and at ca. 8.0 Å (*h'*), respectively. The broad signal at ca. 4.6 Å corresponds to the liquidlike order of the molten aliphatic chains, whereas the broad signal at ca. 8.0 Å likely corresponds to the arrangement of dimers, reminiscent of the crystalline phase. It should be mentioned that the hexagonal columnar phase is only transient and exists over a few degrees only. Once the smectic phase is formed at higher temperatures, the hexagonal columnar phase could not be obtained again. Figure 5.12 shows the optical texture of the smectic phase of L^{VI}·2EtOH between crossed polarizers. Figure 5.13 shows the X-ray pattern of L^{VI}·2EtOH in the smectic phase at 160 °C.

We tried to obtain other ligand:ethanol molar ratios and also adducts with other alcohols (like propanol, butanol), but these trials were unsuccessful.

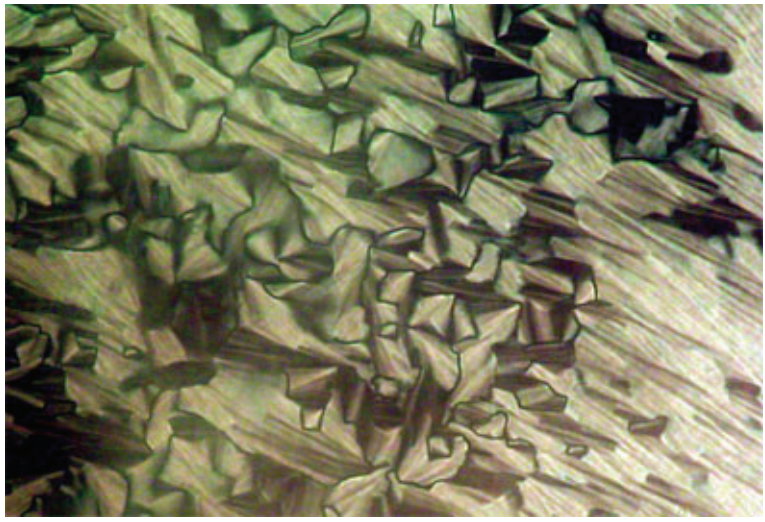


Figure 5.12: Optical texture of the smectic phase of L^{VI}·2EtOH at 155 °C (500× magnification).

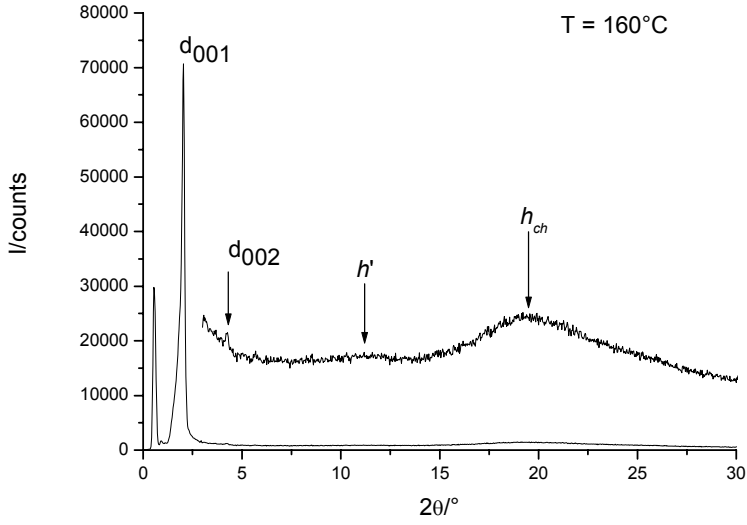


Figure 5.13: X-ray pattern of L^{VI}·2EtOH in the smectic phase at 160 °C.

Looking at the structure of the ligands, mesomorphism was not entirely expected: usually calamitic mesogens having more than one chain at one end are not mesomorphic, unless the rod-like part contains several aromatic rings. The introduction of two or three chains to the relatively short aromatic core reduces the anisotropy of these molecules. Considering also the rigidity of the molecule which cannot adopt for instance a tapered or conical shape, mesomorphism is not favored, only a monotropic thermal behavior is induced.

5.3.2 Thermal behavior of the palladium(II) and platinum(II) complexes

The palladium(II) complex [$PdCl_2L^{XI}$] and platinum(II) complex [$PtCl_2L^{XI}$] were enantiotropic liquid crystals. They were obtained as orange powders, but when dried in a vacuum oven at 50 °C, they transformed into waxy compounds which are room temperature liquid crystals. Their viscosity is high at room temperature, but lowers continuously when heating and decomposition occurs before reaching the isotropic phase (above 300 °C). These complexes are very stable and exhibit a very extended mesophase temperature range. The liquid-crystalline properties were analyzed by POM, DSC and SAXS. In the X-ray pattern were observed at large angles the broad scattering at ca. 4.6 Å, indicative of the liquid-like order of the system, along with an intense and sharp, small-angle reflection indicating that the complexes are self-organized into ordered mesostructures. However, discrimination between a smectic or a hexagonal columnar arrangement is not possible on the basis of XRD only as no additional peaks in the small-angle region were observed (a cubic phase was excluded due to the observation of birefringent textures by POM). In contrary to the 3,4,5-

trisubstituted ligand L^{XI}, these complexes were mesomorphic and the mesophase is likely induced by the introduction of a metal.

5.3.3 Thermal behavior of the rhenium(I) complexes

The rhenium(I) complexes containing the bulky $[ReBr(CO)_3]$ fragment have a large dipole moment due to the polar Re-Br bond. This dipole is expected to influence the arrangement of the molecules in the mesophase and the solid phase. Complexation to rhenium(I) led to an increase of the melting temperatures. None of the rhenium(I) complexes were mesomorphic, except the $[ReBr(CO)_3L^{VIII}]$ and $[ReBr(CO)_3L^{XI}]$ complexes with 3,5-disubstituted and 3,4,5-trisubstituted ligands, which showed a mesophase only on cooling from the isotropic liquid, over a few degrees only. Unfortunately, the mesophase could not be identified unambiguously. The mesomorphic rhenium(I) complexes gave a homeotropic texture when examined by POM, however crystallizing very fast when cooled from the isotropic liquid, hampering any characterization by X-ray diffraction on a powder sample.

5.3.4 Thermal behavior of the ruthenium(II) complexes

No liquid-crystalline behavior was detected for the three ruthenium(II) complexes. Indeed, complexation to ruthenium(II) led to a strong increase of the melting temperatures, and the compounds decomposed at temperatures above 300 °C, before melting.

5.3.5 Thermal behavior of the nickel(II) complexes

All the nickel(II) complexes form enantiotropic liquid crystal phases, except the 3,4-disubstituted complexes $[NiCl(H_2O)(L^{II})_2]Cl$ and $[NiCl(H_2O)(L^{III})_2]Cl$, and the 2,4,5-trisubstituted complex $[NiCl(H_2O)(L^{X})_2]Cl$. After drying in a vacuum oven at 50 °C, the nickel(II) complexes were obtained as waxy

compounds, which were liquid-crystalline at room temperature. Their viscosity is high at room temperature but lowers continuously when heating. Except for the 2,3,4-trisubstituted complex $[NiCl(H_2O)(L^{IX})_2]Cl$, all the nickel(II) complexes decompose before reaching the isotropic liquid (> 300 °C). Like the palladium(II) and platinum(II) complexes, these complexes are very stable and exhibit a very extended mesophase temperature range. Again, X-ray diffraction on powder samples was necessary to identify the type of mesophase. Only the mesophase type of the 3,4-disubstituted complex $[NiCl(H_2O)(L^{VII})_2]Cl$ could be identified and the compound shows a hexagonal columnar mesophase (Col_h). In the small-angle region of the diffraction pattern, 2 sharp reflexions with reciprocal spacings in the ratio 1, $\sqrt{3}$ were observed, corresponding to the indexation (*hk*) = (10), (11) and these are characteristic of a two-dimensional hexagonal lattice. In the wide-angle region of the X-ray pattern, a broad signal is observed at ca. 4.7 Å, corresponding to the liquidlike order of the molten aliphatic chains. Unfortunately, none of the other mesomorphic nickel(II) complexes could be characterized. In the X-ray pattern were observed at large angles the broad scattering at ca. 4.6 Å, indicative of the liquid-like order of the system, along with one single intense and sharp, small-angle reflection indicating that the complexes are self-organized into ordered mesostructures. However, as for the palladium(II) and platinum(II) complexes, discrimination between a smectic or a hexagonal columnar arrangement is not possible on the basis of XRD only as no additional peaks in the small-angle region were observed (a cubic phase was excluded due to the observation of birefringent textures by POM).

5.3.6 Thermal behavior of the uranyl complex

The liquid-crystalline properties of the uranyl complex $[UO_2(L^{XI})_3](OTf)_2$ were examined by POM, DSC and X-ray diffraction on a powder sample. The uranyl complex melts at 95 °C into a mesophase (ΔH = 69.5 kJ mol^{-1}) and clears into the isotropic liquid at 181 °C (ΔH = 2.8 kJ mol^{-1}). The fluid and birefringent optical texture of the uranyl metallomesogen (Figure 5.14) confirms mesomorphism, but the mesophase could not be characterized only on this basis.

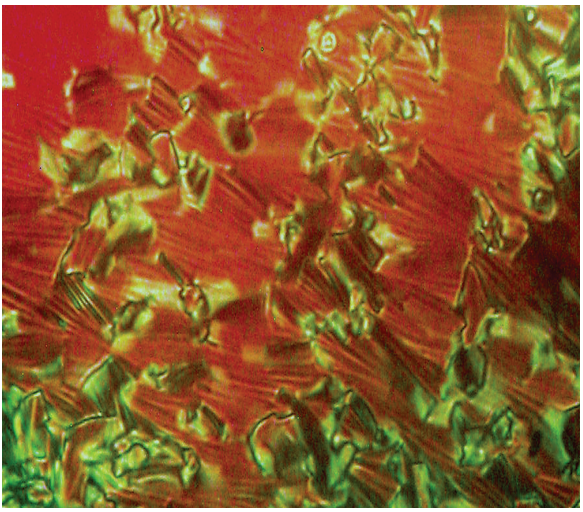


Figure 5.14: Natural optical texture of the uranyl complex at 170 °C (500× magnification).

The X-ray pattern of the uranyl complex (Figure 5.15) is characteristic of a hexagonal columnar phase (Col_h). Two Bragg reflections are observed in the small-angle range: an intense and sharp reflection at $2\theta_1$ = 2.31° (d_1 = 38.2 Å) and another small signal at $2\theta_2$ = 4.012° (d_2 = 22.0 Å). The

reciprocal d-spacings are in the ratio 1:$\sqrt{3}$, which allows their indexation (*hk*) in the hexagonal 2D symmetry as (10) and (11), respectively, the corresponding lattice parameter of the Col_h phase being a = 44.05 Å. A broad scattering band, reflecting the liquid-like organization of the paraffinic chains (h_2 = 4.6 Å), and three other weak signals ascribed to various intermolecular interactions were also seen. The signal observed at 3.5–3.6 Å, h_1, broad and weak, corresponds to the average distance between successive stacking molecular cores (taken hereafter as the stacking periodicity, h_1). The broadness of this signal indicates that such a regular stacking is simply short-range correlated, and also confirms that the bonded ligands are slightly tilted with respect to the hexagonal lattice plane (expected to be due to the propeller-like shape of the complex).

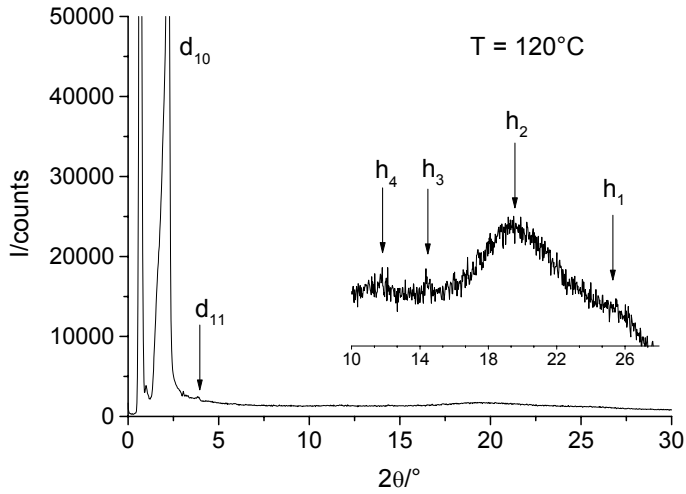
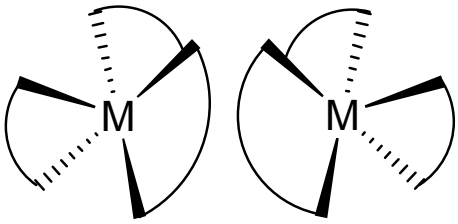


Figure 5.15: X-ray pattern of the uranyl complex in the hexagonal columnar phase at 120 °C.

The Bragg reflection at 6.0–6.2 Å, h_3, is likely due to the strongly scattering uranyl cation $[UO_2]^{2+}$. Comparison with the crystalline structure of a homologous compound,[11,12] leads us to propose that this signal may reflect reticular planes rich in uranium. Finally, the broad signal at 7.2–7.4 Å ($h_4 \approx 2\times h_1$) seems to indicate that the stacking is also alternated (staggered): starting from one molecule, the next one is rotated by 60° in order to "fill" partially the space left unoccupied by the first molecule. The next molecule is also rotated by 60°, therefore totally superposed with the first one, and so on. The volume and the dimensions of the complex are in good agreement with a portion of column defined by $h_1 \cdot S$ (the columnar cross-section S = 1680 Å^2). For one mesogen per such a slice, a density of ca. 1 is deduced for the complex (i.e. a molecular volume of ca. 5600 Å^3 at 120 °C), reasonable in the present case due the presence of the heavy metal atom. The complex, which approximates a D_3 symmetry, exists as two optical isomers, Δ and Λ, present in a 50:50 ratio (Figure 5.16). Thus, packing frustrations can be explained by steric constraints and polar order within the columns.[14,15,16] In order to accommodate an antiferroelectric order in a ternary symmetry lattice (Col_h phase), the columnar phase can result from the random piling of these propeller-like mesogens, however with important stacking faults all along the columns. For a more efficient packing, complexes of identical absolute configuration about the metal center may stack on top of each other into polar aggregates. However, in order to escape from the polar ordering, such molecular bundles made of a few consecutive stacking enantiomers are necessarily randomized within the columns.



Λ and Δ

Figure 5.16: Schematic representation of the two isomers.

Table 5.2 gives an overview of the transition temperatures and phase behavior of all the metal complexes. Table 5.3 gives an overview of the Bragg reflections collected from the X-ray diffraction pattern of L^{VI}·2EtOH and all the mesomorphic metal complexes.

Many of the metal complexes were not liquid-crystalline and this was somewhat disappointing. However, on complexation to rhenium(I), ruthenium(II) and to europium(III), a bulky metal fragment is introduced. Siting the bulky metal fragment in one extremity of the molecule suppressed the formation of a mesophase. This was also observed for the *ortho*-metallated imine complexes of rhenium(I) prepared by Bruce and co-workers,[17] where the introduction of the bulky rhenium(I) fragment at one end of the molecule destabilized the mesomorphism, although it was not suppressed in this case. For the palladium(II) and platinum(II) complexes, the introduction of the metal fragment stabilized the mesomorphism. The metal and chlorine atoms are situated in the same plane as that of the ligand because palladium(II) and platinum(II) form square planar complexes. We can assume that the geometry of the complexes in combination with

favorable interactions between the metal-phenanthroline units results in the formation of more ordered mesophases. For metal complexes with a higher metal-to-ligand ratio, as for the nickel(II) complexes with a 1:2 metal-to-ligand ratio and the uranyl complex with a 1:3 metal-to-ligand ratio, mesophases with a large temperature range were observed. This can be attributed to the higher number of ligands that coordinate to the metal ion and/or to the ionic character of these complexes. In the case of the uranyl complex, the uranyl ion acts as a template to bring the ligands in the correct position so that propeller-like units can arrange into columns. These metallomesogens stack in such a way that the polar order is annihilated.

Table 5.2: Transition temperatures and phase behavior of the metal complexes.

Compound	Transition temperatures (°C)[a]
$[PdCl_2L^{XI}]$	M > 300 dec
$[PtCl_2L^{XI}]$	M > 300 dec
$[ReBr(CO)_3L^{II}]$	Cr 371 I
$[ReBr(CO)_3L^{III}]$	Cr 244 I
$[ReBr(CO)_3L^{IV}]$	Cr 216 I
$[ReBr(CO)_3L^{V}]$	Cr 197 I
$[ReBr(CO)_3L^{VII}]$	Cr 183 I
$[ReBr(CO)_3L^{VIII}]$	Cr 92 (M 69) I
$[ReBr(CO)_3L^{IX}]$	Cr 178 I
$[ReBr(CO)_3L^{X}]$	Cr 180 I
$[ReBr(CO)_3L^{XI}]$	Cr 91 (M 81) I
$[Ru(bipy)_2L^{V}](PF_6)_2$	Cr > 300 dec
$[Ru(bipy)_2L^{VIII}](PF_6)_2$	Cr > 300 dec
$[Ru(bipy)_2L^{XI}](PF_6)_2$	Cr > 300 dec
$[NiCl(H_2O)(L^{II})_2]Cl$	Cr > 300 dec
$[NiCl(H_2O)(L^{III})_2]Cl$	-
$[NiCl(H_2O)(L^{IV})_2]Cl$	M > 300 dec
$[NiCl(H_2O)(L^{V})_2]Cl$	M > 300 dec
$[NiCl(H_2O)(L^{VII})_2]Cl$	Col_h > 300 dec
$[NiCl(H_2O)(L^{VIII})_2]Cl$	M > 300 dec
$[NiCl(H_2O)(L^{IX})_2]Cl$	M 265 I
$[NiCl(H_2O)(L^{X})_2]Cl$	Cr 302 I
$[NiCl(H_2O)(L^{XI})_2]Cl$	M > 300 dec
$[UO_2(L^{XI})_3](OTf)_2$	Cr 95 Col_h 181 I

[a] Abbreviations: Cr = crystalline or semi- or partially crystalline phase; Col_h = hexagonal columnar phase; M = unidentified mesophase; I = isotropic liquid; ( ) metastable monotropic phase; the melting point of $[NiCl(H_2O)(L^{III})_2]Cl$ could not be determined.

Table 5.3: Bragg reflections collected from the X-ray diffraction pattern of L^{VI}·2EtOH and all the mesomorphic metal complexes. For most of the complexes, discrimination between a smectic and a hexagonal columnar arrangement is not possible. Therefore, the parameters of both the smectic and the hexagonal columnar arrangement are given.

Compound	$d_{meas.}$/Å[a]	I[b]	00l[c]	hk[c]	$d_{calc.}$/Å[a]	Parameters of SmX at T/°C[d,e]	Parameters of Col_h at T/°C[d,e]
L^{VI}·2EtOH	45.85	S		10	45.8		T = 135
	26.45	W		11	26.4		V_{mol} = 1562 Å^3
	22.85	S		20	22.9		a = 52.9 Å
	17.3	S		21	17.3		S = 2422.1 Å^2
	15.3	M		30	15.3		N = 12.4
	13.2	W		22	13.2		
	12.7	W		31	12.7		
	8.0	br					
	4.6	br					
	41.5	VS	001		41.25	T = 160	
	20.5	W	002		20.6	V_{mol} = 1590 Å^3	
	8.0	br				A_M = 77.1 Å^2	
	4.6	br				A_{ch} = 38.5 Å^2	
$[PdCl_2L^{XI}]$	39.5	VS	001	10	39.5	T = 160	
	8.1	br				V_{mol} = 1710 Å^3	a = 45.6 Å
	4.6	br				A_M = 86.6 Å^2	S = 1801.6 Å^2
						A_{ch} = 28.9 Å^2	N = 8.5
$[PtCl_2L^{XI}]$	38.5	VS	001	10	38.5	T = 160	
	8.2	br				V_{mol} = 1710 Å^3	a = 44.45 Å
	4.5	br				A_M = 88.6 Å^2	S = 1711.6 Å^2
						A_{ch} = 29.6 Å^2	N = 8.2
$[NiCl(H_2O)(L^{IV})_2]Cl$	32.8	VS	001	10	32.8	T = 200	
	9.1	br				V_{mol} = 2290 Å^3	a = 37.9 Å
	4.5	br				A_M = 69.7 Å^2	S = 1242.3 Å^2
						A_{ch} = 34.8 Å^2	N = 5.0
$[NiCl(H_2O)(L^{V})_2]Cl$	37.2	VS	001	10	37.2	T = 200	
	9.2	br				V_{mol} = 2710 Å^3	a = 42.95 Å
	4.6	br				A_M = 72.8 Å^2	S = 1600.0 Å^2
						A_{ch} = 36.4 Å^2	N = 5.4

$[NiCl(H_2O)(L^{VII})_2]Cl$	37.95	VS		10	37.95		$T = 200$
	21.9	M		11	21.9		$V_{mol} = 3130$ Å^3
	9.3	br					$a = 43.8$ Å
	4.7	br					$S = 1665.0$ Å^2
							$N = 5.4$
$[NiCl(H_2O)(L^{VIII})_2]Cl$	32.8	VS	001	10	32.8	$T = 200$	
	9.0	br				$V_{mol} = 2710$ Å^3	$a = 37.9$ Å
	4.6	br				$A_M = 82.6$ Å^2	$S = 1242.3$ Å^2
						$A_{ch} = 41.3$ Å^2	$N = 4.1$
$[NiCl(H_2O)(L^{IX})_2]Cl$	36.2	S	001	10	36.2	$T = 160$	
	8.3	br				$V_{mol} = 3410$ Å^3	$a = 41.8$ Å
	4.5	br				$A_M = 94.3$ Å^2	$S = 1513.1$ Å^2
						$A_{ch} = 31.4$ Å^2	$N = 3.7$
$[NiCl(H_2O)(L^{XI})_2]Cl$	38.0	VS	001	10	37.6	$T = 100$	
	18.6	W	002	20	18.8	$V_{mol} = 3270$ Å^3	$a = 43.4$ Å
	8.3	br				$A_M = 86.15$ Å^2	$S = 1632.5$ Å^2
	4.4	br				$A_{ch} = 28.79$ Å^2	$N = 4.15$
	37.0	VS	001	10	36.7	$T = 150$	
	18.2	W	002	20	18.3	$V_{mol} = 3390$ Å^3	$a = 42.4$ Å
	8.2	br				$A_M = 91.6$ Å^2	$S = 1555.2$ Å^2
	4.4	br				$A_{ch} = 30.5$ Å^2	$N = 3.8$
	35.9	VS	001	10	36.4	$T = 200$	
	18.5	W	002	20	18.2	$V_{mol} = 3500$ Å^3	$a = 42.1$ Å
	8.5	br				$A_M = 97.6$ Å^2	$S = 1534.1$ Å^2
	4.6	br				$A_{ch} = 32.55$ Å^2	$N = 3.7$
$[UO_2(L^{XI})_3](OTf)_2$	38.2	S		10	38.2		$T = 120$
	22.0	M		11	22.0		$V_{mol} = 5600$ Å^3
	7.3	br					$a = 44.05$ Å
	6.1	br					$S = 1680.0$ Å^2
	4.6	br					$N = 1.0$
	3.5	br					

[a] d_{meas} and d_{calc} are the measured and calculated diffraction spacing.

[b] I is the intensity of the reflections: VS, very strong; S, strong; M, medium; W, weak; br: broad reflection.

[c] 00*l* and *hk* are the indexations of the reflexions.

[d] T is the temperature at which the X-ray pattern was recorded.

[e] Col_h = hexagonal columnar phase; SmX = disordered smectic phase (SmA or SmC); V_{mol}, the molecular volume; A_M, the molecular area; A_{ch}, the cross section of one aliphatic chain; a, the parameter of the hexagonal lattice; S, the columnar cross section; N, the number of molecules within a volume fraction of a column.

5.4 Conclusions

Transformation of 1,10-phenanthroline into substituted 2-aryl-imidazo[4,5-f]-1,10-phenanthroline via condensation of 1,10-phenanthroline-5,6-dione with benzaldehyde in the presence of ammonium acetate is a versatile route to funtionalize 1,10-phenanthrolines. By a proper choice of the substitution pattern of the substituted benzaldehydes, it is possible to obtain lipophilic 1,10-phenanthroline ligands, which are useful for the design of metallomesogens. Depending on the nature of the metal ion 1:1, 1:2 or 1:3 metal-to-ligand ratios are possible, and these structural variations lead to modification of the thermal behavior. Although the ligands are not mesomorphic or exhibit a monotropic mesophase, some of the metal complexes show a mesophase over an extended temperature range. The most stable mesophases are observed for the nickel(II) and uranyl complexes, for which the metal-to-ligand ratio is respectively 1:2 and 1:3. It is of interest to point out the ionic nature of these metallomesogens. At this point, it is not clear yet whether the enhanced mesophase stability of the nickel(II) and uranyl complexes is due to the higher number of ligands or to their ionic character. Unfortunately, none of the lanthanide complexes synthesized with this type of ligands were found to be liquid-crystalline.

5.5 Experimental section

Single-crystal X-ray diffraction was performed by Dr. Peter Nockemann, Kristof Van Hecke and Prof. Dr. Luc Van Meervelt. Two-dimensional ^{1}H-^{13}C correlation spectroscopy and following discussion was performed by Karel Duerinckx and Prof. Dr. Suzanne Toppet. Characterization of the mesophases by X-ray diffraction and following discussion was performed in cooperation with Dr. Bertrand Donnio and Dr. Daniel Guillon.

5.5.1 Techniques

Nuclear magnetic resonance (NMR) spectra were recorded on a Bruker Avance 300 spectrometer (operating at 300 MHz) or a Bruker AMX-400 (operating at 400 MHz). Elemental analyses were obtained on a CE Instruments EA-1110 elemental analyzer. Optical textures of the mesophases were observed with an Olympus BX60 polarizing microscope equipped with a LINKAM THMS600 hot stage and a LINKAM TMS93 programmable temperature-controller. DSC traces were recorded with a Mettler-Toledo DSC821e module. Electrospray ionization (ESI) spectra were recorded on a Thermo Finnigan LCQ Advantage mass spectrometer.
The XRD patterns were obtained with two different experimental setups, and in all cases, the powdered sample was filled in Lindemann capillaries of 1 mm diameter and 10 μm wall thickness. A linear monochromatic CuKα_1 beam (λ = 1.5405 Å) obtained with a sealed-tube generator (900 W) and a bent quartz monochromator were used (both generator and monochromator were manufactured by Inel). One set of diffraction patterns was registered with a curved counter Inel CPS 120, for which the sample temperature is controlled within ±0.05 °C from 20 to 200 °C.; periodicities up to 60 Å can be measured. The other set of diffraction patterns was registered on Image

Plate. Periodicities up to 90 Å can be measured, and the sample temperature is controlled within ±0.3 °C from 20 to 350 °C.

Yellow single crystals of $[Eu(tta)_3L^{XIII}]\cdot MeOH$, $[ReBr(CO)_3L^{XIII}]\cdot DMF$ and $L^{I}\cdot EtOH$ were obtained by slow evaporation of a solution of the compound in methanol, DMF or ethanol, respectively, at 4 °C in a refrigerator. X-ray intensity data were collected on a SMART 6000 diffractometer equipped with CCD detector using Cu-Kα radiation (λ = 1.54178 Å). The images were interpreted and integrated with the program SAINT from Bruker.[18]

$[Eu(tta)_3L^{XIII}]\cdot MeOH$: $C_{46}H_{36}EuF_9N_4O_9S_3$, M = 1205.24, triclinic, P-1 (No. 2), a = 10.8917(8), b = 15.6770(11), c = 15.9877(8) Å, α= 117.819(3), β = 97.656(4), γ = 93.066(5)°, V = 2371.9(3) $Å^3$, T = 100(2) K, Z = 2, ρ_{calc} = 1.688 g cm^{-3}, μ(Cu-Kα) = 11.548 mm^{-1}, F(000) = 1205, crystal size 0.4 × 0.25 × 0.2 mm, 8621 independent reflections (R_{int} = 0.0951). Final R = 0.0581 for 7168 reflections with I > 2σ(I) and ωR2 = 0.1454 for all data.

$[ReBr(CO)_3L^{XIII}]\cdot DMF$: $C_{25}H_{19}BrN_5O_4Re$, M = 719.56, triclinic, P-1 (No. 2), a = 8.890(6), b = 10.729(7), c = 13.263(8) Å, α= 81.23(4), β = 71.34(4), γ = 80.52(4)°, V = 1175.4(13) $Å^3$, T = 100(2) K, Z = 2, ρ_{calc} = 2.033 g cm^{-3}, μ(Cu-Kα) = 12.479 mm^{-1}, F(000) = 692, crystal size 0.4 × 0.2 × 0.2 mm, 3796 independent reflections (R_{int} = 0.0734). Final R = 0.0556 for 3796 reflections with I > 2σ(I) and ωR2 = 0.1803 for all data.

$L^{I}\cdot EtOH$: $C_{37}H_{50}N_4O_2$, M = 582.81, triclinic, P-1 (No. 2), a = 9.9760(13), b = 11.2810(13), c = 15.387(2) Å, α= 70.760(8), β = 81.138(8), γ = 84.700(9)°, V = 1613.8(4) $Å^3$, T = 100(2) K, Z = 2, ρ_{calc} = 1.199 g cm^{-3}, μ(Cu-Kα) = 0.577 mm^{-1}, F(000) = 632, crystal size 0.4 × 0.25 × 0.15 mm, 5869 independent reflections (R_{int} = 0.0741). Final R = 0.0682 for 3358 reflections with I > 2σ(I) and ωR2 = 0.1960 for all data.

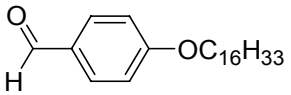
All three structures were solved by direct methods and refined by full-matrix least-squares on F^2 using the SHELXTL program package.[19] Non-hydrogen atoms were anisotropically refined and the hydrogen atoms in the

riding mode with isotropic temperature factors fixed at 1.2 times U(eq) of the parent atoms (1.5 times for methyl groups). CCDC-606328, 606329 and 606330 contain the supplementary crystallographic data for this paper and can be obtained free of charge via www.ccdc.cam.ac.uk/conts/retrieving.html (or from the Cambridge Crystallographic Data Centre, 12, Union Road, Cambridge CB2 1EZ, UK; fax: +44-1223-336033; or deposit@ccdc.cam.ac.uk).

5.5.2 Synthesis

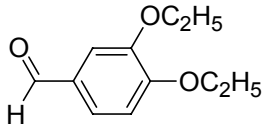
5.5.2.1 Synthesis of precursors and ligands

(a) 4-Hexadecyloxybenzaldehyde (15)



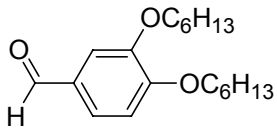
4-Hexadecyloxybenzaldehyde was prepared by adding hexadecyl bromide (0.0073 mol, 2.23 g) to a solution of 4-hydroxybenzaldehyde (0.0072 mol, 1.00 g) and potassium carbonate (0.0073 mol, 1.01 g) in DMF (50 ml). A catalytic amount of potassium iodide was added and the mixture was refluxed for 3 hours under a nitrogen atmosphere. After the reaction mixture was cooled to room temperature, it was poured into 150 ml of a H_2O/HCl (100:50) solution. The solution was extracted with dichloromethane and the combined organic layers were washed with brine, dried over anhydrous $MgSO_4$ and the solvent was removed under reduced pressure. The crude product was purified on a silica column with hexane/ethyl acetate (95:5) as the eluent. The product was recrystallized from methanol. Yield: 60% (1.50 g). δ_H (300 MHz, $CDCl_3$): 0.88 (t, 3H, CH_3), 1.26–1.49 (m, 26H, CH_2), 1.79–1.84 (m, 2H, –C**H**$_2$–CH_2–O–), 4.04 (t, 2H, –C**H**$_2$–O–), 7.00 (d, 2H, H-aryl, J_o = 8.4 Hz), 7.81 (d, 2H, H-aryl, J_o = 8.4 Hz), 9.88 (s, 1H, CH=O). M.p.: 44 °C.

(b) 3,4-Diethyloxybenzaldehyde (16)



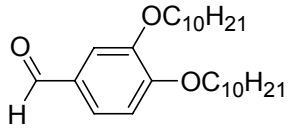
3,4-Diethyloxybenzaldehyde was prepared by adding ethyl bromide (0.015 mol, 1.63 g) to a solution of 3,4-dihydroxybenzaldehyde (0.0072 mol, 1.00 g) and potassium carbonate (0.015 mol, 2.07 g) in DMF (50 ml). A catalytic amount of potassium iodide was added and the mixture was refluxed for 3 hours under a nitrogen atmosphere. After the reaction mixture was cooled to room temperature, it was poured into 150 ml of a H_2O/HCl (100:50) solution. The solution was extracted with dichloromethane and the combined organic layers were washed with brine, dried over anhydrous $MgSO_4$ and the solvent was removed under reduced pressure. The crude product was purified on a silica column with hexane/ethyl acetate (95:5) as the eluent. The product was obtained as a yellow oil. Yield: 53% (0.74 g). δ_H (300 MHz, $CDCl_3$): 1.46–1.55 (m, 6H, CH_3), 4.11–4.24 (m, 4H, –C**H**$_2$–O–), 6.98 (d, 1H, H-aryl, J_o = 7.9 Hz), 7.40–7.46 (m, 2H, H-aryl), 9.83 (s, 1H, CH=O).

(c) 3,4-Dihexyloxybenzaldehyde (17)



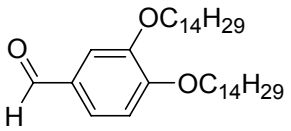
3,4-Dihexyloxybenzaldehyde was prepared by adding hexyl bromide (0.015 mol, 2.48 g) to a solution of 3,4-dihydroxybenzaldehyde (0.0072 mol, 1.00 g) and potassium carbonate (0.015 mol, 2.07 g) in DMF (50 ml). A catalytic amount of potassium iodide was added and the mixture was refluxed for 3 hours under a nitrogen atmosphere. After the reaction mixture was cooled to room temperature, it was poured into 150 ml of a H_2O/HCl (100:50) solution. The solution was extracted with dichloromethane and the combined organic layers were washed with brine, dried over anhydrous $MgSO_4$ and the solvent was removed under reduced pressure. The crude product was purified on a silica column with hexane/ethyl acetate (95:5) as the eluent. The product was recrystallized from ethanol. Yield: 78% (1.72g). δ_H (300 MHz, $CDCl_3$): 0.92 (t, 6H, CH_3), 1.27–1.58 (m, 10H, CH_2), 1.81–1.92 (m, 4H, –C**H**$_2$–CH_2–O–), 4.05–4.12 (m, 4H, –C**H**$_2$–O–), 6.95 (d, 1H, H-aryl, J_o = 8.0 Hz), 7.41–7.45 (m, 2H, H-aryl), 9.85 (s, 1H, CH=O). M.p.: 40 °C.

(d) 3,4-Didecyloxybenzaldehyde (18)



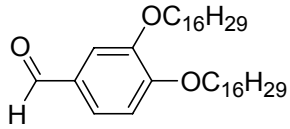
3,4-Didecyloxybenzaldehyde was prepared by adding decyl bromide (0.015 mol, 3.32 g) to a solution of 3,4-dihydroxybenzaldehyde (0.0072 mol, 1.00 g) and potassium carbonate (0.015 mol, 2.07 g) in DMF (50 ml). A catalytic amount of potassium iodide was added and the mixture was refluxed for 3 hours under a nitrogen atmosphere. After the reaction mixture was cooled to room temperature, it was poured into 150 ml of a H_2O/HCl (100:50) solution. The solution was extracted with dichloromethane and the combined organic layers were washed with brine, dried over anhydrous $MgSO_4$ and the solvent was removed under reduced pressure. The crude product was purified on a silica column with hexane/ethyl acetate (95:5) as the eluent. The product was recrystallized from ethanol. Yield: 69% (2.08 g). δ_H (300 MHz, $CDCl_3$): 0.91 (t, 6H, CH_3), 1.29–1.59 (m, 28H, CH_2), 1.81–1.90 (m, 4H, –C**H**$_2$–CH_2–O–), 4.04–4.11 (m, 4H, –C**H**$_2$–O–), 6.98 (d, 1H, H-aryl, J_o = 8.1 Hz), 7.41–7.45 (m, 2H, H-aryl), 9.84 (s, 1H, CH=O). M.p.: 62 °C.

(e) 3,4-Didodecyloxybenzaldehyde (19)



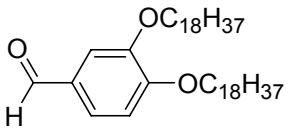
3,4-Didodecyloxybenzaldehyde was prepared by adding tetradecyl bromide (0.015 mol, 4.16 g) to a solution of 3,4-dihydroxybenzaldehyde (0.0072 mol, 1.00 g) and potassium carbonate (0.015 mol, 2.07 g) in DMF (50 ml). A catalytic amount of potassium iodide was added and the mixture was refluxed for 3 hours under a nitrogen atmosphere. After the reaction mixture was cooled to room temperature, it was poured into 150 ml of a H_2O/HCl (100:50) solution. The solution was extracted with dichloromethane and the combined organic layers were washed with brine, dried over anhydrous $MgSO_4$ and the solvent was removed under reduced pressure. The crude product was purified on a silica column with hexane/ethyl acetate (95:5) as the eluent. The product was recrystallized from ethanol. Yield: 69% (2.64 g). δ_H (300 MHz, $CDCl_3$): 0.89 (t, 6H, CH_3), 1.27–1.57 (m, 44H, CH_2), 1.81–1.90 (m, 4H, –C**H**$_2$–CH_2–O–), 4.01–4.11 (m, 4H, –C**H**$_2$–O–), 6.98 (d, 1H, H-aryl, J_o = 8.0 Hz), 7.40–7.45 (m, 2H, H-aryl), 9.84 (s, 1H, CH=O). M.p.: 72 °C.

(f) 3,4-Dihexadecyloxybenzaldehyde (20)



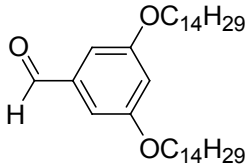
3,4-Dihexadecyloxybenzaldehyde was prepared by adding hexadecyl bromide (0.015 mol, 4.58 g) to a solution of 3,4-dihydroxybenzaldehyde (0.0072 mol, 1.00 g) and potassium carbonate (0.015 mol, 2.07 g) in DMF (50 ml). A catalytic amount of potassium iodide was added and the mixture was refluxed for 3 hours under a nitrogen atmosphere. After the reaction mixture was cooled to room temperature, it was poured into 150 ml of a H_2O/HCl (100:50) solution. The solution was extracted with dichloromethane and the combined organic layers were washed with brine, dried over anhydrous $MgSO_4$ and the solvent was removed under reduced pressure. The crude product was purified on a silica column with hexane/ethyl acetate (95:5) as the eluent. The product was recrystallized from ethanol. Yield: 73% (3.09 g). δ_H (300 MHz, $CDCl_3$): 0.88 (t, 6H, CH_3), 1.19–1.48 (m, 52H, CH_2), 1.79–1.90 (m, 4H, –C**H**$_2$–CH_2–O–), 4.03–4.10 (m, 4H, –C**H**$_2$–O–), 6.94 (d, 1H, H-aryl, J_o = 7.3 Hz), 7.40–7.43 (m, 2H, H-aryl), 9.83 (s, 1H, CH=O). M.p.: 79 °C.

(g) 3,4-Dioctadecyloxybenzaldehyde (21)



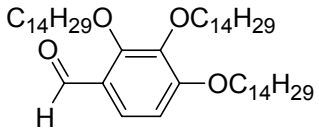
3,4-Dioctadecyloxybenzaldehyde was prepared by adding octadecyl bromide (0.015 mol, 5.00 g) to a solution of 3,4-dihydroxybenzaldehyde (0.0072 mol, 1.00 g) and potassium carbonate (0.015 mol, 2.07 g) in DMF (50 ml). A catalytic amount of potassium iodide was added and the mixture was refluxed for 3 hours under a nitrogen atmosphere. After the reaction mixture was cooled to room temperature, it was poured into 150 ml of a H_2O/HCl (100:50) solution. The solution was extracted with dichloromethane and the combined organic layers were washed with brine, dried over anhydrous $MgSO_4$ and the solvent was removed under reduced pressure. The crude product was purified on a silica column with hexane/ethyl acetate (95:5) as the eluent. The product was recrystallized from ethanol. Yield: 82% (3.80 g). δ_H (300 MHz, $CDCl_3$): 0.89 (t, 6H, CH_3), 1.27–1.57 (m, 60H, CH_2), 1.81–1.89 (m, 4H, –C**H**$_2$–CH_2–O–), 4.04–4.11 (m, 4H, –C**H**$_2$–O–), 6.98 (d, 1H, H-aryl, J_o = 8.1 Hz), 7.41–7.45 (m, 2H, H-aryl), 9.85 (s, 1H, CH=O). M.p.: 83 °C.

(h) 3,5-Didodecyloxybenzaldehyde (22)



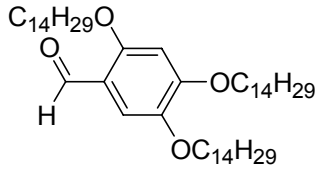
3,5-Didodecyloxybenzaldehyde was prepared by adding tetradecyl bromide (0.015 mol, 4.16 g) to a solution of 3,5-dihydroxybenzaldehyde (0.0072 mol, 1.00 g) and potassium carbonate (0.015 mol, 2.07 g) in DMF (50 ml). A catalytic amount of potassium iodide was added and the mixture was refluxed for 3 hours under a nitrogen atmosphere. After the reaction mixture was cooled to room temperature, it was poured into 150 ml of a H_2O/HCl (100:50) solution. The solution was extracted with dichloromethane and the combined organic layers were washed with brine, dried over anhydrous $MgSO_4$ and the solvent was removed under reduced pressure. The crude product was purified on a silica column with hexane/ethyl acetate (95:5) as the eluent. The product was recrystallized from ethanol. Yield: 77% (2.94 g). δ_H (300 MHz, $CDCl_3$): 0.89 (t, 6H, CH_3), 1.20–1.46 (m, 44H, CH_2), 1.76–1.83 (m, 4H, –C**H**$_2$–CH_2–O–), 3.98–4.02 (m, 4H, –C**H**$_2$–O–), 6.71 (s, 1H, H-aryl), 7.00 (s, 2H, H-aryl), 9.90 (s, 1H, CH=O). M.p.: 47 °C.

(i) 2,3,4-Tridodecyloxybenzaldehyde (23)



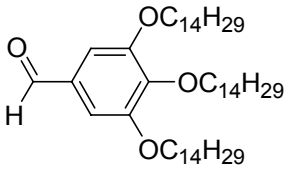
2,3,4-Tridodecyloxybenzaldehyde was prepared by adding tetradecyl bromide (0.0200 mol, 5.55 g) to a solution of 2,3,4-trihydroxybenzaldehyde (0.0065 mol, 1.00 g) and potassium carbonate (0.0200 mol, 2.76 g) in DMF (50 ml). A catalytic amount of potassium iodide was added and the mixture was refluxed for 3 hours under a nitrogen atmosphere. After the reaction mixture was cooled to room temperature, it was poured into 150 ml of a H_2O/HCl (100:50) solution. The solution was extracted with dichloromethane and the combined organic layers were washed with brine, dried over anhydrous $MgSO_4$ and the solvent was removed under reduced pressure. The crude product was purified on a silica column with hexane/ethyl acetate (95:5) as the eluent. The product was recrystallized from ethanol. Yield: 55% (2.66 g). δ_H (300 MHz, $CDCl_3$): 0.89 (t, 9H, CH_3), 1.28–1.55 (m, 66H, CH_2), 1.76–1.88 (m, 6H, –C**H**$_2$–CH_2–O–), 3.99 (t, 2H, –C**H**$_2$–O–), 4.05 (t, 2H, –C**H**$_2$–O–), 4.18 (t, 2H, –C**H**$_2$–O–), 6.74 (d, 1H, H-aryl, J_o = 8.8 Hz), 7.57 (d, 1H, H-aryl, J_o = 8.8 Hz), 10.27 (s, 1H, CH=O). M.p.: 44 °C.

(j) 2,4,5-Tridodecyloxybenzaldehyde (24)



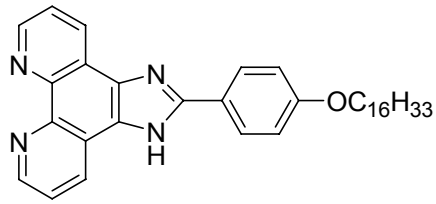
2,4,5-Tridodecyloxybenzaldehyde was prepared by adding tetradecyl bromide (0.0200 mol, 5.55 g) to a solution of 2,4,5-trihydroxybenzaldehyde (**8**) (0.0065 mol, 1.00 g) and potassium carbonate (0.0200 mol, 2.76 g) in DMF (50 ml). A catalytic amount of potassium iodide was added and the mixture was refluxed for 3 hours under a nitrogen atmosphere. After the reaction mixture was cooled to room temperature, it was poured into 150 ml of a H_2O/HCl (100:50) solution. The solution was extracted with dichloromethane and the combined organic layers were washed with brine, dried over anhydrous $MgSO_4$ and the solvent was removed under reduced pressure. The product was recrystallized from petroleum ether. Yield: 51% (2.46 g). δ_H (300 MHz, $CDCl_3$): 0.89 (t, 9H, CH_3), 1.28–1.53 (m, 66H, CH_2), 1.77–1.91 (m, 6H, –C**H**$_2$–CH_2–O–), 3.96–4.08 (m, 6H, –C**H**$_2$–O–), 6.46 (s, 1H, H-aryl), 7.33 (s, 1H, H-aryl), 10.34 (s, 1H, CH=O). M.p.: 79 °C.

(k) 3,4,5-Tridodecyloxybenzaldehyde (25)



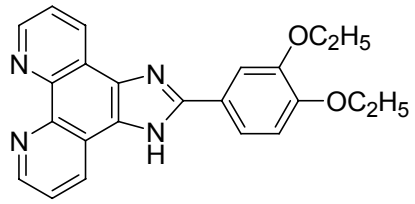
3,4,5-Tridodecyloxybenzaldehyde was prepared by adding tetradecyl bromide (0.0180 mol, 4.99 g) to a solution of 3,4,5-trihydroxybenzaldehyde monohydrate (0.0058 mol, 1.00 g) and potassium carbonate (0.0180 mol, 2.49 g) in DMF (50 ml). A catalytic amount of potassium iodide was added and the mixture was refluxed for 3 hours under a nitrogen atmosphere. After the reaction mixture was cooled to room temperature, it was poured into 150 ml of a H_2O/HCl (100:50) solution. The solution was extracted with dichloromethane and the combined organic layers were washed with brine, dried over anhydrous $MgSO_4$ and the solvent was removed under reduced pressure. The crude product was purified on a silica column with hexane/ethyl acetate (95:5) as the eluent. The product was recrystallized from ethanol. Yield: 41% (1.72 g). δ_H (300 MHz, $CDCl_3$): 0.89 (t, 9H, CH_3), 1.27–1.49 (m, 66H, CH_2), 1.72–1.88 (m, 6H, –C**H**$_2$–CH_2–O–), 4.02–4.17 (m, 6H, –C**H**$_2$–O–), 7.09 (s, 2H, H-aryl), 9.84 (s, 1H, CH=O). M.p.: 58 °C.

(l) L^I



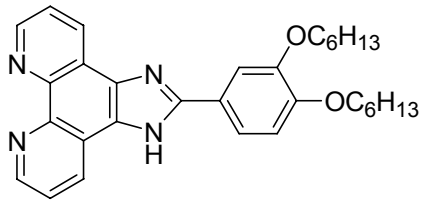
Ligand L^I was prepared by adding 4-hexadecyloxybenzaldehyde (**15**) (0.0020 mol, 0.69 g) to a warm solution of 1,10-phenanthroline-5,6-dione (**10**) (0.0020 mol, 0.42 g) and ammonium acetate (0.0170 mol, 1.32 g) in 20 ml of glacial acetic acid. The mixture was heated to 85 °C for 5 hours. After the reaction mixture was cooled to room temperature, it was poured into 100 ml of water and neutralized to pH 7 with an aqueous ammonia solution. The precipitate was filtered off, washed with distilled water and dried. The crude product was purified on a silica column with $CHCl_3$/hexane/MeOH (50:50:10) as the eluent. Since the compound holds solvents firmly, it was dried in a vacuum oven at 50 °C. Yield: 62% (0.67 g). δ_H (400 MHz, 363 K, DMSO-d6): 0.86 (t, 3H, CH_3), 1.26–1.52 (m, 26H, CH_2), 1.75–1.82 (m, 2H, –C**H**$_2$–CH_2–O–), 4.11 (t, 2H, –C**H**$_2$–O–), 7.14 (d, 2H, H-aryl, J_o = 8.8 Hz), 7.77–7.80 (b, m, 2H, H-aryl), 8.21 (d, 2H, H-aryl, J_o = 8.8 Hz), 8.95 (d, 2H, H-aryl, J_o = 8.00 Hz), 9.03 (b, s, 2H, H-aryl). δ_C (100 MHz, DMSO-d6): 13.57, 21.86, 25.45, 28.51, 28.64, 28.74, 28.83, 28.89, 31.16, 115.19, 122.96, 127.98, 129.56, 143.52, 147.35, 151.07, 160.21. Calcd. for $C_{35}H_{44}N_4O{\cdot}0.5H_2O$: C 77.03, H 8.31, N 10.27. Found: C 77.00, H 8.44, N 9.96. ESI-MS (Methanol, m/z): 537.5, $[M + H]^+$. M.p.: 162 °C.

(m) L^{II}



Ligand L^{II} was prepared by adding 3,4-diethyloxybenzaldehyde (**16**) (0.0020 mol, 0.39 g) to a warm solution of 1,10-phenanthroline-5,6-dione (**10**) (0.0020 mol, 0.42 g) and ammonium acetate (0.0170 mol, 1.32 g) in 20 mL of glacial acetic acid. The mixture was heated to 85 °C for 5 hours. After the reaction mixture was cooled to room temperature, it was poured into 100 ml of water and neutralized to pH 7 with an aqueous ammonia solution. The precipitate was filtered off, washed with distilled water and dried. The crude product was purified on a silica column with $CHCl_3$/hexane/MeOH (50:50:10) as the eluent. Since the compound holds solvents firmly, it was dried in a vacuum oven at 50 °C. Yield: 41% (0.32 g). δ_H (300 MHz, DMSO-d6): 1.36–1.45 (m, 6H, CH_3), 4.10–4.24 (m, 4H, –C**H**$_2$–O–), 7.20 (d, 1H, H-aryl, J_o = 8.2 Hz), 7.84–7.86 (m, 4H, H-aryl), 8.92 (d, 2H, H-aryl, J_o = 6.4 Hz), 9.02 (d, 2H, H-aryl, J_o = 2.8 Hz), 13.59 (b, s, 1H, N–H). δ_C (75 MHz, DMSO-d6): 15.60, 15.72, 64.73, 65.04, 80.06, 112.16, 114.08, 120.24, 123.49, 124.07, 130.47, 144.30, 148.53, 149.20, 150.58, 151.73. Calcd. for $C_{23}H_{20}N_4O_2 \cdot 0.5H_2O$: C 70.21, H 5.38, N 14.24. Found: C 69.78, H 5.77, N 13.91. ESI-MS (Methanol, m/z): 385.4, $[M + H]^+$. M.p.: 345 °C.

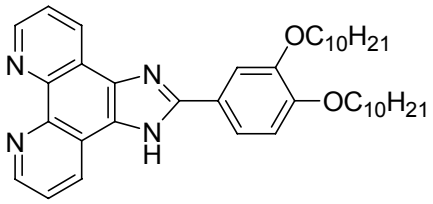
(n) L^{III}



Ligand L^{III} was prepared by adding 3,4-dihexyloxybenzaldehyde (**17**) (0.0020 mol, 0.61 g) to a warm solution of 1,10-phenanthroline-5,6-dione (**10**) (0.0020 mol, 0.42 g) and ammonium acetate (0.0170 mol, 1.32 g) in 20 ml of glacial acetic acid. The mixture was heated to 85 °C for 5 hours. After the reaction mixture was cooled to room temperature, it was poured into 100 ml of water and neutralized to pH 7 with an aqueous ammonia solution. The precipitate was filtered off, washed with distilled water and dried. The crude product was purified on a silica column with $CHCl_3$/hexane/MeOH (50:50:10) as the eluent. Since the compound holds solvents firmly, it was dried in a vacuum oven at 50 °C. Yield: 68% (0.68 g). δ_H (300 MHz, THF-d8): 0.83 (t, 3H, CH_3), 0.89 (t, 3H, CH_3), 1.12–1.37 (m, 8H, CH_2), 1.43–1.52 (m, 4H, CH_2), 1.72–1.88 (m, 4H, –C**H**$_2$–CH_2–O–), 3.51 (t, 2H, –C**H**$_2$–O–), 3.96 (t, 2H, –C**H**$_2$–O–), 6.93 (d, 1H, H-aryl, J_o = 6.2 Hz), 7.30 (b, m, 1H, H-aryl), 7.73 (b, m, 1H, H-aryl), 7.93–7.96 (m, 2H, H-aryl), 8.70– 8.73 (b, m, 2H, H-aryl), 8.95 (b, s, 1H, H-aryl), 9.12 (d, 1H, H-aryl, J_o = 5.7 Hz), 14.42 (b, s, 1H, N–H). δ_C (75 MHz, THF-d8): 14.20, 23.27, 26.35, 26.50, 29.95, 30.10, 32.26, 32.35, 68.97, 69.45, 112.50, 114.08, 120.20, 121.03, 123.43, 123.98, 124.47, 125.75, 127.61, 130.62, 131.11, 137.57, 144.60, 144.88, 147.56, 148.11, 150.21, 151.27, 152.74. Calcd. for $C_{31}H_{36}N_4O_2 \cdot 0.5H_2O$: C 73.63, H 7.38, N 11.08. Found: C 73.67, H 7.88, N

10.71. ESI-MS (Methanol, m/z): 497.6, $[M + H]^+$. The compound is an enantiotropic liquid crystal: g 91 N 128 I.

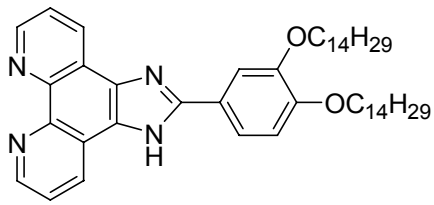
(o) L^{IV}



Ligand L^{IV} was prepared by adding 3,4-didecyloxybenzaldehyde (**18**) (0.0020 mol, 0.84 g) to a warm solution of 1,10-phenanthroline-5,6-dione (**10**) (0.0020 mol, 0.42 g) and ammonium acetate (0.0170 mol, 1.32 g) in 20 ml of glacial acetic acid. The mixture was heated to 85 °C for 5 hours. After the reaction mixture was cooled to room temperature, it was poured into 100 ml of water and neutralized to pH 7 with an aqueous ammonia solution. The precipitate was filtered off, washed with distilled water and dried. The crude product was purified on a silica column with $CHCl_3$/hexane/MeOH (50:50:10) as the eluent. Since the compound holds solvents firmly, it was dried in a vacuum oven at 50 °C. Yield: 41% (0.50 g). δ_H (400 MHz, THF-d8): 0.83–0.87 (m, 6H, CH_3), 1.16–1.75 (m, 32H, CH_2), 3.43 (m, 2H, –C**H**$_2$–O–), 3.94 (m, 2H, –C**H**$_2$–O–), 6.91 (d, 1H, H-aryl, J_o = 8.4 Hz), 7.26 (b, m, 1H, H-aryl), 7.74 (b, m, 1H, H-aryl), 7.92–7.99 (m, 2H, H-aryl), 8.67 (b, s, 1H, H-aryl), 8.76 (b, d, 1H, H-aryl), 8.95 (b, s, 1H, H-aryl), 9.16 (b, d, 1H, H-aryl), 14.68 (b, s, 1H, N–H). δ_C (100 MHz, THF-d8): 14.20, 14.24, 23.34, 26.69, 30.02, 30.10, 30.15, 30.32, 30.40, 32.65, 32.70, 69.02, 69.55, 112.64, 114.27, 120.30, 121.10, 123.46, 123.98, 124.53, 125.82, 127.68, 130.80, 131.21, 137.59, 144.56, 144.84, 147.51, 148.06, 150.25, 151.29,

152.83. Calcd. for $C_{39}H_{52}N_4O_2 \cdot 0.5H_2O$: C 75.81, H 8.65, N 9.07. Found: C 76.08, H 8.99, N 8.73. ESI-MS (Methanol, m/z): 609.7, $[M + H]^+$. The compound is an enantiotropic liquid crystal: g 60 N 95 I.

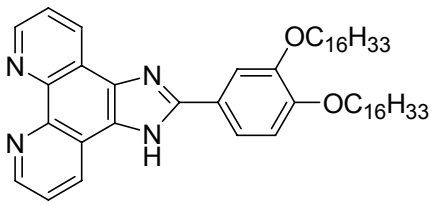
(p) L^V



Ligand L^V was prepared by adding 3,4-didodecyloxybenzaldehyde (**19**) (0.0020 mol, 1.06 g) to a warm solution of 1,10-phenanthroline-5,6-dione (**10**) (0.0020 mol, 0.42 g) and ammonium acetate (0.0170 mol, 1.32 g) in 20 ml of glacial acetic acid. The mixture was heated to 85 °C for 5 hours. After the reaction mixture was cooled to room temperature, it was poured into 100 ml of water and neutralized to pH 7 with an aqueous ammonia solution. The precipitate was filtered off, washed with distilled water and dried. The crude product was purified on a silica column with $CHCl_3$/hexane/MeOH (50:50:10) as the eluent. Since the compound holds solvents firmly, it was dried in a vacuum oven at 50 °C. Yield: 69% (1.00 g). δ_H (400 MHz, THF-d8): 0.85 (t, 6H, CH_3), 1.23–1.88 (m, 48H, CH_2), 3.57 (t, 2H, –C**H**$_2$–O–), 3.96 (t, 2H, –C**H**$_2$–O–), 6.94 (d, 1H, H-aryl, J_o = 8.0 Hz), 7.34 (b, s, 1H, H-aryl), 7.71 (b, s, 1H, H-aryl), 7.92–7.96 (m, 2H, H-aryl), 8.73 (b, s, 2H, H-aryl), 8.95 (b, s, 1H, H-aryl), 9.10 (b, s, 1H, H-aryl), 14.22 (b, s, 1H, N–H). δ_C (100 MHz, THF-d8): 13.73, 22.86, 26.29, 26.37, 29.63, 29.71, 29.92, 29.97, 32.19, 68.80, 69.10, 78.89, 112.33, 113.79, 119.67, 120.38, 122.88, 123.29, 124.04, 125.12, 127.01, 129.83, 130.41, 144.37, 147.20, 147.66,

149.83, 150.92, 152.07. Calcd. for $C_{47}H_{68}N_4O_2 \cdot 0.5H_2O$: C 77.32, H 9.53, N 7.67. Found: C 77.72, H 9.77, N 7.23. ESI-MS (Methanol, m/z): 721.8, $[M + H]^+$. The compound is an enantiotropic liquid crystal: g 64 M 82 I.

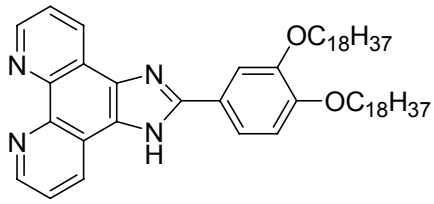
(q) L^{VI}



Ligand L^{VI} was prepared by adding 3,4-dihexadecyloxybenzaldehyde (**20**) (0.0020 mol, 1.17 g) to a warm solution of 1,10-phenanthroline-5,6-dione (**10**) (0.0020 mol, 0.42 g) and ammonium acetate (0.0170 mol, 1.32 g) in 20 ml of glacial acetic acid. The mixture was heated to 85 °C for 5 hours. After the reaction mixture was cooled to room temperature, it was poured into 100 ml of water and neutralized to pH 7 with an aqueous ammonia solution. The precipitate was filtered off, washed with distilled water and dried. The crude product was purified on a silica column with $CHCl_3$/hexane/MeOH (50:50:10) as the eluent. Since the compound holds solvents firmly, it was dried in a vacuum oven at 50 °C. Yield: 60% (1.55 g). δ_H (400 MHz, 363 K, DMSO-d6): 0.86 (t, 6H, CH_3), 1.26–1.56 (m, 52H, CH_2), 1.76–1.84 (m, 4H, –C**H**$_2$–CH_2–O–), 4.11 (t, 2H, –C**H**$_2$–O–), 4.18 (t, 2H, –C**H**$_2$–O–), 7.16 (d, 1H, H-aryl, J_o = 8.5 Hz), 7.91–7.98 (m, 4H, H-aryl), 9.08 (b, s, 2H, H-aryl), 9.20 (b, d, 2H, H-aryl). δ_C (100 MHz, 363 K, DMSO-d6): 13.57, 21.86, 25.55, 25.59, 28.51, 28.70, 28.73, 28.85, 28.91, 28.98, 29.10, 31.16, 69.29, 69.80, 113.94, 115.01, 120.34, 123.12, 123.87, 131.70, 146.49, 149.44, 151.06, 151.74. Calcd. for $C_{51}H_{76}N_4O_2 \cdot 0.5H_2O$: C 77.91, H 9.87, N 7.13.

Found: C 77.80, H 10.20, N 6.83. ESI-MS (Methanol, m/z): 777.7, $[M + H]^+$. M.p.: 113 °C (a monotropic phase is formed upon cooling at 79 °C).

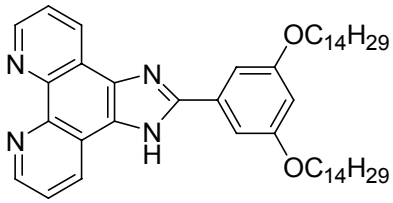
(r) L^{VII}



Ligand L^{VII} was prepared by adding 3,4-dioctadecyloxybenzaldehyde (**21**) (0.0020 mol, 1.29 g) to a warm solution of 1,10-phenanthroline-5,6-dione (**10**) (0.0020 mol, 0.42 g) and ammonium acetate (0.0170 mol, 1.32 g) in 20 ml of glacial acetic acid. The mixture was heated to 85 °C for 5 hours. After the reaction mixture was cooled to room temperature, it was poured into 100 ml of water and neutralized to pH 7 with an aqueous ammonia solution. The precipitate was filtered off, washed with distilled water and dried. The crude product was purified on a silica column with $CHCl_3$/hexane/MeOH (50:50:10) as the eluent. Since the compound holds solvents firmly, it was dried in a vacuum oven at 50 °C. Yield: 30% (0.50 g). δ_H (400 MHz, THF-d8): 0.87 (t, 6H, CH_3), 1.28–1.76 (m, 64H, CH_2), 3.52 (t, 2H, –C**H**$_2$–O–), 3.96 (t, 2H, –C**H**$_2$–O–), 6.93 (d, 1H, H-aryl, J_o = 8.4 Hz), 7.30 (b, m, 1H, H-aryl), 7.72 (b, m, 1H, H-aryl), 7.92–7.96 (m, 2H, H-aryl), 8.73 (b, m, 2H, H-aryl), 8.95 (b, s, 1H, H-aryl), 9.13 (b, d, 1H, H-aryl), 14.40 (b, s, 1H, N–H). δ_C (100 MHz, THF-d8): 14.22, 23.34, 26.75, 26.86, 30.09, 30.11, 30.20, 30.39, 30.45, 30.47, 30.51, 30.54, 32.67, 69.17, 69.58, 112.75, 114.28, 120.23, 120.97, 123.37, 123.86, 124.56, 125.73, 127.57, 130.48, 131.04, 137.60, 144.70, 144.93, 147.61, 148.09,150.30, 151.36, 152.68.

Calcd. for $C_{55}H_{84}N_4O_2 \cdot 0.5H_2O$: C 78.43, H 10.17, N 6.65. Found: C 78.47, H 9.77, N 6.78. ESI-MS (Methanol, m/z): 833.9, $[M + H]^+$. M.p.: 116 °C (a monotropic phase is formed upon cooling at 77 °C).

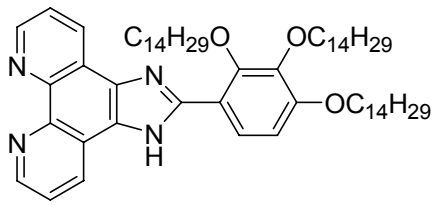
(s) L^{VIII}



Ligand L^{VIII} was prepared by adding 3,5-didodecyloxybenzaldehyde (**22**) (0.0020 mol, 1.06 g) to a warm solution of 1,10-phenanthroline-5,6-dione (**10**) (0.0020 mol, 0.42 g) and ammonium acetate (0.0170 mol, 1.32 g) in 20 ml of glacial acetic acid. The mixture was heated to 85 °C for 5 hours. After the reaction mixture was cooled to room temperature, it was poured into 100 ml of water and neutralized to pH 7 with an aqueous ammonia solution. The precipitate was filtered off, washed with distilled water and dried. The crude product was purified on a silica column with $CHCl_3$/hexane/MeOH (50:50:10) as the eluent. Since the compound holds solvents firmly, it was dried in a vacuum oven at 50 °C. Yield: 34% (0.49 g). δ_H (300 MHz, THF-d8): 0.87 (t, 6H, CH_3), 1.24 (m, 44H, CH_2), 1.55 (m, 4H, –C**H**$_2$–CH_2–O–), 3.57 (t, 4H, –C**H**$_2$–O–), 6.41 (s, 1H, H-aryl), 7.32 (b, m, 1H, H-aryl), 7.53 (s, 2H, H-aryl), 7.77 (b, m, 1H, H-aryl), 8.68 (b, s, 1H, H-aryl), 8.77 (b, d, 1H, H-aryl), 8.98 (b, m, 1H, H-aryl), 9.15 (b, d, 1H, H-aryl), 14.70 (b, s, 1H, N–H). δ_C (75 MHz, THF-d8): 14.33, 23.43, 26.84, 30.10, 30.20, 30.29, 30.53, 32.75, 68.39, 103.61, 105.34, 121.00, 123.68, 124.08, 125.78, 127.80, 130.84, 131.12, 133.13, 137.51, 145.04, 148.14, 148.30, 152.41,

161.52. Calcd. for $C_{47}H_{68}N_4O_2 \cdot 0.5H_2O$: C 77.32, H 9.53, N 7.67. Found: C 77.29, H 9.23, N 7.48. ESI-MS (Methanol, m/z): 721.8, $[M + H]^+$. M.p.: 158 °C.

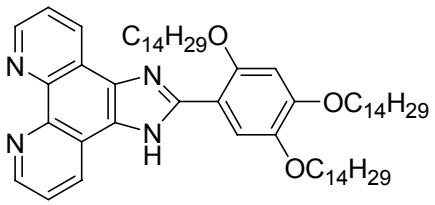
(t) L^{IX}



Ligand L^{IX} was prepared by adding 2,3,4-tridodecyloxybenzaldehyde (**23**) (0.0020 mol, 1.50 g) to a warm solution of 1,10-phenanthroline-5,6-dione (**10**) (0.0020 mol, 0.42 g) and ammonium acetate (0.0170 mol, 1.32 g) in 20 ml of glacial acetic acid. The mixture was heated to 85 °C for 5 hours. After the reaction mixture was cooled to room temperature, it was poured into 100 ml of water and neutralized to pH 7 with an aqueous ammonia solution. The precipitate was filtered off, washed with distilled water and dried. The crude product was purified on a silica column with $CHCl_3$/hexane/MeOH (50:50:10) as the eluent. Since the compound holds solvents firmly, it was dried in a vacuum oven at 50 °C. Yield: 42% (0.78 g). δ_H (400 MHz, $CDCl_3$): 0.85–0.89 (m, 9H, CH_3), 1.22–1.59 (m, 66H, CH_2), 1.82–1.96 (m, 6H, –C**H**$_2$–CH_2–O–), 4.07 (t, 4H, –C**H**$_2$–O–), 4.30 (t, 2H, –C**H**$_2$–O–), 6.88 (d, 1H, H-aryl, J_o = 8.8 Hz), 7.66 (dd, 1H, H-aryl, J_o = 8.2 Hz, J_m = 4.2 Hz), 7.70 (dd, 1H, H-aryl, J_o = 8.2 Hz, J_m = 4.2 Hz), 8.23 (d, 1H, H-aryl, J_o = 8.8 Hz), 8.28 (d, 1H, H-aryl, J_o = 8.2 Hz), 9.04 (d, 1H, H-aryl, , J_o = 8.2 Hz), 9.14 (s, 2H, H-aryl), 11.46 (s, 1H, N–H). δ_C (100 MHz, $CDCl_3$): 14.06, 22.66, 26.13, 26.19, 26.45, 29.33, 29.35, 29.41, 29.59, 29.62, 29.64, 29.69,

29.73, 30.40, 30.96, 31.91, 68.95, 73.92, 74.93, 109.29, 115.41, 118.90, 122.60, 123.19, 123.85, 124.28, 124.49, 127.86, 130.37, 136.10, 141.52, 144.35, 144.42, 148.04, 148.52, 149.19, 150.83, 155.02. Calcd. for $C_{61}H_{96}N_4O_3 \cdot 0.5H_2O$: C 77.74, H 10.37, N 5.94. Found: C 78.22, H 10.40, N 5.61. ESI-MS (Methanol, m/z): 933.9, $[M + H]^+$. M.p.: 77 °C.

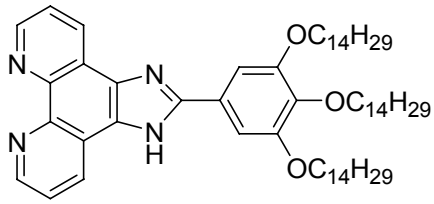
(u) L^X



Ligand L^X was prepared by adding 2,4,5-tridodecyloxybenzaldehyde (**24**) (0.0020 mol, 1.50 g) to a warm solution of 1,10-phenanthroline-5,6-dione (**10**) (0.0020 mol, 0.42 g) and ammonium acetate (0.0170 mol, 1.32 g) in 20 ml of glacial acetic acid. The mixture was heated to 85 °C for 5 hours. After the reaction mixture was cooled to room temperature, it was poured into 100 ml of water and neutralized to pH 7 with an aqueous ammonia solution. The precipitate was filtered off, washed with distilled water and dried. The crude product was purified on a silica column with $CHCl_3$/hexane/MeOH (50:50:10) as the eluent. Since the compound holds solvents firmly, it was dried in a vacuum oven at 50 °C. Yield: 45% (0.84 g). δ_H (300 MHz, THF-d8): 0.86–0.88 (m, 9H, CH_3), 1.22–2.03 (m, 72H, CH_2), 4.06–4.10 (m, 4H, –C**H**$_2$–O–), 4.22 (t, 2H, –C**H**$_2$–O–), 6.76 (s, 1H, H-aryl), 7.58–7.67 (m, 2H, H-aryl), 8.09 (s, 1H, H-aryl), 8.51 (d, 1H, H-aryl, J_o = 7.8 Hz), 8.98–9.00 (m, 3H, H-aryl), 11.82 (s, 1H, N–H). δ_C (75 MHz, THF-d8): 14.32, 23.44, 27.00, 27.05, 27.22, 30.22, 30.32, 30.51, 30.58, 32.76, 69.84, 70.59, 101.23,

111.64, 116.03, 120.01, 122.92, 123.38, 125.12, 125.73, 128.84, 130.30, 136.60, 144.86, 145.27, 145.43, 147.99, 148.39, 149.91, 152.12, 152.65. Calcd. for $C_{61}H_{96}N_4O_3 \cdot 0.5H_2O$: C 77.74, H 10.37, N 5.94. Found: C 77.63, H 10.77, N 5.95. ESI-MS (Methanol, m/z): 933.9, $[M + H]^+$. M.p.: 81 °C.

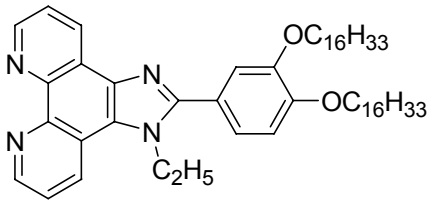
(v) L^{XI}



Ligand L^{XI} was prepared by adding 3,4,5-tridodecyloxybenzaldehyde (**25**) (0.0020 mol, 1.50 g) to a warm solution of 1,10-phenanthroline-5,6-dione (**10**) (0.0020 mol, 0.42 g) and ammonium acetate (0.0170 mol, 1.32 g) in 20 ml of glacial acetic acid. The mixture was heated to 85 °C for 5 hours. After the reaction mixture was cooled to room temperature, it was poured into 100 ml of water and neutralized to pH 7 with an aqueous ammonia solution. The precipitate was filtered off, washed with distilled water and dried. The crude product was purified on a silica column with $CHCl_3$/hexane/MeOH (50:50:10) as the eluent. Since the compound holds solvents firmly, it was dried in a vacuum oven at 50 °C. Yield: 55% (1.03 g). δ_H (300 MHz, THF-d8): 0.87 (t, 9H, CH_3), 1.25–1.67 (m, 72H, CH_2), 3.57–3.62 (m, 4H, –C**H**$_2$–O–), 3.88 (t, 2H, –C**H**$_2$–O–), 7.30 (b, m, 1H, H-aryl), 7.68 (s, 2H, H-aryl), 7.74 (b, m, 1H, H-aryl), 8.66 (b, s, 1H, H-aryl), 8.80 (b, d, 1H, H-aryl), 8.97 (b, s, 1H, H-aryl), 9.19 (b, d, 1H, H-aryl), 14.82 (b, s, 1H, N–H). δ_C (75 MHz, THF-d8): 14.36, 23.46, 26.91, 27.03, 30.23, 30.59, 31.26, 32.79, 69.25, 73.51, 105.86, 121.15, 123.68, 124.17, 125.88, 126.39,

127.92, 131.02, 131.42, 137.57, 140.35, 144.67, 144.94, 147.75, 148.24, 152.80, 154.24. Calcd. for $C_{61}H_{96}N_4O_3 \cdot 0.5H_2O$: C 77.74, H 10.37, N 5.94. Found: C 78.16, H 10.59, N 5.44. ESI-MS (Methanol, m/z): 933.9, $[M + H]^+$. M.p.: 83 °C.

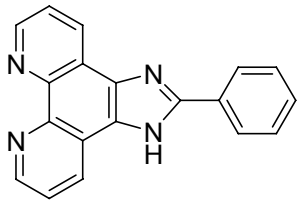
(w) L^{XII}



Under a nitrogen atmosphere, sodium hydride (0.00075 mol, 0.030 g of a 60% dispersion in mineral oil) was added to a solution of ligand L^{VI} (0.00036 mol, 0.28 g) in dry DMF (10 ml). The mixture was heated to 100 °C under a nitrogen atmosphere. Then ethylbromide (0.00046 mol, 0.050 g) was added dropwise and the mixture was heated to reflux for 12 hours under a nitrogen atmosphere. NaBr formed upon cooling was filtered off and the solvent was removed under reduced pressure. The crude product was purified on a silica column with $CHCl_3$/hexane/MeOH (50:50:10) as the eluent. Yield: 41% (0.12 g). δ_H (400 MHz, $CDCl_3$): 0.86–0.89 (m, 6H, CH_3), 1.25–1.63 (m, 55H, CH_2 and N–CH_2–C**H**$_3$), 1.84–1.90 (m, 4H, –C**H**$_2$–CH_2–O–), 4.07–4.12 (m, 4H, –C**H**$_2$–O–), 4.64–4.69 (m, 2H, N–C**H**$_2$–), 7.05 (d, 1H, H-aryl, J_o = 8.2 Hz), 7.23–7.27 (m, 2H, H-aryl), 7.69–7.73 (m, 2H, H-aryl), 8.62 (d, 1H, H-aryl, J_o = 8.4 Hz), 9.07 (d, 1H, H-aryl, J_o = 8.4 Hz), 9.17–9.18 (m, 2H, H-aryl). δ_C (75 MHz, $CDCl_3$): 14.08, 16.04, 22.67, 26.05, 29.24, 29.35, 29.43, 29.65, 29.70, 31.92, 41.62, 69.39, 69.58, 113.61, 115.52, 120.03, 122.56, 122.69, 123.44, 124.22,

124.56, 127.93, 130.36, 136.61, 144.23, 144.82, 147.59, 148.87, 149.42, 150.77, 153.68. Calcd. for $C_{53}H_{80}N_4O_2 \cdot 0.5H_2O$: C 78.18, H 10.03, N 6.88. Found: C 78.15, H 9.90, N 6.68. ESI-MS (Methanol, m/z): 805.9, $[M + H]^+$. M.p.: 122 °C.

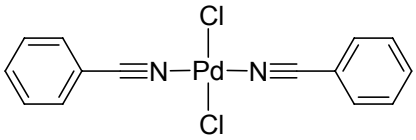
(x) L^{XIII}



Ligand L^{XIII} was prepared by adding benzaldehyde (0.0020 mol, 0.21 g) to a warm solution of 1,10-phenanthroline-5,6-dione (**10**) (0.0020 mol, 0.42 g) and ammonium acetate (0.0170 mol, 1.32 g) in 20 ml of glacial acetic acid. The mixture was heated to 85 °C for 5 hours. After the reaction mixture was cooled to room temperature, it was poured into 100 ml of water and neutralized to pH 7 with an aqueous ammonia solution. The precipitate was filtered off, washed with distilled water and dried. The crude product was recrystallized from ethanol. Since the compound holds solvents firmly, it was dried in a vacuum oven at 50 °C. Yield: 86% (0.51 g). δ_H (300 MHz, DMSO-d6): 7.50–7.54 (m, 1H, H-aryl), 7.59–7.64 (m, 2H, H-aryl), 7.81–7.85 (m, 2H, H-aryl), 8.28 (d, 2H, H-aryl, J_o = 7.3 Hz), 8.92 (d, 2H, H-aryl, J_o = 8.2 Hz), 9.02 (d, 2H, H-aryl, J_o = 3.7 Hz). Calcd. for $C_{19}H_{12}N_4 \cdot EtOH$: C 73.67, H 5.30, N 16.36. Found: C 73.66, H 5.79, N 16.38. ESI-MS (Methanol, m/z): 297.1, $[M + H]^+$. M.p.: 388 °C.

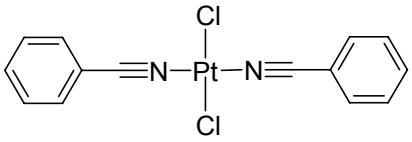
5.2.2.2 Synthesis of metal precursors

(a) Bis(phenylnitrile)palladiumdichloride (26)



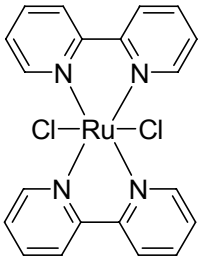
Palladium(II) chloride (0.011 mol, 2.00 g) was suspended in benzonitrile (50 ml) and the mixture was heated to 100 °C. After 20 minutes the greater part of palladium(II) chloride was dissolved to give a red solution. This solution was filtered while still hot and the filtrate was poured into petroleum ether (300 ml). The yellow precipitate was filtered off and dried. Yield: 92% (3.88 g). Calcd. for $C_{14}H_{10}Cl_2N_2Pd{\cdot}2H_2O$: C 40.07, H 3.36, N 6.68. Found: C 39.57, H 3.30, N 6.57.

(b) Bis(phenylnitrile)platinumdichloride (27)



Bis(phenylnitrile)platinumdichloride was prepared starting from platinum(II) chloride (0.0075 mol, 2.00 g) and benzonitrile (50 ml) using the procedure described for bis(phenylnitrile)palladiumdichloride. Yield: 90% (3.19 g). Calcd. for $C_{14}H_{10}Cl_2N_2Pt$: C 35.61, H 2.13, N 5.93. Found: C 35.99, H 2.32, N 5.95.

(c) *Cis*-[$RuCl_2(bipy)_2$] (28)

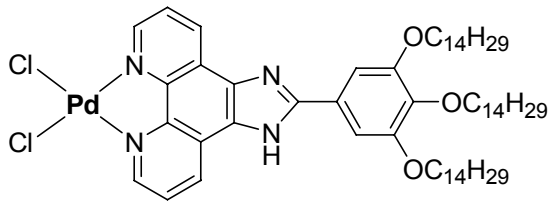


A mixture of $RuCl_3 \cdot 3H_2O$ (0.007 mol, 1.83 g), bipyridine (0.014 mol, 2.20 g), LiCl (0.047 mol, 2.00 g) and 20 ml of DMF was refluxed for 8 hours. Then the mixture was cooled and 150 ml of acetone was added. The precipitate was filtered off and washed 3 times with 25 ml of water and 3 times with 25 ml of diethyl ether. The dark green micro-crystalline product was dried under vacuum. Yield: 47% (1.61 g). Calcd. for $C_{20}H_{16}Cl_2N_4Ru \cdot 0.5H_2O$: C 48.69, H 3.47, N 11.36. Found: C 48.88, H 3.65, N 11.49. ESI-MS (Methanol, m/z): 485.1, $[M + H]^+$.

5.2.2.3. Synthesis of metal complexes

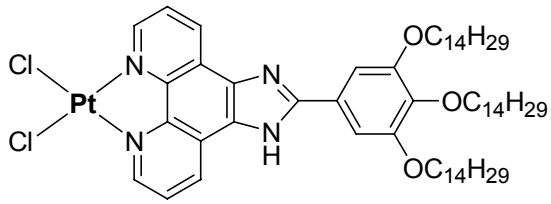
Palladium(II) and platinum(II) complexes

(a) [$PdCl_2L^{XI}$]



The palladium(II) complex was prepared by slowly adding a solution of $[PdCl_2(NCPh)_2]$ (**26**) (0.140 mmol, 0.054 g) in chloroform to a solution of ligand L^{XI} (0.107 mmol, 0.100 g) in chloroform. The mixture was refluxed for 30 minutes. Then the solvent was removed under reduced pressure and diethyl ether was added. The excess of $[PdCl_2(NCPh)_2]$ was removed by filtration and ethanol was added until precipitation occurred. The orange precipitate was filtered off and dried in a vacuum oven at 50 °C. Yield: 86% (0.102 g). Calcd. for $C_{61}H_{96}Cl_2N_4O_3Pd{\cdot}3H_2O$: C 62.90, H 8.83, N 4.81. Found: C 62.48, H 8.39, N 4.77. ESI-MS (Methanol/Ammonium acetate, m/z): 1149.3, $[M + Na + H_2O]^+$. The compound is an enantiotropic liquid crystal: M > 300 dec.

(b) [$PtCl_2L^{XI}$]

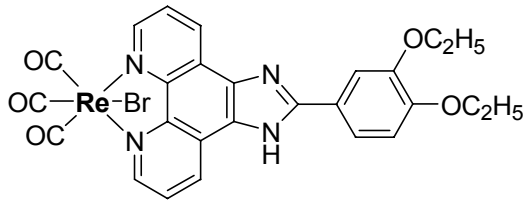


The platinum(II) complex was prepared by slowly adding a solution of $[PtCl_2(NCPh)_2]$ (**27**) (0.140 mmol, 0.066 g) in chloroform to a solution of ligand L^{XI} (0.107 mmol, 0.100 g) in chloroform. The mixture was refluxed for 5 hours. Then the solvent was removed under reduced pressure and diethyl ether was added. The excess of $[PtCl_2(NCPh)_2]$ was removed by filtration and ethanol was added until precipitation occurred. The orange precipitate was filtered off and dried in a vacuum oven at 50 °C. Yield: 54% (0.069 g). Calcd. for $C_{61}H_{96}Cl_2N_4O_3Pt{\cdot}0.5H_2O$: C 60.63, H 8.09, N 4.64. Found: C 60.87, H 8.19, N 4.32. ESI-MS (Methanol/Ammonium acetate, m/z): 1276.0, $[M + CH_3COONH_4 + H]^+$. The compound is an enantiotropic liquid crystal: M > 300 dec.

Rhenium(I) complexes

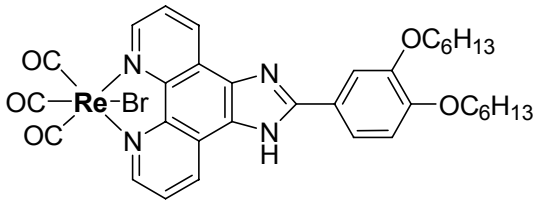
Except from $[ReBr(CO)_3L^{XIII}]$, all the rhenium(I) complexes were prepared following the same procedure: rhenium(I) pentacarbonyl bromide (1 eq.) was added to a solution of the ligand (1 eq.) in toluene. The mixture was refluxed for 3 hours. Then the solvent was removed under reduced pressure and the crude product was purified on a silica column with $CHCl_3$/hexane (50:50) as the eluent. The complex was dissolved in a minimum amount of $CHCl_3$ and precipitated in hexane or ethanol. The yellow precipitate was filtered off and dried in a vacuum oven at 50 °C.

(a) [ReBr(CO)$_3$L^{II}]



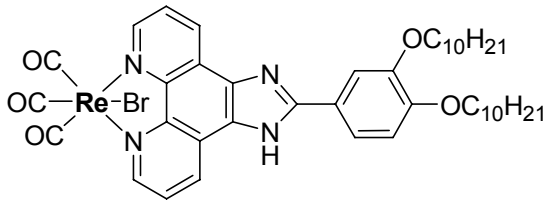
Yellow powder. Yield: 87%. Calcd. for $C_{26}H_{20}BrN_4O_5Re \cdot H_2O$: C 41.49, H 2.95, N 7.44. Found: C 41.25, H 3.33, N 7.55. ESI-MS (Methanol, m/z): 756.9, $[M + Na]^+$. M.p.: 371 °C.

(b) [ReBr(CO)$_3$L^{III}]



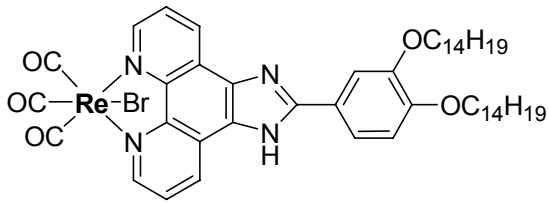
Yellow powder. Yield: 65%. Calcd. for $C_{34}H_{36}BrN_4O_5Re \cdot 0.5H_2O$: C 47.72, H 4.36, N 6.55. Found: C 47.56, H 4.73, N 6.39. ESI-MS (Methanol, m/z): 847.1, $[M + H]^+$. M.p.: 244 °C.

(c) [ReBr(CO)$_3$L^{IV}]



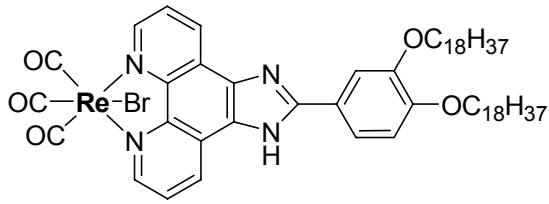
Yellow powder. Yield: 59%. Calcd. for $C_{42}H_{52}BrN_4O_5Re \cdot 0.5H_2O$: C 52.11, H 5.52, N 5.79. Found: C 52.13, H 5.26, N 5.84. ESI-MS (Methanol, m/z): 958.8, $[M + H]^+$. M.p.: 216 °C.

(d) [ReBr(CO)$_3$L^{V}]



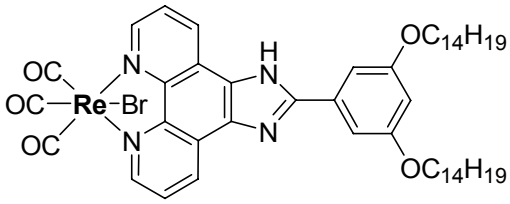
Yellow powder. Yield: 51%. Calcd. for $C_{50}H_{68}BrN_4O_5Re \cdot 0.5H_2O$: C 55.59, H 6.44, N 5.19. Found: C 55.61, H 6.16, N 5.30. ESI-MS (Methanol, m/z): 991.6, $[M - Br]^+$. M.p.: 197 °C.

(e) [ReBr(CO)$_3$L^{VII}]



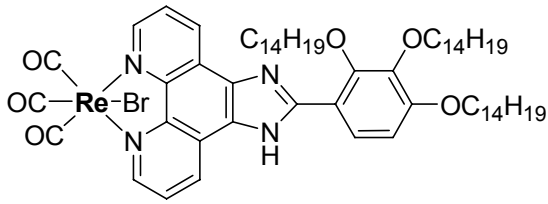
Yellow powder. Yield: 55%. Calcd. for $C_{58}H_{84}BrN_4O_5Re{\cdot}0.5H_2O$: C 58.42, H 7.18, N 4.70. Found: C 58.48, H 6.76, N 4.72. ESI-MS (Methanol, m/z): 1102.7, $[M - Br]^+$. M.p.: 183 °C.

(f) [ReBr(CO)$_3$L^{VIII}]



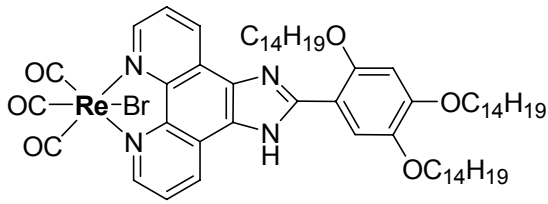
Yellow powder. Yield: 53%. Calcd. for $C_{50}H_{68}BrN_4O_5Re{\cdot}0.5H_2O$: C 55.59, H 6.44, N 5.19. Found: C 56.09, H 6.78, N 4.93. ESI-MS (Methanol, m/z): 1071.5, $[M + H]^+$. M.p.: 92 °C (a monotropic phase is formed upon cooling at 69 °C).

(g) [ReBr(CO)$_3$L^{IX}]



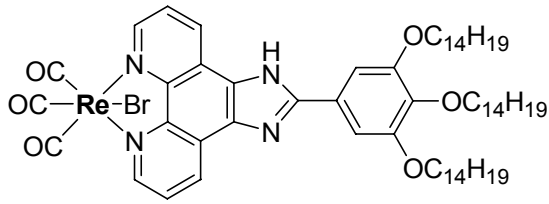
Yellow powder. Yield: 11%. Calcd. for $C_{64}H_{96}BrN_4O_6Re{\cdot}0.5H_2O$: C 59.47, H 7.56, N 4.33. Found: C 59.52, H 7.79, N 3.91. ESI-MS (Methanol, m/z): 1283.8, $[M + H]^+$. M.p.: 178 °C.

(h) [ReBr(CO)$_3$L^{X}]



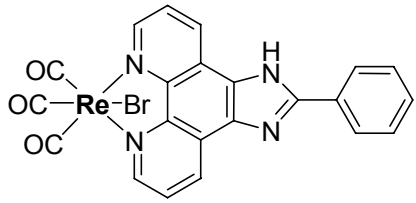
Yellow powder. Yield: 55%. Calcd. for $C_{64}H_{96}BrN_4O_6Re{\cdot}0.5H_2O$: C 59.47, H 7.56, N 4.33. Found: C 59.79, H 7.63, N 4.42. ESI-MS (Methanol, m/z): 1283.8, $[M + H]^+$. M.p.: 180 °C.

(i) [ReBr(CO)$_3$L^{XI}]



Yellow powder. Yield: 58%. Calcd. for $C_{64}H_{96}BrN_4O_6Re{\cdot}0.5H_2O$: C 59.47, H 7.56, N 4.33. Found: C 59.70, H 7.94, N 3.94. ESI-MS (Methanol, m/z): 1203.2, $[M - Br]^+$. M.p.: 91 °C (a monotropic phase is formed upon cooling at 81 °C).

(j) [ReBr(CO)$_3$L^{XIII}]

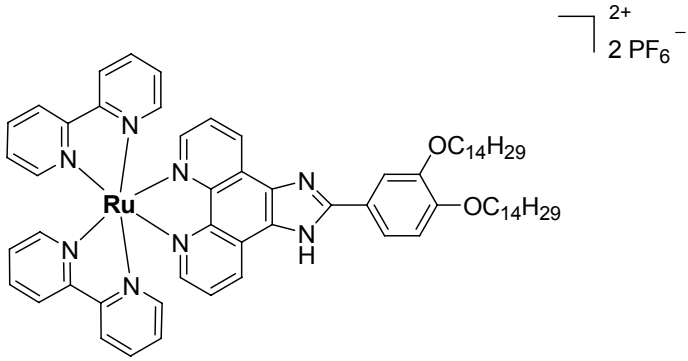


Rhenium(I) pentacarbonyl bromide (1 eq.) was added to a solution of ligand L^{XIII} (1 eq.) in toluene. The mixture was refluxed for 3 hours. Then the solvent was removed under reduced pressure and the crude product was recrystallized from acetone. Since the compound holds solvents firmly, it was dried in a vacuum oven at 50 °C. Yield: 71%. Calcd. for $C_{22}H_{12}BrN_4O_3Re{\cdot}H_2O$: C 40.31, H 2.00, N 8.55. Found: C 40.69, H 2.45, N 8.52. ESI-MS (Acetone/methanol, m/z): 645.0, $[M - H]^-$. M.p.: 439 °C.

Ruthenium(II) complexes

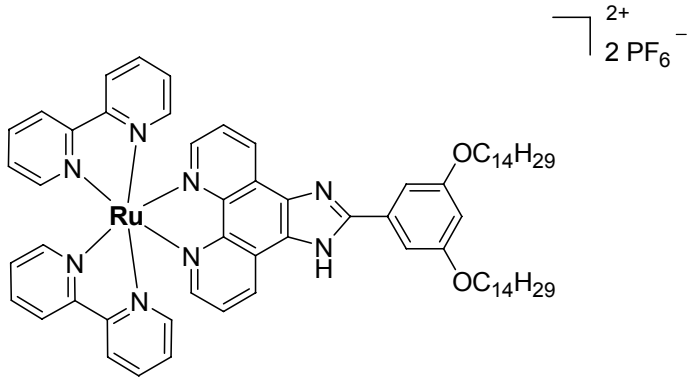
All the ruthenium(II) complexes were prepared following the same procedure: *cis*-[$RuCl_2(bipy)_2$] (**28**) (1 eq.) was dissolved in a warm ethanol/water (50:50) mixture under a nitrogen atmosphere. The ligand (1 eq.) was dissolved in warm ethanol and added to the solution. Then the mixture was refluxed overnight under a nitrogen atmosphere and the solution became clearly red. Ethanol was removed under reduced pressure and a saturated solution of KPF_6 in water was added. A red precipitate was formed, filtered off and washed with water. The crude product was purified on an alumina column with acetone as the eluent. The product was dissolved in a minimum amount of ethanol and precipitated in hexane. The red precipitate was filtered off and dried in a vacuum oven at 50 °C.

(a) $[Ru(bipy)_2L^V](PF_6)_2$



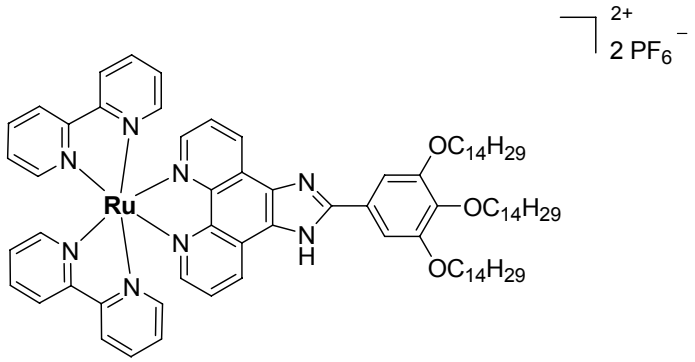
Red powder. Yield: 84%. Calcd. for $C_{67}H_{84}F_{12}N_8O_2P_2Ru \cdot 3H_2O$: C 54.43, H 6.14, N 7.58. Found: C 54.36, H 5.81, N 7.83. ESI-MS (Methanol, m/z): 1312.9, $[M - PF_6 + H_2O]^+$. The compound decomposes before melting.

(b) $[Ru(bipy)_2L^{VIII}](PF_6)_2$



Red powder. Yield: 51%. Calcd. for $C_{67}H_{84}F_{12}N_8O_2P_2Ru \cdot H_2O$: C 55.79, H 6.01, N 7.77. Found: C 55.84, H 5.92, N 7.80. ESI-MS (Methanol, m/z): 1312.4, $[M - PF_6 + H_2O]^+$. The compound decomposes before melting.

(c) $[Ru(bipy)_2L^{XI}](PF_6)_2$

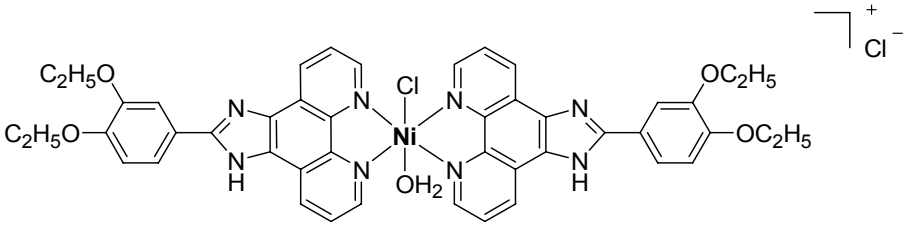


Red powder. Yield: 38%. Calcd. for $C_{81}H_{112}F_{12}N_8O_3P_2Ru \cdot 3H_2O$: C 57.54, H 7.03, N 6.63. Found: C 57.14, H 6.68, N 6.66. ESI-MS (Methanol, m/z): 1525.7, $[M - PF_6 + H_2O]^+$. The compound decomposes before melting.

Nickel(II) complexes

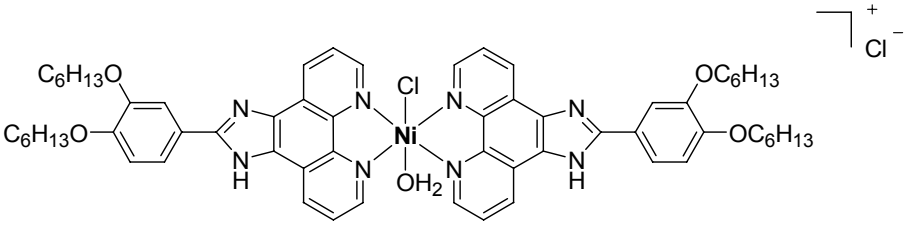
All the nickel(II) complexes were prepared following the same procedure: $NiCl_2 \cdot 6H_2O$ (1 eq.) was dissolved in ethanol and added slowly to a solution of the ligand (2 eq.) in hot ethanol. The solution was stirred for 30 minutes at 65 °C. The yellow precipitate was filtered off, washed with ethanol and dried in a vacuum oven at 50 °C.

(a) $[NiCl(H_2O)(L^{II})_2]Cl$



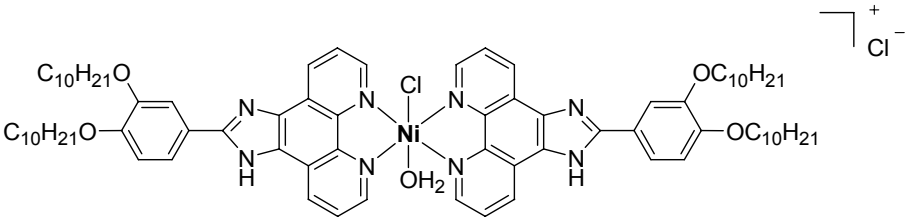
Yellow powder. Yield: 43%. Calcd. for $C_{46}H_{40}Cl_2N_8NiO_4 \cdot H_2O$: C 60.28, H 4.62, N 12.23. Found: C 60.27, H 4.99, N 12.34. ESI-MS (Methanol, m/z): 413.3, $[M - 2Cl]^{2+}/2$. The compound decomposes before melting.

(b) $[NiCl(H_2O)(L^{III})_2]Cl$



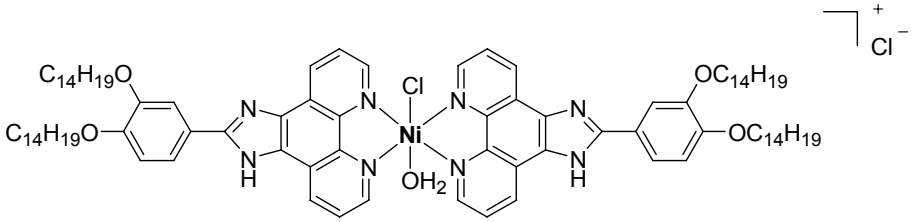
Yellow powder. Yield: 12%. Calcd. for $C_{62}H_{72}Cl_2N_8NiO_4 \cdot H_2O$: C 65.27, H 6.54, N 9.82. Found: C 65.09, H 7.08, N 9.78. ESI-MS (Methanol, m/z): 525.5, $[M - 2Cl]^{2+}/2$. The melting point could not be determined.

(c) $[NiCl(H_2O)(L^{IV})_2]Cl$



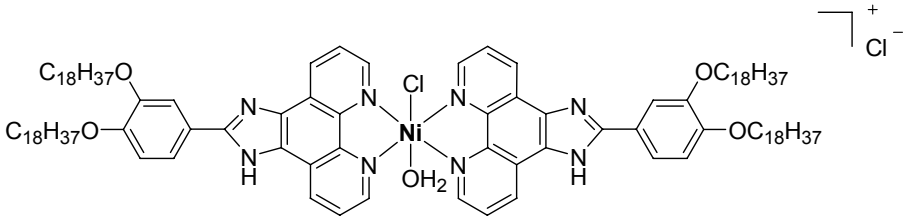
Yellow powder. Yield: 32%. Calcd. for $C_{78}H_{104}Cl_2N_8NiO_4 \cdot H_2O$: C 68.62, H 7.83, N 8.21. Found: C 68.79, H 7.90, N 8.27. ESI-MS (Methanol, m/z): 637.6, $[M - 2Cl]^{2+}/2$. The compound is an enantiotropic liquid crystal: M > 300 dec.

(d) $[NiCl(H_2O)(L^V)_2]Cl$



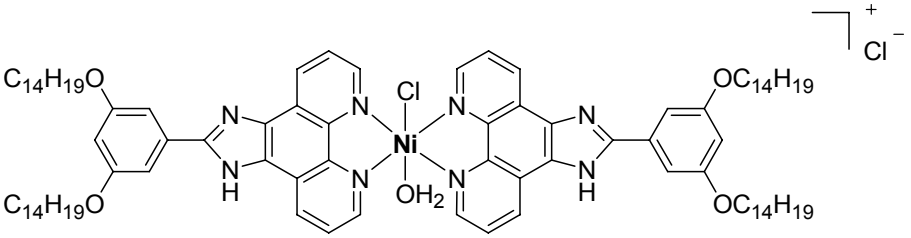
Yellow powder. Yield: 35%. Calcd. for $C_{94}H_{136}Cl_2N_8NiO_4 \cdot H_2O$: C 71.02, H 8.75, N 7.05. Found: C 71.08, H 8.64, N 7.18. ESI-MS (Methanol, m/z): 750.1, $[M - 2Cl]^{2+}/2$. The compound is an enantiotropic liquid crystal: M > 300 dec.

(e) $[NiCl(H_2O)(L^{VII})_2]Cl$



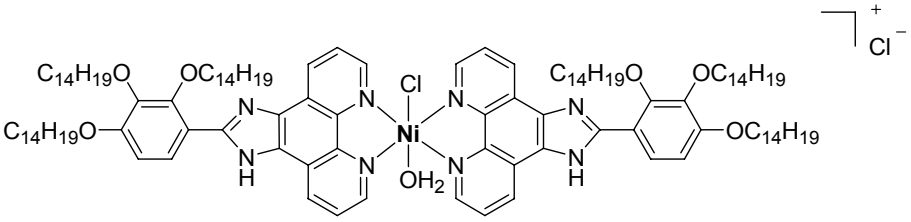
Yellow powder. Yield: 32%. Calcd. for $C_{110}H_{168}Cl_2N_8NiO_4 \cdot H_2O$: C 72.83, H 9.45, N 6.18. Found: C 73.28, H 9.68, N 6.27. ESI-MS (Methanol/Ammonium acetate, m/z): 1782.5, $[M - 2Cl + CH_3COO]^+$. The compound is an enantiotropic liquid crystal Col_h > 300 dec.

(f) $[NiCl(H_2O)(L^{VIII})_2]Cl$



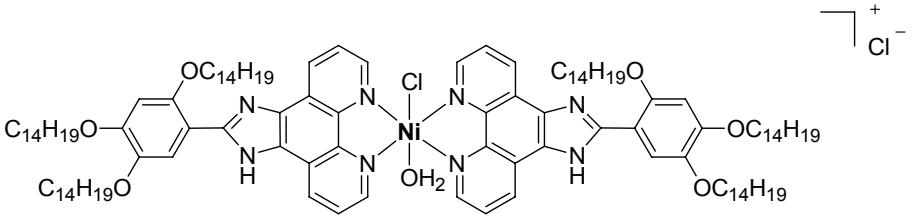
Yellow powder. Yield: 78%. Calcd. for $C_{94}H_{136}Cl_2N_8NiO_4 \cdot H_2O$: C 71.02, H 8.75, N 7.05.Found: C 71.26, H 8.40, N 7.33. ESI-MS (Methanol/Ammonium acetate, m/z): 1558.3, $[M - 2Cl + CH_3COO]^+$. The compound is an enantiotropic liquid crystal: M > 300 dec.

(g) $[NiCl(H_2O)(L^{IX})_2]Cl$



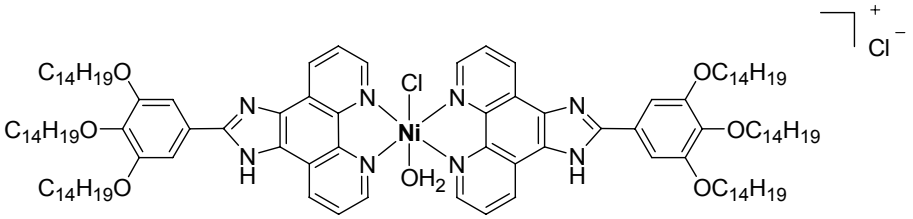
Yellow powder. Yield: 14%. Calcd. for $C_{122}H_{192}Cl_2N_8NiO_6 \cdot H_2O$: C 72.74, H 9.71, N 5.56. Found: C 72.58, H 9.95, N 5.54. ESI-MS (Methanol, m/z): 1960.6, $[M - Cl]^+$. The compound is an enantiotropic liquid crystal: M 265 I.

(h) $[NiCl(H_2O)(L^X)_2]Cl$



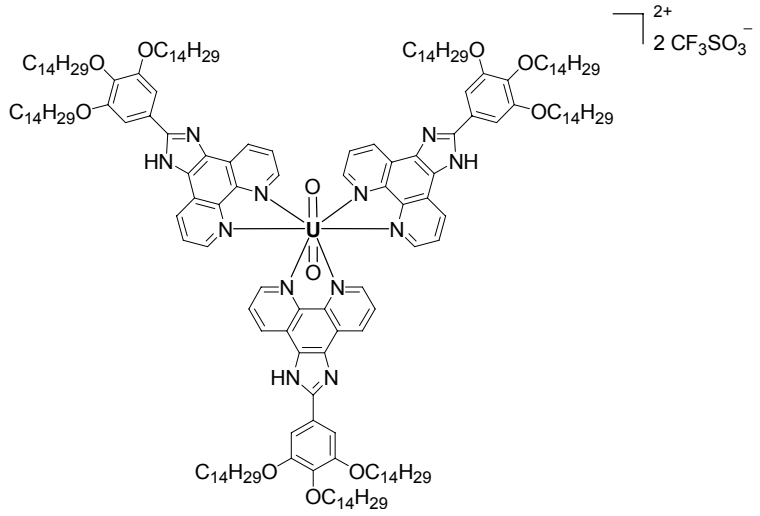
Green powder. Yield: 56%. Calcd. for $C_{122}H_{192}Cl_2N_8NiO_6 \cdot H_2O$: C 72.74, H 9.71, N 5.56. Found: C 73.24, H 9.90, N 5.16. ESI-MS (Methanol/Ammonium acetate, m/z): 1983.0, $[M - 2Cl + CH_3COO]^+$. M.p.: 302 °C.

(i) $[NiCl(H_2O)(L^{XI})_2]Cl$



Yellow powder. Yield: 65%. Calcd. for $C_{122}H_{192}Cl_2N_8NiO_6 \cdot H_2O$: C 72.74, H 9.71, N 5.56. Found: C 72.61, H 9.76, N 5.15. ESI-MS (Methanol/Ammonium acetate, m/z): 1983.2, $[M - 2Cl + CH_3COO]^+$. The compound is an enantiotropic liquid crystal: M > 300 dec.

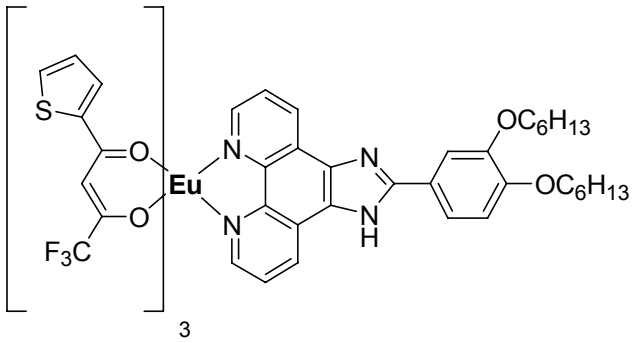
Uranyl complex $[UO_2(L^{XI})_3](OTf)_2$



The uranyl complex was prepared by slowly adding a solution of $UO_2(CF_3SO_3)_2$ (0.036 mmol, 0.020 g) in ethanol to a warm solution of ligand L^{XI} (0.107 mmol, 0.100 g) in ethanol. The mixture was stirred for 30 minutes at 65 °C. The orange precipitate was filtered off, washed with ethanol and dried in a vacuum oven at 50 °C. Yield: 83% (0.100 g). δ_H (400 MHz, THF-d8): 0.87–0.88 (m, 27H, CH_3), 1.30–1.83 (m, 216H, CH_2), 3.99–4.07 (m, 18H, –C**H**$_2$–O–), 7.49 (s, 6H, H-aryl), 7.88 (b, s, 6H, H-aryl), 8.92 (b, s, 6H, H-aryl), 9.20 (b, s, 6H, H-aryl). IR (KBr-pellet, cm^{-1}): 3530 (m, ν(N–H)), 2920, 2850 (s, C–H and C–F stretch), 1242, 1028 (s, S–O stretch), 918 (s, ν(U=O)), 636, 517 (s, ν(S–O)). Calcd. for $C_{185}H_{288}F_6N_{12}O_{17}S_2U$: C 65.96, H 8.62, N 4.99. Found: C 65.59, H 8.87, N 4.74. The compound is an enantiotropic liquid crystal: Cr 95 Col_h 181 I.

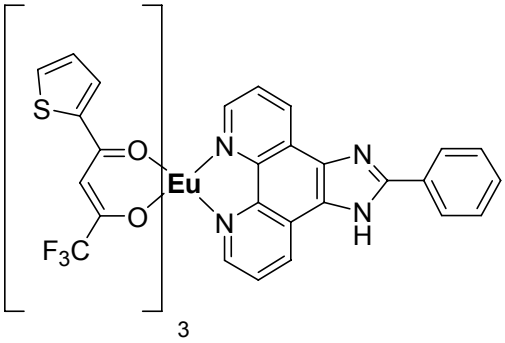
Europium complexes

(a) [Eu(tta)$_3$L^{III}]



Eu(tta)$_3$·2H$_2$O (1 eq.) was dissolved in ethanol and added slowly to a solution of ligand L^{III} (1 eq.) in hot ethanol. The solution was stirred for 30 minutes at 65 °C. The mixture was cooled to room temperature and the precipitate was filtered off, washed with ethanol and dried in a vacuum oven at 50 °C. Yield: 49%. Calcd for $C_{55}H_{48}EuF_9N_4O_8S_3·H_2O$: C 49.66, H 3.79, N 4.21. Found: C 50.25, H 3.81, N 4.24. ESI-MS (Methanol, m/z): 1335.4, [M + Na]$^+$. M.p.: 135 °C.

(b) [Eu(tta)$_3$L^{XIII}]



$Eu(tta)_3 \cdot 2H_2O$ (1 eq.) was dissolved in ethanol and added slowly to a solution of ligand L^{XIII} (1 eq.) in a hot ethanol/$CHCl_3$ mixture. The solution was stirred for 30 minutes at 65 °C. Then the mixture was cooled to room temperature and hexane was added until precipitation occurred. The precipitate was filtered off, washed with hexane and dried in a vacuum oven at 50 °C. Yield: 66%. Calcd for $C_{43}H_{24}EuF_9N_4O_6S_3 \cdot 2H_2O$: C 44.99, H 2.46, N 4.88. Found: C 45.13, H 2.47, N 4.50. ESI-MS (Methanol, m/z): 1111.1, $[M - H]^-$. M.p.: 278 °C.

5.6 References

1. Steck, E. A.; Day, A. R. *J. Am. Chem. Soc.* **1943**, *65*, 452.
2. Hiort, C.; Lincoln, P.; Norden, B. *J. Am. Chem. Soc.* **1993**, *115*, 3448.
3. Li, H. R.; Fu, L. S.; Lin, J.; Zhang, H. J. *Thin Solid Films* **2002**, *416*, 197.
4. (a) Xu, H.; Zheng, K. C.; Chen, Y.; Li, Y. Z.; Jin, L. J.; Li, H.; Zhang, P. X.; Ji, L. N.; *Dalton Trans.* **2003**, 2260. (b) Xiong, Y.; Zou, X. H.; Wu, J. Z.; Ji, L. N.; Li, R. J.; Zhou, J. Y.; Yu, K. B. *Transit. Met. Chem.* **1999**, *24*, 263. (c) Xiong, Y.; He, X. F.; Zou, X. H.; Wu, J. Z.; Chen, X. M.; Ji, L. N.; Li, R. H.; Zhou, J. Y.; Yu, K. B. *J. Chem. Soc., Dalton Trans.* **1999**, 19. (d) Chao, H.; Li, R. H.; Ye, B. H.; Li, H.; Feng, X. L.; Cai, J. W.; Zhou, J. Y.; Ji, L. N. *J. Chem. Soc., Dalton Trans.* **1999**, 3711. (e) Chao, H.; Yuan, Y. X.; Ji, L. N. *Transit. Met. Chem.* **2004**, *29*, 774.
5. (a) Anbei, J.; Kruger, C.; Pfeil, B. *Acta Crystallogr., Sect.C: Cryst. Struct. Commun.* **1987**, *43*, 2334. (b) Fanizzi, F. P.; Intini, F. P.; Maresca, L.; Natile, G.; Lanfranchi, M.; Tiripicchio, A. *J. Chem. Soc., Dalton Trans.* **1991**, 1007. (c) Gaballa, A.; Wagner, C.; Schmidt, H.; Steinborn, D. *Z. Anorg. Allg. Chem.* **2003**, *629*, 703.
6. (a) Ferbinteanu, M.; Cimpoesu, F.; Andruh, M.; Rochon, F. D. *Polyhedron* **1998**, *17*, 3671. (b) Yang, J.; Ma, J. F.; Wu, D. M.; Guo, L. P.; Liu, J. F. *J. Mol. Struct.* **2003**, *657*, 333. (c) Travnicek, Z.; Kopel, P.; Marek, J. *Z. Kristallogr. - New Cryst. Struct.* **1998**, *213*, 149. (d) Freire, E.; Baggio, S.; Suescun, L.; Baggio, R. *Acta Crystallogr., Sect.C: Cryst. Struct. Commun.* **2001**, *57*, 905.
7. Brewer, B.; Brooks, N. R.; Abdul-Halim, S.; Sykes, A. G.; *J. Chem. Cryst.* **2003**, *33*, 651.

8. Norman, R. E.; Xie, M. *J. Coord. Chem.* **2004**, *57*, 425.
9. Rice, C. R.; Anderson, K. M. *Polyhedron* **2000**, *19*, 495.
10. Werner, A. Z. *Anorg. Chem.* **1893**, *3*, 267.
11. Berthet, J. -C.; Nierlich, M; Ephritikhine, M. *Chem. Commun.* **2003**, 1660.
12. Berthet, J. -C; Nierlich, M.; Ephritikhine M. *Dalton Trans.* **2004**, 2814.
13. Donnio, B.; Bruce, D. W. *J. Chem. Soc., Dalton Trans*. **1997**, 2745.
14. (a) Zheng, H.; Swager, T. M. *J. Am. Chem. Soc.* **1994**, *116*, 761. (b) Trzaska, S. T.; Hsu, H. F.; Swager, T. M. *J. Am. Chem. Soc.* **1999**, *121*, 4518. Corrigendum 4544.
15. Serrano, J. L.; Sierra, T. *Coord. Chem. Rev.* **2003**, *242*, 73.
16. (a) Xu, B.; Swager, T. M. *J. Am. Chem. Soc.* **1993**, *115*, 1159. (b) Gorecka, E.; Pociecha, D.; Mieczkowski, J.; Matraszek, J.; Guillon, D.; Donnio, B. *J. Am. Chem. Soc.* **2004**, *126*, 15946.
17. Guillevic, M.-A.; Danks, M. J.; Harries, S. K.; Collinson, S. R.; Pidwell, A. D.; Bruce, D. W. *Polyhedron* **2000**, *19*, 249.
18. SAINT, Bruker Analytical X-ray Systems Inc., Madison, WI, Manual Version 5/6.0, 1997.
19. SHELXTL-PC, Bruker Analytical X-ray Systems Inc., Madison, WI, Manual Version 5.1, 1997.

General conclusions and summary

Starting from the facts that 1,10-phenanthroline is a frequently used ligand in coordination chemistry and that it is able to form stable complexes with a wide variety of d-block and f-block metals, we have selected 1,10-phenanthroline as a building block for the synthesis of a new class of metal-containing liquid crystals. The aim of this work was to design luminescent liquid crystals and liquid crystals with an unusual geometry.

Although different substitution patterns are possible for 1,10-phenanthroline, 3,8-disubstituted 1,10-phenanthrolines were selected as the first target molecules (this work was performed in collaboration with Prof. Duncan W. Bruce, who carried out pioneering research on liquid-crystalline phenanthrolines). This substitution pattern is a logical choice if one wants to obtain compounds with an extended rodlike aromatic core and thus with the necessary anisotropic shape for the formation of mesophases. For the synthesis, 3,8-dibromo-1,10-phenanthroline was used as the starting product, which can be functionalized by Sonogashira coupling reactions. The advantage of this approach is that the aromatic rings, which build up the rigid part of the mesogenic molecule, are linked to one another by an acetylene linking group. It is known from the literature that acetylene linking groups are in general much more stable than for instance ester groups. The dibromation of 1,10-phenanthroline in the 3- and 8-positions turned out to be a difficult task because different brominated species were obtained. The side products include not only the monobrominated 3-bromo-1,10-phenanthroline, but also other isomers of the dibrominated product and polybrominated species. Even small quantities of impurities of these side

products cause serious problems for the purification of the final product after Sonogashira coupling reactions. Due to the tedious purification of the mesomorphic 1,10-phenanthroline derivatives, we were able to synthesize only one 1,10-phenanthroline derivative, i.e. a tetracatenar compound with four terminal alkoxy chains. The structure of this ligand was determined by single-crystal X-ray diffraction and examination of the thermal behavior indicated that the ligand exhibits a smectic C phase. Unfortunately, the ligand could not be obtained in sufficient quantities to allow the synthesis of metal complexes.

Facing the problems with the 3,8-disubstituted 1,10-phenanthrolines, another type of functionalized 1,10-phenanthrolines was considered, i.e. 1,10-phenanthrolines mono-functionalized in the 5-position or difunctionalized in the 5- and 6-positions. In a search for the most suitable precursor, we first worked with 5-amino-1,10-phenanthroline, but it turned out that the 1,10-phenanthroline-5,6-dione is a more useful starting product. 1,10-Phenanthroline-5,6-dione is easily accessible in high purity by oxidation of 1,10-phenanthroline and the product itself is much more stable than 5-amino-1,10-phenanthroline. By reaction between 1,10-phenanthroline-5,6-dione and a benzaldehyde in the presence of ammonium acetate and acetic acid, a 2-phenyl-imidazo[4,5-f]-1,10-phenanthroline can be obtained. This is a versatile approach because the imidazo[4,5-f]-1,10-phenanthroline can be modified by replacing the benzaldehyde by a substituted benzaldehyde. Another route to modify the ligand is the alkylation of one of the nitrogen atoms of the imidazole ring.
In first instance, we decided to promote mesomorphism in the imidazo-[4,5-f]-1,10-phenanthrolines by coupling mesogenic 4-cyanobiphenyl groups via a long, flexible alkyl spacer to a substituted imidazo[4,5-f]-1,10-phenanthroline, which acts as the coordinating group. Three different

ligands were designed, bearing one, two, and three mesogenic groups, respectively. Complexes of rhenium(I), yttrium(III), lanthanum(III), neodymium(III), samarium(III), europium(III), erbium(III), and ytterbium(III) were synthesized. In the case of the rare-earth complexes, 2-thenoyltrifluoroacetonate was used as the coligand. The rhenium(I) complexes contain the bromotricarbonylrhenium(I) moiety. All the compounds exhibit enantiotropic mesophases, except the rhenium(I) complex of the ligand bearing only one mesogenic group, which forms only a monotropic mesophase. The ligands and corresponding rhenium(I) complexes show a nematic or a *lamello-columnar* phase, depending on the number of attached mesogenic groups. All the rare-earth complexes systematically exhibit a nematic mesophase. The luminescence properties of the neodymium(III), samarium(III), europium(III), erbium(III), and ytterbium(III) complexes were examined. The spectroscopic and photophysical properties of these complexes are comparable with those of the $[Ln(tta)_3(phen)]$ complexes, where Ln = Nd, Sm, Eu, Er, Yb, tta = 2-thenoyltrifluoroacetonate, and phen = 1,10-phenanthroline. However, an interesting feature of these rare-earth complexes is their good solubility in nematic liquid-crystal solvents, so that by a doping procedure luminescent liquid crystals can be obtained. These could be of interest as active components in emissive liquid crystal displays. Although a 4-cyanobiphenyl group was chosen as the mesogenic promoter and a 1,10-phenanthroline derivative as the coordinating group, the concept of decoupling of the mesophase-inducing groups and the coordination groups can be extended to other mesogenic groups and ligands. The advantage of this approach is that high coordination number metallomesogens showing a nematic mesophase can be obtained. Traditionally, to obtain high coordination number metallomesogens, a large number of long alkyl chains are attached to the central metal core, which usually leads to (viscous) columnar mesophases.

There are however some problems associated with this new approach. The most serious problem is that such compounds with complex molecular architectures cannot be easily aligned by external electric or magnetic fields, even not when they exhibit a nematic phase. The linker avoids that phase separation occurs but the mesogenic groups and the coordination group act rather independently.

Finally, in the third strategy, 2-aryl-substituted imidazo[4,5-f]-1,10-phenanthrolines were used as building blocks for the synthesis of metal-containing liquid crystals by attaching alkoxy chains in different positions of the phenyl ring. Their molecular shape and space filling requirements can be tuned by the choice of an appropriate alkoxy-substituted benzaldehyde for the ligand synthesis. Metal complexes were made with different d-block transition metals, including nickel(II), palladium(II), platinum(II), ruthenium(II), and rhenium(I), as well as with lanthanides and uranyl. The ligands do not form a stable mesophase; they show at best a monotropic mesophase. The most striking feature is the influence of solvent molecules on the thermal behavior of the ligands, as the ethanol adduct of the ligand with hexadecyloxy chains in the 3- and 4-positions shows two mesophases, a transient hexagonal columnar phase and a smectic phase. Mesomorphism can be induced in the ligands by coordination to a metal center. The thermal behavior of the metal complexes depends on the metal-to-ligand ratio, but also on the substitution pattern and on the alkyl chain length. Although the palladium(II) and platinum(II) complexes exhibit enantiotropic (unidentified) mesophases with an extended temperature range, complexes with a metal-to-ligand ratio of 1:1 are in general not liquid-crystalline or they exhibit only a monotropic mesophase. Nickel(II) complexes with a 1:2 metal-to-ligand ratio form enantiotropic mesophases with an extended temperature range for most types of ligands. The uranyl complex, with a 1:3

metal-to-ligand ratio, has a propeller-like shape and exhibits a hexagonal columnar mesophase. The uranyl ion acts as a template to bring the ligands in the correct position so that propeller-shaped units can arrange into columns. It was somewhat disappointing that we were not able to synthesize liquid-crystalline lanthanide complexes of this type of imidazo[4,5-f]-1,10-phenanthrolines. This is due to the small differences in solubility behavior of the ligands and metal complexes. Lanthanide complexes with shorter alkyl chains could be synthesized, but these complexes were not mesomorphic. The photophysical properties of the rhenium(I) complexes and of the (non-mesomorphic) lanthanide complexes are being investigated at the moment (ongoing work by Jan Ramaekers). The attachment of long alkyl chains to the 2-phenyl-imidazo[4,5-f]-1,10-phenanthroline core was a more classic approach. Although stable mesophases were observed for some complexes (for instance for the uranyl compound), the stability of the mesophases did in general not meet the expectations. Relatively few metal complexes were mesomorphic and the mesophases were difficult to characterize or were not stable. No new types of mesophases were observed.

This PhD work is hopefully the initiation of further research using 1,10-phenanthroline derivatives as building blocks for liquid crystals and especially for metallomesogens. It is possible to highlight some directions for further research concerning these systems. The functionalization of 1,10-phenanthroline in the 3- and 8-positions deserves a more careful investigation, because our research illustrates that such compounds can indeed exhibit mesomorphic behavior. This further work could include variation of the alkoxy chain length of the tetracatenar compound, in order to examine the polymorphism as a function of the chain length. Although we observed a smectic C phase for the compound we synthesized, analogous series of compounds described in the literature show a gradual

change from smectic to columnar mesomorphism. The mesophase behavior can also be tuned by choosing other substitution patterns. However, the most interesting study concerns the synthesis of corresponding metal complexes and to examine the influence of metal fragments on the thermal behavior. In order to avoid purification problems, the synthetic methodology should be reconsidered. One approach is to develop a new method for the synthesis of 3,8-dibromo-1,10-phenanthroline in high yield and purity. A second approach is to synthesize the mesomorphic branches in the first stage and to form the 1,10-phenanthroline core in the last step via methods similar to the Skraup synthesis of 1,10-phenanthroline.

The idea of linking mesogenic units via a flexible alkyl chain to a coordinating unit can of course be generalized. Variations of the coordinating unit, metal ion, coligand, length of the flexible linker, type and number of mesogenic groups could be made and could result in a large number of different metallomesogens. Such molecules are of interest from a fundamental point of view because these complex molecular architectures can lead to new types of mesophases. The results obtained from a systematic variation of the constituents of these complexes could be useful to make predictions on the mesophase behavior of this type of mesomorphic compounds.

The approach of attaching long alkyl chains to the 2-phenyl-imidazo[4,5-f]-1,10-phenanthroline core was not as successful as that of attaching mesogenic groups via a flexible linker, although there are at least two aspects that deserve further investigation. First of all, the thermal behavior of the nickel(II) and uranyl complexes give the impression that the ionic character of these compounds aid to the stabilization of the mesophases. Research in the future can be directed to the design of ionic metallomesogens based on 1,10-phenanthroline. Another aspect for further study is the influence of H-bonding on the stability of the mesophases of

these complexes. Indeed, it was observed that mesomorphism was lost when the proton on the nitrogen atom of the imidazole ring was replaced by an alkyl group, and cocrystallization of the mesogenic compounds with protic solvents has a large influence on the mesophase behavior.

Finally, further research will be directed to the functionalization of 1,10-phenanthroline in the 4- and 7-positions in order to design bent-core liquid crystals.

Samenvatting

De ontdekking van de vloeibaar-kristallijne fase op het einde van de 19e eeuw heeft een enorme impact op het wetenschappelijk onderzoek gehad. Onderzoek naar vloeibare kristallen is één van de snelst groeiende onderzoeksgebieden geworden van waaruit voortdurend nieuwe toepassingen ontstaan. De laatste jaren is er veel interesse voor metaalhoudende vloeibare kristallen, de zogenaamde *metallomesogenen*, die de vloeibaar-kristallijne eigenschappen en de eigenschappen van transitiemetalen (magnetische en fotofysische eigenschappen, redoxactiviteit) combineren. Dit onderzoeksgebied heeft veel potentieel en de synthese van nieuwe liganden en complexen vormt een uitdaging voor iedereen die in dit gebied werkzaam is.

In het kader van deze doctoraatsthesis werden vloeibaar-kristallijne metaalcomplexen van gesubstitueerde 1,10-fenantrolines gesynthetiseerd. Er zijn nauwelijks voorbeelden van vloeibaar-kristallijne verbindingen op basis van 1,10-fenantroline bekend. De reden waarom er zo weinig vloeibare kristallen van dit type onderzocht zijn, is zonder twijfel de relatief moeilijke synthetische toegankelijkheid van de precursorliganden. Er zijn immers slechts weinig gefunctionaliseerde fenantrolines commercieel beschikbaar. 1,10-Fenantroline is uitermate geschikt als basismolecule voor de vorming van mesofasen. Het is opgebouwd uit een vlak, uitgebreid geconjugeerd π-systeem en bezit een dipoolmoment. Dit is gunstig voor een goede stapeling van de moleculen in de mesofase door π-π en dipool-dipool interacties. 1,10-Fenantroline is ook één van de meest veelzijdige liganden in de coördinatiechemie en kan met een hele reeks metalen complexen vormen.

Er werden drie verschillende strategieën gebruikt voor de synthese van metallomesogenen op basis van 1,10-fenantroline. In de eerste strategie werd 1,10-fenantroline gesubstitueerd in de 3- en 8-posities om zo een lange, staafvormige kern te verkrijgen, waaraan lange alifatische ketens werden gekoppeld. Via Sonogashira-koppelingsreacties werd een rigide en chemisch stabiele *tetracatenar* verbinding gesynthetiseerd. De moleculaire structuur werd bepaald door middel van X-stralendiffractie en de verbinding vormt een smectische C fase.
Spijtig genoeg was het niet mogelijk om een voldoende grote hoeveelheid aan zuiver product te verkrijgen door het moeilijke zuiveringsproces en konden geen metaalcomplexen worden gesynthetiseerd. Tetracatenar mesogenen vertonen een uitzonderlijk mesofasegedrag aangezien eenzelfde verbinding nematische, smectische, kubische en kolomvormige mesofasen kan vormen voor een verschillende ketenlengte. Daarom is verder onderzoek aangewezen op de synthese van de andere ketenlengtehomologen en overeenkomstige metaalcomplexen.

In de tweede strategie werden mesogene 4-cyanobifenylgroepen gekoppeld aan een gesubstitueerd imidazo[4,5-f]-1,10-fenantroline via een lange, flexibele spacer. Het imidazo[4,5-f]-1,10-fenantroline functioneert als de coördinerende groep. Drie verschillende liganden werden gesynthetiseerd met respectievelijk één, twee en drie mesogene groepen. Metaalcomplexen van rhenium(I), yttrium(III), lanthaan(III), neodymium(III), samarium(III), europium(III), erbium(III), en ytterbium(III) werden gesynthetiseerd. Voor de complexen van zeldzame aarden werd 2-thenoyltrifluoroacetonaat als coligand gebruikt. De rhenium(I)-complexen bevatten de bromotricarbonyl-rhenium(I)-eenheid.
Al de verbindingen vormen enantiotrope mesofasen, uitgezonderd het rhenium(I)-complex van het ligand met één mesogene groep dat enkel een

monotrope mesofase vormt. Afhankelijk van het aantal mesogene groepen, vormen de liganden en overeenkomstige rhenium(I)-complexen een nematische of een *lamellair-kolomvormige* mesofase. Alle lanthanide-complexen vormen een nematische mesofase.

Hoewel een 4-cyanobifenylgroep werd gekozen als de mesogene groep en 1,10-fenantroline als de coördinerende groep kan het concept van ontkoppeling van de mesofase-inducerende groepen van de coördinerende groepen naar andere mesogene groepen en liganden uitgebreid worden. Het voordeel van deze benadering is dat nematische mesofasen worden gevormd door metallomesogenen met een hoog coördinatiegetal. Traditioneel worden metallomesogenen met een hoog coördinatiegetal verkregen door lange alkylketens te koppelen aan het metaalcentrum. Meestal worden dan kolomvormige mesofasen gevormd.

De luminescentie-eigenschappen werden onderzocht voor de neodymium(III)-, samarium(III)-, europium(III)-, erbium(III)- en ytterbium(III)-complexen. De spectroscopische en fotofysische eigenschappen zijn vergelijkbaar met deze van de $[Ln(tta)_3(fen)]$-complexen waarbij Ln = Nd, Sm, Eu, Er, Yb, tta = 2-thenoyltrifluoroacetonaat en fen = 1,10-fenantroline. Een interessant aspect van deze lanthanidecomplexen is hun goede oplosbaarheid in nematische vloeibaar-kristallijne solventen. Via een dopingprocedure kunnen zo luminescerende vloeibare kristallen worden verkregen. Verder onderzoek zou moeten gericht worden op 1,10-fenantrolines waaraan andere mesogene groepen gekoppeld worden. Voorbeelden van andere mesogene groepen zijn 4-alkoxybifenylgroepen en cholesterylgroepen. Ook metaalcomplexen met een andere metaal-ligand verhouding zijn interessant. Bijvoorbeeld nikkel(II)-complexen met een metaal-ligand verhouding 1:2 of een uranylcomplex met een metaal-ligand verhouding 1:3. Op deze manier wordt het aantal mesogene groepen per

coördinerende groep verhoogd wat een invloed op het mesofasegedrag heeft.

Ten slotte werden in de derde strategie 2-aryl-gesubstitueerde imidazo[4,5-f]-1,10-fenantrolines gebruikt als bouweenheid voor de synthese van metallomesogenen door alkoxyketens te koppelen in verschillende posities. Hun moleculaire vorm en ruimtevullende eigenschappen kunnen gecontroleerd worden door de keuze van een geschikt alkoxygesubstitueerd benzaldehyde voor de ligandsynthese. Metaalcomplexen van verschillende transitiemetalen, uranyl en zeldzame aarden werden gesynthetiseerd. Als transitiemetalen werden nikkel(II), palladium(II), platina(II), ruthenium(II) en rhenium(I) gebruikt.
De liganden vormen geen stabiele mesofase. Zij vormen hoogstens een monotrope mesofase. Zeer opvallend is de invloed van solventmoleculen op het thermisch gedrag van de liganden. Zo vormt het ethanoladduct van het ligand met een hexadecyloxyketen in de 3- en 4-posities twee mesofasen, een hexagonale kolomvormige mesofase en een smectische mesofase. Mesomorfisme kan geïnduceerd worden in de liganden door coördinatie met een metaalcentrum. Het thermisch gedrag van de metaalcomplexen is eerst en vooral afhankelijk van de metaal-ligand verhouding maar ook van het substitutiepatroon en de ketenlengte. Over het algemeen zijn metaalcomplexen met een metaal-ligand verhouding 1:1 niet vloeibaar-kristallijn, met uitzondering van de palladium(II)- en platina(II)-complexen. Deze vormen (niet ondubbelzinnig-identificeerbare) enantiotrope mesofasen over een zeer uitgebreid temperatuursgebied. De nikkel(II)-complexen met een metaal-ligand verhouding 1:2 vormen enantiotrope mesofasen over een zeer uitgebreid temperatuursgebied voor de meeste ligandtypes. Het uranylcomplex met een metaal-ligand verhouding 1:3 heeft een propellervormige moleculaire structuur en vormt een hexagonale

kolomvormige mesofase. Het uranyl-ion brengt als templaat de liganden in de correcte positie zodat propellervormige eenheden kunnen stapelen in kolommen. Deze metallomesogenen stapelen op een apolaire manier in de mesofase.
Verder onderzoek zou gericht moeten worden op de bepaling van de moleculaire structuur van de nikkel(II)-complexen. Ook de synthese van gesubstitueerde pyrazino[2,3-f]-1,10-fenantrolines (en overeenkomstige metaalcomplexen) is interessant omdat hun structuur analoog is aan deze van de imidazo[4,5-f]-1,10-fenantrolines beschreven in deze thesis.

Om te besluiten werd een nieuwe methode ontwikkeld voor het ontwerpen van metaalhoudende vloeibare kristallen met een complexe geometrie. Dit werk leidt tot een beter inzicht in de relatie tussen moleculaire vorm en de mesofasestructuur in supramoleculaire coördinatieverbindingen.

List of publications

1. Sleven, J.; Cardinaels, T.; Binnemans, K.; Guillon, D.; Donnio, B.; *"Thermal and optical behaviour of octa-alkoxy substituted phthalocyaninatovanadyl complexes", Liquid Crystals* **2002**, *29*, 1425-1433.

2. Sleven, J.; Cardinaels, T.; Binnemans, K.; Nelis, D.; Mullens, J.; Hinz-Hübner, D.; Meyer, G.; *"Mesophase behaviour and thermal stability of octa-alkoxy substituted phthalocyaninatocobalt(II) complexes", Liquid Crystals* **2003**, *30*, 143-148.

3. Sleven, J.; Cardinaels, T.; Görller-Walrand, C.; Binnemans, K.; *"Liquid-crystalline metallophthalocyanines containing late first-row transition metals", Arkivoc* **2003**, Part IV, 68-82.

4. Cardinaels, T.; Driesen, K.; Parac-Vogt, T. N.; Heinrich, B.; Bourgogne, C.; Guillon, D.; Donnio, B.; Binnemans, K.; *"Design of high coordination number metallomesogens by decoupling of the complex-forming and mesogenic groups: Nematic and lamello-columnar mesophases", Chemistry of Materials* **2005**, *17*, 6589-6598.

5. Cardinaels, T.; Ramaekers, J.; Guillon, D.; Donnio, B.; Binnemans, K.; *"A propeller-like uranyl metallomesogen", Journal of the American Chemical Society* **2005**, *127*, 17602-17603.

6. Binnemans, K.; Lodewyckx, K.; Cardinaels, T.; Parac-Vogt, T. N.; Bourgogne, C.; Guillon, D.; Donnio, B.; *"Dinuclear lanthanide Schiff-Base complexes forming a rectangular columnar mesophase", European Journal of Inorganic Chemistry* **2006**, 150-157.

X-ray diffraction of mesophases Appendix A

This appendix is meant to give a basic introduction to the application of X-ray diffraction for the identification of mesophases.

A.1 Nematic phase

Diffuse peaks are observed in both the small-angle and the wide-angle region of the X-ray pattern of the nematic phase. The broad signal in the wide-angle region corresponds to the average lateral separations of the close-packed molecules and to the short-range order of the molten chains. The signal in the small-angle region, with distances of the order of the molecular length, corresponds to cybotactic groups (i.e. local smectic ordering), a consequence of the molecular anisotropy and amphipathic character of the molecule. In many cases, the diffraction pattern of the isotropic phase is very similar to that of the nematic phase. However, a nematic phase can be aligned by an external magnetic field. This is not the case for the isotropic phase. The alignment of the nematic phase in a magnetic field can be observed by X-ray diffraction if a 2D detector is used.

A.2 Smectic phases

Lamellar structures are characterized by the layer periodicity d. To get a better understanding of the molecular packing in smectic phases, it is necessary to consider the molecular area, A_M, and to compare it with the cross-sectional area of the rigid core of the molecules A_{core} and the cross-sectional area of the aliphatic chains of the molecules A_{chains}. In general, if at

the interface between the rigid core and the aliphatic chains, the cross-sectional area of the chains is similar to that of the core, a non-tilted SmA phase is obtained. However, if the cross-sectionnal area of the chains is greater than that of the core, the cores must tilt in order to fill space efficiently and a SmC phase is obtained. Thus, as a rule of thumb, there must be a balance between the molecular area and the cross-sectional area of the aliphatic chains: $A_M \approx A_{chains}$. Figure A.1 shows a schematic representation of the cross-sectional area of the rigid cores in the SmA ($A_{core} \approx A_{chains} \approx A_M$) and SmC ($A_{core} < A_{chains} \approx A_M$) phase.

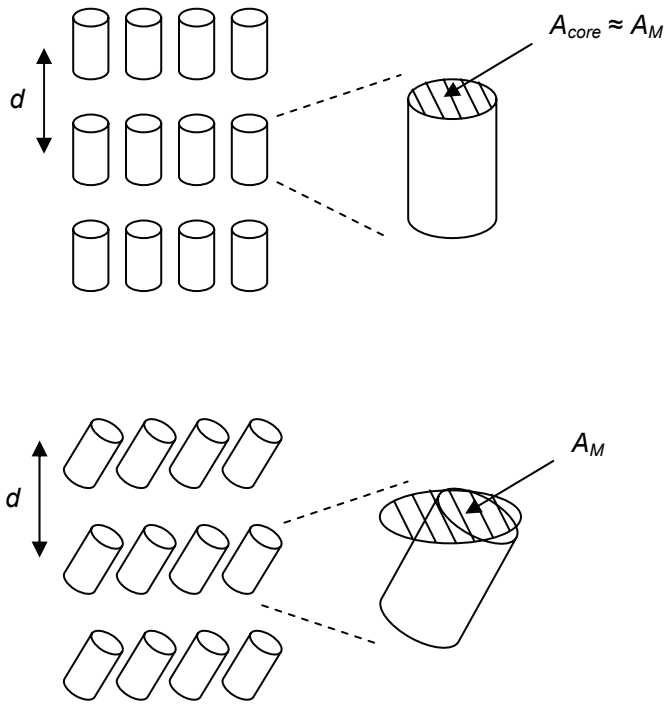


Figure A.1: Schematic representation of the molecular area in the SmA phase (top) and the SmC phase (bottom).

The molecular area A_M is directly deduced from the molecular volume V_{mol} and the layer thickness d: $A_M = V_{mol}/d$.

In some cases, two molecules aggregate in a head-to-head arrangement ((d) in Figure A.2). The rigid part, build up by the rigid cores of two molecules, can be considered as a cylindrical unit with molecular area A_M. In this case, $A_M = 2V_{mol}/d$.

In general, for a cylindrical unit build up by the rigid cores of N molecules, the molecular area A_M is related to the layer thickness d and the molecular volume V_{mol} as follows:

$$A_M = \frac{NV_{mol}}{d} \qquad \text{(A.1)}$$

A comparison of the molecular length L with the layer thickness d also provides useful information about the molecular packing. L can be determined via molecular modeling (computer calculations) or can be obtained from X-ray diffraction on a single crystal (although this provides information about the molecular structure in the crystalline state). Figure A.2 shows a schematic representation of different lamellar arrangements. In case (a) of Figure A.2, there is one rigid core per cylindrical unit and the molecules are non-tilted. In case (b) of Figure A.2, there is one rigid core per cylindrical unit and the molecules are tilted within the layers to compensate the cross-sectional area of the aliphatic chains. In case (c) of Figure A.2, there is one rigid core per cylindrical unit and the molecules are non-tilted. In addition, the aliphatic chains are interdigitated. Finally in case (d) of Figure A.2, there are two rigid cores per cylindrical unit and the molecules are non-tilted.

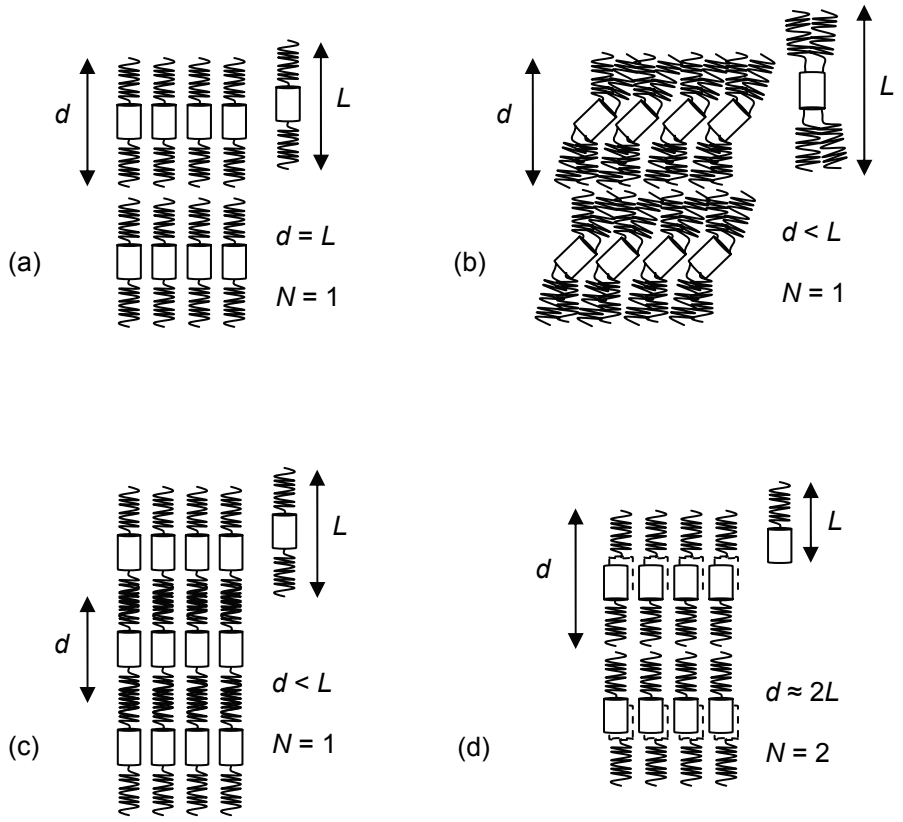


Figure A.2: Schematic representation of different lamellar arrangements; d is the layer thickness, N is the number of molecules per cylindrical unit and L is the molecular length.

For smectic mesophases, the d-spacings are correlated as follows:

$$d_{00l} = \frac{d}{l} \qquad \text{(A.2)}$$

where d is the layer thickness and l is the diffraction order.
Thus, in the small-angle region of the X-ray pattern, sharp reflections with reciprocal spacings in the ratio 1, 2, 3… are observed, corresponding to the indexation (00*l*) = (001), (002), (003)… The higher order reflections have much lower intensities than the first order reflection (001). In the wide-angle region of the X-ray pattern, a broad signal is observed at ca. 4.5 Å, corresponding to the liquidlike order of the molten aliphatic chains.

A.3 Columnar phases

From a geometrical point of view, the columnar structures are characterized mainly by two parameters: the columnar cross section S and the stacking periodicity along the columnar axis h (Figure A.3). Knowledge of these two structural parameters permits the interpretation of the molecular packing inside the columns and a better understanding of the influence of this packing on the 2D arrangement of the columns, and, therefore on the mesophase symmetry.

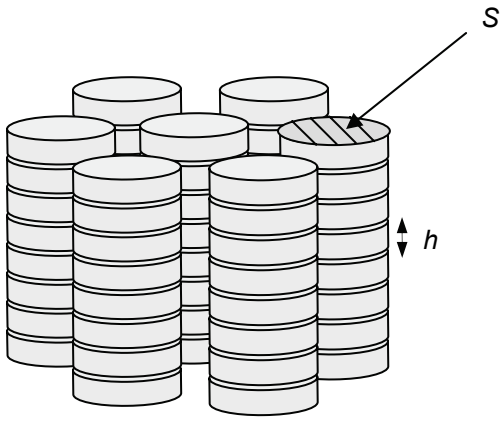


Figure A.3: Schematic representation of a hexagonal arrangement of columns. S is the columnar cross section and h is the stacking periodicity along the columnar axis.

The periodicity h, the columnar cross section S, and the molecular volume V_{mol} are linked analytically through the relation:

$$hS = NV_{mol} \qquad \text{(A.3)}$$

in which N is the number of molecules within a volume fraction of a column. The cross-sectional area of the columns S can be calculated from the lattice parameters obtained from X-ray diffraction and h can usually be obtained directly from the X-ray pattern (or can be determined experimentally by dilatometry).

Although the molecular volume V_{mol} can be determined experimentally by dilatometry, it can also be estimated as follows:

$$V_{mol} = \frac{M}{0.6022\rho} \tag{A.4}$$

where M is the molecular mass (g/mol) and ρ (g/cm^3) the molecular density, which can be estimated as follows:

$$\rho = \frac{27.0673}{V_{CH_2}} \tag{A.5}$$

where V_{CH_2} is the volume of one methylene unit, which can be calculated via the following relation:

$$V_{CH_2} = 26.5616 + 0.02023T \tag{A.6}$$

The number of molecules within a repeat unit of a column depends on the shape and the size of the molecules. For large discotic molecules, there is usually one molecule per repeat unit and for hemidisclike molecules, there are usually two molecules per repeat unit. Polycatenar molecules also form columnar phases at long chain lengths and usually three or four molecules arrange into a repeat unit. Figure A.4 gives a schematic overview of these arrangements.

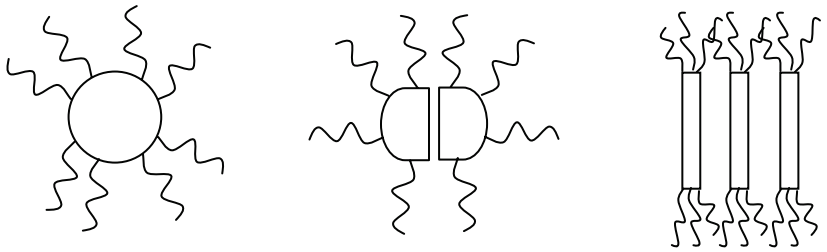


Figure A.4: Schematic overview of the arrangement of large discotic molecules (left), hemidisclike molecules (center) and polycatenar molecules (right) into a repeat unit.

A.3.1 Hexagonal columnar phase

The hexagonal symmetry results from the hexagonal close-packing of cylindrical columns. Their projection onto the lattice plane perpendicular to the columnar axis leads to circular columnar cross sections, separated from one other by the molten aliphatic medium (aliphatic continuum). A representation of the arrangement of the columns in the hexagonal columnar mesophase is shown in Figure A.5.

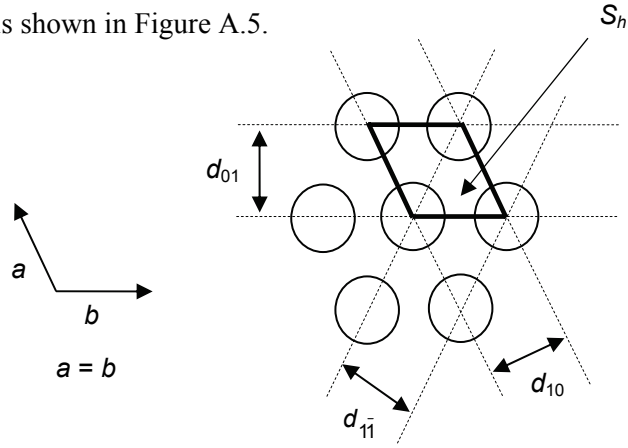


Figure A.5: Schematic representation of the 2D lattice of the hexagonal columnar mesophase (plane group p6mm).

For the hexagonal lattice, the d-spacings are correlated as follows:

$$d_{hk} = \frac{a}{\sqrt{\frac{4}{3}(h^2 + k^2 + hk)}} \qquad \text{(A.7)}$$

where h and k are miller indices defining a set of planes in the hexagonal lattice and a is the lattice parameter.
Thus, in the small-angle region of the X-ray pattern, sharp reflections with reciprocal spacings in the ratio 1, $\sqrt{3}$, 2, $\sqrt{7}$, 3… are observed, corresponding to the indexation (hk) = (10), (11), (20), (21), (30)… In general, the higher order reflections have much lower intensities than the fundamental reflection (10). In the wide-angle region of the X-ray pattern, a broad signal is observed at ca. 4.5 Å, corresponding to the liquidlike order of the molten aliphatic chains.

As the unit cell of the hexagonal lattice contains only one column, the cross section S of the columns corresponds exactly to the lattice area S_h (Figure A.5), and can be directly calculated from the measurement of d_{10}:

$$S = \frac{2}{\sqrt{3}} d_{10}^2 \qquad \text{(A.8)}$$

Note that the lattice parameter a corresponds to the diameter of a circular columnar cross section and can also be directly calculated from the measurement of d_{10}:

$$a = \frac{2}{\sqrt{3}} d_{10} \qquad \text{(A.9)}$$

If the diameter of the circular cross section is smaller than the molecular length, the molecules are tilted within the columns.

A.3.2 Rectangular columnar phase

The rectangular symmetry results from the packing non-cylindrical columnar cores, and their projection onto the lattice plane perpendicular to the columnar axis leads to elliptical, columnar cross sections, separated from one other by the molten aliphatic medium. Such elliptical cross sections are generated either by the molecular shape itself, hindered molecular rotation of non-disclike molecules around the columnar axis, or by the tilt of the molecular discs perpendicular to the columnar axis.

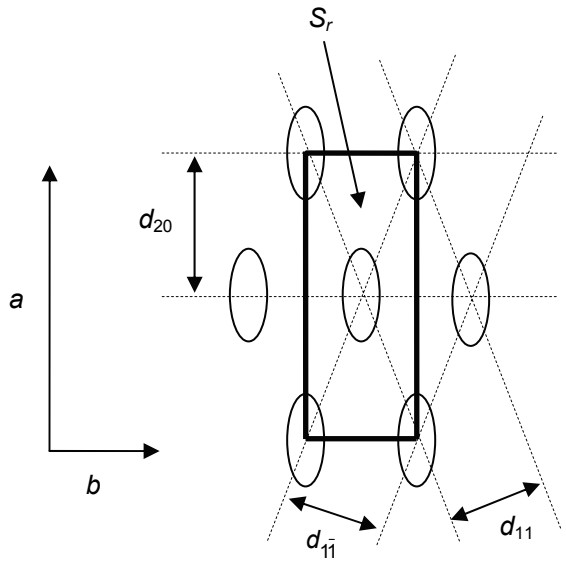


Figure A.6: Schematic representation of the 2D centered lattice of the rectangular columnar mesophase (plane group c2mm).

Two types of 2D rectangular arrangements of columns are possible for the rectangular columnar mesophases, characterized by two different plane groups, namely *c2mm* and *p2gg* depending on the mutual orientation of these ellipses in the rectangular lattice. The ellipses are either oriented along a unique direction (*c2mm,* Figure A.6) or are alternatively oriented along two different directions (*p2gg,* Figure A.7).

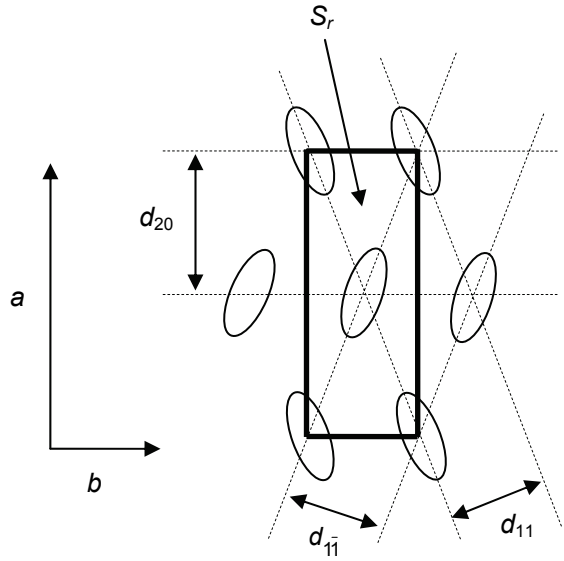


Figure A.7: Schematic representation of the 2D centered lattice of the rectangular columnar mesophase (plane group p2gg).

The distinction between the centered *c*2*mm* and *p*2*gg* lattices depends on the number of reflections obtained, allowing the specific conditions of the (*hk*) reflections to be tested. For *p*2*gg* symmetry, there exists the condition that $h0 = 2n$ and $0k = 2n$, whereas, in *c*2*mm* symmetry, all the (*hk*) reflections must additionally satisfy the condition $h + k = 2n$, so that the presence of

forbidden reflections ($h + k = 2n + 1$) excludes *c*2*mm* symmetry. However, in most cases, two fundamental reflections, one corresponding to the (20) reflection and the other to the (11) and $(1\bar{1})$ pair, are in general intense, and the higher order reflections, very weak or absent, so that discrimination between the two symmetries is often not possible using powder patterns alone. Oriented samples are then necessary to provide the necessary additional information.

As for the hexagonal columnar mesophase, in the wide-angle region of the X-ray pattern, a broad signal is observed at ca. 4.5 Å, corresponding to the liquidlike order of the molten aliphatic chains.

The lattice parameter a is connected directly to the d_{20} spacing:

$$a = 2d_{20} \tag{A.10}$$

The lattice parameter b and the lattice area S_r are defined by the three fundamental reflections:

$$b = \sqrt{\frac{2}{\frac{1}{d_{11}^2} + \frac{1}{d_{1\bar{1}}^2} - \frac{1}{2d_{20}^2}}} \tag{A.11}$$

$$S_r = ab \tag{A.12}$$

In contrary to the hexagonal lattice, the unit cell of the rectangular lattice contains two columns (Figure A.6 and Figure A.7). Thus, $S = S_r/2$ for the columnar cross sections of the rectangular columnar mesophase.

A.4 Cubic phases

The cubic lattice is defined by the lattice parameter a, which can be calculated from the lattice parameters obtained from X-ray diffraction. The volume of the cubic cell, V_{cell}, can be calculated as follows:

$$V_{cell} = a^3 \tag{A.13}$$

By determination or estimation of the molecular volume V_{mol} (vide supra) and by comparing the molecular volume to the volume of the cubic cell V_{cell}, the number of molecules per cubic cell N can be determined:

$$\frac{V_{cell}}{V_{mol}} = N \tag{A.14}$$

For the cubic lattice, the d-spacings are correlated as follows:

$$d_{hkl} = \frac{a}{\sqrt{h^2 + k^2 + l^2}} \tag{A.15}$$

Thus, in the small-angle region of the X-ray pattern, sharp reflections with reciprocal spacings in the ratio 1, $\sqrt{2}$, $\sqrt{3}$, 2, $\sqrt{5}$, $\sqrt{6}$ … are observed, corresponding to the indexation (hkl) = (100), (110), (111), (200), (210), (211)… For a primitive lattice, all (hkl) reflexions are allowed; for a body-centered lattice, there exists the condition that $h + k + l = 2n$; for a face-centered lattice, h, k and l must be all even or odd. In the wide-angle region of the X-ray pattern, a broad signal is observed at ca. 4.5 Å, corresponding to the liquidlike order of the molten aliphatic chains.

A.5 Bibliography

Bruce, D. W.; Donnio, B.; Hudson, S. A.; Levelut, A.-M.; Megtert, S.; Petermann, D.; Veber, M. *J. Phys. II France* **1995**, *5*, 289.

Donnio, B.; Heinrich, B.; Allouchi, H.; Kain, J.; Diele, S.; Guillon, D.; Bruce, D. W. *J. Am. Chem. Soc.* **2004**, *126*, 15258.

Guillon, D. *Struct. Bonding* **1999**, *95*, pp 41-82.

Morale, F.; Date, R. W.; Guillon, D.; Bruce, D. W.; Finn, R. L.; Wilson, C.; Blake, A. J.; Schröder, M.; Donnio, B. *Chem. Eur. J.* **2003**, *9*, 2484.

Treatment of glass cover slips Appendix B

When examined by polarizing optical microscopy (POM), some compounds tend to give a homeotropic texture: the rodlike molecules orient themselves nearly perpendicular to glass slide surface. For uniaxial mesophases (for example the nematic phase and the smectic A phase), a black image will appear between crossed polarizers. In this case, it is impossible to identify the type of mesophase and a planar orientation of the sample is necessary to characterize the mesophase. On the other hand, if a black image appears when the sample is homeotropically aligned, the mesophase must be uniaxial. Therefore, both the homeotropic and the planar orientations provide complementary information and it is useful to examine the same sample in both orientations. This appendix describes a procedure to treat glass cover slips in order to induce a planar or a homeotropic orientation of the sample.

The rigid part of a mesogen can be considered as being more polar than the apolar aliphatic chains. When the glass cover slips are treated with sulfochromic acid (B.1), a thin layer of water will bind via hydrogen bonding to the hydrophilic glass cover slip surface. In this case, the apolar aliphatic chains will avoid the hydrophilic water layer and a planar orientation is energetically more favorable (Figure B.1). When the glass cover slips are treated with *n*-octadecyltrichlorosilane (B.2), the glass cover slip surface becomes hydrophobic. Hydrophobic interactions will induce a homeotropic orientation, which is energetically more favorable (Figure B.1).

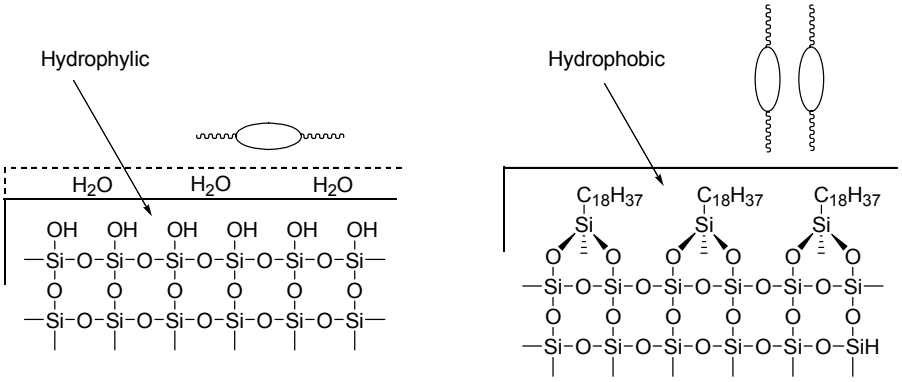


Figure B.2: Glass cover slip surface treated with sulfochromic acid (left) and with n-octadecyltrichlorosilane (right).

B.1 Treatment of glass cover slips to obtain planar orientation

Small glass containers were filled with a sulfochromic acid solution, which was prepared by dissolving $K_2Cr_2O_7$ (0.17 mol, 50 g) in H_2O (500 ml) and conc. H_2SO_4 (400 ml). The glass cover slips were placed in containers, which were then covered to prevent evaporation of the solvent. The containers were placed in a bath of H_2SO_4 and H_2O and heated to 80 °C overnight. The glass cover slips were removed from the sulfochromic acid solution, washed with water and stored in a fresh sulfochromic acid solution.

Use: the glass cover slips were washed with water and dried. After drying, the glass cover slips should be used immediately. In order to obtain the desired orientation, the sample should be heated into the isotropic phase and then cooled very slowly (1 °C/min or slower).

B.2 Treatment of glass cover slips to obtain homeotropic orientation

Small glass containers were filled with a 1% solution of *n*-octadecyltrichlorosilane in $CHCl_3$, saturated with water (which acts as a catalyst). Glass cover slips, which were treated with sulfochromic acid (see B.1), were placed in the glass containers, which were then covered to prevent evaporation. After 16 hours, the glass cover slips were removed from the solution, placed in dry containers and dried for 2 hours at 120 °C. The glass cover slips were washed with $CHCl_3$ (to remove the excess of *n*-octadecyltrichlorosilane) and dried. No special storage conditions are necessary.

Use: in order to obtain the desired orientation, the sample should be heated into the isotropic phase and then cooled very slowly (1 °C/min or slower).